Candida glabrata ace2 hypervirulence: Looking at the genes behind the effect

Samuel Russell Stanley Gibbs

A thesis submitted to fulfil the requirements for a Doctor of Philosophy degree from Imperial College London, Faculty of Medicine.

Imperial College London, South Kensington, London, United Kingdom

Dedication

To my parents for all their love and support and putting me through the best education possible. I appreciate their sacrifices and I wouldn't have been able to get to this stage without them.

To Deborah for her unending support, level-headedness and love. I wouldn't have gotten through this doctorate if it wasn't for her.

Abstract

Our current understanding of virulence in the opportunistic pathogen *Candida glabrata* is in its infancy. To expand our understanding of *C. glabrata* virulence, an investigation into the genes transcriptionally regulated by the first virulence-moderating gene to be discovered in *Candida*, *ACE2,* was undertaken. For the first time in *C. glabrata*, a partial Ace2p regulon containing 12 previously univestigated genes that show Ace2p-dependent expression has been defined. Study of their promoter regions discovered possible Ace2p DNA binding sites, with 10 genes showing possible direct regulation by Ace2p in *C. glabrata.* A reductionist approach was employed in an effort to study the effects of the deletion of each of the 12 partial Ace2p-regulon genes in *C. glabrata* individually. Both phenotypic and virulence analyses were used to analyse the results of the individual deletions with regard to the extreme hypervirulence displayed by the *ace2* null cells. The results indicate that out of the 10 genes successfully disrupted, six were shown to be significantly different when compared with the *C. glabrata* wild type in a neutropenic murine model of systemic candidiasis and therefore hypervirulent.

Each of the six hypervirulent genes showed 100% mortality after five days post infection, markedly different to the hypervirulence displayed by the *ace2* null, which displayed 100% mortality within 18 hours post infection, and to the wild type, which displayed 40% mortality after 14 days post infection. The *C. glabrata sic1* null was also found to elicit significantly increased cytokine release in an *in vitro* macrophage infection assay, as measured by IL-6 and TNFα ELISA. The results presented in this thesis therefore indicate that the hypervirulence and immune over-stimulation shown by the *ace2* mutant in *C. glabrata* is most likely multifactorial with a combination of antivirulence genes contributing to the extreme hypervirulence and immune over-stimulation.

During the course of investigation into the Ace2p regulon, a novel gene lacking homology to putative glucanases or other yeast genes was highlighted. Therefore the uncharacterised Ace2p regulon gene *DSE1*, whose function is currently unknown, was investigated. Using *C. glabrata* and its close genetic relative, the model organism *Saccharomyces cerevisiae*, a study of the localisation, phenotype and structural prediction revealed a possible enzymatic or regulatory function for Dse1p, localised to the cell budding area and daughter cell, with a likely role in cell wall metabolism and cell separation within *C. glabrata*.

Declaration

I certify that the work described within this thesis is entirely my own, unless otherwise stated.

Samuel Russell Stanley Gibbs

Acknowledgements

Throughout this project many people have helped me, both through hands on direction and as walls to bounce ideas off. I want to thank all the members of the Haynes, Bignell and Arst groups for making the lab a decent place to work, and for your help, tips and tricks. I want to thank Biao Ma for his help in kick starting my project – I wouldn't have got this far if it wasn't for the methods, tips and tricks I learnt from him in my first year. I would also like to thank Lara, for her help initially with my undergraduate project and her help and advice throughout my PhD, she showed me what was possible and lead the way by example. To Hsueh-lui, thanks for all your help throughout the last four years and for putting up with inane questions, you've been a Saint and a good friend.

I'd also like to thank the newer members of the Haynes lab, particularly Daniel and Florencia, who have often served as extremely helpful idea bouncing boards, sorry for that. Marghe and Ana-Maria, thank you both for your help on many occasions in the lab. Thanks also to Elaine for your help with the CBS work and with transition after Ken's move to Exeter, most appreciated.

I'd of course like to thank Ken for the opportunity to do the PhD in the first place, for his help and tips throughout the four years, and for wading through this thesis at the end.

Thanks go to Dr. David Talavera from Manchester University for his structural prediction work and also to Maxime for his help with statistics and bioinformatics. A special thanks goes to Daniel and the rest of the team in the CBS, without which I wouldn't have been able to complete a large chunk of the work that went into this thesis – cheers mate!

And finally, thanks go to Deborah, without whom I would have gone loopy by this stage. Thank you for your support, level headedness and love; I couldn't have done it without you.

To any and all who read this, thanks, but you can stop here if you'd like.

List of abbreviations and acronyms

µ	Micro
µF	Microfarads
µg	Microgram
µL	Microlitre
µm	Micrometre
Ω	Ohm
°C	Degrees Celsius
3D	Three-dimensional
AIDS	Acquired immunodeficiency syndrome
ABC	ATP-binding cassette
AMEN	Antagonist of the mitotic exit network
ANOVA	Analysis of variance
ATP	Adenosine triphosphate
BLAST	Basic Local Alignment Search Tool
BSI	Bloodstream infection
cAMP	Cyclic adenosine monophosphate
CDK	cyclin-dependent protein kinase
daddH_2O	Double autoclaved double distilled water
ddH_2O	Double distilled water
DIC	Differential interference microscopy
DIG	Digoxigenin
DMEM	Dulbecco's Modified Eagle Medium
DMSO	Dimethyl sulfoxide
DNA	Deoxyribonucleic acid
ECM	Extracellular matrix

EDTA	Ethylenediaminetetraacetic acid
EGTA	Ethylene glycol-bis(2-aminoethylether)-N'-N'-N'-N'-tetraacetic acid
ELISA	Enzyme Linked ImmunoSorbent Assay
FCS	Foetal calf serum (also known as FBS, Foetal bovine serum)
FRT	Flippase recognition target
g	Gram
GEN	Geneticin (G418)
GEN_R	Geneticin (G418) resistance marker
GFP	Green fluorescent protein
GM-CSF	Granulocyte monocyte colony-stimulating factor
GMS	Grocott's methenamine silver and light green
GPI	Glycosylphosphatidylinositol
H&E	Haemotoxylin and eosin
hBD	Human beta-densins
ICU	Intensive care unit
IL	Interleukin
IP	Intraperitoneal
IV	Intravenous
kb	Kilobase
kg	Kilogram
kV	Kilovolts
L	Litre
LB	Luria Bertani
LEU/Leu	Leucine
LiAc	Lithium acetate
M	Molar
MAP	Mitogen-activated protein

MAPK	Mitogen-activated protein kinase
MDR	Multidrug resistance
MEN	Mitotic exit network
mg	Miligram
mL	Mililitre
mM	Milimolar
NAT	Nourseothricin
NAT_R	Nourseothricin resistance marker
nm	Nanometer
ng	Nanogram
OD	Optical density
ORF	Open reading frame
PBS	Phosphate buffered saline
PCR	Polymerase chain reaction
PEG	Polyethylene glycol
pH	Measure of acidity/alkalinity of a solution
PKC	Protein kinase C
PL	Phospholipases
POI	Points of interest
RAM	Regulation of Ace2p transcription factor and polarised morphogenesis
RNA	Ribonucleic acid
RNA-seq	High-throughput sequencing of cDNA made from RNA
ROS	Reactive oxygen species
rpm	Revolutions per minute
s	Second
SAPs	Secreted aspartic proteases
SD	Synthetic dropout

SDS	Sodium dodecyl sulphate
SGD	Saccharomyces genome database
TBE	Tris-borate EDTA
TBOOH	t-butylhydroperoxide
Tet	Tetracycline
TNF	Tumour necrosis factor
TRP/Trp	Tryptophan
TV	Tail vein
URA/Ura	Uracil
US	United States of America
UV	Ultra violet
V	Volts
v/v	Volume/volume
w/v	Weight/volume
X-Gal	5-bromo-4-chloro-3-indoyl-b-D-galactopyranoside
YKO	Yeast Knockout
YNB	Yeast nitrogen base
YPD	Yeast peptone dextrose
YPG	Yeast peptone glucose

Table of Contents

Title 1
Dedication 2
Abstract 3
Declaration 4
Acknowledgments 5
List of abbreviations and acronyms 6
Table of Contents 10
List of Figures 14
List of Tables 24

1 Introduction 25
1.1 Fungal human pathogens 25
1.1.1 Antifungals 26
1.2 Non-human fungal pathogens 27
1.3 *Candida* epidemiology 28
1.3.1 Superficial candidiasis 29
1.3.2 Invasive candidiasis and candidaemia 30
1.4 *Candida glabrata* and candidiasis 31
1.4.1 *Candida albicans* virulence factors 32
1.4.2 *Candida glabrata* virulence factors 33
1.4.3 *C. glabrata* virulence analysis using *Caenorhabditis elegans* 35
1.5 The evolutionary relationship between *C. glabrata* and S*. cerevisiae* 36
1.5.1 Phylogeny 36
1.5.2 Host environment adaptation 37
1.5.3 Virulence and drug resistance 38
1.6 Ace2p and the cell cycle 39
1.6.1 Yeast cell cycle 39
1.6.2 Cytokinesis and cell separation 39
1.6.3 The RAM network 41
1.7 Current knowledge of the Ace2p regulon 42
1.7.1 *AMN1* 43
1.7.2 *ASH1* 43
1.7.3 *BUD9* 44
1.7.4 *DSE1* 44
1.7.5 *DSE2* 45
1.7.6 *DSE3* 46
1.7.7 *DSE4/ACF2* 46
1.7.8 *EGT2* 46
1.7.9 *RME1* 47
1.7.10 *SCW11* 47
1.7.11 *SIC1* 48

1.8 Role of cell wall components in the septum 49
1.8.1 Glucan 49
1.8.2 Chitin 49
1.9 General aims of the project 50
1.10 Specific aims of the project 50
2 Materials and Methods 52
2.1 Chemicals and reagents 52
2.2 Culture media, strains and plasmids 52
2.2.1 Fungal strains and growth media 52
2.2.2 Bacterial strains and growth media 52
2.2.3 Plasmids 52
2.3 Molecular biology techniques 53
2.3.1 Primers 53
2.3.2 Polymerase chain reaction 53
2.3.3 Colony polymerase chain reaction 53
2.3.4 Linear DNA and PCR extraction and purification 53
2.3.5 Enzymatic manipulation of DNA 53
2.3.6 Agarose gel electrophoresis 53
2.3.7 DNA and RNA quantification 54
2.3.8 Isolation of yeast DNA 54
2.3.9 Isolation of yeast RNA 54
2.3.10 Plasmid DNA extraction 54
2.3.11 Yeast transformation – Electroporation 54
2.3.12 Yeast Transformation – Lithium acetate 55
2.3.13 Quick transformation of yeast cells 55
2.3.14 Bacterial transformation 55
2.3.15 Northern Analysis 55
2.3.16 Southern Analysis 56
3 Confirmation of the Ace2p regulon 57
3.1 Overview 57
3.2 Materials and methods 59
3.2.1 Northern analysis of Ace2p regulon in *C. glabrata* Ace2p tet-regulated strain 59
3.2.2 Analysis of the upstream regions of Ace2p regulon genes in *C. glabrata* for potential Ace2p binding sites 59
3.3 Results 60
3.3.1 Ace2p transcriptionally regulates 12 genes 60
3.3.2 Potential Ace2p binding sites in the promoter regions of the Ace2p regulon genes 60
3.3.3 Selection of target genes for deletion 63
3.4 Discussion 64
3.4.1 Ace2p transcriptional regulation: direct or indirect? 65
3.4.2 *C. glabrata ace2* clumping phenotype 66
4 Study of the Ace2 regulon and its role in hypervirulence 69
4.1 Overview 69

4.1.1 Conventional virulence factors in *C. glabrata* 69
4.1.2 A novel antivirulence gene in *C. glabrata* 70
4.1.3 The Ace2p regulon 70
4.2 Materials and Methods 72
4.2.1 Construction of *ash1, bud9, dse1, dse3, egt2* and *rme1* null mutants by fusion PCR 72
4.2.2 Construction of *amn1, acf2, scw11b* and *sic1* null mutants by Edlind method 74
4.2.3 Reconstitution of *C. glabrata* gene deletions 75
4.2.4 Solid agar phenotypic screen 77
4.2.5 Difference interference microscopy (DIC) 79
4.2.6 Growth rate analysis 79
4.2.7 Murine virulence studies 79
4.2.8 Histological examination of murine samples 79
4.2.9 Fungal burden 79
4.2.10 Macrophage stimulation with yeast 80
4.2.11 Enzyme-Linked ImmunoSorbent Assay (ELISA) cytokine analysis 80
4.3 Results 81
4.3.1 Southern blot analysis 81
4.3.2 Solid agar phenotypic screen 81
4.3.3 Phenotypic microscopy 89
4.3.4 Growth rate analysis 92
4.3.5 Immune suppression survival pilot 93
4.3.6 Murine virulence model of systemic candidiasis 94
4.3.7 Fungal burden 105
4.3.8 Histology 106
4.3.9 Macrophage stimulation assay 116
4.3.10 Reconstitution Northern Analysis 118
4.4 Discussion 119
4.4.1 Deletion of the Ace2p regulon in *C. glabrata* 119
4.4.2 Deletion screening 119
4.4.3 Virulence screening 121
4.4.4 Immune activation and septic shock in Ace2p regulon hypervirulence 122
4.4.5 Potential effects of deletion of the Ace2p regulon genes 123
4.4.6 Ace2p regulon hypervirulence and *ace2* 126
4.4.7 Implications of antivirulence 127
5 Study of the novel gene *DSE1* in yeast 129
5.1 Overview 129
5.2 Materials and Methods 132
5.2.1 Analysis of the upstream region of *DSE1* in *S. cerevisiae* for potential Ace2p binding sites 132
5.2.2 *C. glabrata* Dse1p structural prediction 132
5.2.3 *C. glabrata* and *S. cerevisiae dse1* null vanadate sensitivity screen 132
5.2.4 Yeast *dse1* null polarization study 132
5.2.5 Construction of Dse1p-GFP Gateway plasmid 133
5.2.6 Localisation study of *S. cerevisiae* Dse1p in known interactor nulls 133

5.2.7 Growth rate analysis 133
5.3 Results 134
5.3.1 *DSE1* expression is Ace2p-dependent in *S. cerevisiae* and *C. glabrata* 134
5.3.2 Potential Ace2p binding sites in the promoter region of both *C. glabrata* and *S. cerevisiae* *DSE1* 134
5.3.3 *C. glabrata* Dse1p structural prediction 135
5.3.4 C. glabrata *dse1* null phenotypic screen 136
5.3.5 *C. glabrata* and *S. cerevisiae* vanadate sensitivity screen 136
5.3.6 Yeast *dse1* null polarization study 138
5.3.7 Localisation study of *S. cerevisiae* Dse1p in known interactor nulls 139
5.3.8 Growth rate analysis of *C. glabrata dse1* 140
5.4 Discussion 141
5.4.1 Ace2p direct transcriptional regulation is likely in both *C. glabrata* and *S. cerevisiae*. 141
5.4.2 β-propeller 141
5.4.3 Deletion of *DSE1* induces a cell separation defect 142
5.4.4 Localisation of Dse1p 143
5.4.5 Results and roles from the literature 144
5.4.6 Summary 146
6 Summary and Conclusions 147
6.1 Summary 147
6.1.1 The Ace2p regulon in *C. glabrata* 147
6.1.2 *DSE1* a novel gene likely to be involved in cell separation in *C. glabrata* 148
6.2 Future work 149
6.3 Conclusions 151
7 References 153
Appendix 1 - Strains 167
A1.1 Yeast Strains 167
Appendix 2 - Plasmids 169
A2.1 Yeast plasmids 169
A2.2 *E. coli* plasmids 169
Appendix 3 – Primers 170
Appendix 4 – Gene deletion confirmations 175
Appendix 5 185
A5.1 *C. elegans* invertebrate model of innate immune response 185
A5.1.1 Materials and Methods 186
A5.2 Study and comparison of the transcriptome of *Candida* species infection of murine model 187
A5.2.1 Materials and Methods 188

Figure 1.1 – *C. glabrata* belongs to the *Saccharomyces* clade, not the *Candida* clade. Phylogenetic tree showing the evolutionary relationships of *C. glabrata* and selected *Candida* species with that of *S. cerevisiae* and selected *Saccharomyces* species. Adapted from Roetzer et al. 2010 [104]. The tree was built using maximum likelihood analysis of concatenated alignments of 1137 protein familys that exist with single-copy orthologues in the 21 species. CTG marks genetic code transition event that recoded CUG to Serine (the non-CTG branch). 37

Figure 1.2 – *S. cerevisiae* and *C. glabrata ace2* display a clumpy, cell separation deficient phenotype. Yeast was grown over night at 30°C or 37°C, 180 rpm, and visualised under DIC. A) *S. cerevisiae* BY4741 cells (B) *C. glabrata* (HSL122) *ace2* cells (C) *S. cerevisiae ace2* cells. Both *ace2* strains display a cell separation deficient phenotype, although this is less severe in *S. cerevisiae*. Scale bar 10 μm. 40

Figure 1.3 – Predicted model of the RAM network [132]. Interacting Kic1p, Sog2p and Hym1p form a complex and activate Mob2p-Cbk1p [135, 136]. Tao3p and Ssd1p are also thought to activate the Mob2p-Cbk1p complex; the activated Mob2p-Cbk1p complex activates Ace2p, which in turn activates the transcription of genes required for cell separation, the cell separation machinery, which leads to hydrolysis of the primary and secondary septum and cell separation [135, 136]. *SSD1,* however, has been shown to not be essential for RAM regulation of Ace2p [135, 136]. . 41

Figure 3.1 – *C. glabrata* Ace2p regulates the expression of 12 genes putatively involved in cell wall biology, daughter cell specific expression and cell cycle regulation. *C. glabrata* HLS119 was cultured overnight in YPD in the absence (-, *ACE2* de-repressed) and presence (+, *ACE2* repressed) of 200 mg/mL doxycycline. Total RNA was extracted using a modified acid phenol method, and 7 μg was loaded per lane. The upper panels show Northern analysis. Probes were constructed using internal primer pairs from the relevant gene indicated above each pair of panels. Primers are listed in Appendix 3. The lower panels show methylene blue loading controls. In the presence of doxycycline *ACE2* expression is repressed as shown by the lack of a band in the *ACE2* + lane. All other genes analysed show a loss of band in the absence of *ACE2* expression demonstrating that their expression in *C. glabrata* is dependent, either directly or indirectly, on Ace2p. 60

Figure 3.2a – Potenial Ace2p binding sites exist in the intergene regions upstream of the Ace2p regulon ORFs in *C. glabrata*. The intergene region upstream of the Ace2p regulon genes in *C. glabrata* is displayed with potential Ace2p binding sites (ACCAGC) [220] marked for position relative to the ATG of the Ace2p-dependent gene of interest. All co-ordinates and measurements are in base pairs, all sequences were taken from Génolevures [171]. Diagrams are not to scale. *AMN1* has two potential Ace2p binding sites between it and *FAB1*; *ASH1* has four potential Ace2p binding sites between it and *MTR2*; *BUD9* has two potential Ace2p binding sites between it and *KSS1*; *DSE1* has two potential Ace2p binding sites between it and *RSP5*; *DSE2* has three potential Ace2p binding sites between it and *CH37*; and *DSE3* has three potential Ace2p binding sites between it and *CAGL0C02805g*..... 61

Figure 3.2b – Potenial Ace2p binding sites exist in the intergene regions upstream of the Ace2p regulon ORFs in *C. glabrata.* The intergene region upstream of the Ace2p regulon genes in *C. glabrata* is displayed with potential Ace2p binding sites (ACCAGC) [215] marked for position relative to the ATG of the Ace2p---dependent gene of interest. All co---ordinates and measurements are in base pairs, all sequences were taken from Génolevures [165]. Diagrams are not to scale. *ACF2* lacks any potential Ace2p binding sites between it and *RMP1; EGT2* has four potential Ace2p binding sites between it and *MDJ2; RME1* lacks any potential Ace2p binding sites between it and *SCM4; SCW11α* has three potential Ace2p binding sites between it and *CWH41; SCW11β* has three potential Ace2p binding sites between it and *RRN6;* and *SIC1* has two potential Ace2p binding sites between it and *BOS1.* *61*

Figure 3.2c – Four Potenial Ace2p binding sites exist in the intergene region upstream of *CTS1* in *C. glabrata.* The intergene region upstream of *CTS1* in *C. glabrata* is displayed with potential Ace2p binding sites (ACCAGC) [215] marked for position relative to the ATG. All co---ordinates and measurements are in base pairs, all sequences were taken from Génolevures [165]. Diagrams are not to scale. *CTS1* has four potential Ace2p binding sites between it and CAGL0M09757g. 62

Figure 4.1 – Construction of *C. glabrata* deletion mutants by homologous recombination of a fusion PCR deletion cassette. Primers, as listed in Appendix 3, were designed to produce products containing 500 bp of homology with the 5' and 3' UTRs of the target gene and 20 bp tails of the U2 and D2 regions of the NAT^R cassette. The deletion cassette was then created by fusion PCR essentially as described by [240, 244] and transformed into the *C. glabrata his3* strain using electroporation. Flippase recognition target (FRT) sites for marker recycling and barcodes from the *S. cerevisiae* gene deletion project [242, 243] have been included for genes with *S. cerevisiae* homologues. 72

Figure 4.3 – Plasmid map of pBM51. The target ORF for reconstitution was cloned into pBM51 [Biao Ma (personal communication)] between either 2172 (Sal1) and 2211 (Xma1) or between 2199 (EcoR1) and 211 (Xma1) using the respective restriction digests..... 77

Figure 4.4 – *C. glabrata ash1, bud9, dse1, egt2* and *rme1* show no sensitivity to seven test conditions. Growth phenotypes of 18 Ace2p regulon null mutants, three nulls for each gene: *ASH1*, *BUD9*, *DSE1, DSE3*, *EGT2* and *RME1* and the parental strain *C. glabrata his3* (*Δhis3*). No sensitivity was shown by any of the null mutants when compared with the parental control. 5 µL of each strain was spotted in serial dilutions of 1×10^7, 1×10^6, 1×10^5 and 1×10^4 cells/ml. Strains were grown for three days on YPD at 37°C unless otherwise stated. 82

Figure 4.5 – *C. glabrata ash1, bud9, dse1, egt2* and *rme1* show no sensitivity to seven test conditions. Growth phenotypes of 18 Ace2p regulon null mutants, three nulls for each gene: *ASH1*, *BUD9*, *DSE1, DSE3*, *EGT2* and *RME1* and the parental strain *C. glabrata his3* (*Δhis3*). No sensitivity was shown by any of the null mutants when compared with the parental control. 5 µL of each strain was spotted in serial dilutions of 1×10^7, 1×10^6, 1×10^5 and 1×10^4 cells/ml. Strains were grown for three days on YPD at 37°C unless otherwise stated. 83

Figure 4.6 – *C. glabrata ash1, dse1, egt2* and *rme1* show mild sensitivity to vanadate and *ash1* and *dse1* show mild sensitivity to caffeine test conditions. Growth phenotypes of 18 Ace2p regulon null mutants, three nulls for each gene: *ASH1*, *BUD9*, *DSE1, DSE3*, *EGT2* and *RME1* and the parental strain *C. glabrata his3* (*Δhis3*). No sensitivity was shown by any of the null mutants when compared with the parental control apart from 2.5mM vanadate in which *Δash1 #5, Δash1 #7, Δash1 #8, Δdse1 #4, Δdse1 #5, Δdse1 #6, Δdse3 #18, Δdse3 #19, Δegt2 #4, Δegt2 #6, Δegt2 #14, Δrme1 #5,* and *Δrme1 #6* showed sensitivity, and 10 mM caffeine to which *Δash1 #5, Δash1 #7, Δash1 #8, Δdse1 #4* and *Δdse1 #5* showed a sensitivity. 5 µL of each strain was spotted in serial dilutions of 1 x 10^7, 1 x 10^6, 1 x 10^5 and 1 x 10^4 cells/ml. Strains were grown for three days on YPD at 37°C unless otherwise stated. 84

Figure 4.7 – *C. glabrata amn1, acf2, scw11β,* and *sic1* show no sensitivity to seven test conditions. Growth phenotypes of 12 Ace2p regulon null mutants, three nulls for each gene: *AMN1*, *ACF2*, *SCW11β,* and *SIC1* and the parental strain Cg*ΔΔΔ*. No sensitivity was shown by any of the null mutants when compared with the parental control. 5 µL of each strain was spotted in serial dilutions of 1 x 10^7, 1 x 10^6, 1 x 10^5 and 1 x 10^4 cells/ml. Strains were grown for three days on YPD at 37°C unless otherwise stated. 86

Figure 4.8 – *C. glabrata amn1, acf2, scw11β,* and *sic1* show no sensitivity to seven test conditions. Growth phenotypes of 12 Ace2p regulon null mutants, three nulls for each gene: *AMN1*, *ACF2*, *SCW11β,* and *SIC1* and the parental strain Cg*ΔΔΔ*. No sensitivity was shown by any of the null mutants when compared with the parental control. 5 µL of each strain was spotted in serial dilutions of 1 x 10^7, 1 x 10^6, 1 x 10^5 and 1 x 10^4 cells/ml. Strains were grown for three days on YPD at 37°C unless otherwise stated. 87

Figure 4.9 – *C. glabrata amn1, acf2* and *sic1* show mild sensitivity to vanadate and *amn1, acf2, scw11β,* and *sic1* show mild sensitivity to caffeine test conditions. Growth phenotypes of 12 Ace2p regulon null mutants, three nulls for each gene: *AMN1*, *ACF2*, *SCW11β,* and *SIC1* and the parental strain Cg*ΔΔΔ*. No sensitivity was shown by any of the null mutants when compared with the parental control apart from 2.5 mM vanadate in which all the *amn1, acf2* and *sic1* mutants showed mild sensitivity. All the mutants also showed mild sensitivity to 10 mM caffeine. 5 µL of each strain was spotted in serial dilutions of 1 x 10^7, 1 x 10^6, 1 x 10^5 and 1 x 10^4 cells/ml. Strains were grown for three days on YPD at 37°C unless otherwise stated. 88

Figure 4.10 – *C. glabrata dse1* and *egt2* display a cell seperation defect similar to HLS122 (*ace2*) in liquid media. DIC microscopy of a representitive sample of each of the Ace2p regulon null mutants, their parental control and an *ace2* null, HLS122. No phenotype difference was shown between the parental control and the *ash1, bud9, dse3* and *rme1* null mutants. Both *dse1* and *egt2* null cells displayed a cell seperation defect similar, but not as pronounced, as that displayed by HLS122. This shows that both *DSE1* and *EGT2* may encode proteins that play a more significant role in cell seperation than those gene nulls that didn't display a cell separation phenotype. Yeast strains were grown overnight in YPD at 37°C, 180 rpm, diluted, and grown to OD_{600} 0.5-1, washed, mounted and visualised. 90

Figure 4.11 – *C. glabrata amn1, acf2, scw11β* and *sic1* show a cell separation competent phenotype similar to the parental strain Cg ΔΔΔ in liquid media. DIC microscopy of a representitive sample of each of the Ace2p regulon null mutants and their parental control Cg ΔΔΔ. No phenotypic difference was shown between the parental control and the *amn1, acf2, scw11β* and *sic1* null mutants. Yeast strains were grown overnight in YPD at 37°C, 180 rpm, diluted, and grown to OD_{600} 0.5-1, washed, mounted and visualised. 91

Figure 4.12 – *C. glabrata amn1, ash1, acf2, bud9, dse1, dse3, egt2, rme1, scw11β* and *sic1* show similarity to wild type and parental growth rates. The growth rate of each of the mutants, their parental types Cg *his3* and Cg *ΔΔΔ*, as well as the *C. glabrata* wild type (Cg2001) over 24 hours. The growth rates of *amn1, ash1, acf2, bud9, dse1, dse3, egt2, rme1, scw11β* and *sic1* showed similarity to that of their respective parental types and Cg2001. 92

Figure 4.13 – The addition of an extra immune suppression step at day -1 does not effect uninfected control group survival. Survival of unifected mice (n = 10, open squares) subjected to the modified immune suppression regime with IP injection of 200 mg/kg cyclophosphamide at day 0, 2 and every fourth day remained at 100% through a 21 day experiment..... 93

Figure 4.14 – *C. glabrata amn1* cells are not hypervirulent in a neutropenic murine model of systemic candidasis. Virulence was assayed in a modified neutropenic murine model of systemic infection [81] (n = 5 for wild type (open squares), n = 5 for null mutant (closed triangles)). Intravenous infection with the *C. glabrata amn1* null mutant at 7 x 10^7 cells/mouse resulted in a phenotype that was not significantly different when compared to the wild type strain resulting in 60% survival over 14 days..... 95

Figure 4.15 – *C. glabrata ash1* cells are not hypervirulent in a neutropenic murine model of systemic candidasis. Virulence was assayed in a modified neutropenic murine model of systemic infection [81] (n = 5 for wild type (open squares), n = 5 for null mutant (closed triangles)). Intravenous infection with the *C. glabrata ash1* null mutant at 7 x 10^7 cells/mouse resulted in a phenotype that was not significantly different when compared to the wild type strain resulting in 20% survival over 14 days..... 96

Figure 4.16 – *C. glabrata bud9* cells are not hypervirulent in a neutropenic murine model of systemic candidasis. Virulence was assayed in a modified neutropenic murine model of systemic infection [81] (n = 5 for wild type (open squares), n = 5 for null mutant (closed triangles)). Intravenous infection with the *C. glabrata bud9* null mutant at 7 x 10^7 cells/mouse resulted in a phenotype that was not significantly different when compared to the wild type strain resulting in 20% survival over 14 days..... 97

Figure 4.17 – *C. glabrata dse1* cells are not hypervirulent in a neutropenic murine model of systemic candidasis. Virulence was assayed in a modified neutropenic murine model of systemic infection [81] (n = 5 for wild type (open squares), n = 5 for null mutant (closed triangles)). Intravenous infection with the *C. glabrata dse1* null mutant at 7 x 10^7 cells/mouse resulted in a phenotype that was not significantly different when compared to the wild type strain resulting in 60% survival over 14 days..... 98

Figure 4.18 – *C. glabrata dse3* cells are hypervirulent in a neutropenic murine model of systemic candidasis. Virulence was assayed in a modified neutropenic murine model of systemic infection [81] (n = 5 for wild type (open squares), n = 5 for null mutant (no symbol), n = 5 for the reconsituted strain (closed triangles)). Intravenous infection with the *C. glabrata dse3* null mutant at 7 x 10^7 cells/mouse resulted in a hypervirulent phenotype that was significantly different when compared to the wild type strain resulting in 100% mortality after five days ($p < 0.05$, Log-rank (Mantel-Cox) analysis). Reconsitution of *DSE3* resulted in a return to wild type virulence levels. 99

Figure 4.19 – *C. glabrata acf2* cells are hypervirulent in a neutropenic murine model of systemic candidasis. Virulence was assayed in a modified neutropenic murine model of systemic infection [81] (n = 5 for wild type (open squares), n = 5 for null mutant (no symbol), n = 5 for the reconsituted strain (closed triangles)). Intravenous infection with the *C. glabrata acf2* null mutant at 7 x 10^7 cells/mouse resulted in a hypervirulent phenotype that was significantly different when compared to the wild type strain resulting in 100% mortality after five days ($p < 0.05$, Log-rank (Mantel-Cox) analysis). Reconsitution of *ACF2* resulted in a return to wild type virulence levels. 100

Figure 4.20 – *C. glabrata egt2* cells are hypervirulent in a neutropenic murine model of systemic candidasis. Virulence was assayed in a modified neutropenic murine model of systemic infection [81] (n = 5 for wild type (open squares), n = 5 for null mutant (no symbol), n = 5 for the reconsituted strain (closed triangles)). Intravenous infection with the *C. glabrata egt2* null mutant at 7 x 10^7 cells/mouse resulted in a hypervirulent phenotype that was significantly different when compared to the wild type strain resulting in 100% mortality after five days ($p < 0.05$, Log-rank (Mantel-Cox) analysis). Reconsitution of *EGT2* resulted in a return to wild type virulence levels. 101

Figure 4.21 – *C. glabrata rme1* cells are hypervirulent in a neutropenic murine model of systemic candidasis. Virulence was assayed in a modified neutropenic murine model of systemic infection [81] (n = 5 for wild type (open squares), n = 5 for null mutant (no symbol), n = 5 for the reconsituted strain (closed triangles)). Intravenous infection with the *C. glabrata rme1* null mutant at 7 x 10^7 cells/mouse resulted in a hypervirulent phenotype that was significantly different when compared to the wild type strain resulting in 100% mortality after five days ($p < 0.05$, Log-rank (Mantel-Cox) analysis). Reconsitution of *RME1* resulted in a return to wild type virulence levels. 102

Figure 4.22 – *C. glabrata sw11β* cells are hypervirulent in a neutropenic murine model of systemic candidasis. Virulence was assayed in a modified neutropenic murine model of systemic infection [81] (n = 5 for wild type (open squares), n = 5 for null mutant (no symbol), n = 5 for the reconsituted strain (closed triangles)). Intravenous infection with the *C. glabrata scw11β* null mutant at 7 x 10^7 cells/mouse resulted in a hypervirulent phenotype that was significantly different when compared to the wild type strain resulting in 100% mortality after five days ($p < 0.05$, Log-rank (Mantel-Cox) analysis). Reconsitution of *SCW11β* resulted in a return to wild type virulence levels. 103

Figure 4.23 – *C. glabrata sic1* cells are hypervirulent in a neutropenic murine model of systemic candidasis. Virulence was assayed in a modified neutropenic murine model of systemic infection [81] (n = 5 for wild type (open squares), n = 5 for null mutant (no symbol), n = 5 for the reconsituted strain (closed triangles)). Intravenous infection with the *C. glabrata sic1* null mutant at 7 x 10^7 cells/mouse resulted in a hypervirulent phenotype that was significantly different when compared to the wild type strain resulting in 100% mortality after five days ($p < 0.05$, Log-rank (Mantel-Cox) analysis). Reconsitution of *SIC1* resulted in a return to wild type virulence levels. 104

Figure 4.24 – *C. glabrata dse3*, *acf2*, *egt2*, *rme1*, *scw11β* and *sic1* show increased fungal burden when compared with the wild type in a neutropenic murine model of candidaisis. The fungal burden as measured by kidney CFU/g from infected mice. Kidneys were extracted at the point of sacrifice, weighed, homogenised, diluted, plated out in triplicate, grown overnight at 37°C and colony forming units counted. The CFU per gram per kidney per infected animal was calculated and compared to the the wild type with *dse3*, *acf2*, *egt2*, *rme1*, *scw11β* and *sic1* showing a significant increase in fungal burden when compared to the wild type (unpaired two tailed t-test, $p < 0.0001$). Reconstitution of *dse3*, *acf2*, *egt2*, *rme1*, *scw11β* and *sic1* returned the fungal burden to the wild type levels. 105

Figure 4.25a – Histological examination of tissues taken from *C. glabrata* wild type experimentally infected mice. The kidney, liver and lung from *C. glabrata* wild type infected mice were removed at sacrifice and stained using GMS. Staining revealed the lung to be the primary target organ for yeast colonisation. 107

Figure 4.26 – *C. glabrata sic1* shows a significant increase in TNFα production in a macrophage stimulation assay compared to the wild type. *C. glabrata* 2001, *dse3*, *acf2*, *egt2*, *rme1*, *scw11β, sic1* and *sic1::SIC1* were exposed to RAW 264.7 macrophages at a ratio of 30:1 fungi:macrophage. After washing off unbound fungi, macrophages were incubated for 6 hours at 37°C, with supernatants then collected for TNFα quantification by ELISA kit (R&D Systems, UK). Results (mean with standard deviation) are pooled triplicate data from three separate experiments. *C. glabrata sic1* showed statistically significant increased levels of TNF-α elicitation compared to the wild type *C. glabrata* 2001 ($p < 0.005$, one-way ANOVA). Reconsitution of *SIC1* restored TNFα elicitation to wild type levels. 116

Figure 4.27 – *C. glabrata sic1* shows a significant increase in IL-6 production in a macrophage stimulation assay compared to the wild type. *C. glabrata* 2001, *dse3*, *acf2*, *egt2*, *rme1*, *scw11β, sic1* and *sic1::SIC1* were exposed to RAW 264.7 macrophages at a ratio of 30:1 fungi:macrophage. After washing off unbound fungi, macrophages were incubated for 6 hours at 37°C, with supernatants then collected for IL-6 quantification by ELISA kit (R&D Systems). Results (mean with standard deviation) are pooled triplicate data from three separate experiments. *C. glabrata sic1* showed statistically significant increased levels of IL-6 elicitation compared to the wild type *C. glabrata* 2001 ($p < 0.05$, one-way ANOVA). Reconsitution of *SIC1* restored IL-6 elicitation to wild type levels. 117

Figure 4.28 – *C. glabrata dse3::DSE3, acf2::ACF2, egt2::EGT2, rme1::RME1, scw11β::SCW11β* and *sic1::SIC1* reconstitutions display expression of the reconstituted gene. *C. glabrata dse3, dse3::DSE3, acf2, acf2::ACF2, egt2, egt2::EGT2, rme1, rme1::RME1, scw11β, scw11β::SCW11β, sic1* and *sic1::SIC1* were cultured in selective media over night, diluted down to 0.1 OD_{600} and allowed to grow for three hours. Total RNA was extracted using a Qiagen RNeasy mini kit as per the manufacturers instructions. Probes were constructed using internal primer pairs from the relevant gene as indicated above each pair of panels. Primers are listed in Appendix 3. The lower panels show methylene blue loading controls. The target gene expression is suppressed in the null strains as indicated by a lack of a band in the KO lane. All reconstituted strains display a black band in the R lane indicating expression of the reconstituted target gene. 118

Figure 5.1 – Potential Ace2p binding sites exist in the intergene regions upstream of *DSE1*. The intergene region upstream of the *DSE1 S. cerevisiae* is displayed with potential Ace2p binding sites (ACCAGC) [220] marked for position relative to the ATG of *DSE1*. *C. glabrata DSE1* is included from Figure 3.2 for reference. All co-ordinates and measurements are in base pairs, all sequences were taken from Génolevures [171] or SGD [170]. Diagrams are not to scale. A. *C. glabrata DSE1* has two potential Ace2p binding sites between it and *RSP5*. B. *S. cerevisiae DSE1* has three potential Ace2p binding sites between it and *RSP5*. 134

Figure 5.2 – Structural prediction of *C. glabrata* Dse1p reveals a β-propeller structure. Analysis of the predicted structure, kindly performed by Dr. Talavera, University of Manchester, of the N-terminus, minus 20bps, of *C. glabrata* Dse1p predicts a β-propeller structure. The arrows represent β-sheets and the coil an α-helix. This predicted functional structure may indicate an enzymatic function for the N-terminus of Dse1p [269]. 135

Figure 5.3 – *C. glabrata dse1* and *S. cerevisiae dse1* display no difference in vanadate sensitivity when compared to their respective wild type strains. Growth phenotypes of the wild type *C. glabrata* strain Cg2001, *C. glabrata dse1*, the *S. cerevisiae* wild type strain BY4741, and *S. cerevisiae dse1*. No sensitivity was shown by any of the null mutants when compared with the wild type control. *S. cerevisiae* shows increased vanadate resistance when compared with *C. glabrata*. 5 µL of each strain was spotted in serial dilutions of 1 x 10^7, 1 x 10^6, 1 x 10^5 and 1 x 10^4. Strains were grown for three days on YPD with the 0.5 mM, 1 mM, 2 mM, 4 mM, 5 mM or 6 mM of vanadate at 30°C. 137

Figure 5.4 – Polarisation of *C. glabrata* and *S. cerevisiae dse1* is unchanged compared to the wild type. Chart showing cell polarisation as measured the ratio of Length:Width for a sample of *C. glabrata* wild type (Cg2001), *C. glabrata dse1* null (Cg Δdse1), *S. cerevisiae* wild type (BY4741) and *S. cerevisiae dse1* null (Sc Δdse1). No significant difference was observed between the polarity of either of the *dse1* nulls and their associated wild type strains in their respective species. Yeast strains were grown overnight in YPD at 30°C/37°C, 180 rpm, diluted, and grown to OD_{600} 0.5-1, washed, mounted and visualised. Photos were then analysed for cell polarity using Image J. 138

Figure 5.5 – Localisation of *S. cerevisiae* Dse1p-GFP is altered in *zds2* null mutant. Florescence microscopy of a representitive sample of the *S. cerevisiae* Dse1p-GFP library strain, as well as BY4741 and known interactors *boi1*, *boi2, zds2, ste4* and *ste11* with pSRSG-GD1 (Dse1-GFP) and their parental control BY4741. All strains show similar localisation to the Dse1-GFP library strain, with Dse1p primarily located to the bud neck area, apart from *zds2* in which Dse1p localised to the cell wall but not the bud neck. Yeast strains were grown overnight in YPD at 30°C, 180 rpm, diluted, and grown to OD_{600} 0.5-1, washed, mounted and visualised. 139

Figure S.1 – Construction and confirmation of the *C. glabrata amn1* null mutant. A null allele of *C. glabrata AMN1* was constructed as described in Chapter 4. A. The *C. glabrata AMN1* locus. Coding regions are shown in blue, ATG (+1) and stop codon (+1536) of *AMN1* are shown. The upstream and downstream genes are also shown. B. The *C. glabrata AMN1* deletion cassette. A 675 bp fragment of *S. cerevisiae TRP1* was amplified flanked by 60 bps of *AMN1* 5' and 3' as described in Chapter 4. C. Targeted integration of the *AMN1* deletion cassette at the *AMN1* locus removing 1536 bps of *AMN1* from +1 to +1536. D. Southern analysis of putative null alleles of *AMN1*. Total genomic DNA was digested with NsiI and probed with 672 bp fragment of Sc*TRP1* as described in Chapter 4. The null allele yielded a 1023 bp NSiI fragment. The presence of a band confirms that correct integration of the cassette has occurred in mutants 3, 5 and 9. The coordinates are shown relative to the start codon of *AMN1* (A) or Sc*TRP1* (B, C). The diagram is not to scale. 175

Figure S.2 – Construction and confirmation of the *C. glabrata ash1* null mutant. A null allele of *C. glabrata ASH1* was constructed as described in Chapter 4. A. The *C. glabrata ASH1* locus. Coding regions are shown in blue, ATG (+1) and stop codon (+2139) of *ASH1* are shown. The upstream and downstream genes are also shown. B. The *C. glabrata ASH1* deletion cassette. A NAT cassette was amplified flanked by 471 bps and 538 bps of *ASH1* 5' and 3' respectively as described in Chapter 4. C. Targeted integration of the *ASH1* deletion cassette at the *ASH1* locus removing 2229 bps of *ASH1* from -68 to +2161. D. Southern analysis of putative null alleles of *ASH1*. Total genomic DNA was digested with ClaI and probed with 567 bp fragment of the NAT cassette as described in Chapter 4. The null allele yielded a 4744 bp ClaI fragment. The presence of a band confirms that correct integration of the cassette has occurred in mutants 5, 7 and 8, with a slanted gel resulting in sloping bands. The coordinates are shown relative to the start codon of *ASH1* (A) or the NAT cassette (B, C). The diagram is not to scale. 176

Figure S.3 – Construction and confirmation of the *C. glabrata bud9* null mutant. A null allele of *C. glabrata BUD9* was constructed as described in Chapter 4. A. The *C. glabrata BUD9* locus. Coding regions are shown in blue, ATG (+1) and stop codon (+1590) of *BUD9* are shown. The upstream and downstream genes are also shown. B. The *C. glabrata BUD9* deletion cassette. A NAT cassette was amplified flanked by 504 bps and 484 bps of *BUD9* 5' and 3' respectively as described in Chapter 4. C. Targeted integration of the *BUD9* deletion cassette at the *BUD9* locus removing 1693 bps of *BUD9* from -29 to +1664. D. Southern analysis of putative null alleles of *BUD9*. Total genomic DNA was digested with NSiI and probed with 567 bp fragment of the NAT cassette as described in Chapter 4. The null allele yielded a 3138 bp NsiI fragment. The presence of a band confirms that correct integration of the cassette has occurred in mutants 6, 7 and 8. The coordinates are shown relative to the start codon of *BUD9* (A) or the NAT cassette (B, C). The diagram is not to scale. 177

Figure S.4 – Construction and confirmation of the *C. glabrata dse1* null mutant. A null allele of *C. glabrata DSE1* was constructed as described in Chapter 4. A. The *C. glabrata DSE1* locus. Coding regions are shown in blue, ATG (+1) and stop codon (+1704) of *DSE1* are shown. The upstream and downstream genes are also shown. B. The *C. glabrata DSE1* deletion cassette. A NAT cassette was amplified flanked by 516 bps and 531 bps of *DSE1* 5' and 3' respectively as described in Chapter 4. C. Targeted integration of the *DSE1* deletion cassette at the *DSE1* locus removing 1747 bps of *DSE1* from -4 to +1743. D. Southern analysis of putative null alleles of *DSE1*. Total genomic DNA was digested with FspI and probed with 567 bp fragment of the NAT cassette as described in Chapter 4. The null allele yielded a 3100 bp FspI fragment. The presence of a band confirms that correct integration of the cassette has occurred for mutants 4, 5, 6. The coordinates are shown relative to the start codon of *DSE1* (A) or the NAT cassette (B, C). The diagram is not to scale..... 178

Figure S.5 – Construction and confirmation of the *C. glabrata dse3* null mutant. A null allele of *C. glabrata DSE3* was constructed as described in Chapter 4. A. The *C. glabrata DSE3* locus. Coding regions are shown in blue, ATG (+1) and stop codon (+1317) of *DSE3* are shown. The upstream and downstream genes are also shown. B. The *C. glabrata DSE3* deletion cassette. A NAT cassette was amplified flanked by 492 bps and 494 bps of *DSE3* 5' and 3' respectively as described in Chapter 4. C. Targeted integration of the *DSE3* deletion cassette at the *DSE3* locus removing 1364 bps of *DSE3* from -44 to +1320. D. Southern analysis of putative null alleles of *DSE3*. Total genomic DNA was digested with SpeI and probed with 567 bp fragment of the NAT cassette as described in Chapter 4. The null allele yielded a 7508 bp SpeI fragment. The presence of a band confirms that correct integration of the cassette has occurred for mutants 10, 12, 18, 19 and 21. The coordinates are shown relative to the start codon of *DSE3* (A) or the NAT cassette (B, C). The diagram is not to scale..... 179

Figure S.6 – Construction and confirmation of the *C. glabrata acf2* null mutant. A null allele of *C. glabrata ACF2* was constructed as described in Chapter 4. A. The *C. glabrata ACF2* locus. Coding regions are shown in blue, ATG (+1) and stop codon (+2313) of *ACF2* are shown. The upstream and downstream genes are also shown. B. The *C. glabrata ACF2* deletion cassette. A 675 bp fragment of *S. cerevisiae TRP1* was amplified flanked by 60 bps of *ACF2* 5' and 3' as described in Chapter 4. C. Targeted integration of the *ACF2* deletion cassette at the *ACF2* locus removing 2313 bps of *ACF2* from +1 to +2313. D. Southern analysis of putative null alleles of *ACF2*. Total genomic DNA was digested with XbaI and probed with 672 bp fragment of Sc*TRP1* as described in Chapter 4. The null allele yielded a 1182 bp XbaI fragment. The presence of a band confirms that correct integration of the cassette has occurred. The coordinates are shown relative to the start codon of *ACF2* (A) or Sc*TRP1* (B, C). The diagram is not to scale..... 180

Figure S.7 – Construction and confirmation of the *C. glabrata egt2* null mutant. A null allele of *C. glabrata EGT2* was constructed as described in Chapter 4. A. The *C. glabrata EGT2* locus. Coding regions are shown in blue, ATG (+1) and stop codon (+2031) of *EGT2* are shown. The upstream and downstream genes are also shown. B. The *C. glabrata EGT2* deletion cassette. A NAT cassette was amplified flanked by 494 bps and 483 bps of *EGT2* 5' and 3' respectively as described in Chapter 4. C. Targeted integration of the *EGT2* deletion cassette at the *EGT2* locus removing 2101 bps of *EGT2* from -27 to +2031. D. Southern analysis of putative null alleles of *EGT2*. Total genomic DNA was digested with BstBI and probed with 567 bp fragment of the NAT cassette as described in Chapter 4. The null allele yielded a 4778 bp BstBI fragment. The presence of a band confirms that correct integration of the cassette has occurred for mutants 4, 6 and 14. The coordinates are shown relative to the start codon of *EGT2* (A) or the NAT cassette (B, C). The diagram is not to scale. 181

Figure S.8 – Construction and confirmation of the *C. glabrata rme1* null mutant. A null allele of *C. glabrata RME1* was constructed as described in Chapter 4. A. The *C. glabrata RME1* locus. Coding regions are shown in blue, ATG (+1) and stop codon (+1644) of *RME1* are shown. The upstream and downstream genes are also shown. B. The *C. glabrata RME1* deletion cassette. A NAT cassette was amplified flanked by 463 bps and 508 bps of *RME1* 5' and 3' respectively as described in Chapter 4. C. Targeted integration of the *RME1* deletion cassette at the *RME1* locus removing 1850 bps of *RME1* from -150 to +1700. D. Southern analysis of putative null alleles of *RME1*. Total genomic DNA was digested with NsiI and probed with 567 bp fragment of the NAT cassette as described in Chapter 4. The null allele yielded a 5624 bp NsiI fragment. The presence of a band confirms that correct integration of the cassette has occurred for mutants 1, 5, 6, 7 and 8. The coordinates are shown relative to the start codon of *RME1* (A) or the NAT cassette (B, C). The diagram is not to scale. 182

Figure S.9 – Construction and confirmation of the *C. glabrata scw11β* null mutant. A null allele of *C. glabrata SCW11β* was constructed as described in Chapter 4. A. The *C. glabrata SCW11β* locus. Coding regions are shown in blue, ATG (+1) and stop codon (+1497) of *SCW11β* are shown. The upstream and downstream genes are also shown. B. The *C. glabrata SCW11β* deletion cassette. A 675 bp fragment of *S. cerevisiae TRP1* was amplified flanked by 60 bps of *SCW11β* 5' and 3' as described in Chapter 4. C. Targeted integration of the *SCW11β* deletion cassette at the *SCW11β* locus removing 1497 bps of *SCW11β* from +1 to +1497. D. Southern analysis of putative null alleles of *SCW11β*. Total genomic DNA was digested with ClaI and probed with 672 bp fragment of Sc*TRP1* as described in Chapter 4. The null allele yielded a 848 bp ClaI fragment. The presence of a band confirms that correct integration of the cassette has occurred for mutants 1, 4 and 5. The coordinates are shown relative to the start codon of *SCW11β* (A) or Sc*TRP1* (B, C). The diagram is not to scale. 183

Figure S.10 – Construction and confirmation of the *C. glabrata sic1* null mutant. A null allele of *C. glabrata SIC1* was constructed as described in Chapter 4. A. The *C. glabrata Sic1* locus. Coding regions are shown in blue, ATG (+1) and stop codon (+849) of *SIC1* are shown. The upstream and downstream genes are also shown. B. The *C. glabrata SIC1* deletion cassette. A 675 bp fragment of *S. cerevisiae TRP1* was amplified flanked by 60 bps of *Sic1* 5' and 3' as described in Chapter 4. C. Targeted integration of the *Sic1* deletion cassette at the *Sic1* locus removing 849 bps of *SIC1* from +1 to +849. D. Southern analysis of putative null alleles of *SIC1*. Total genomic DNA was digested with NsiI and probed with 672 bp fragment of Sc*TRP1* as described in Chapter 4. The null allele yielded a 1062 bp NsiI fragment. The presence of a band confirms that correct integration of the cassette has occurred for mutants 2, 9 and 13. The coordinates are shown relative to the start codon of *SIC1* (A) or Sc*TRP1* (B, C). The diagram is not to scale..... 184

List of Tables

Table 4.1 – Phenotypic conditions used to test the conditional sensitivity of the Ace2p-dependent gene nulls in a phenotypic screen [240]. 78

1 Introduction

1.1 Fungal human pathogens

Fungi form part of the normal flora of humans colonising the skin, mucosal surfaces, the gastrointestinal and urinary tracts, as well as practically every surface we touch; but for the most part they cause no clinical symptoms. The human immune system has proven quite adept at managing most fungal species, which has led to the common belief that fungi are not important contributors to human disease [1]. Within the last 20 to 30 years, advances in medical science have brought about increased life expectancy, even for the most critically ill patients. It is this development that has caused a dramatic increase in the 'at risk' demographic, and has allowed fungal pathogens to thrive and flourish in the human environment, becoming a not insignificant clinical burden [2]. Fungal species now make up a significant proportion of nosocomial infections with *Candida* species alone accounting for between 10 and 15% of all nosocomial blood stream infections (BSIs) acquired from the various surfaces and commensal colonisation found within the clinical setting [3], and have played critical roles in patient survival worldwide.

Most pathogenic species of fungi can be classified as deep or superficial of which dermatophyte opportunistic pathogens are a subset of superficial. For instance, a reduction in the immune competency of patients allows *Candida* species to turn from a commensal organism into a pathogen. The subject of this study, *Candida glabrata*, falls within that classification as a true opportunistic pathogen, which fails to cause disease in immunocompetent patients, and is only virulent in the immunocompromised population.

Fungal pathogens range from the superficial, yet extremely irritating, *Trichophyton* and *Candida* species that cause Athlete's Foot [4] and vulvovaginal candidiasis respectively, to the deadly systemic infections of immunocompetent individuals caused by *Cryptococcus gattii* [5]. The majority of clinical burden comes from a combination of superficial and systemic infections caused by opportunistic pathogens in the immunocompromised. For instance, it is estimated that systemic infections caused by *Candida* species alone account for an $800 million burden on medical treatment in the US [6], not to mention the cost of over the counter medication, practitioner visitation hours and prescriptions for superficial *Candida* infections.

The list of pathogenic mycoses is still expanding to this day, and ranges from yeasts such as *C. glabrata* and *Cryptococcus neoforms,* through dimorphic fungi like *Candida albicans* and *Histoplasma capsulatum*, to true hyphal fungi such as *Aspergillus fumigatus* [2]. The most common cause of fungal pathogenesis in the US has been shown to be *Candida* species, which alone account for 10-15% of hospital-acquired BSIs [3, 7, 8]. This represents an incidence of 72.8 cases per million per year, with a case-fatality percentage of 33.9% for first episode infections [2, 8]. The next most prevalent invasive fungal species is *C. neoformans*, with 65.5 cases per million per year; then *Coccidioides immitis*, with 15.3 cases per million per year; and rounding out the double figure percentages are *Aspergillus* species with 12.4 cases per million per year [2, 8].

1.1.1 Antifungals

Treating pathogenic fungi has always been a clinical challenge due to many factors. The eukaryotic nature of fungi has posed a serious obstacle to be overcome because the similarities in cellular processes between fungi and other eukaryotes makes specifically targeting fungi very difficult [1]. For instance, amphotericin-B can cause significant levels of toxicity in the patient due its ability to bind to host sterols as well as those of a fungal nature [1]. Another issue is the increasing resistance found in species, like *A. fumigatus* and *C. glabrata,* to another effective antifungal species, azoles, in particular fluconazole [1], which further limits the effective list of available active antifungals. Diagnosis and successful treatment of fungal pathogens is also hampered by the poor sensitivity of current detection methods, which are especially weak for cases of invasive aspergillosis, where blood culture tests often fail [9].

Coming into the turn of the millennium, although only having a short list to choose from, the availability of antifungals stood at an all-time high, which combined with improved clinical practices including prophylaxis, has meant that the incidence of systemic fungal infections in neutropenic and other immune deficient patients is on the decline [10, 11]. Instead a shift of the primary focus of fungal pathogens from the intensive care unit (ICU) to other general and surgery wards has been observed [12], meaning that fungal disease is no longer only an affliction of the critically ill, but one that effects a wider hospitalised population.

Most commonly used antifungal agents act against ergosterol, a component of fungal cell membranes, which either have an inhibitory action on its biosynthesis or bind directly to ergosterol disrupting the proper form and function of plasma membranes within fungi [1]. The antifungal agents currently in clinical use can be divided into five groups. First the azoles, which include both imidazoles and triazoles, target the demethylation of lanosterol to zymosterol during ergosterol synthesis by binding to and inhibiting the heme component of the cytochrome P450-dependent 14α-demethylase encoded by *ERG11*, thereby blocking ergosterol production [1]. The second, polyenes such as terbinafine and amphotericin-B, are thought to bind to ergosterol directly in the cell membrane and possibly create aqueous pores changing the permeability of the cells and leading to cell death [1]. The third group, fluoropyrimidines such as 5-fluorocytosine, are used to a lesser extent by clinicians and display a limited spectrum of activity [1]; they are therefore primarily used in combination with amphotericin-B [1]. The 5-fluorocytosine is thought to be taken up by sensitive cells and converted to 5-fluorouracil, and then to 5-fluorouridylic acid, which is then incorporated into the fungal RNA inhibiting protein synthesis [1, 13]. Strains without cytosine deaminase are therefore immune to 5-fluorocytosine treatment [13]. The fourth group of antifungals are the allylamines and thiocarbamates, which inhibit ergosterol synthesis upstream of the action of azoles, by inhibiting squalene epoxidase, which works in conjunction with (2,3)-oxidosqualene cyclase to convert squalene to lanosterol [1, 14]. The fifth group, the echinocandins such as caspofungin and micafungin, are currently thought to be the gold standard for treatment of candidaemia [15]. They are fungicidal, binding to and inhibiting the fungal cell wall enzyme complex β-1,3-D-glucan synthase, preventing the production of the β-1,3-glucan that forms the major structural component of the fungal cell wall along with β-1,6-glucan [16, 17]. Both polyenes and echinocandins are therefore fungicidal, and as such show a lower potential for resistance development [1]. The rest of the antifungal drugs in clinical use are fungistatic, and therefore have shown a propensity to cause resistance development in certain fungal species [1].

Antifungal resistance can develop via several routes within different fungal species, including the overexpression of targeted pathway genes, amino acid substitutions within subunits of drug targets and upregulation of drug efflux pumps. Like many species of bacteria, fungal species are able to rapidly acquire resistance to certain antifungals, such as azoles, through the over expression of multidrug resistance transporters, such as the major facilitator and ATP-binding cassette (ABC) classes. For instance, *C. glabrata* can upregulate the expression of two ABC transporter genes *CDR1* and *PDH1 (CDR2)*, which actively export azoles from the fungal cell [18]. In this way, increased efflux of the antifungal compound from the cell enables the fungus to rapidly decrease the concentration of the active antifungal agent within the cell, restoring normal cell function. Another method of antifungal resistance can take the form of upregulation of the antifungal drug's target gene expression. For instance, *C. glabrata* upregulates the expression of the target of azole species itself, *ERG11,* reducing the impact of the antifungal drug on the production of ergosterol [19]. Some fungal species are also capable of developing mutations within the target of the antifungal agent. For instance, a common resistance mechanism of fungal species to the antifungal action of echinocandins takes the form of small mutations of the target itself, Fks1p – a major subunit of the fungal glucan synthase [20]. Two amino acid substitutions in two so called "hot-spots" within the structure of Fks1p reduce its sensitivity to echinocandins by several thousand fold, conferring resistance to the antifungal drug's disruption of the glucan synthase pathway [20].

Due to the potential for resistance development to antifungal therapy by pathogenic fungal species, it is crucial that continuing research is performed into novel fungal specific drug targets, in an effort to combat the inevitable development of resistant strains. Some examples of promising target areas currently under investigation for potential drug development include the fungal cell wall, its maintenance, biosynthesis and structural integrity; fungal fatty acid synthase, which shows significant structural differences to that of the human housekeeping proteins filling the same role; two-component regulatory systems that play a role in sensing of the environment in fungi, but crucially have not been described in mammalian cells, and so pose suitable drug targets; and virulence genes bespoke to fungi, which are obvious targets for drug discovery and may have the potential to not only have effective therapeutic value as virulence attenuators, but also to avoid the development of resistance [1].

1.2 Non-human fungal pathogens

Although this project focuses on pathogenic fungi that target man, it's important to note that pathogenic fungi pose problems for many forms of life, including those that we cultivate or require for human survival. Microbial plant pathogens are a major limiting factor of global crop production accounting for losses in the region of 14% of potential yield, which equates to about US$220 billion lost per annum [21]. Fungal plant pathogens account for some of the most notorious microbial plant diseases including the potato late blight, wheat stem rust, rice blast and grapevine downy mildew, which have impacted heavily on global economies and caused famine and economic collapse throughout the ages [21]. The first description of a fungal plant pathogen was the potato late blight, which was defined by Anton de Barry, the father of Plant Pathology, in 1861 [21, 22]. Since then, many fungal plant pathogens have been the focus of research into both crop resistance and pesticide development.

Non-human animal fungal pathogens are also an issue in the global environment. Amphibians are particularly susceptible to fungal infection. The fungal pathogen *Batrachochytrium dendrobatidis*, which causes the disease Chytridiomycosis has been blamed for the current population decline in frog species in certain areas [23]. It infects the keratinized epidermis of metamorph and adult stages of the amphibian life cycle, as well as the tooth rows and jaw sheaths of larvae, leaving populations crippled especially in Ranid frog species [23, 24]. Unfortunately, *B. dendrobatidis,* survives in the larval stages of the amphibians without causing significant mortality, and so creates an endemic disease with a larval stage reservoir [23].

Fungal pathogens have also been demonstrated to be a significant burden on insect populations. A critical example of this on the global scale is the recent decline in managed honeybee populations. Managed honeybees carry out approximately 90% of commercial pollination for agriculture, and so their decline in health has, and will have, a serious impact on human food security [25]. The obligate microsporidial fungal parasite, *Nosema ceranae,* has been implicated in playing a major role in the population decline of the western honeybee, *Apis mellifera* [25, 26]. Microsporidia exist outside the host only in a metabolically inactive, spore form, with its life cycle totally dependent on entry into host cells [25]. The spore germinates within the host and injects sporoplasm into target cells through a physical puncture in the cell membrane. From there the fungi proliferate and form more spores for dissemination [25]. Study of the molecular and cellular mechanisms of interactions between *Nosema* species and *Apis* species have been restricted due to the lack of cell culture systems for *Nosema*, something that has thankfully recently been resolved [25].

It is clear that fungal pathogens pose significant burden on not only human health, but also the health of the wider environment and human managed agriculture. It is therefore imperative that research into all areas of pathogenic fungal biology is carried out with an aim to discover cellular processes, structure and virulence mechanisms for both a better understanding of fungal burden, but also in aid of therapeutic discovery.

1.3 *Candida* epidemiology

Candida species form a group of fungi consisting of approximately 154 separate species belonging to the class Ascomycetes, order of the Saccharomycetales and the family Saccharomycetaceae [27]. The name *Candida* comes from the Latin phrase *toga candida* meaning a special white robe worn by the Roman Senate, so called because of the whitish appearance of colonies on solid plate agar [27]. The name was first applied to the agent of thrush, which was later isolated and classified as *C. albicans. Candida* species exist primarily as non-pathogenic commensals, forming up part of the normal flora of human beings and are found wildly throughout the environment including the soil, water and on plants [27]. Despite their majority commensal status, more than 17 *Candida* species have been reported as etiologic agents of BSIs [11, 28]. About 95% of these BSIs are caused by four *Candida* species, *C. albicans*, *C. glabrata*, *Candida parapsilosis* and *Candida tropicalis,* with the remaining 5% made up by approximately 13 different species [28, 29]. The majority of *Candida* species do not exhibit a true sexual cycle, but are polymorphic in form, able to exist in colonies as budding yeast, or projecting hyphae or pseudohyphae. The ability to form true or pseudohyphae is thought to play a role in colonisation, dissemination and virulence within host systems [30], although

C. glabrata, a haploid yeast, lacks any real form of pseudo or true hyphal formations except when cultured on solid nitrogen starvation media [31].

Having been considered clinically insignificant for many years, life-threatening infections due to opportunistic and pathogenic fungi have shown a dramatic increase in incidence in the past 20 years [32-34]. This has primarily been due to the increasing size of at risk groups, which includes patients on immunosuppressive regimes such as those receiving transplants and cancer patients, patients with AIDs and other immunodeficiency disease patients, as well as the elderly [33, 34]. Opportunistic fungi such as *Candida, Aspergillus, Cryptococcus* and other non-*Candida* yeasts, have become an increasing threat, not helped by broad-spectrum antibiotics use and increasingly invasive procedures with prolonged catheter use in ICUs [32-34]. However, with approximately 73 million cases worldwide per year, *Candida* infections remain one of the most dominant and important of opportunistic mycoses [8].

1.3.1 Superficial candidiasis

Candida species cause a wide range of infections, from superficial candidiasis of the skin and mucosal surfaces, which are frequently community acquired and cause significant morbidity, to invasive or deep candidiasis infections [11]. The most widespread and well known of *Candida* infections is vulvovaginal candidiasis, colloquially known as thrush, which an estimated 75% of the female population will suffer from at least once in their lives [35], with between 5-10% of suffers acquiring reoccurring infections of at least three cases a year [36]. *C. albicans* represents the most common cause of vulvovaginal candidiasis [35], but it also exists as a commensal organism in both the gastrointestinal and genitourinary tracts [37]. Some individuals may have developed a *Candida*-specific adaptive immune response, which could protect them from the commensal turning into an opportunistic pathogen under normal conditions; however it is also possible that *C. albicans* fails to invade the host epithelia and therefore remains commensal under these conditions. [37], Of course conditions can change for both the host and organism, leading to symptomatic infections, and while they are largely treatable with modern antifungals including azoles and amphotericin B, the high prevalence correlates with large amounts of money spent on over-counter medication, physician visits and prescriptions [37].

Candiduria, yeast infection of the urine, is another common urinary tract infection. Patients are often asymptomatic, but *C. albicans* has been shown to be the most common isolate, even though tracing the cause of infection can be difficult due to the lack of diagnostic tests that effectively discriminate between infection and colonisation [38, 39]. An estimated 50,000 episodes of candiduria occur annually in the United States, with risk factors including catheterisation, antibiotic exposure, diabetes, age and sex [38, 40, 41]. While antifungal therapy is effective at reducing patient symptoms, candiduria in asymptomatic patients seems to be unaffected, and therefore only certain groups of patients, mainly those at risk of developing candidiasis such as neutropenic patients, are recommended for treatment [39].

Candida species are often found in the oral cavity as part of the natural flora but cause particular issues for cancer patients, who have reduced immune protection as a result of their therapy, and patients with immune deficiency disorders [42]. Although the pathogenesis of oral candidiasis is

currently not well understood, common superficial infections can progress and penetrate the host tissue, with BSI-Oral complications remaining a major source of illness despite a variety of antifungals being clinically available to treat them [42].

1.3.2 Invasive candidiasis and candidaemia

Invasive infection, as opposed to superficial infection, of *Candida* species, systemic/invasive candidiasis or candidaemia, are a significant cause of life threatening infection, and are a common and important cause of morbidity and mortality within hospitalised patients [10, 11]. The most common form of deep *Candida* infection is candidaemia, which has an associated overall mortality rate of between 30-40% [43-45]. *Candida* species form an important part of hospital-acquired infections and remain the fourth leading cause of nosocomial BSIs in the United States [44, 45]. They account for between roughly 7000 to 28000 hospital-acquired cases a year, and approximately 63000 cases from all points of infection [10], with about 11200 deaths in total per annum [10]. It was estimated that each case of candidaemia in the US cost between $34000 and $44000 to treat, bringing the total annual attributable cost to $800 million in the US alone [6]. Despite this, the sources of candidaemia are poorly understood, although it has been assumed that gut colonization could possibly be responsible for onset of systemic candidiasis in some immune compromised patients [46].

Population based epidemiological study of candidaemia has shown that the incidence of different *Candida* infection varies by geographic region. For instance, studies from Canada and Europe, show that with the exception of Denmark, incidence of candidaemia is significantly lower than the US [11]. This is most likely due to the differences in population demographics, with certain sectors of the population found to be at greater risk. For example, although age was a primary risk factor across all races, with infants less than one year of age and adults over the age of 65 showing higher rates of infection, studies conducted in the US found that incidence of candidaemia was over fourfold higher in blacks from any age group [11]. Other risk factors for candidaemia and candidiasis are similar to those of superficial *Candida* infections, with the use of systemic antibiotics, corticosteroids, catheterisation, plus chemotherapy and radiotherapy within cancer patients, immune suppression and diabetics all showing higher rates and risks of infection [10, 11].

Incidence rates of *Candida* BSIs within hospitals have changed in recent years, from the ICUs towards a general ward setting [10, 11]. It has been shown that only 36% of *Candida* BSIs occur in the ICU, while 28% were community acquired, representing a 10% increase over five year period in the Baltimore area of the US [12]. Other studies have corroborated this showing that more candidaemia cases are now reported from general medical and surgery wards than those dealing with patients with immune deficiencies [10, 45]. This change has been brought about by the increased use of antifungal chemoprophylaxis and shortened periods of neutropenia preventing colonization by *Candida* species [47]. Although it is not clear why the incidence of candidiasis has increased within non-ICU wards it is likely that increased catheterisation and antibiotic use in clearance of bacteraemia, an aging population and extensive colonisation of surfaces within the clinical setting have contributed to the apparent increased or sustained level of candidiasis in non-ICU wards. It is also possible that the shift towards non-*albicans Candida* species has also contributed to the non-ICU candidiasis incidence, being more prevalent in different at risk, yet not ICU-bound groups [10].

Epidemiological data, however, maintains that candidaemia incidence has not decreased over the last 20 years as a whole and remains a significant global problem [11].

While *C. albicans* remains the largest single cause of invasive candidiasis globally, a recent shift in the distribution of *Candida* species causing candidiasis has meant that, in the US for instance, non-*albicans Candida* species now account for 54.4% of candidaemia cases [48]. The change in proportion of *albicans* isolation has revolved around the increasing incidence of the azole resistant *C. glabrata* and *C. tropicalis* [10]. This shift has been suggested as being caused in part, by the widespread use of azoles, and in particular fluconazole, for treatment of candidaemia and associated *Candida* infections [49, 50]. Given that other non-*albicans* species show greater resistance to azoles than *C. albicans*, extensive use of fluconazole has potentially selected against *C. albicans* and positively selected for the most resistant of them all, *C. glabrata* [51]. The reason for the increased clinical prevalence of non-*albicans Candida* species is still up for debate and has been suggested as being down to one (or both) of two causes [50]. Either non-*albicans Candida* species infections are actually growing in number as some studies have suggested [49], or their increasing isolation is simply due to a reduction in *C. albicans* incidence, which has altered the proportion of isolation of non-*albicans Candida* species but not their overall number. Whether non-*albicans Candida* infections are actually increasing in number or not, *C. glabrata*'s innate and acquired resistance to fluconazole combined with its recorded increasing prevalence poses a real problem for current candidaemia treatment.

1.4 *Candida glabrata* and candidiasis

C. glabrata displays a varying distribution within *Candida* BSIs depending heavily on patient demographics. For instance, *C. glabrata* was found predominantly in older patients with the highest percentage found in the over 80 years old group of the SENTRY Antimicrobial Surveillance Program [52]. Interestingly the same study found that the most resistant strains to antifungals including anidulafungin, caspofungin, micafungin, fluconazole, all showing a 16.7% resistance rate, posaconazole showing 5.6%, and voriconazole showing 11.1%, were found from isolates taken from the 20-39 years old age group [52]. These results indicate that although prevalence of *C. glabrata* increases with age, the percentage rates of resistance actually decrease with age [52, 53]. This also suggests that as the world's population experiences greater and greater life expectancy, *C. glabrata* will become more and more prevalent in hospitalised candidaemia patients within that aging population.

The *C. glabrata* prevalence also varies with geographical region. Almost all studies from the US indicate that *C. glabrata* has over taken *C. tropicalis* as the second most common cause of *Candida* BSIs after *C. albicans* with between a 20-24% share [10]. However, in other countries such as those that form part of Latin America, only about 4-7% of candidaemia cases were caused by *C. glabrata* [10]. It is unknown why such geographic differences occur in *C. glabrata* prevalence, although the mechanism by which blood isolates are taken and identified has been suggested as contributing to the variation, along with azole use and median patient age [10].

The risk factors associated with *C. glabrata* isolation as opposed to other *Candida* species are largely unclear. Certain studies have pointed to the use of fluconazole as a predisposing factor, which would

make sense when combined with the knowledge that *C. glabrata* is innately less sensitive to azole treatment [54]. However, various studies have also confused the issue, finding that azole use did not contribute to an increase in *C. glabrata* isolation [55, 56]. The age of the patient certainly has an impact on the incidence of *C. glabrata*, with Malani et al. showing that *C. glabrata* colonisation of the oral cavity increased with age, as well as with the use of psychotropic drugs and denture use [57]. Unfortunately, other than age, these studies show how complex an issue identifying risk factors for species specificity can be, with many conflicting factors reported [47]. For clinicians, a lack of a clear-cut set of risk factors for clinical identification of *C. glabrata* prevalence impacts on their ability to choose appropriate antifungal strategy due to the azole resistance of the species. Delay in initiation of appropriate antifungal therapy has been linked to increased mortality [58], but non-clinical methods of antifungal susceptibility tests can take 48-96 hours to complete, while conventional biochemical species identification also takes a significant amount of time [47]. The recent introduction of matrix-assisted laser desorption ionization–time of flight (MALDI-TOF) mass spectrometry for fungal species identification has proved to be a both rapid and reliable method of identification of yeasts and yeast-like fungi [59], allowing faster confirmation of species and therefore the correct therapeutic agent or combination.

1.4.1 *Candida albicans* virulence factors

Most *Candida* species are opportunistic pathogens that can survive in both a commensal or pathogenic form, inhabiting most surfaces and organs of the human body [60]. Unlike the model organism *Saccharomyces cerevisiae*, many *Candida* specific genes encode catabolic proteins that likely account for its ability to survive in either commensal or pathogenic state. This ability of *Candida* to survive in various distinct environments contributes to its versatility as an opportunistic pathogen and its ability to cause disease at several anatomical sites in the host [60].

C. albicans has several characterised virulence factors described in the literature. Cell surface host interaction genes are an important part of virulence in *C. albicans* like so many other pathogenic organisms. Adhesins, cell surface biomolecules that help *C. albicans* adhere to host cells and surfaces, are crucial to virulence in *C. albicans* shown by the avirulence of non-adherent strains [61]. Adhesins aid in the avoidance of clearance through adherence to host cells, host proteins and other microbial competitors [60] forming the first stage of colonization and persistence in the host. Several *C. albicans* proteins have been found to bind to host cell extracellular matrix (ECM) proteins including collagen (I and IV), fibrinogen, fibronectin and laminin [62-64]. Two such genes, *ALS1* and *ALS5 (ALA1)* have been shown to be essential for virulence [65]. The proteins they encode have been shown to play a role in adherence similar to the α-agglutinin cell-cell recognition protein in *S. cerevisiae* [66-68]. Int1p, an ECM binding protein similar to mammalian integrins, has also been shown to be important in virulence, adherence and filamentation in *C. albicans* [69]. Hwp1p, an outer surface mannoprotein, has recently been shown to be crucial to adherence and virulence [70, 71]. An α-1,2-mannosyl transferase residing in the medial Golgi, Mnt1p, has also been shown to play a role in adherence through O-linked mannosylation of proteins and virulence, with null mutants displaying an avirulent phenotype [72]. Many other adhesin like genes have been identified and are currently under investigation with a likelihood most will play a role in virulence [60].

Other important molecules that play a role in *C. albicans* virulence include those associated with morphogenesis, a characteristic only *C. albicans* shares with *Candida dubliniensis* in the *Candida* family [60]. Morphogenesis is the process of reversible conversion between an isotropic, unicellular yeast phenotype and an apical, hyphal and pseudohyphal phenotype [60]. Current understanding of the link between phenotype switching and virulence is in its infancy, but it's clear from preliminary findings that the dimorphic nature of *C. albicans* plays a significant role in its ability to cause disease [73, 74]. Proteins involved in invasion have also been shown to play a role in virulence using animal models. *C. albicans* has two families of proteins related to the invasion of host cells. The secreted aspartyl proteinases (SAPs) form a family of at least nine genes of which six, *SAP1-6*, have a role in virulence [69, 71]. The second invasion related family of genes, the phospholipases (PL), consist of at least four genes of which *PLB1* has been identified to play a role in virulence with *plb1* cells found to exhibit a 60% reduction in mortality compared to wild type *C. albicans* [75]. Phenotype switching [76], where a yeast colony changes phenotype appearing rough, smooth or changing colour in response to stress, such as low level UV light doses, may also play a role in virulence. The plasticity this switching provides has been suggested as the route by which asexual fungi, including some *Candida* species, gain phenotypic diversity [77]. Isolated *C. albicans* strains from systemically infected patients show higher levels of switching than the wild type [78], inferring there might be a link between their ability to cause disease and their ability to switch phenotype. This link is, however, still open to interpretation and has yet to be thoroughly investigated [60]. For an extensive review of virulence in *C. albicans* please see Calderone et al. 2001 [60] and Brown et al. 2007 [79].

1.4.2 *Candida glabrata* virulence factors

Our current understanding of the virulence and host interactions of *C. glabrata* is limited when compared with *C. albicans*. *C. glabrata* is a phylogenetically distinct fungus to *C. albicans* [77] and shows a high degree of synteny within its haploid genome with the model organism *S. cerevisiae* [77]. *C. glabrata*, however, shares similarities and differences with *C. albicans* when it comes to virulence. SAPs show less importance in *C. glabrata* compared with *C. albicans*. *C. glabrata* has multiple orthologues of *S. cerevisiae* extracellular glycosyl phosphatidylinositol (GPI)-linked aspartyl proteases, but appears not to produce significant levels of proteinase activity *in vitro* [80]. In contrast phospholipase genes in *C. glabrata* show similar activity to their *C. albicans* counterparts. They exhibit higher activity from persistent candidiasis isolates than from non [75], however the link between *C. glabrata PLB* genes, orthologues of *S. cerevisiae PLB* genes, and virulence has yet to be proven [77]. *C. glabrata* also lacks the true morphological switching that aids the tissue infiltration demonstrated by *C. albicans*, showing only pseudohyphal formation in nitrogen starvation conditions [31]. Ste12p is a highly conserved transcriptional regulator, which is also found in *S. cerevisiae* [81]. It is activated by the mitogen-activated protein (MAP) kinase signalling cascade involved in pseudohyphal formation and has been characterised in *C. glabrata* showing importance for virulence [81]. Clinical isolates however, lack any pseudohyphal forms [77] questioning the significance of pseudohyphal formation in *C. glabrata* pathogenesis. *STE11* and *STE20* have also been highlighted in virulence in *C. glabrata*. Both genes encode protein kinases that play important roles in several signalling cascades including the response to hypertonic stress, an important factor in the host-pathogen interaction and therefore, unsurprisingly, both proteins are required for wild type levels of virulence [82, 83]. Another virulence factor in *C. albicans* has recently been identified in *C.*

glabrata. Phenotypic switching has been shown in *C. glabrata* and was observed to be selective to anatomical site of clinical isolation [84]. This indicates that phenotypic switching likely plays a role in environmental adaptation in *C. glabrata* [77] and therefore a role in virulence.

Adherence in *C. glabrata* is, for the most part, mediated by a family of GPI-anchored cell wall proteins similar to the *ALS* and *HWP1* genes found in *C. albicans* called the Epithelial Adhesion (*EPA*) family [85]. Investigation of the *EPA* family of genes has shown strains of *C. glabrata* that encode at least 23 *EPA* genes [77]. Most of the *EPA* genes are encoded on sub-telomeric loci and are subject to chromatin-based transcriptional silencing [86, 87]. *EPA1* has been shown to be crucial for *in vitro* adherence [86, 87] likely due to the unusually low level expression of the other *EPA* genes under laboratory culture conditions. The same cannot be said for *in vivo* adherence [88] in which other *EPA* genes play a role that indicates redundancy in the *EPA* gene family. Transcriptional silencing mutants have been found to be hyperadherent and show greater infiltration of the kidney than the wild type from a disseminated candidiasis model [86, 89]. *EPA1*, *EPA6* and *EPA7* have all been shown to play roles in this hyperadherent phenotype indicating that *EPA* expression could be a significant factor in virulence [86]. *EPA6* has also been shown to be important in biofilm formation [90]. Biofilm formation can be a significant clinical burden with colonization of inert surfaces like catheters, which not only causes unintentional *C. glabrata* inoculation, but also allows for a synergistic binding of *C. albicans* to an existing *C. glabrata* biofilm [91]. Nicotinamide adenine dinucleotide (NAD^+) abundance has been shown to play a crucial role in *EPA* expression within *C. glabrata* due to its auxotrophy for nicotinic acid [89]. Low environmental niacin levels, representing the vitamin precursors for NAD^+ synthesis, have been shown to inhibit transcriptional silencing of the *EPA* genes, due to the lack of NAD^+ co-substrate binding, resulting in increased adhesion and infiltration of host urinary tract [89, 92].

Clinical treatment failure of *C. glabrata* infection is often attributed to the yeast's innate resistance to azoles such as fluconazole. Azoles selectively inhibit lanosterol 14-α-demethylase, which is involved in the ergosterol biosynthesis pathway [19]. This in turn affects many other biosynthesis pathways and the cell membrane structure [19]. *C. glabrata* is not only innately resistant to azole action but is able to rapidly acquire resistance to azoles through over expression of two ATP-binding cassette (ABC) transporter genes *CDR1* and *PDH1 (CDR2)* [18], which cause azole efflux from the cell or upregulation of the target gene itself *ERG11* [19]. *C. glabrata*'s haploid nature allows it to rapidly acquire resistance mutations that might otherwise be blocked by the presence of a dominant allele in diploid genomes like that possessed by *C. albicans* [52]. Recent work by Polakova et al. [93] has shown that clinical isolates of *C. glabrata* exhibit rapid changes in chromosomal organisation creating duplicated genes including ABC transporters, proteases and phospholipase B genes. This enhances survival in host systems, due to the subsequent upregulation of the effector proteins [93]. Petite strains of *C. glabrata* also show high levels of azole resistance through their self-inhibition of mitochondrial function that results in a greater quantity of free ergosterols [94]. This loss of mitochondrial function can be either permanent or reversible [94] and shows some evidence of an epigenetic mechanism utilised to switch between respiratory-competent and –incompetent states [95]. This may explain the difference shown between *in vitro* and *in vivo* pharmacological results from clinical isolate azole treatment [95].

C. glabrata is also more resistant than other *Candida* species to most antimicrobial proteins secreted by mammalian cells. Human beta-defensins (hBD), a family of small antimicrobial and antiviral

proteins secreted by epithelial cells, show a lower fungicidal activity against *C. glabrata* than *C. albicans* for example [96]. Both histatins, a group of salivary antifungal proteins and magainins, a group of cationic antifungal proteins derived from frog dermal glands, also showed a lower fungicidal activity against *C. glabrata* than *C. albicans* [97]. It should be noted that other studies have shown human histatin-5 to be an effective fungicidal agent against *C. glabrata* [98, 99]. *C. glabrata* also shows a decreased cytokine response from the host when compared with *C. albicans* using a reconstituted human epithelial *in vitro* model [100]. *C. glabrata* oral candidiasis clinical isolates failed to show significant interleukin-1α (IL-1α), IL-8 or tumour necrosis factor (TNF) induction and only weak increases in granulocyte monocyte colony-stimulating factor (GM-CSF) levels [95, 100]. Variation in cytokine response was, however, found between strains of *C. glabrata* with isolates from oesophageal candidiasis showing higher cytokine induction than oral candidiasis isolates [95]. Also of note was the fact that although *C. glabrata* killed up to 60% of oral epithelial cells in a 36-hour co-culture system, it was found to be less cytotoxic than *C. albicans* and failed to infiltrate an *in vitro* 3D model of human oral mucosa [95]. This could explain the difficulty that immune compromised patients experience in clearing *C. glabrata* candidiasis even with heavy antifungal treatments. Failure of *C. glabrata* to induce an appropriate cytokine response therefore stifles recruitment of immune cells to the site of infection and subsequent immune clearance.

In 2004 the first virulence moderating gene or antivirulence factor in *Candida*, *ACE2* was characterised by Kamran et al. [7]. The *S. cerevisiae* homologue *ACE2* encodes a transcription factor associated with cell separation [7]. It exhibits transcriptional control, either directly or indirectly over some 11 known genes, and has been shown to regulate the transcription of machinery essential to cell separation in budding yeast including the chitinase *CTS1* [101, 102]. The *C. glabrata* strain HLS122, an *ace2* null, was shown to be hypervirulent in a neutropenic murine model of candidiasis, with 100% mortality within 18-hours post infection [7]. The extreme hypervirulence was shown to be independent of the clumpy phenotype exhibited by HLS122 through chitinase treatment of the yeast cells prior to inoculation, which allowed the clumped daughter cells, deficient in *CTS1* expression, to separate from their mothers [7]. Inoculation of the separated strain resulted in an overwhelming, fatal systemic disease with a 200-fold lower inoculum required for 100% mortality than similarly treated wild type cells and *ACE2* reconstituted HLS121 cells [7]. This discovery of a virulence-moderating factor in *C. glabrata* may have power to reveal novel insights into the host-pathogen interactions crucial to the development of disease by this opportunistic pathogen.

1.4.3 *C. glabrata* virulence analysis using *Caenorhabditis elegans*

Virulence analysis of *C. glabrata* is commonly conducted using a neutropenic murine model of disseminated candidiasis [7, 81]. In an effort to define a complementary invertebrate model, the nematode *Caenorhabditis elegans* was investigated as a suitable virulence model organism. A feeding infection assay was adapted from previous work with *S. cerevisiae* [103] for use with *C. glabrata*, including an intermediate disease phenotype marked by post anal region swelling. Unfortunately a baseline of *C. glabrata* infectivity of *C. elegans* could not be set. An overview of the experiments is presented in Appendix 5.1.

1.5 The evolutionary relationship between *C. glabrata* and *S. cerevisiae*

1.5.1 Phylogeny

Much of the work in *C. glabrata* is aided by inferences from its close genetic relative the model organism *S. cerevisiae*. *C. glabrata* shares a recent common ancestor with seven of the *Saccharomyces* family as displayed in Figure 1.1 [104]. It belongs to a different clade than other *Candida* species including *albicans*, which display a recoding of the CUG codon to Serine, and belongs to the clade that includes *Saccharomyces* species, *Kluyveromyces* species and *Ashbya gossypii* [104]. This likely evolutionary separation means that the perceived species ability of *Candida* to act as opportunistic pathogens could have potentially developed independently for *C. glabrata* to the rest of the *Candida* species, including *C. albicans* [104], although that is still open to interpretation.

As a result of the close phylogenetic link between *C. glabrata* and *S. cerevisiae*, the two budding yeasts show very similar genetic homology with a similar G+C content of 38.8% and 38.3% respectively [77]. *C. glabrata* and *S. cerevisiae* have a total of 5448 and 5988 identified ORFs respectively, out of which they share some 4945 orthologues with an average 65% amino acid identity between them [77, 105]. Both show a similar stress response and respiratory metabolism [106, 107], similar cellular processes such as cytokinesis and cell separation, while many genes can be complemented between the two strains, which is common practice in the investigation of *C. glabrata* gene function [108].

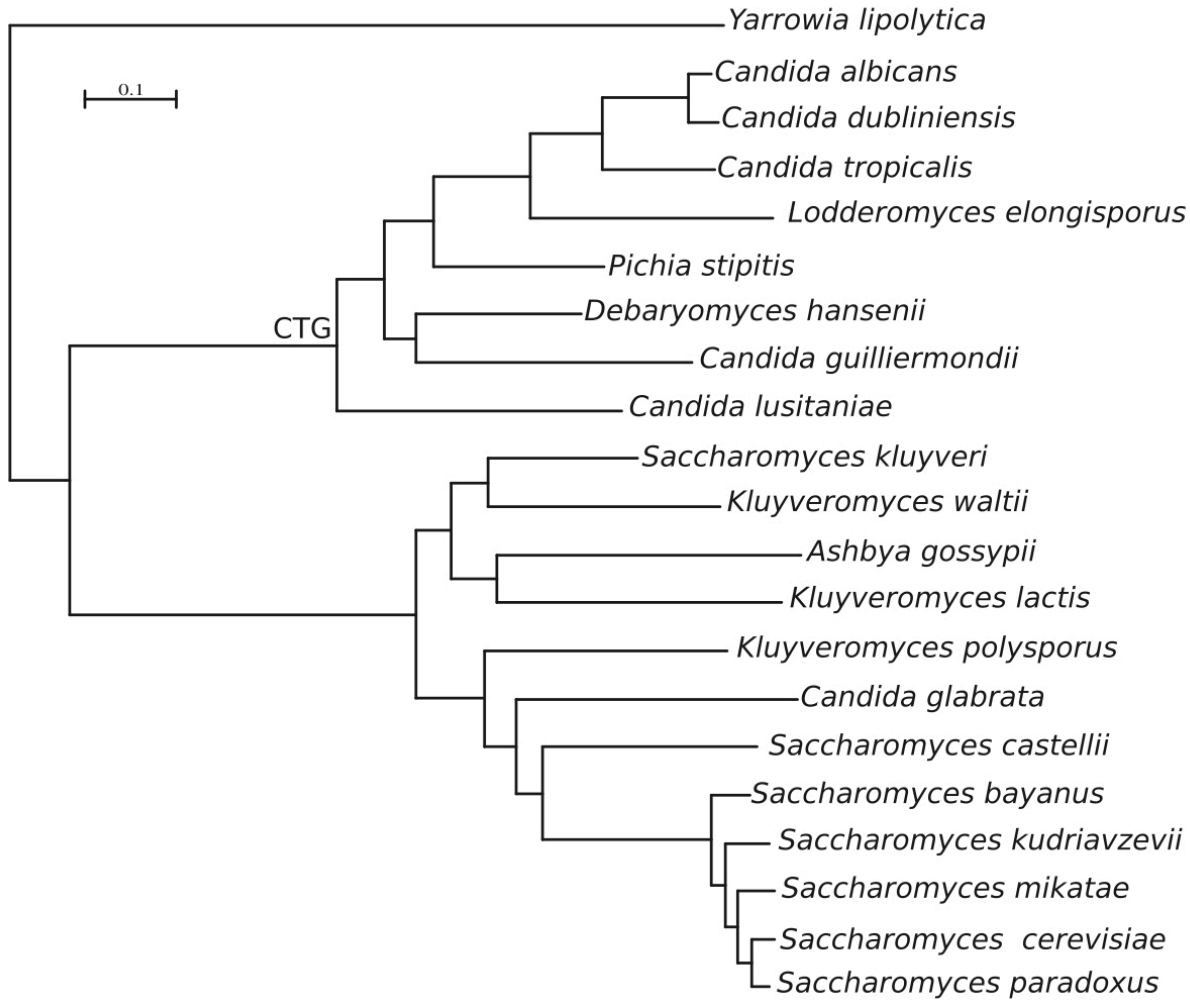


Figure 1.1 – *C. glabrata* belongs to the *Saccharomyces* clade, not the *Candida* clade. Phylogenetic tree showing the evolutionary relationships of *C. glabrata* and selected *Candida* species with that of *S. cerevisiae* and selected *Saccharomyces* species. Adapted from Roetzer et al. 2010 [104]. The tree was built using maximum likelihood analysis of concatenated alignments of 1137 protein familys that exist with single-copy orthologues in the 21 species. CTG marks genetic code transition event that recoded CUG to Serine (the non-CTG branch).

1.5.2 Host environment adaptation

Despite the apparent similarities, *C. glabrata* and *S. cerevisiae* show crucial differences when it comes to environmental adaption and ability to cause disease. The first difference in terms of environmental adaptation is the variation in optimal growth temperature. *S. cerevisiae*, like many other yeasts optimally grows at 30°C and below [104]. In contrast, *C. glabrata* grows faster overall than *S. cerevisiae* with its optimum growth temperature being 37°C, but showing good growth rates up to around 39°C [104]. This evolutionary shift between optimum growth at 30°C and 37°C is crucial to the ability of *C. glabrata* to colonise the host as both a commensal and opportunistic pathogen. *C. glabrata* has also been considered to have undergone an increased rate of gene loss, or reductive evolution, from its common ancestor with *S. cerevisiae,* with loss of galactose, phosphate, nitrogen and sulphur metabolism being standout examples, as well as auxotrophies to nicotinic acid, pyridoxine and thiamine, which *C. glabrata* relies on its host to overcome [77, 104, 109, 110].

The *C. glabrata* genome also contains several genes that are not found within the *S. cerevisiae* or *Saccharomyces* family genome. These include a putative aspartate racemase that appears to have originated from a bacterial origin and acts to inter-convert optical isomers of aspartate [111], as well as a variable number of *EPA* genes that although they have functional homologues in *S. cerevisiae FLO* genes, do not show sequence similarity [104]. *C. glabrata* also features expanded sets of genes that have *S. cerevisiae* homologues, but are more numerous. Several relate to the cell wall and include six extra genes encoding extracellular GPI-linked aspartyl proteases and eight genes encoding α-1,3-mannosyltransferases involved in cell wall biosynthesis [104]. These genes are linked with adhesion and cell wall structure and likely evolved through adaptation to the host environment.

1.5.3 Virulence and drug resistance

In virulence terms, *C. glabrata* and *S. cerevisiae* are quite different. *S. cerevisiae* has only been shown to be able to cause fungemia in certain immunocompromised patients that are given *Saccharomyces boulardii* supplements as a treatment for *Clostridium difficile*-associated diarrhoea [112]. In contrast, *C. glabrata* has been found be much more adept at causing disease, albeit in similarly immunocompromised patients and the elderly, as previously discussed. It is likely that the genetic differences linked to cell adhesion and adaptation to the host environment between *C. glabrata* and *S. cerevisiae* account for the apparent virulence of *C. glabrata*.

The pathogenic yeast *C. glabrata* also exhibits much greater antifungal drug resistance than that of *S. cerevisiae*. *C. glabrata* is both innately resistant to azoles and can also quickly acquire resistance to other antifungals [104]. The two yeasts share some of the signalling pathways that create the anti-toxicity and drug response revolving around *PRD1* [104]. Crucially the *C. glabrata* genes *CDR1* and *CDR2,* which encode drug efflux pumps that actively eject antifungals and are transcriptionally regulated by *PRD1*, can be upregulated through gain of function mutations within *PRD1* and loss of mitochondrial function, which is also linked with increased ergosterol availability [18, 113]. As these drug resistant adaptations evolved in *C. glabrata* before the introduction of azoles into the clinical setting, it is thought that they were formed by adaptation to frequent exposure to toxic substances as part of the mucosal flora [104].

It is clear that *C. glabrata* shares a close common ancestor with *S. cerevisiae*, which makes them genetically similar and means that many cellular processes are carried out by both functional and genetic homologues between the two species. This means that *S. cerevisiae* can be used as a model for studying and inferring gene function within *C. glabrata* for genes that share genetic homologues. It's also very clear that *C. glabrata* is a distinct fungus from both *S. cerevisiae* and its frequently associated *Candida* species relative, *C. albicans*. Therefore caution must be applied when making inferences between *C. glabrata* and either *C. albicans* or *S. cerevisiae*.

1.6 Ace2p and the cell cycle

1.6.1 Yeast cell cycle

Ace2p plays a significant role in the final act of the cell cycle in budding yeast, cell separation. The budding yeast cell cycle, as characterised in *S. cerevisiae*, is a complex and closely controlled series of events concluding in the production of progeny. The cell cycle can be arbitrarily divided into four phases: M, which encompasses mitosis and cell division; G_1, the longest part of the cell cycle, which forms a period of growth and preparation including START initiation; S, a phase exclusive to eukaryotes in which DNA synthesis occurs; and G_2, in which the cell prepares for mitosis [114]. Each mother cell can bud once during its cell cycle and development is closely controlled by G-protein signalling through Cdc42p [115]. Checkpoints in the cell cycle closely regulate the transition to the next phase and prevent premature progression. START is one such checkpoint that allows conditional transition through late G_1 and budding initiation in the mother cell, dependent on several conditions including the size of the cell and the nutrient content of the growth media [116]. As the cell cycle progresses the daughter cell must reach a critical size before cell division can take place allowing the mother and daughter cells to undergo cytokinesis and cell separation [116]. The budding yeast *S. cerevisiae* regulates its cell cycle progression through cyclical activation of at least nine cell-cycle dependent transcription factors, which can be divided into three sets [115] and many cyclin-dependent protein kinases (CDKs), which synchronise at least 800 transcripts [117]. In *S. cerevisiae MBF*, a complex of Mbp1p and Swi6p, and *SBF*, a complex of Swi4p and Swi6p, regulate the expression of genes involved in the late G_1 phase [115, 118, 119]. Gene transcription in G_2/M is normally controlled by Mcm1p together with Ndd1p, which is recruited by the forkhead factors Fkh1p or Fkh2p in late G_2 [115, 118, 119]. However, it has been shown that Fkh1p and Fkh2p are able to bind directly to the promoters of G_1/S phase genes in the absence of Mcm1p [115, 118, 119]. Mcm1p has also been shown to activate the expression of M/G_1 genes independently of Fkh1p and Fkh2p [120, 121]. This shows that transcription factors are able to alter their own transcriptional co-operativity in order to activate expression of phase specific genes, which adds another level of complexity and fine tuning to cell cycle regulation [115]. Ace2p and a closely related transcription factor Swi5p regulate gene transcription throughout the cell cycle and activate gene transcription in the final stages, G_1/M phase, of the cell cycle leading to cytokinesis and cell separation [101]. All the cycle dependent transcription factors are serially linked to one another, each one activating the expression of the next to control the subsequent phase of the cell cycle [115].

1.6.2 Cytokinesis and cell separation

The final stage of the cell cycle in most eukaryotes is cytokinesis, where by the mother and daughter cells become compartmentalised [122]. Cytokinesis occurs through the division and isolation of the cytoplasm by the mother cell membranes after duplication and segregation of the genetic material has taken place, producing two independent cells [122]. In *S. cerevisiae,* the **m**itotic **e**xit **n**etwork (MEN) group of proteins ensure chromosome segregation is complete before cytokinesis, the penultimate step in the cell cycle, can take place through ubiquitin ligase mediated proteolytic degradation and inactivation of the mitotic kinase complex formed by Cdc28p plus one of the regulatory subunits encoded by *CLB1-4* [123]. The process of cytokinesis encompasses three phases; the first is appropriate selection of a division site, chosen late in G_1 as the bud begins to emerge

[124]. The second is the assembly of protein complexes at the site of division where a septin ring is assembled as a scaffold for the eventual assembly of the contractile actomyosin ring [122]. The final phase of cytokinesis can be thought of as the operation of the pre-assembled machinery at the site of division, leading to constriction of the actomyosin ring that in turn allows septum formation and the division of the cytoplasm [122]. In this way, all cell cycle ties are severed between mother and daughter allowing uncoupling in subsequent rounds of cell division [125]. On completion of cytokinesis the two discrete cell units, mother and daughter cells, remain attached via a tri-laminar septum to each other until cell separation can take place, allowing dispersal of the cells.

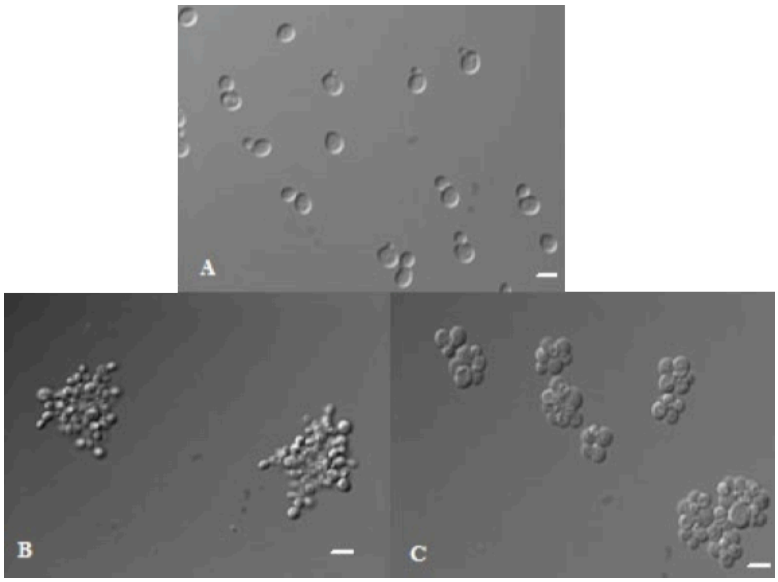


Figure 1.2 – *S. cerevisiae* and *C. glabrata ace2* display a clumpy, cell separation deficient phenotype. Yeast was grown over night at 30°C or 37°C, 180 rpm, and visualised under DIC. A) *S. cerevisiae* BY4741 cells (B) *C. glabrata* (HSL122) *ace2* cells (C) *S. cerevisiae ace2* cells. Both *ace2* strains display a cell separation deficient phenotype, although this is less severe in *S. cerevisiae*. Scale bar 10 µm.

Cell separation is the process of degradation of the cell wall ring and the tri-laminar septum that separates the mother and daughter cells; allowing the daughter cell to dissociate from the mother cell [126]. Successful completion of cell separation is the result of the highly regulated assembly of a series of components to the mother-daughter neck throughout the cell division cycle [125]. In *S. cerevisiae* many proteins have been shown to play important roles in the final stage of cytokinesis. Glucan β1,3-glucosidases such as Dse2p and Scw11p have been shown to be directed to the site of cell separation along with an endoglucanase Egt2p [127, 128]. Chitinase activity has also been shown to play an important part with Cts1p directed to the site of the bud neck [129]. Other proteins have subsequently been shown to be important to cell separation including Dse4p (also known as Eng1p), an endo glucan β1,3-glucosidase [130] and Gpi7p, which plays a role in the biosynthesis of glycosylphosphatidylinositol, another component of the cell wall [131].

Misregulation or disruption of these proteins has been shown to effect cell separation and cause cell separation defective cells such as the clumpy phenotype cells illustrated in Figure 1.2 [132]. In budding yeast the cell wall consists of a complex of glucose polysaccharides (glucans), manno-proteins and chitin [125]. Chitin itself is mainly found in the mother-daughter bud neck and primary septum [125]. Cts1p is responsible for hydrolysis of the chitin components of the primary septum that contributes to cell separation [125]. It has also been found by several groups studying budding

yeast cell separation that absence of glucanases, such as Dse4p [133], Dse2p [101] and Scw11p [134], leads to failure of cell separation with loss of hydrolysis of the secondary septum and surrounding cell wall that hold the mother and daughter cells together [125]. The series of hydrolytic enzymes that are responsible for completion of cell separation are closely regulated in their expression and function [125].

Some of the genes involved in cell separation are expressed asymmetrically in the daughter cell due to the localisation of two transcription factors Swi5p and Ace2p, which show a high degree of similarity between themselves and overlapping transcriptional regulation in *S. cerevisiae* [101, 133]. Swi5p has been shown to regulate the expression of *AIM44, PCL9, PIR1* and the uncharacterised gene *YNL046W* [101, 130], whereas Ace2p exhibits transcriptional control over *CTS1*, *DSE1*, *DSE2* and *SCW11* among others [101, 132]. The asymmetrical transcription of these important cell separation components is due to the localisation of Swi5p and Ace2p to the daughter cell nucleus [101, 133]. Localisation of the transcribed products to the daughter side of the bud neck has also been suggested to be very important for correct function [129]. An investigation using C-terminal deletions of *CTS1* showed alteration in the trafficking of Cts1p resulted in cell separation defective mutants [129].

1.6.3 The RAM network

Ace2p is a zinc finger-like DNA binding transcription factor associated with the regulation of genes that participate in the early G_1 to M phase of the cell cycle in *S. cerevisiae* [101]. Ace2p exhibits transcriptional control over the cell separation machinery and has been shown to cause a clumpy growth phenotype when deleted in both *S. cerevisiae* and *C. glabrata* [132]. The transcription and localisation of Ace2p is controlled by a network of proteins, similar to MEN, called the **r**egulation of **A**ce2p transcription factor and polarised **m**orphogenesis (RAM) signalling network shown in Figure 1.3 [135]. The RAM network also controls polarised growth, cellular morphogenesis and maintenance of cellular integrity, and has been shown to be crucial for cell viability except in the absence of Ssd1p [136].

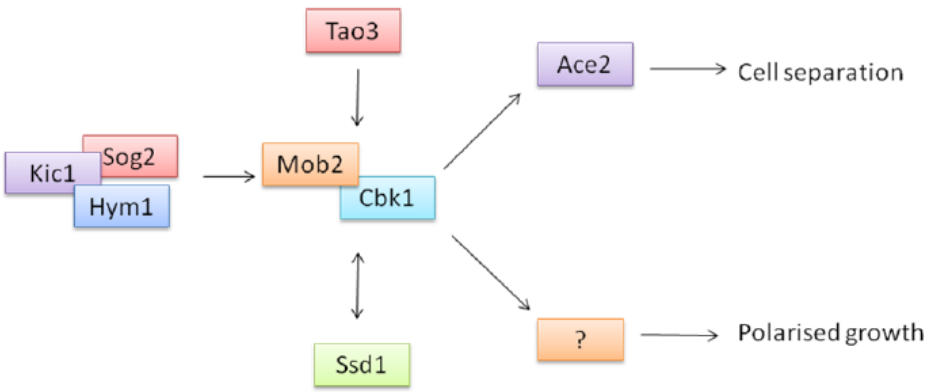


Figure 1.3 – Predicted model of the RAM network [132]. Interacting Kic1p, Sog2p and Hym1p form a complex and activate Mob2p-Cbk1p [135, 136]. Tao3p and Ssd1p are also thought to activate the Mob2p-Cbk1p complex; the activated Mob2p-Cbk1p complex activates Ace2p, which in turn activates the transcription of genes required for cell separation, the cell separation machinery, which leads to hydrolysis of the primary and secondary septum and cell separation [135, 136]. *SSD1,* however, has been shown to not be essential for RAM regulation of Ace2p [135, 136].

The RAM network is known to contain at least six proteins: Mob2p, Cbk1p, Tao3p, Sog2p, Hym1p and Kic1p [135]. Disruption of any one of the six encoding genes results in cell separation defective mutants and low levels of *ACE2* transcription [135]. The current model of the RAM network (Figure 1.3) shows that Kic1p, Sog2p and Hym1p interact to activate a Mob2p-Cbk1p complex, which in turn activates *ACE2* transcription leading to cell separation [135]. Tao3p and Ssd1p are also believed to activate Mob2p-Cbk1p, however RAM regulation of *ACE2* expression has been shown to be independent of *SSD1* [136]. In *Schizosaccharomyces pombe* the protein kinase Kic1p has been shown to regulate septum formation and hence is involved in polarised growth and cell wall integrity, interacting with a centrin related Cdc31p [137]. Sog1p shares a weak similarity with the amino terminus of the adenylate cyclase of *S. cerevisiae* and is necessary for Cbk1p activity and cell morphogenesis [135]. *HYM1*, an orthologue of the *Aspergillus nidulans* hyphal growth factor *HYMa*, encodes a protein with a likely role in polarised morphogenesis in association with Kic1p [135, 138]. Not much is currently known about *TAO3* although it has been shown to be conserved in both yeast and human genomes indicating a possible important biological function [139]. Ssd1p has been implicated in the function of Sit4p, a phosphatase, and is believed to be a suppressor of *TAO3* and *CBK1* expression as it has been shown that disruption of *SSD1* rescues the growth defect of *tao3* and *cbk1* null mutants therefore indicating a role in polarised morphogenesis [139, 140]. Cbk1p itself plays a role in polarised growth and controls the localisation of Ace2p to the daughter nucleus [135, 141]. In the other half of the complex Mob2p is a member of the *MOB* family and is related to the MEN proteins Mob1p and Dbf2p [135, 141]. The RAM network has therefore been shown to be crucial for cell separation and dissemination of progeny. Investigation into the genes responsible for the end result of cell separation induced by *ACE2* expression is therefore needed to fully understand the mechanism of cell separation and the role it plays in virulence.

1.7 Current knowledge of the Ace2p regulon

The genes currently known to be transcriptionally regulated, either directly or indirectly, by Ace2p [101, 133] have been characterised individually, some to a greater extent than others in *S. cerevisiae*. Considering Ace2p's role as a regulator of cell separation, it's not surprising that most of them play a role in cell separation, forming part of the cell separation machinery. *CTS1* for example encodes a cell wall associated chitinase that hydrolyses the chitin in the septum, which together with other hydrolytic enzymes, allows mother and daughter cells to separate [129]. *CTS1* and its Ace2p-depenence have been well characterised in *S. cerevisiae,* as well as previously being investigated in relation to virulence in *C. glabrata* [142]. The other genes of the Ace2p regulon, *AMN1*, *ASH1*, *BUD9*, *DSE1*, *DSE2*, *DSE3*, *ACF2/DSE4*, *EGT2*, *RME1*, *SCW11α, SCW11β* and *SIC1,* have yet to be investigated in *C. glabrata* in relation to their Ace2p-dependence and possible antivirulence, or virulence moderating, activity, but their functions in *S. cerevisiae* have been widely documented, ranging from cell wall glucanases that help hydrolyse the secondary septum, to cell cycle regulators, regulators of mating-type and bud site selection.

1.7.1 *AMN1*

In *S. cerevisiae*, Amn1p, a daughter-cell expressed protein, has been shown to localise to the daughter cell cytoplasm and nucleus [143] performing a role in cell cycle progression and inactivation of the MEN group of proteins as part of the AMEN (antagonist of MEN) group of proteins [144]. Wang et al. showed that *AMN1* overexpression was toxic to MEN mutants and also slowed the growth of wild type cells causing cell cycle arrest or delays in mitotic exit [144]. They also showed that *amn1* null mutants present with inappropriate mitotic exit during spindle assembly or nuclear orientation checkpoints [144] indicating that Amn1p is involved in a cell cycle progression checkpoint that occurs at the completion of mitotic exit. *AMN1* expression is induced as part of the AMEN upon completion of mitotic exit and blocks G-protein signalling by binding to Tem1p, a G protein located on the spindle pole body [144]. This in turn prevents Tem1p binding to and activating Cdc15p, resulting in inhibition of both Cdc14p and MEN activation [144]. With MEN inhibited, the cells are then able to progress into START and enter S phase, in which Amn1p is actively destroyed reversing AMEN [144]. Amn1p has also been shown to display strong self-linkage meaning that its expression level is linked to its own locus in the genome and local variation, therefore it has been proposed to indirectly negatively regulate itself in *trans* in the diploid *S. cerevisiae* [145]. Amn1p may also play a role in mating having been shown to regulate the binding of Ste12p to the pheromone response elements (PREs), with *AMN1* deletion increasing Ste12p binding to PREs, inferring that Amn1p plays a role in regulating transcription under a vegetative state through Ste12p [146]. The *C. glabrata* homologue of *S. cerevisiae AMN1* is *CAGL0H07491g*.

1.7.2 *ASH1*

ASH1, **a**symmetric **s**ynthesis of ***HO***, is a protein involved in the control of mating-type switching, and therefore cell fate, in *S. cerevisiae* [147]. Regulation of *HO*, a gene that encodes an endonuclease that initiates replacement of the mating-type locus with code from one of two mating-type cassettes (a or α) in haploid *S. cerevisiae* cells*,* prevents daughter cells or those that have yet to bud, from being able to switch mating-type [148]. Ash1p is expressed in daughter cells and is localized to the daughter cell nucleus in G_1, controlling the initiation of mating-type switching by repressing the transcription of *HO* in G_1, but also shows some control over the frequency of mating-type switching in mother cells through perdurance [147, 149]. Over expression of Ash1p in mother cells has been shown to prevent mating-type switching [147]. Likewise, disruption of *ASH1* causes de-repression of *HO* transcription and therefore mating-type switching [147]. Ash1p has also been shown to affect the expression of *SWI5* in *S. cerevisiae* daughter cells [147]. *ASH1* encodes a GATA-like transcription factor that binds to the promoter region of *HO* with its C-terminal zinc-finger-like domain and suppressing the transcription of *HO* with its N-terminal in a mechanism that is independent of Swi5p binding [149]. Ash1p binds to a consensus sequence similar to that of GATA-1 (YTGAT) that has also been shown to exist in promoter regions of genes other than *HO* and could indicate a greater regulatory role for Ash1p [149, 150]. *ASH1* has been shown to be essential for pseudohyphal growth in both haploid and diploid *S. cerevisiae* cells independently of the previously described MAPK cascade and Ste12p for instance, with *ASH1* over expression causing an increase in the number of pseudohyphal projections in response to nitrogen starvation [150]. *ASH1* transcription is regulated by Ace2p, but its translation is thought to be regulated through the action of several RNA-binding proteins, including Puf6p, that are thought to supress *ASH1* translation, which is released by *CK*

phosphorylation and the general transcription factor Fun12p that acts to promote *ASH1* expression [151]. Localisation of *ASH1* mRNA to the bud tip is actin cytoskeleton-dependent involving *SHE2-5*, *LOC1* and the type V myosin Myo4p (*SHE1*), through She2p binding [152-154]. The *C. glabrata* homologue of *S. cerevisiae ASH1* is *CAGL0D00462g*.

1.7.3 *BUD9*

Bud9p, as the name suggests, is thought to be involved in the bipolar budding formation in diploid *S. cerevisiae* cells acting as a cortical landmark [155-157]. *BUD9* encodes a cell membrane targeted protein that is predicted to have two hydrophobic membrane-spanning domains separated by a short hydrophilic domain that likely performs the signalling function of the protein, and a large, heavily glycosylated N-terminal extracytoplasmic domain, which may play a role in anchoring the protein in position in the cell membrane by interacting with the cell wall [156]. Bud9p is partnered by another bud site selection associated protein, Bud8p, which although not thought to play a role in the axial budding pattern displayed by haploid *S. cerevisiae* cells, together they are thought to mark the distal and proximal poles for bud site selection respectively in diploid cells [155, 156]. Diploid *S. cerevisiae bud8* and *bud9* mutants display almost exclusive budding to the proximal and distal poles respectively [156]. Bud9p has also been shown to be localised to the daughter cell side of the mother-daughter bud neck [143] and remains in place during cell division [156]. Correct expression and localisation of Bud9p is both cell cycle dependent and Rax1p/Rax2p-dependent [158], and has been shown to be dependent on actin and septin for correct delivery to the bud neck and proximal pole [157, 159]. Kato et al. have also shown Bud9p localisation to be dependent on the EKC/KEOPS complex, a group of proteins involved in telomere maintenance and transcriptional regulation [160, 161], separate from Bud9p's dependence on of Rax2p and septin [157], which they suggest might be involved with the timing of *BUD9* expression rather than playing a direct role in localisation or as a downstream element from Rax2p and septin. Once properly localised it is thought that Bud9p acts as a landmark for the proximal pole, recruiting a GTPase signalling complex formed from Rsr1p, Bud2p and Bud5p when appropriate, which then transmits the positional information to Cdc42p and Cdc24p for establishment of cell polarity via recruitment of the budding machinery [157, 162]. The *C. glabrata* homologue of *S. cerevisiae BUD9* is *CAGL0K04191g*.

1.7.4 *DSE1*

DSE1 is an Ace2p regulated gene that currently has no known function in *S. cerevisiae* [101, 163]. It is known to be expressed other Ace2p regulated genes in the run up to cell separation along with the rest of the cell separation machinery, is repressed by Swi5p and shows daughter cell specific expression [101, 133, 143]. Doolin et al. also showed that *dse1* null *S. cerevisiae* diploid cells display a cell separation defect that was not found in haploid lab strains, and a sensitivity to cell wall targeted conditions such as SDS, calcofluor white and caffeine, indicating a possible role in cell separation and cell wall metabolism [101]. Interaction data from *S. cerevisiae* shows 32 different interactions, with Boi1p, Boi2p, Ste4p and Zds2p physical interactions possibly indicating a role in bud formation or bud site selection [163-165]. Dse1p has also been shown to physically interact with Ste11p, which is involved in pseudohyphal growth, plays a role in virulence in *C. glabrata* and, along

with Ste4p, has been implicated in pheromone sensing [82, 165, 166]. Both Boi1p and Boi2p are thought to play a role in polar growth localising to the bud cortex with double null mutants displaying an abnormally large, round phenotype that is prone to lysis, plus buds showing defective bud formation and disruption of cell polarity maintenance [167]. Boi1p and Boi2p have been shown to interact with Bem1p a protein that helps establish the cellular polarity required for budding [168]. Recent evidence also points to a possible bud site selection role for Dse1p in haploid *S. cerevisiae* cells, with over expression causing a budding-within-birth-scar phenotype, a typically highly protected area that forbids budding, and activation of the cell wall integrity pathway [163]. Draper et al. also showed that in *S. cerevisiae* over expression of Dse1p induced invasive growth, and was presumed to be a positive regulator of invasive growth through its interaction with Ste11p [166]. It was also shown that overexpression of Dse1p caused interference with the pheromone sensing pathway, conferring resistance to cell cycle arrest in G_1 in response to mating factor and equally causing two-fold sensitivity to pheromone-induced cell cycle arrest in *dse1* null cells [166]. Draper et al. also hypothesised that Dse1p had a role in cross-talk between the pheromone and invasive growth pathways due to its ability to bind to both a Ste4p complex and Ste11p [166]. In *C. albicans,* Daher et al. hypothesised *DSE1* to be an essential gene due to their inability to construct a null strain, only managing a heterozygote haploinsufficient strain [169]. The haploinsuffient *DSE1 C. albicans* strain showed increased sensitivity to calcofluor white, SDS and oxidative stress, with slightly decreased levels of chitin deposition in the cell wall, as well as increased filamentous growth levels on both solid and liquid media [169]. Daher et al. also found their *DSE1* haploinsufficient strain to be attenuated in virulence with a delayed adhesion [169]. *DSE1* has little homology to other genes regulated by Ace2p, however, including Dse2p or Dse4p/Acf2p, or any other gene in the *S. cerevisiae*, *C. glabrata* or *C. albicans* genome [170, 171]. The *C. glabrata* homologue of *S. cerevisiae DSE1* is *CAGL0K02277g*.

1.7.5 *DSE2*

DSE2 encodes a putative GPI-anchored cell surface protein with similarities to another Ace2p controlled gene, *DSE4,* and sequence similarity to previously characterised glucanases [101]. *DSE2* expression is also reduced by the transcriptional regulator and Ace2p homologue, Sw15p, with *swi5* cells showing at least a 25% increase in *DSE2* expression compared to wild type *S. cerevisiae* cells [101]. In haploid *S. cerevisiae* cells *DSE2* disruption showed no appreciable phenotype, but diploid *dse2* cells exhibit cell separation defects forming long chains of cells with unipolar budding [101]. *DSE2* disruption also causes enhanced pseudo-hyphal production on nitrogen-poor medium and increased resistance to lactic acid media [101, 172]. *DSE2* expression is also down regulated in response to bovine protein kinase C-α (PKCα) activation and by cAMP [173, 174]. Dse2p is localised to the cell wall and the septum separating the mother and daughter cells [101]. Dse2p is therefore thought to be involved in cell separation, helping to hydrolyse the septum or surrounding cell wall after cytokinesis [133]. The *C. glabrata* homologue of *S. cerevisiae DSE2* is *CAGL0G05896g*.

1.7.6 *DSE3*

DSE3 unlike *DSE2* and *DSE4/ACF2* does not share a sequence similarity with other known yeast glucanases and has yet to be characterised, but is likely involved in daughter cell fate due to its daughter cell specific expression and localisation to the bud neck [133, 143]. Doolin et al. found *DSE3* expression to be regulated by both Ace2p and its homologue Swi5p, with a double deletion *ace2 swi5* required to produce minimal *DSE3* expression in haploid *S. cerevisiae* cells [101]. *DSE3* expression was also shown to not be induced by α-factor [133], and was enhanced twofold by the deletion of *AMN1* in a *S. cerevisiae* diploid natural isolate derivative [175], which could indicate a down-stream role for Dse3p from the MEN activation inhibitor. The *C. glabrata* homologue of *S. cerevisiae DSE3* is *CAGL0C02827g*.

1.7.7 *DSE4/ACF2*

In *C. glabrata* one of the Ace2p regulon genes, *CAGL0M04565g*, has homology to both *DSE4* and *ACF2* in *S. cerevisiae,* which form part of the glycosyl hydrolase family 81 (GHF81) [171, 176, 177]. Up until recently the gene was designated as *DSE4* within *C. glabrata*, but is currently designated as *ACF2* as it has been discovered that *CAGL0M04565g* has good synteny with *ACF2,* sharing a similar spot in the *C. glabrata* genome to the orthologous ORF within *S. cerevisiae* genome [105, 171]. In *S. cerevisiae DSE4* (*ENG1*) and *ACF2* (*ENG2*) encode endo-1,3-β-glucanases with highly specific 1,3-β-linkage activity and little sequence similarity to other yeast 1,3-β-glucanase encoding genes [130]. *DSE4* is transcriptionally regulated by Ace2p, peaking in expression during the M/G_1 transition and is heavily glycosylated [130]. *ACF2*, however, shows no periodic fluctuation in expression levels throughout the cell cycle, but has increased expression during sporulation, matching the temporal pattern of midterm meiosis genes such as *SPO12* [130]. Baladron et al also showed Dse4p to be localised to the bud neck, accumulating on the daughter cell side of the septum [130]. Diploid *S. cerevisiae* null cells for both *dse4* and *acf2,* as well as double mutants, displayed no sensitivity to cell wall targeted conditions such as calcofluor white and congo red, indicating that neither *DSE4* nor *ACF2* play a significant role in general cell wall architecture [130]. However, diploid *dse4* cells in both *S. cerevisiae* and *C. albicans* showed a cell separation defect, with small clusters of cells visible, which, coupled with the septum localisation, indicates that Dse4p helps to degrade the septum for cell separation [130, 177]. *S. cerevisiae acf2* null cells showed no appreciable phenotype, but in *S. pombe* diploid *acf2* cells showed a failure in ascus cell wall hydrolysis and ascospore release, which coupled with the increased expression during sporulation in *S. cerevisiae* clearly indicates a role in intracellular 1,3-β-glucan hydrolysis in sporulation [130, 178]. The *C. glabrata* gene *CAGL0M04565g*, will be referred to as *ACF2* hence forth, in-line with its current annotation within the Génolevures database [171].

1.7.8 *EGT2*

EGT2 encodes a glycosylphosphatidylinositol (GPI)-anchored cell wall endoglucanase that has been shown to be involved in cell separation due to a delay in cell separation shown by *egt2* null *S. cerevisiae* cells [127]. It is expressed in the early stages of G_1 immediately after mitosis and is not expressed in cells arrested with α-factor [127]. In exponentially growing cells Kovacech et al. and

others showed that *S. cerevisiae EGT2* can be transcriptionally regulated by both Swi5p and Ace2p in both mother and daughter cells [101, 127, 133, 179]. However, Colman-Lerner et al. showed that saturated culture daughter cell specific expression of *EGT2* was dependent on Ace2p and independent of Swi5p [133]. Recent analysis in *C. glabrata* has also showed that *EGT2* could be under the sole regulation of Ace2p and not Swi5p [180]. It is thought that Egt2p plays a role in cell separation through the hydrolysis of mother-daughter septum [127, 133]. The *C. glabrata* homologue of *S. cerevisiae EGT2* is *CAGL0D02530g*.

1.7.9 *RME1*

Rme1p, as its name suggests, is a zinc finger protein that acts as a **r**egulator of **me**iosis, which in *S. cerevisiae* is a haploid specific gene with its transcription directly suppressed in *MATa*/α diploid cells by the *a1-α2* gene product complex [181, 182]. *RME1* has been shown to prevent meiosis and subsequent sporulation in haploid cells [182]. Rme1p acts to transcriptionally repress the expression of *IME1,* a protein required for expression of *IME2* and other meiotic genes, by binding to an upstream element directly, acting independently of the environmental signal [181-185]. As a distal repressor, Rme1p represses *IME1* expression by binding to two binding sites over 1600 base pairs upstream of the *IME1* ORF and blocks the binding of the transcriptional activator Hap1p to an upstream activation sequence, known as activator exclusion [186, 187]. Rme1p transcriptional repression is dependent on specific sequences flanking the Rme1p binding sites, which together are called the Rme1p response element (RRE), on a modulation region, and on *RGR1* and *SIN4* expression forming two subunits of the Mediator RNA polymerase II associated complex [185-188]. Rme1p has also been found to be able to promote mitosis through direct activation of the expression of the G_1 cyclin, *CLN2* through binding to two RREs present in the *CLN2* promoter [189, 190]. Overexpression of *RME1* has been shown to cause a reduction in cell size that is dependent on Cln2p, bypassing the *CLN2* activation requirement for the SBF (Swi4p-Swi6p) or MBF (Mbp1-Swi6p) transcription factor complexes, while *rme1* mutants display increased cell size and reduced steady-state levels of *CLN2* expression [189, 190]. In *S. cerevisiae RME1* expression is transcriptionally regulated by Swi5 and Ace2p, shows cell cycle regulated transcript levels peaking at the M/G_1 boundary in both haploid and diploid cells, and shows nuclear localisation in G_1 [191]. The *C. glabrata* homologue of *S. cerevisiae RME1* is *CAGL0K04257g*.

1.7.10 *SCW11*

SCW11 encodes a SDS-soluble cell wall protein and shows sequence homology to other cell wall glucanase genes including *BGL2*, which encodes an endo-β-glucanase, and Dse2p and Dse4p/Acf2p, which have been highlighted in playing a role in degradation of the cell wall during cell separation as previously discussed [133, 134]. In *S. cerevisiae* and *C. albicans, SCW11* has been shown to be transcriptionally regulated by Ace2p but not Swi5p [101, 192], down regulated in response to genotoxicity, and also to be regulated by Ste12p and therefore may have roles in conjugation [134, 193, 194]. Cappellaro et al. found *S. cerevisiae scw11* cells to display a cell separation defect, which strengthens the theory that Scw11p may be involved in the cell separation-dependent glucan hydrolysis of the septum [134]. Teparić et al. also found that Scw11p acts antagonistically with other

closely related cell wall proteins Scw3p and Scw10p, relieving an increased mortality phenotype shown by *scw3scw10* double deletion mutants when disrupted itself [195]. This suggests that Scw11p forms part of catabolic side of the dynamic equilibrium displayed by the cell wall in yeast, which ties in well with the assumption that it plays a role in septum hydrolysis during cell separation [125, 195]. In *C. albicans SCW11* has shown altered expression in response to certain conditions like caspofungin treatment, which decreases expression, and high iron concentration that increases expression, while conversely in *S. cerevisiae,* reduced *SCW11* expression has been shown under high iron conditions [196, 197]. As expected, reduced expression of *SCW11* is also found in hyphal *C. albicans* compared to yeast form, as well as pseudohyphal *S. cerevisiae* cells [197-200]. It has also been suggested that *SCW11* is essential in *C. albicans* due to the apparent inability to create a homozygous *scw11* null strain, and has been shown to be a consistent part of the *C. albicans* secretome [201-203]. Two *C. glabrata* homologues of *S. cerevisiae SCW11* have been found, *CAGL0A01474g* and *CAGL0E02915g*, henceforth referred to as *SCW11α* and *SCW11β* respectively.

1.7.11 *SIC1*

SIC1, a Swi5p and Ace2p regulated gene encoding a cyclin dependent kinase inhibitor, plays a role in the control of the G_1/S-phase transition [101, 204]. In *S. cerevisiae* Swi5p has been shown to control *SIC1* transcription at the end of mitosis ready for G_1 as part of the '*SIC1* cluster' [204-207]. Over expression of *SIC1* has been shown to cause a subset of elongated, single nucleate budding cells, while *sic1* null cells display partial mitotic arrest, premature DNA replication and genome instability [208]. Sic1p binds to and inhibits the Cdk1p-Clbp (previously known as Cdc28p) histone kinase complexes, which are responsible for initiation of DNA replication in budding cells [209, 210]. Cdk1-Clbp complex inhibition acts as a checkpoint preventing premature S-phase progression and ensures genomic integrity [209, 210]. Sic1p has been shown to be destroyed by ubiquitin-dependent proteolysis, which releases the Cdk1-Clbp complex to then initiate DNA replication and transition into S-phase [211]. Sic1p is targeted for ubiquitination by multi-site phosphorylation by the Cdk1p-Clnp kinase complexes at a minimum of six out of nine possible suboptimal phosphorylation sites, which then allows it to be recognised by the F-box protein Cdc4p [210, 212]. By requiring at least six phosphorylation events at suboptimal CDK sites, Sic1p recognition by the Skp1p-Cdc53p-Cdc4p (SCF^{Cdc4p}) complex is Cdk1p-Clnp concentration dependent, imposing a Cdk1p-Clnp kinase threshold on Sic1p recognition by SCF^{Cdc4p}, which allows fine-tuning of the de-inhibition of Cdk1p-Clnp [211, 212]. Once phosphorylated, Sic1p is recognised by SCF^{Cdc4p}, which then recruits Cdc34p to form the ubiquitin ligase complex for Sic1p ubiquitination, destroying it and releasing the Cdk1-Clbp complex allowing it to initiate DNA replication and transition into S-phase [211]. Sic1p has also been shown to be a functional homologue of mammalian Kip1p [209] and is localised to both the cytoplasm and the nucleus of the daughter cell [143, 205]. The *C. glabrata* homologue of *S. cerevisiae SIC1* is *CAGL0L13222g*.

The Ace2p regulon therefore includes genes involved in cell separation, cell cycle regulation and bud site selection, as well as two genes of as yet unknown function. From hydrolytic enzymes to transcriptional regulators, Ace2p maintains their cell cycle regulated expression and contributes to their daughter cell specific localisation.

1.8 Role of cell wall components in the septum

The fungal cell wall is responsible for maintaining cell shape, protecting the fungal cell from the environment, enabling adherence to host surfaces and acts as an anchor point for many cell wall associated proteins. In budding yeast, the cell wall also forms the septum that binds mother to daughter until cell separation can take place. The main constituents of the cell wall, glucan and chitin, form critical linkages between budding cells and it is their hydrolysis by components of the cell separation machinery that allows dissemination of progeny [125].

1.8.1 Glucan

The glucan component of the cell wall is comprised of chains of glucose molecules primarily linked in a β-1,3 configuration with some β-1,6-glucan linkages interspersed across the chains. Glucan forms the major structural component of the cell wall in *S. cerevisiae* [16], and is formed by the glucan synthase that creates β-1,3-linkages between glucose residues creating long polysaccharide chains [213]. The glucan chains are branched at every 50-60 or so residues to other β-1,3-glucans, which in turn are cross-linked with chitin, β-1,6-glucans and other mannoproteins to form a strong core for the cell wall [214]. Glucan has been shown to be an integral part of the fungal cell wall and essential for viability in both *S. cerevisiae* and *C. albicans*, and others, through disruption of the glucan synthase complex [215, 216]. This indicates that the glucan synthase pathway is a viable target for antifungal drug development, and indeed it has been shown that the action of echinocandins revolves around inhibition of the β-1,3-glucan synthase [217].

1.8.2 Chitin

Chitin, although only a small part of the cell wall by mass [126], forms the other major component of structural integrity of the cell wall due to its high tensile strength. Like glucan, chitin is made up of a long chain of glucose-derived molecules, this time in the form of N-acetylglucosamine, which are linked together by the chitin synthase. The long chains of chitin are linked by hydrogen bonds, which combine to create a strong crystalline, microfibrillar structure, which is then in turn linked with glucan and other components of the cell wall. Chitin, like glucan, has been shown to be essential for viability in both *S. cerevisiae* and *C. albicans*, as disruption of all the chitin synthase redundant genes results in non-viable strains [218, 219]. Chitin has been shown to form the main structural link within the primary septum that holds mother and daughter together, as disruption of the chitinase *CTS1* forms large cell clumps deficient in cell separation [129]. Like the glucan synthase pathway, the chitin synthase pathway forms a viable antifungal drug target.

1.9 General aims of the project

This study aims to investigate the underlying cause of the antivirulence potential of the cell separation associated transcription factor Ace2p in *C. glabrata* by studying the genes that show Ace2p-dependent expression. Through analysis of the genes regulated by Ace2p it is hoped that we can begin to understand the mechanism for the antivirulence and the genes that play a role in it, building further insight into *C. glabrata* virulence both *in vitro* and *in vivo*, which is still very much in its infancy when compared to other human pathogens.

1.10 Specific aims of the project

To further study the effect of *ace2* within *C. glabrata* by defining the Ace2p regulon -- the genes under the transcriptional regulation of Ace2p. This will enable us to see which genes in *C. glabrata* contribute to the antivirulence of *ACE2* and will provide targets for deletion and further study within this project. Due to the unavailability of suitable and cost effective array tools for *C. glabrata* at the time, to achieve this Northern analysis of a tet-regulated *ACE2* strain (HLS119) will be conducted to show whether the genes highlighted as being controlled by Ace2p, through homology to *S. cerevisiae* genes, localisation studies and promoter analysis, show Ace2p-dependent expression in *C. glabrata.*

To investigate the potential for direct control of expression by Ace2p by promoter analysis. This will allow us to highlight those genes that are potentially directly transcriptionally regulated by Ace2p and define whether the Ace2p binding sites, homologous to those found in *S. cerevisiae*, exist in *C. glabrata*. To achieve this, the promoter region sequences of the Ace2p-dependent genes will be searched for the central consensus sequence of the Ace2p binding site as defined by Dohrmann et al. [220] using a GIBBS analysis or similar.

To create deletions of each of the previously uninvestigated genes of the Ace2p regulon in *C. glabrata*. Through individual deletion of the previously uninvestigated genes shown to be Ace2p-dependent in *C. glabrata*, it will then be possible to conduct both *in vitro* and *in vivo* analysis of their antivirulent potential and in turn, their contribution to the hypervirulence displayed by *ace2* cells in *C. glabrata* [7]. To achieve this gene deletion techniques, including the high throughput fusion PCR and Edlind methods, will be employed to disrupt the genes, which will then be confirmed via PCR and Southern analysis.

To study the potential hypervirulent effects of previously uninvestigated Ace2p regulon gene deletions to determine their contribution to the extreme hypervirulence displayed by *C. glabrata ace2* cells [7]. This will be achieved through the use of *in vivo* virulence analysis. A neutropenic murine model of candidiasis will be used to assay the virulence of each individual Ace2p regulon deletion and compared to the *C. glabrata* wild type.

To study the potential immune over-stimulation effects of previously uninvestigated Ace2p regulon gene deletions to determine their contribution to the extreme immune activation displayed by *C. glabrata ace2* cells [7]. This will be achieved through the use of an *in vitro* macrophage infection assay. After a short infection the supernatant will be assayed for cytokine release via ELISA as a measure of immune activation and compared to that elicited by the *C. glabrata* wild type.

To investigate the role and function of the novel gene *DSE1* within *C. glabrata*. This will be achieved through the study of the gene in both *C. glabrata* and its close genetic relative *S. cerevisiae,* by studying its possible Ace2p-dependence, by disrupting it within *C. glabrata*, and by studying its sensitivity to phenotypic stress conditions. The localisation of Dse1p will also be looked at in *S. cerevisiae*, while structural prediction will be conducted using the sequence of *DSE1* from *C. glabrata*.

2 Materials and Methods

These are the general materials and methods common throughout the study. Specific materials and methods that only apply to particular chapters are included in the appropriate chapter.

2.1 Chemicals and reagents

All chemicals used within this study were purchased from Sigma or Fisher Chemicals unless otherwise stated.

2.2 Culture media, strains and plasmids

2.2.1 Fungal strains and growth media

Please see Appendix 1 for all strains used within this study. Fungal cells were routinely cultured using yeast extract peptone dextrose (YPD) (2% (*w/v*) peptone, 2% (*w/v*) glucose, 1% (*w/v*) yeast extract) or synthetic dropout medium (SD) (0.68% (*w/v*) yeast nitrogen base without amino acids (Difco, BD, UK), 2% (*w/v*) glucose) and the appropriate dropout mix (Clontech, France) at 30°C (*S. cerevisiae*, *C. glabrata* or *C. albicans*) or 37°C (*C. glabrata* or *C. albicans*) at 180 rpm. Selective agents and stress condition chemicals were added prior to growth for specific strains and for specific experiments. For culture on solid media 2% (*w/v*) agar was added prior to autoclaving. Strains were stored at room temperature for up to 4 weeks or 2 months at 4°C on solid agar plates, or for long term storage in 50% (*v/v*) glycerol at -80°C. Specific descriptions of strain constructions are given in the relevant chapters.

2.2.2 Bacterial strains and growth media

XL-10 and TOP10 *Escherichia coli* competent cells were cultured in standard Luria Bertani (LB) medium, 2% (*w/v*) GibcoBRL LB Broth Base (Life Technologies, UK). Liquid cultures were routinely incubated at 30°C or 37°C, 180 rpm. Solid medium was produced by the addition of 2% (*w/v*) agar prior to autoclaving. When required, ampicillin, geneticin or gentamycin was added to a final concentration of 100 µg/mL after autoclaving and once the media had cooled to below 55°C. Strains were stored for up to 4 weeks at 4°C in a fridge or cold room.

2.2.3 Plasmids

Please see Appendix 2 for a list of all the plasmids either used or constructed during this study. Details regarding construction of plasmids made during this study are given in the relevant chapters.

2.3 Molecular biology techniques

2.3.1 Primers

Oligonucleotides were purchased from Sigma-Genosys (Dorset, UK) or Integrated DNA Technologies (Leuven, Belgium). Primers are listed in the text where appropriate, or in Appendix 3.

2.3.2 Polymerase chain reaction

PCRs were performed as described by Saiki et al. [221] using protocols dependent on the enzyme manufacturer. Each reaction was optimised individually specific to the template and oligonucleotides in use. Enzymes used included GoTaq Flexi DNA Polymerase (Promega, UK), RedTaq™ DNA polymerase (Sigma-Genosys, UK), Advantage™ 2 PCR Enzyme System (BD Biosciences, UK), BIO-X-ACT™ Short Polymerase (Bioline, UK), BIO-X-ACT™ Long Polymerase (Bioline, UK) and Platinum Taq (Invitrogen, UK).

2.3.3 Colony polymerase chain reaction

Colony PCRs were performed as described by Liang and Richardson [222] using protocols dependent on the enzyme manufacturer. Each reaction was optimised individually specific to the colony and oligonucleotides in use. The enzymes used primarily were GoTaq Flexi DNA Polymerase (Promega, UK) and RedTaq DNA polymerase (Sigma-Genosys, UK).

2.3.4 Linear DNA and PCR extraction and purification

Linear DNA and PCR fragments were routinely purified from 1% (*w/v*) agarose gels or from solution using a QIAquick® Gel Extraction Kit (Qiagen Ltd, UK) according to manufacturer's instructions.

2.3.5 Enzymatic manipulation of DNA

DNA was modified as appropriate by restriction endonuclease digestion and blunt ending [223] using appropriate enzymes purchased from New England Biolabs (UK). All enzymatic reactions were performed according to manufacturer's instructions.

2.3.6 Agarose gel electrophoresis

Samples of DNA were routinely separated on 1% (*w/v*) agarose gels made with TBE (Tris-Borate: 4 mM EDTA, 0.089 M trizma base) with the addition of 0.5 µg/mL Sybr safe (Invitrogen, UK).

Samples of RNA were routinely separated on 1% (*w/v*) agarose gels made with 10 mM phosphate buffer pH 7.4.

2.3.7 DNA and RNA quantification

Nucleic acid concentrations were quantified via spectrophotometric measurement using a NanoDrop-1000 spectrophotometer (Labtech International, UK).

2.3.8 Isolation of yeast DNA

DNA extractions were performed using a MasterPure Yeast DNA purification kit (Epicentre Biotechnologies, UK) according to manufacturer's instructions.

2.3.9 Isolation of yeast RNA

RNA was extracted using an acid phenol method modified from that described previously [224]. Briefly, 50 mL of saturated culture was collected by centrifugation, washed in ice cold ddH_2O and resuspended in 400 µL TES (10 mM Tris-HCl (pH 7.5), 10 mM EDTA, 0.5% (*w/v*) SDS). Then 400 µL acid phenol was added and the cells vortexed and incubated for 65°C for 1 hour. Cells were collected by centrifugation and the aqueous phase transferred to a new microfuge tube. A further 400 µL acid phenol was added, vortexed vigorously and then centrifuged. Next, 400 µL chloroform was added to the aqueous phase, vortexed and then centrifuged. Finally, 40 µL 3 M sodium acetate (pH 5.2) and 1 mL of ice-cold 100% ethanol was added to the supernatant and the mixture incubated at -80°C for 1 hour, the pellet collected by centrifugation and washed in ice-cold 70% (*w/v*) ethanol, air-dried and resuspended in 50 µL ddH_2O to be stored at -80°C.

2.3.10 Plasmid DNA extraction

Plasmids were extracted from overnight LB cultures of appropriate *E. coli* strains using a QIAprep®Spin Miniprep Kit (Qiagen Ltd, UK) according to manufacturer's instructions. Plasmids were stored at 4°C or -20°C in O.1 x TE (10 mM Tris-HCl (pH 8), 1 mM EDTA (pH 8)).

2.3.11 Yeast transformation – Electroporation

Yeast cells were transformed using a modification of the electroporation protocol [225]. Briefly, 1 mL of a saturated overnight culture was transferred into 50 mL pre-warmed YPD and incubated for a further 3 hours at 37°C (*C. glabrata*) or 30°C (*S. cerevisiae*), 180 rpm. Cells were harvested by centrifugation, washed in sterile water and resuspended in 8 mL ddH_2O, 1 mL 10 x TE (10 mM Tris-HCl (pH 8), 1 mM EDTA (pH 8)) and 1 mL 1 M Lithium acetate and incubated at 30°C for 30 min at 130 rpm. Then 250 µL 1 M dithiotheitol (DTT) was added and incubated for a further 60 min at 30°C, 130 rpm. Cells were then harvested, after the 40 mL of ddH_2O, by centrifugation. All consequent procedures were performed at 4°C. The cells were resuspended in 25 mL ice-cold ddH_2O, harvested by centrifugation, washed in 5 mL sorbitol (1 M) and resuspended in 550 µL sorbitol (1 M). The competent cells (45 µL per reaction) were transferred to pre-chilled microfuge tubes and 100 ng DNA added, mixed and left at 4°C for 10 minutes. The competent cell mixture was then transferred to pre-chilled electroporation cuvettes and pulsed at 1.5 kV, 25 µF, 200 Ω. The cells were recovered

by gentle mixing with 950 µL YPD. For cells transformed with a CloneNAT deletion cassette the cells were incubated for four hours at 30°C and plated onto YPD plates containing 200 µg/mL nourseothricin. For deletion cassettes with other markers, the cells were incubated for 30 minutes at 30°C and plated out onto appropriate SC drop out media. Both were incubated for two to four days at 30°C or 37°C.

2.3.12 Yeast Transformation – Lithium acetate

Yeast cells were transformed using a modification of the lithium acetate protocol [226]. Briefly, 1 mL of a saturated overnight culture was transferred into 50 mL pre-warmed YPD and incubated for a further two hours at 37°C (*C. glabrata*) or 30°C (*S. cerevisiae*), 180 rpm. Cells were harvested by centrifugation, washed in sterile water with 1 x 10^8 cells were used for each transformation. The cells were resuspended in 1 mL lithium acetate (LiAc) (100 mM) and incubated at 30°C for 15 min. Cells were pelleted, the supernatant removed and 360 µL transformation mix (33% (w/v) polyethylene glycol (PEG) 3350, 0.1 M LiAc, 0.3 mg/mL boiled and chilled salmon sperm DNA, 200-500 ng DNA per transformation) was added. The mixture was vortexed, incubated at 30°C for 30 minutes, then subjected to heat-shock at 42°C for 20 min. The cells were harvested by centrifugation, resuspended into 50 µL ddH_2O, plated onto appropriate SC dropout media and incubated for two to four days at 30°C or 37°C.

2.3.13 Quick transformation of yeast cells

A colony of cells was added to 500 µL transformation mix (50% (w/v) PEG 4000, 0.1 M LiAc, 10 mM Tris-HCl (pH 7.5), 0.0025 mM EDTA pH8), 500-1000 ng DNA for transformation and 0.05 mg/mL boiled and chilled salmon sperm DNA. The mixture was vortexed, and incubated at 25°C overnight, then plated onto appropriate media and incubated for two to five days at 30°C or 37°C.

2.3.14 Bacterial transformation

E. coli cells were transformed using the heat shock method previously described [227].

2.3.15 Northern Analysis

Northerns were performed using a modification of the Northern technique [228]. All glassware was cleaned of RNAase prior to use and double autoclaved ddH_2O (daddH_2O) used throughout. Briefly, 7 µL RNA (10 µg RNA plus daddH_2O) and 15 µL master mix (11.25 µL DMSO, 0.45 µL phosphate buffer (100 mM), 3.3 µL glyoxal) were incubated at 50°C for one hour, then chilled on ice. The RNA was separated by agarose gel electrophoresis at 100 V until the samples had run ⅔ of the way though the gel. The gel was blotted overnight onto positively charged nylon membrane (Roche Diagnostics, UK). The RNA was fixed by UV cross linking then 5% (v/v) acetic acid, stained in methylene blue buffer, rinsed in sterile water. The blot was pre-hybridised in pre-warmed DIG Easy Hyb (Roche Diagnostics, UK) for two hours and hybridised overnight at 50°C against a DIG DNA probe prepared using a PCR

DIG probe synthesis kit (Roche Diagnostics, UK). The membrane was then washed in a low stringency buffer (2 x SSC, 0.1% (w/v) SDS) at room temperature, high stringency buffer (0.1 x SSC, 0.1% (w/v) SDS) at 50°C and washing buffer (0.1 M maleic acid, 0.15 M NaCl, pH 7.5, 0.3% (v/v) Tween 20) at room temperature. The membrane was blocked with blocking solution (1% (w/v) blocking powder (Roche Diagnostics, UK) in 0.1 M maleic acid, 0.15 M NaCl (pH 7.5)) for one hour at 25°C and subsequently incubated with 75 mU/mL anti-DIG-AP antibody (Roche Diagnostics, UK) for 30 minutes. The membrane was washed in washing buffer followed by a three minute incubation in detection buffer (0.1 M Tris-HCl, 0.1 M NaCl, pH 9.5) and detection was performed with CDP-Star (Roche Diagnostics, UK) and using Kodak biomax MR film (Hertfordshire, UK).

2.3.16 Southern Analysis

Southerns were performed using a modification of the Southern technique [229]. Briefly, 1-5 µg of digested DNA was separated by agarose gel electrophoresis overnight. Following depurination (250 mM HCl), denaturation (0.5 M NaOH, 1.5 M NaCl), neutralisation (0.5 M Tris-HCl (pH 7.5), 1.5 M NaCl) and equilibration in 20 x SSC (3 M NaCl, 300 mM sodium citrate (pH 7)) the gel was blotted overnight onto positively charged nylon membrane (Roche Diagnostics, UK). The DNA membrane was fixed by UV cross-linking then rinsed in sterile water and allowed to dry. The blot was pre-hybridised in pre-warmed digoxigenin (DIG) Easy Hyb (Roche Diagnostics, UK) for two hours and hybridised overnight against a DIG DNA probe prepared from the PCR fragment of the target DNA using a PCR DIG probe synthesis kit (Roche Diagnostics, UK). The membrane was then washed in low stringency buffer (2 x SSC, 0.1% (w/v) SDS) at room temperature, high stringency buffer (0.5 x SSC, 0.1 % (w/v) SDS) at 65°C and washing buffer (0.1 M maleic acid, 0.15 M NaCl (pH 7.5), 0.3% (v/v) Tween 20) at room temperature. The membrane was blocked (1% (w/v) blocking powder (Roche Diagnostics, UK) in 0.1 M maleic acid, 0.15 M NaCl (pH 7.5)) for one hour at 25°C and subsequently incubated with 75 mU/mL anti-DIG-AP antibody (Roche Diagnostics, UK) for 30 minutes. The membrane was washed in washing buffer followed by a 3 minute incubation in detection buffer (0.1 M Tris-HCl, 0.1 M NaCl, pH 9.5) and detection was performed with CDP-Star (Roche Diagnostics, UK) and using Kodak biomax MR film (Hertfordshire, UK).

3 Confirmation of the Ace2p regulon

3.1 Overview

The principle aim of this study is to unearth the cause of the hypervirulent phenotype shown by *ace2 C. glabrata* cells by Kamran et al. [7]. Understanding the mechanisms behind *Candida* virulence is crucial to our ability to develop new strategies to combat the increasing microbial problem presented by pathogenic fungi. Recent data from genetic and proteomic research into *Candida* virulence should provide greater targeting accuracy for both new and existing antifungal treatments, on their own or in combination, toward essential fungal virulence mechanisms. It is also hoped that new directly-virulence related gene or protein targets can be identified for novel antifungal therapy development such as direct inhibition, degradation, or even signature masking to prevent septic shock. The fungal cell wall serves as the primary layer of defence in a hostile environment and is therefore a common antifungal target. It also serves as the anchor point that ties mother to daughter prior to cell separation and in cell separation deficient mutants. Several components of the cell separation machinery, which interact directly with the cell wall during budding, show Ace2p-dependent expression in *S. cerevisiae* [101]. It is hoped that by investigating the mechanism underlying the hypervirulent effect displayed by *ace2*, our understanding of the mechanics of a virulence moderating gene and its effects on or via the cell separation machinery will shed new light on the pathogenicity of *C. glabrata* and other *Candida* species, as resilient fungal pathogens.

Ace2p, a transcription factor regulated by the RAM network of proteins [135] and involved in the regulation and maintenance of the cell separation machinery, has been shown to cause a clumpy, cell separation deficient growth phenotype in its absence in both *S. cerevisiae* and *C. glabrata* [132]. In *C. glabrata*, *ace2* null cells have been shown to cause hypervirulence in a neutropenic murine model of systemic candidiasis, independent of the cell clumping shown on solid and liquid media [7]. Interaction data from *S. cerevisiae* has shown that Ace2p interacts with and influences the transcription of several genes [230]. Out of these genes several are known to form part of the cell separation machinery including the chitinase Cts1p, glucan β1,3-glucosidases Dse2p, Acf2p (previously known as Dse4p in *C. glabrata*) and Scw11p, plus an endoglucanase Egt2p.

The experiments contained within this chapter were designed to define a partial Ace2p regulon in *C. glabrata,* a collection of genes that show Ace2p-dependent expression, to be used throughout the rest of this project. In *S. cerevisiae* Ace2p and its homologue Swi5p, have been shown to exhibit transcription regulation over an overlapping group of genes [101, 133]. Included in the Ace2p dependent, Swi5p-independent, group were the genes *CTS1*, *DSE1*, *DSE2, DSE4* and *SCW11*, while the Swi5p-dependent, Ace2p-independent group included then genes *AIM44, PCL9, PIR1* and the uncharacterised gene *YNL046W* [101, 130]. A group of genes were also found to be regulated by both Ace2p and Swi5p, which included *AMN1*, *ASH1, DSE3, EGT2, RME1* and *SIC1* [101]. *BUD9* was also highlighted as showing possible Ace2p-dependent expression, having been shown to be daughter cell specific with G_1 expression, localised to the bud neck and to possess two adjacent potential Ace2p binding sequences in its promoter region in *C. glabrata* [143, 158, 171, 220]. Due to the lack of easily accessible and cost efficient microarray technologies for *C. glabrata* at the time [231], and the availability of the tet-regulated *ACE2* strain HLS119, it was decided that the Ace2p

dependence of a selection of *C. glabrata* homologues of genes shown to be Ace2p-dependent in their expression in *S. cerevisiae* [101], were to be analysed by Northern analysis. The mRNA transcripts from the previously uninvestigated genes *AMN1*, *ASH1*, *BUD9*, *DSE1*, *DSE2*, *DSE3*, *ACF2/DSE4*, *EGT2*, *RME1*, *SCW11α, SCW11β* and *SIC1* were shown to be undetectable in the absence of *ACE2* expression, while detectable in the presence of *ACE2* expression, and therefore transcriptionally regulated in an Ace2p-dependent manner in *C. glabrata.* Once Ace2p-dependent expression was confirmed for the set of 12 *C. glabrata* genes, they were identified as candidates for targeted deletion and virulence analysis in a systemic model of candidiasis going forward. The 12 genes therefore define the partial Ace2p regulon in *C. glabrata* as used throughout the rest of this study, which lacks the previously investigated *CTS1* [142] and possibly other genes yet to be found to be regulated by Ace2p.

The 12 genes of the partial Ace2p regulon studied within this project, have been shown play roles in cell separation, cell wall and cell cycle progression within *S. cerevisiae,* as detailed in section 1.7 of the Introduction. Briefly, Amn1p is an inhibitor of G-protein signalling involved in cell cycle progression and inhibition of mitotic exit through Tem1p binding, which prevents Cdc15p activation and subsequent activation of the MEN [144]. Ash1p plays a role in the control of cell fate through regulation of mating-type switching [149]. It directly inhibits *HO* expression, which prevents the mating-type locus switching between *a* and α. Bud9p is a cell membrane targeted protein involved in bud site selection, which acts as a cortical landmark in bipolar budding formation in diploid *S. cerevisiae* cells [155-157]. *DSE1* encodes a protein that currently has no known function. It shows little homology to other yeast genes, but is suggested to play a role in bud site selection; invasive growth, or mating [163, 166]. *DSE2, DSE4/ACF2, EGT2* and *SCW11* are all thought to encode cell wall targeted glucanases, and display daughter cell specific expression, localising to the bud neck [101, 127, 130, 195]. They therefore likely play a role in septum hydrolysis and cell separation [101, 127, 130, 195]. *DSE3* encodes another protein of unknown function. However, it has been shown to exhibit daughter cell specific expression and localisation to the bud neck. It therefore is likely to play a role in determining daughter cell fate [133, 143]. *RME1* encodes a zinc finger-like distal repressor protein, which regulates meiosis through inhibition of *IME1* expression [181-185]. Finally, *SIC1* encodes a cyclin-dependent kinase inhibitor, which binds to and inhibits the Cdk1p-Clbp histone kinase complexes, preventing premature transition to S-phase and ensuring genomic integrity [209, 210].

Another gene that displays Ace2p-dependent expression, *CTS1,* has already been investigated in *C. glabrata* for virulence phenotypes. Although *C. glabrata cts1* null mutants display a hypervirulent phenotype, CTS1 deletion does not completely explain the extent of the hypervirulent phenotype shown by *C. glabrata ace2* null mutants [142]. *CTS1* encodes a cell wall chitinase that is responsible for hydrolysis of the chitin septum for cell separation [102, 129].

In an effort to discover the effects of *ACE2* deletion within *C. glabrata*, in this chapter we will show that 12 genes display Ace2p-dependent expression and that out of those 12 genes, 10 contain potential Ace2p-binding sites within their promoter regions, indicating that they are likely directly transcriptionally regulated by Ace2p in *C. glabrata*. We will also define the partial Ace2p regulon to be used throughout the rest of this study in an effort to study the virulence moderating effect of Ace2p in *C. glabrata*.

3.2 Materials and methods

3.2.1 Northern analysis of Ace2p regulon in *C. glabrata* Ace2p tet-regulated strain

HLS119, a tet-regulatory mutant of *C. glabrata ACE2* [180], was grown overnight in 50 mL YPD at 37°C, 180 rpm shaking, with and without the presence of doxycycline (200 µg/mL). The cells were harvested by centrifugation and total RNA was then extracted via a modified acid phenol method, as described in section 2.3.9.

Northern analysis was then performed on the total RNA samples as described in section 2.3.15. Briefly, the total RNA was quantified by Nanodrop and then incubated at 50°C for one hour with DMSO, 100 mM phosphate buffer and glyoxal. The RNA was then loaded at 7 µg per well for gel electrophoresis and then blotted overnight. A DIG DNA-based probe was constructed for each gene using internal primers listed in Appendix 3 and a Roche DIG probe kit, according to the manufacturer's instructions. The membranes were then probed overnight, washed and developed on film.

3.2.2 Analysis of the upstream regions of Ace2p regulon genes in *C. glabrata* for potential Ace2p binding sites

C. glabrata gene sequences were downloaded from the Génolevures *C. glabrata* genome database [171] and analysed for potential consensus motifs using Gibbs analysis [232]. The sequences were also imported into Serial Cloner, version 2.1, Serial Basics, France. The open reading frames (ORFs) were then mapped, while the intergene regions upstream of the target genes highlighted with Gibbs analysis were analysed for potential Ace2p binding sites (ACCAGC) and their reverse complements as defined in *S. cerevisiae* by Dohrmann et al. [220]. The potential binding sites were then marked and the distance in base pairs to the start codon of the target gene was calculated for each.

3.3 Results

3.3.1 Ace2p transcriptionally regulates 12 genes

As discussed previously, expression and interaction data from *S. cerevisiae* [101, 133, 230] indicated that Ace2p could exhibit transcriptional control over a group of genes that includes 12 previously uninvestigated genes. To confirm that the genes selected to take forward for virulence analysis were part of the Ace2p regulon in *C. glabrata*, a tet-regulated mutant strain for *ACE2* (HLS119) was used to assay for the presence or absence of the 12 gene transcripts thought to exhibit Ace2p-dependent expression. Northern analysis was used to detect the presence of mRNA for each of the 12 genes in the presence or absence of Ace2p. The results show (Figure 3.1) that the expression of *AMN1*, *ASH1*, *BUD9*, *DSE1*, *DSE2*, *DSE3*, *ACF2* (*DSE4*), *EGT2*, *RME1*, *SCW11α, SCW11β*, and *SIC1* is Ace2p-dependent and therefore form part of the Ace2p regulon as defined here.

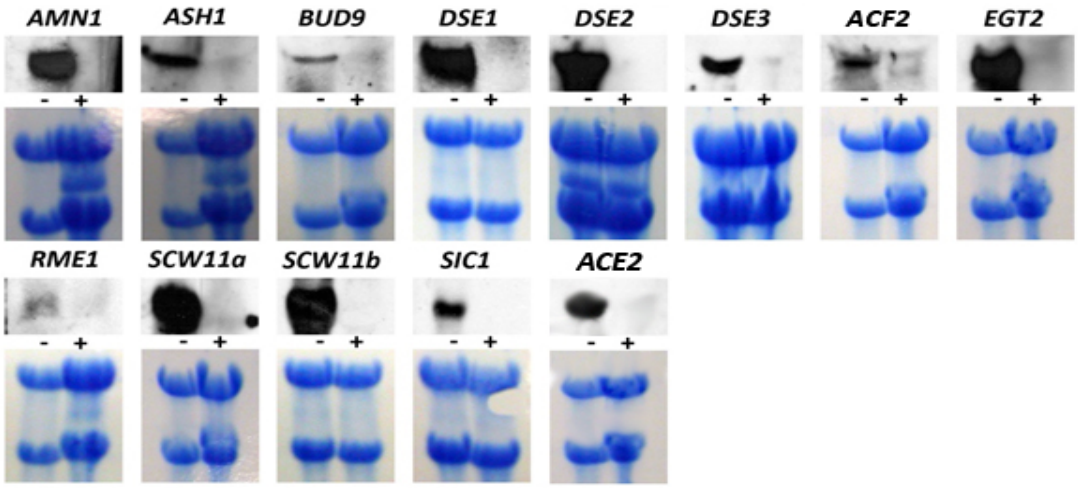


Figure 3.1 – *C. glabrata* Ace2p regulates the expression of 12 genes putatively involved in cell wall biology, daughter cell specific expression and cell cycle regulation. *C. glabrata* HLS119 was cultured overnight in YPD in the absence (-, *ACE2* de-repressed) and presence (+, *ACE2* repressed) of 200 mg/mL doxycycline. Total RNA was extracted using a modified acid phenol method, and 7 μg was loaded per lane. The upper panels show Northern analysis. Probes were constructed using internal primer pairs from the relevant gene indicated above each pair of panels. Primers are listed in Appendix 3. The lower panels show methylene blue loading controls. In the presence of doxycycline *ACE2* expression is repressed as shown by the lack of a band in the *ACE2* + lane. All other genes analysed show a loss of band in the absence of *ACE2* expression demonstrating that their expression in *C. glabrata* is dependent, either directly or indirectly, on Ace2p.

3.3.2 Potential Ace2p binding sites in the promoter regions of the Ace2p regulon genes

Having shown that the expression of *AMN1*, *ASH1*, *BUD9*, *DSE1*, *DSE2*, *DSE3*, *ACF2* (*DSE4*), *EGT2*, *RME1*, *SCW11α*, *SCW11β*, and *SIC1* is Ace2p-dependent in *C. glabrata*, the upstream regions of each of the Ace2p regulon genes was analysed for potential Ace2p binding sites (ACCAGC) as defined by Dohrmann et al. [220]. Using sequences from the Génolevures *C. glabrata* genome database [171] and Gibbs analysis [232] it was possible to identify a potential shared motif in 10 out of the 12 genes, as well as the *C. glabrata* homologue of *CTS1*. Screening of each of the 10 genes and *CTS1* showed at least two Ace2p binding sites within the intergene region upstream of the start codon and downstream of the next closest gene ORF. The site positions are mapped below in Figures 3.2a, b

and c in relation to the start codon of the target gene, with all co-ordinates and sizes measured in base pairs.

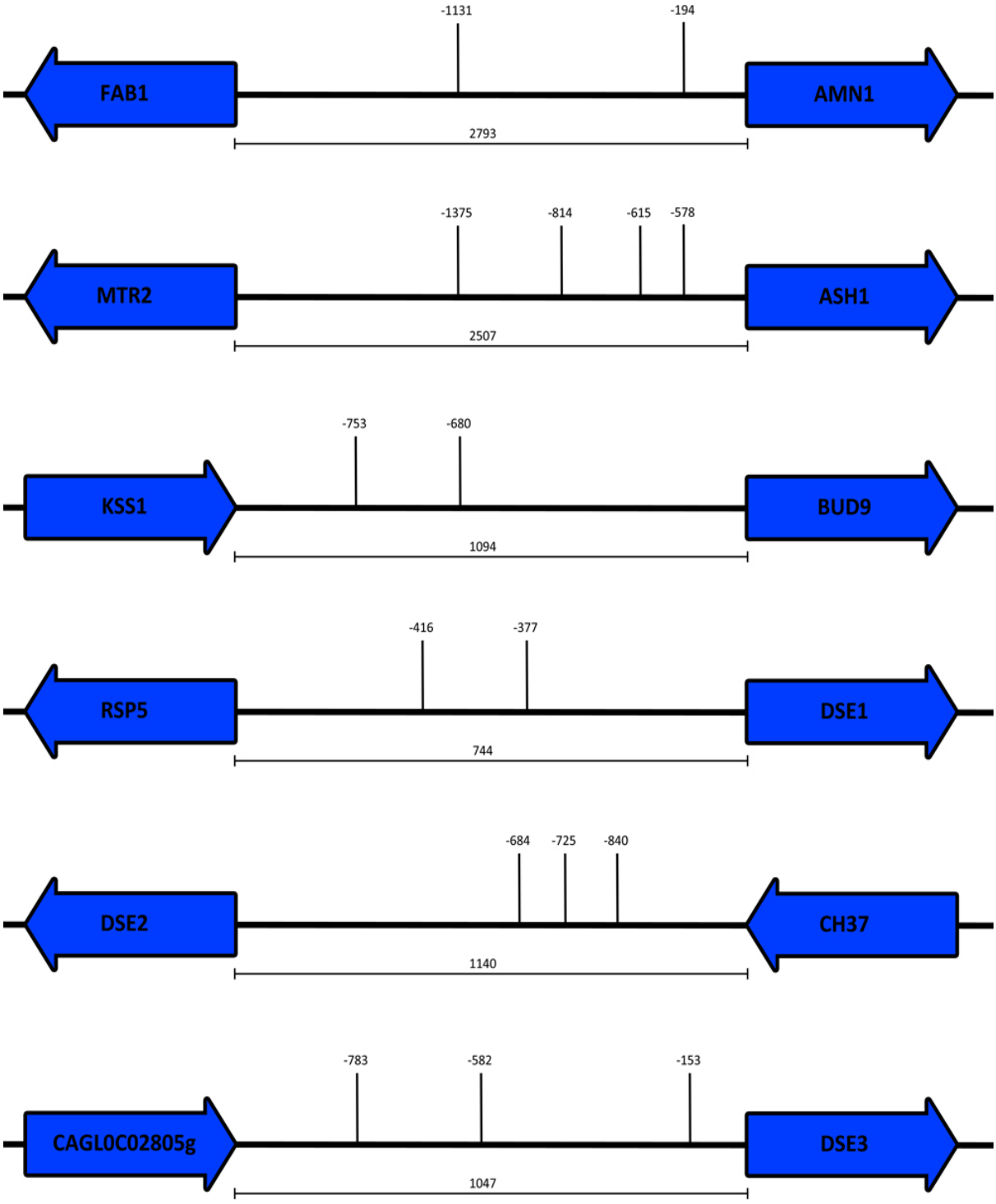


Figure 3.2a – Potenial Ace2p binding sites exist in the intergene regions upstream of the Ace2p regulon ORFs in *C. glabrata*. The intergene region upstream of the Ace2p regulon genes in *C. glabrata* is displayed with potential Ace2p binding sites (ACCAGC) [220] marked for position relative to the ATG of the Ace2p-dependent gene of interest. All co-ordinates and measurements are in base pairs, all sequences were taken from Génolevures [171]. Diagrams are not to scale. *AMN1* has two potential Ace2p binding sites between it and *FAB1*; *ASH1* has four potential Ace2p binding sites between it and *MTR2*; *BUD9* has two potential Ace2p binding sites between it and *KSS1*; *DSE1* has two potential Ace2p

binding sites between it and *RSP5*; *DSE2* has three potential Ace2p binding sites between it and *CH37*; and *DSE3* has three potential Ace2p binding sites between it and *CAGL0C02805g*.

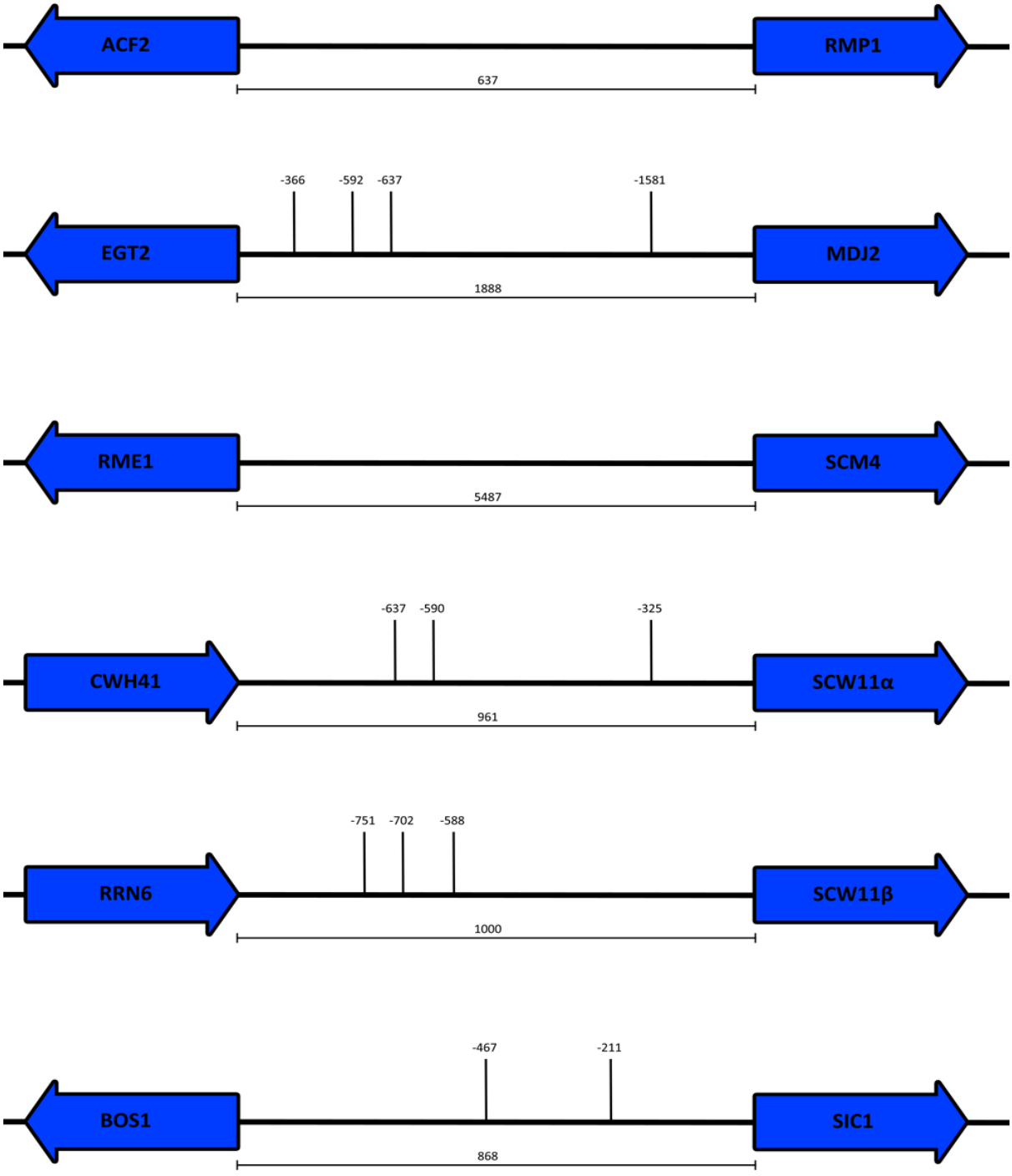


Figure 3.2b – Potenial Ace2p binding sites exist in the intergene regions upstream of the Ace2p regulon ORFs in *C. glabrata*. The intergene region upstream of the Ace2p regulon genes in *C. glabrata* is displayed with potential Ace2p binding sites (ACCAGC) [220] marked for position relative to the ATG of the Ace2p-dependent gene of interest. All co-ordinates and measurements are in base pairs, all sequences were taken from Génolevures [171]. Diagrams are not to scale. *ACF2* lacks any potential Ace2p binding sites between it and *RMP1*; *EGT2* has four potential Ace2p binding sites between it and *MDJ2*; *RME1* lacks any potential Ace2p binding sites between it and *SCM4*; *SCW11α* has three potential

Ace2p binding sites between it and *CWH41*; *SCW11β* has three potential Ace2p binding sites between it and *RRN6*; and *SIC1* has two potential Ace2p binding sites between it and *BOS1*.



Figure 3.2c – Four Potenial Ace2p binding sites exist in the intergene region upstream of *CTS1* in *C. glabrata*. The intergene region upstream of *CTS1* in *C. glabrata* is displayed with potential Ace2p binding sites (ACCAGC) [220] marked for position relative to the ATG. All co-ordinates and measurements are in base pairs, all sequences were taken from Génolevures [171]. Diagrams are not to scale. *CTS1* has four potential Ace2p binding sites between it and *CAGL0M09757g*.

3.3.3 Selection of target genes for deletion

Having identified that the 12 previously uninvestigated genes show Ace2p-dependent expression in *C. glabrata* as shown in Figure 3.1, all 12 genes were selected for genetic deletion for further study into the effects of the partial Ace2p regulon on virulence within chapter 4.

3.4 Discussion

The experiments outlined in this chapter have shown for the first time that a group of 12 genes exhibit Ace2p-dependent expression in *C. glabrata*. Through the use of Northern analysis and HLS119, a tetracycline transcriptionally-regulated mutant for *C. glabrata ACE2,* it was shown that in the presence of *ACE2* expression all 12 gene transcripts were detectable by Northern blot, illustrated in Figure 3.1. It was also shown that in the absence of *ACE2* expression under doxycycline conditions, all 12 gene transcripts were undetectable (Figure 3.1). It is therefore possible to define part of the Ace2p regulon in *C. glabrata* and confirm the Ace2p-dependence of the expression of the *C. glabrata* orthologues of *S. cerevisiae* genes *AMN1*, *ASH1*, *BUD9*, *DSE1*, *DSE2*, *DSE3*, *ACF2* (*DSE4*), *EGT2*, *RME1*, and *SIC1* in *C. glabrata*. The majority of these results show similarity to the observations of Doolin et al. in *S. cerevisiae* [101], in which it was found that some genes, *DSE1, DSE2* and *SCW11* display Ace2p-dependance independent of Swi5p. It is interesting to note however, that the results also indicate that in *C. glabrata, AMN1, ASH1, DSE3, EGT2, RME1* and *SIC1* show Ace2p-dependent expression independent of Swi5p and aren't detectable by Northern analysis in stationary cells in the absence of *ACE2* expression. Doolin et al. showed that in *S. cerevisiae,* the expression of the five genes is regulated by both Ace2p and Swi5p, requiring a double knockout of *ace2-swi5* to result in near total suppression of expression [101]. The difference in results between the two studies could indicate that the Ace2p-Swi5p transcriptional regulation overlap is different in *C. glabrata* than *S. cerevisiae*. The two budding yeast, although close genetic relatives, are distinct species and show differences in their cellular processes, not least of all virulence, drug resistance and ploidy (reviewed by Roetzer et al. [104]). Recently in *C. glabrata, EGT2* expression was suggested as being solely Ace2p-dependent and independent on Swi5p [180], which the results from this study corroborate.

The dependence difference could also be down to the disparity in cell growth phase at the time of harvesting in the experiments, as Doolin et al. harvested cells in mid-logarithmic or exponential growth phase, whereas the cells used in this study were harvested from overnight cultures, which were therefore in the stationary growth phase. It has been shown that at least one gene shows a different pattern of Ace2p-Swi5p regulation in exponential and stationary phase cells, with *EGT2* expression being shown to be Ace2p-dependent and Swi5p-independent in a saturated *S. cerevisiae* culture [133]. To fully clarify the difference in Ace2p-Swi5p dependent regulation between *C. glabrata* and *S. cerevisiae*, further analysis of gene expression from HLS119 cells in exponential growth phase would be needed. Northern analysis of the expression of *C. glabrata* genes with and without the presence of Swi5p would also clarify whether Swi5p plays a role in the regulation of the Ace2p regulon and Ace2p-dependent genes.

Having been shown to exhibit Ace2p-dependent expression, it has also been shown for the first time that *BUD9* expression is Ace2p-dependent in *C. glabrata*. Ace2p-dependent expression was hypothesised based on the presence of two adjacent Ace2p binding sites within the promoter region of *BUD9* [171], which have been shown to be required for Ace2p binding and direct transcriptional regulation [220].

The expression of two separate orthologues of *S. cerevisiae SCW11* was found to be Ace2p-dependent in *C. glabrata* and have been named *SCW11α* (*SCW11a*) (*CAGL0A01474g*) and *SCW11β* (*SCW11b*) (*CAGL0E02915g*) henceforth.

3.4.1 Ace2p transcriptional regulation: direct or indirect?

By studying the upstream promoter regions of the known Ace2p-dependent gene *CTS1* and the known Swi5p-dependent gene *HO* in *S. cerevisiae*, Dohrmann et al. showed that both Ace2p and Swi5p share a common binding site marked by a six base core sequence, ACCAGC [220]. They hypothesised that Ace2p bound co-operatively to two adjacent sites to enhance Ace2p-specificity and regulation of *CTS1* expression, although they could not prove co-operative binding *in vitro* [220]. They also suggested that Swi5p binding to Ace2p-dependent genes was inhibited by a negative sequence element that was downstream of the potential Ace2p binding sites [220], and suggested that an unmapped gene, which they referred to as *NCE3*, was responsible for Swi5p inhibition, due to the ability of Swi5p to induce *CTS1* expression in *ace2 nce3* double mutants [220]. Because the *NCE3* region is as yet unmapped in *S. cerevisiae*, it is not possible to search for a homologue in *C. glabrata*.

Although only DNA-binding assays like those originally implemented by Dohrmann et al. [220] could conclusively show the binding site of *C. glabrata* Ace2p and Swi5p, it is interesting to consider that due to the sequence conservation between *S. cerevisiae* and *C. glabrata* with respect to the *ACE2* and *SWI5* genes, BLAST scores of 413_{E}^{-115} and 209_{E}^{-84} respectively [171], it could be possible that the core of the binding sites for *C. glabrata* Ace2p and Swi5p could be similar or the same to that of the *S. cerevisiae* genes. To that end the upstream intergene sequence between *CTS1* and the next ORF, the uncharacterised gene *CAGL0M09757g*, was analysed in *C. glabrata* to see if potential Ace2p binding sites were detectable. As shown in Figure 3.2c, four potential Ace2p binding sites were found in the upstream region. The number, four instead of the three found in the *S. cerevisiae CTS1* promoter, the spacing between the potential sites, and the sequences surrounding them differ to what was found by Dohrmann et al. [220], but each of the potential sites were within relatively close proximity of one another, ranging between 116 and 26 base pairs separation. Using this knowledge combined with Gibbs analysis of the promoter regions of each of the target genes, once Ace2p-dependent expression was confirmed for the Ace2p regulon genes in *C. glabrata*, the next step was to look at their upstream regulatory regions to see if potential Ace2p binding sites exist in their promoters similar to the ones found for *CTS1*.

The results displayed in Figures 3.2a and 3.2b show that for 10 of the 12 genes, at least two potential Ace2p binding sites were found. Some of the potential Ace2p binding sites were placed outside of the assumed size of the normal upstream promoter region, being over 1000 base pairs from the start codon of the ORF. *AMN1* has an ACCAGC site at -1131 base pairs from the ATG, while another one is much closer to the ORF at -194 base pairs from the start codon. This could indicate that the promoter region of *AMN1* is quite large, extending past -1137 base pairs from the ATG. It could also show that *AMN1* only has one active potential Ace2p binding site in its promoter and that one is enough to exert control over its transcription. *ASH1* and *EGT2* also have one potential Ace2p binding site beyond 1000 base pairs upstream of the ATG at -1375 and -1581 respectively. However, both genes have three other potential Ace2p binding sites closer to the ORF and within close proximity to each other, the -814 to -578 and -637 to -366 base pair region respectively. Again this could indicate that the site located past 1000 base pairs upstream of the ORF is out of range of the promoter region and that potential Ace2p direct transcriptional regulation revolves around the three clustered together closer to the start codon. The other genes, *BUD9*, *DSE1*, *DSE2*, *DSE3*, *SCW11*α, *SCW11*β and *SIC1*, each have at least two potential Ace2p binding sites within 256 base pairs of each other. These

results, combined with their Ace2p-dependent expression, shows that this group of 10 genes, *AMN1*, *ASH1*, *BUD9*, *DSE1*, *DSE2*, *DSE3*, *EGT2*, *SCW11*α, *SCW11*β and *SIC1* are likely to be directly transcriptionally regulated by Ace2p binding to the promoter, although possibly not as positively compared to *CTS1* due to the larger spacing between potential binding sites. To confirm this assumption, further work using DNA binding assays to look at the protein-DNA interaction would be needed to prove whether Ace2p can bind directly to the DNA sequence in *C. glabrata* and therefore exert direct transcriptional regulation over the genes.

A look at the sequence of the other two genes of the Ace2p regulon, *ACF2* and *RME1*, shows that they lack any form of the Ace2p binding site in their upstream regions in *C. glabrata* (Figure 3.2b), while Gibbs analysis failed to detect any consensus motif found in the other 10 genes. Because both *ACF2* and *RME1* display Ace2p-dependent expression, but lack potential Ace2p binding sites in their promoter regions, it's likely that they are transcriptionally regulated through an intermediary or series of intermediaries and not directly by Ace2p. It is therefore possible that they are transcriptionally regulated by Ace2p via unknown proteins or mechanisms, which in turn exhibit control over *ACF2* and *RME1* expression. It's also possible that *ACF2* and *RME1* may be transcriptionally regulated by one or more of the other Ace2p-dependent genes in other potential parts of Ace2p regulon, or even by the uncharacterised Dse1p. Further analysis of the regulation of *ACF2* and *RME1*, their expression and the ability of other proteins to bind to their promoter regions *in vitro* and *in vivo* will be required to determine the mechanism of their Ace2p-dependent expression.

3.4.2 *C. glabrata ace2* clumping phenotype

In both *S. cerevisiae* and *C. glabrata*, *ace2* null mutants display a clumpy, cell separation deficient phenotype on both solid and liquid media [7, 129]. This is partly due to the lack of expression of the Ace2p-dependent chitinase, Cts1p, which hydrolyses the chitin components of the primary septum to allow for separation of mother and daughter cells [102]. Cts1p, although it plays a major structural degradation role in separating mother from daughter, isn't the sole arbiter of cell separation. Many other components form the cell separation machinery and are necessary for correct separation and dissemination of progeny in *S. cerevisiae* (reviewed by Yeong [125]). Glucanases and other cell wall associated proteins have been shown to be crucial to cell separation, displaying chains of linked cells or clumpy phenotypes when disrupted [125, 133]. It is thought that, in conjunction with Cts1p-mediated chitin degradation, glucanases act to hydrolyse the secondary septum and/or the surrounding cell wall, allowing mother and daughter to separate [125].

The extreme clumpy phenotype displayed by *ace2 C. glabrata* cells [7] is likely due to a combination of failure of expression and therefore loss of action of Cts1p and the cell wall glucanases. Looking at the reported functions of the *C. glabrata* Ace2p regulon homologues in *S. cerevisiae*, it is clear that at least some of them play a role in glucan hydrolysis as part of the cell separation machinery. Four genes, *DSE2*, *DSE4*, *EGT2* and *SCW11*, are thought to encode cell wall associated glucanases [101, 127, 130, 133, 134], which are bud neck localised [143] and are therefore thought to play a role in glucan hydrolysis. It is possible that they also play a role in cell wall maintenance. *C. glabrata ace2* mutants show a 16- and 38-fold increase in release of the inflammatory cytokines, IL6 and TNFα respectively, during infection [233], which have been shown to play a role in host defence against

Candida infections [234]. It has been suggested that the massive inflammatory cytokine over-stimulation by *ace2* mutants represents a septic shock response; an inappropriate extreme host response to infection, which can trigger multiple organ failure and subsequent death due in part to reduced blood volume and pressure (reviewed by Sriskandan and Cohen) [233, 235]. It is therefore possible that a change in the cell wall structure attributed to the absence of *DSE2*, *DSE4*, *EGT2* and *SCW11* expression, and therefore the cell wall activities of their encoded glucanases, in *ace2* cells causes a change in the immune recognition of the mutant *C. glabrata* cells, leading to the inappropriate immune response. To test this theory macrophage stimulation assays using individual *dse2*, *dse4*, *egt2* and *scw11*α and *scw11*β *C. glabrata* cells will be required, which will be able to show whether or not their absence of expression causes changes in the cytokine response *in vitro*.

Two other genes in the Ace2p regulon, *DSE1* and *DSE3* encode proteins of unknown function [133, 143]. Dse1p is thought to play a role in cell wall metabolism due to the increased cell wall targeted condition sensitivity shown by *dse1 S. cerevisiae* cells [101]. This could mean that the absence of Dse1p function may change cell wall metabolism, and therefore impact immune recognition in the host and also may contribute to the cell separation defect of *ace2* cells. It is unknown what the deletion of *DSE3* might cause, with regard to cell separation or immune recognition.

Bud9p has been highlighted as a cell wall associated cortical landmark, which plays a role in bipolar budding [155-157]. It is known to be cell wall anchored and to have a large, heavily glycosylated N-terminal extracytoplasmic domain [156], which in theory, may contribute to immune recognition and cell wall structure. This means that absence of *BUD9* expression may cause changes in the cell wall structure and therefore alter the host pathogen interaction. Its role in the cell separation defect displayed by *ace2 C. glabrata* cells is unknown; however, its absence may disrupt the normal budding pattern of *C. glabrata* cells.

The remaining genes of the Ace2p regulon, *AMN1*, *ASH1*, *RME1* and *SIC1* all play a role in cell cycle control, and have no known direct effect on the cell wall or cell separation. Amn1p is a regulator of mitotic exit that blocks G-protein signalling, inhibiting MEN and allowing the cell to progress into START and S-phase [144]. The absence of *AMN1* expression may play a role in the clumpy phenotype by slowing the growth of cells and causing cell cycle arrest or delays. Equally *amn1* causes cells to arrest, which could mean that it reduces budding frequency and therefore could also act to inhibit the clumpy phenotype. It is unclear what role Amn1p would play in virulence or immune activation. Ash1p has been shown to be involved in the control of mating-type switching through the repression of *HO* [147]. It is unclear what role Ash1p has in *C. glabrata* due to its lack of a mating-locus, or what affect its deletion would have on immune activation or virulence. Rme1p represses *IME1* expression and therefore the initiation of meiosis [181-185]. It has also been shown to promote mitosis through Cln2p activation [189, 190]. *S. cerevisiae rme1* mutants have been shown to have reduced steady-state levels of *CLN2* expression and increased cell size [189, 190]. Absence of *RME1* expression could therefore affect cell size and rate of budding, although it is unclear how this could promote a clumpy phenotype. Finally, Sic1p has been shown to bind to and inhibit the Cdk1p-Clbp histone kinase complexes preventing premature progression to S-phase and ensuring genomic integrity [209, 210]. *S. cerevisiae sic1* mutants have been shown to exhibit partial mitotic arrest, premature DNA replication and genome instability [208]. It is unknown what contribution this could make to the *ace2* clumpy phenotype, but it is possible that it could increase the generation time and therefore

reduce the number of budding cells progressing through mitotic arrest, which could reduce the clumpy phenotype.

For the first time in *C. glabrata*, it has been shown that 12 genes have Ace2p-dependent expression and that of the 12 genes, 10 of them are likely to be directly transcriptionally regulated by Ace2p binding. It is now possible to use that data to expand upon our understanding of Ace2p within the cell cycle, cell separation and virulence. Concurrently, now that the core of potential Ace2p binding sites has been shown to exist within the promoter regions of Ace2p expression dependent genes in *C. glabrata*, it is also possible to screen genes within the *C. glabrata* genome for potential direct Ace2p transcriptional regulation via their sequence alone, as was shown with the investigation of *BUD9*.

The extreme hypervirulence shown by *ace2* in *C. glabrata* [7] is most likely attributable to a combination of gene absences and removal of their biological functions or physical interactions. It is also possible that Ace2p exerts direct and indirect control over more genes than those defined here, and that it is their change in expression levels that causes the hypervirulent phenotype.

In chapter 4, to investigate the hypothesis that the partial Ace2p regulon, as defined within this chapter, is responsible for the hypervirulent phenotype displayed by *C. glabrata ace2* cells, deletion of each of the named genes, *AMN1*, *ASH1*, *BUD9*, *DSE1*, *DSE2*, *DSE3*, *ACF2*, *EGT2*, *RME1*, *SCW11α, SCW11β*, and *SIC1*, will be carried out. The effects of their deletion with regard phenotype, sensitivity to stress conditions, and growth rate will be studied, in an effort to discern the effect of their absence on *C. glabrata*. The null mutants will also be studied with regard for virulence in both *in vitro* and *in vivo,* using immune stimulation assays and a murine model of systemic candidiasis, to unearth the potential for each of the 12 genes to be antivirulence or virulence-moderating genes.

An investigation into the uncharacterised gene *DSE1* will be carried out in chapter 5 using both *C. glabrata* and *S. cerevisiae* in an effort to further our understanding of the cellular function and role or roles that Dse1p has within *C. glabrata*. To that end phenotypic analysis, sensitivity screening and a study of cell polarity using *dse1* nulls from both species of yeast will be conducted. Cellular localisation of Dse1p within known interactor [165] nulls and structural prediction of Dse1p from *C. glabrata* will also be employed in an attempt to gather enough data to identify possible roles, and dismiss others suggested in the literature, for the previously unknown function of Dse1p.

4 Study of the Ace2 regulon and its role in hypervirulence

4.1 Overview

4.1.1 Conventional virulence factors in *C. glabrata*

Our understanding of the virulence of *C. glabrata* is in its infancy. Nevertheless, certain virulence factors for *C. glabrata* have been identified and discussed in the Introduction. Briefly, phenotypic switching has been suggested to play a role in host environment adaptation and therefore virulence, displaying selectivity to anatomical site in clinical isolates [77, 84]. Adhesion is also known to play an important role in *C. glabrata* virulence and biofilm formation, mediated by the *EPA* family of genes, which are GPI-anchored cell wall proteins similar to the *ALS* and *HWP1* genes found in *C. albicans* [85]. *In S. cerevisiae,* the *EPA* genes are predominantly located at sub-telomeric loci and are subject to *SIR*-dependent transcriptional silencing (reviewed by Rusche et al. [236]). It is thought that the transcriptional silencing found in *S. cerevisiae* is maintained within *C. glabrata* and that NAD^+ is required as a co-substrate for the Sir2p-dependent deacetylation reaction that leads to repression of *C. glabrata EPA* genes [89, 92]. Because *C. glabrata* lacks the ability to synthesise NAD^+ from tryptophan, relying solely on salvaging pathways from vitamin precursors such as nicotinic acid, nicotinamide and nicotinamide ridoside, it has been shown that in environments low in NAD^+ vitamin precursors, such as the urine tract, cause the derepression of *EPA* expression and an increase in adherence and therefore virulence [89]. The highly conserved *STE*-family of genes have also been suggested to play a role in *C. glabrata* virulence with *ste11*, *ste12* and *ste20* null mutants all showing attenuated virulence in murine models of disseminated candidiasis [81-83]. Ste12p, a highly conserved transcriptional regulator, is activated by the MAP kinase signalling cascade and is involved in pseudohyphal formation in *S. cerevisiae*, something that has yet to be proven as playing a role in *C. glabrata* pathogenesis due to the lack of clinical isolates displaying pseudohyphal formation [77]. *STE11* and *STE20* encode protein kinases that play important roles in several signalling cascades including the response to hypertonic stress, an important factor in the host-pathogen interaction and therefore unsurprisingly both proteins are required for wild type levels of virulence [82, 83].

C. glabrata's virulence has often been put down to its innate and adaptive resistance to antifungals, especially azoles, which target the ergosterol biosynthesis pathway. *C. glabrata* achieves resistance though over expression of two ABC transporter genes *CDR1* and *CDR2*, which are overexpressed causing azole efflux [18]. The target of azoles, the lanosterol 14-α-demethylase encoded by *ERG11*, can also be upregulated in response to azole attack, which helps *C. glabrata* stave off the effects of ergosterol synthesis disruption [19]. Finally, *C. glabrata* can also increase free ergosterol concentration through permanent or reversible loss of mitochondrial function, which not only aids in resistance to azoles, but also to drugs that target and bind to ergosterol directly such as amphotericin-B and the rest of the polyene family [94]. Another interesting virulence related factor in *C. glabrata*'s favour over other *Candida* species is its reduced immune activation footprint [100]. Failure to induce appropriate levels of immune cytokine release could be the root of the difficulty patients and clinicians experience in clearing *C. glabrata* infection from the immune compromised.

4.1.2 A novel antivirulence gene in *C. glabrata*

In 2004, a novel antivirulence or virulence-moderating gene was discovered in *C. glabrata* by Kamran et al. in *ACE2* [7]. This was the first discovery of an antivirulence gene in *Candida* species, and was characterised by an extreme hypervirulence displayed by *ace2* cells, causing 100% mortality in under 18-hours post infection in a neutropenic murine model of disseminated candidiasis [7]. *ACE2*, as previously described, encodes a transcriptional regulator of the cell separation machinery that hydrolyses the septum and allows for dissemination of progeny [101, 102]. The hypervirulence effect was demonstrated to be independent of the clumpy, cell separation deficient phenotype displayed by *ace2* cells, through manual separation of *ace2* cells by enzymatic digestion of the primary septum using chitinase prior to inoculation [7]. This conclusion was reinforced by the finding that *ace2* null cells were avirulent in immunocompetent mice [237], and by the discovery of other clumpy strains of *C. albicans* that have been shown to be avirulent *in vivo* such as *tup1* and *och1* [238, 239].

As a fungal pathogen, it seems illogical on an evolutionarily scale to maintain a gene that causes such a rapid and extreme hypervirulence advantage in its absence, unless its product has a crucial role in cell survival and dissemination. As a cell separation machinery transcriptional regulator, it is therefore likely that *ACE2*'s advantage must lie in its ability to aid dissemination of progeny. In fact *C. glabrata*, unlike *S. cerevisiae* or *C. albicans*, lacks any known form of true morphological switching between yeast and hyphal states, other than the formation of pseudohyphae *in vitro* [31]. Therefore, budding and subsequent cell separation is *C. glabrata*'s only currently known mode of dissemination and therefore transmission, which might explain why such a potent antivirulence gene is maintained as an evolutionary advantage [233].

4.1.3 The Ace2p regulon

As previously discussed Ace2p controls a suite of previously uninvestigated genes in *C. glabrata* as defined in Chapter 3 as the partial Ace2p regulon. The Ace2p regulon includes many of the genes of the cell separation machinery, including genes that encode cell wall associated glucanases (*DSE2, ACF2* (*DSE4*)*, EGT2, SCW11*α and *SCW11*β) and a chitinase (*CTS1*) [101, 102, 127, 129, 130, 195]. Ace2p also controls the transcription of a regulator of mitotic exit (*AMN1*) [144], a regulator of mating type-switching, which is a process that as yet hasn't been shown to exist in *C. glabrata,* (*ASH1*) [149], a bud site selection marker (*BUD9*) [155-157], a regulator of meiosis (*RME1*) [181-185], and a cyclin-dependent kinase inhibitor involved in control of the G_1 to S-phase transition (*SIC1*) [209, 210]. Two genes of currently unknown function are also transcriptionally regulated by Ace2p in *C. glabrata*: *DSE1* and *DSE3*. *DSE1* has recently been suggested as playing a role in cell separation, bud site selection, invasive growth or mating in *S. cerevisiae*. *DSE3* shows daughter cell specific expression and is localised to the bud neck, and therefore has been proposed to play a role in determining daughter cell fate. *CTS1* has already been investigated in *C. glabrata* in relation to its potential antivirulence effect [142], and although it was shown to cause a hypervirulent phenotype in its absence, does not fully explain the extent of the *ace2* hypervirulence effect [7]. The partial Ace2p regulon genes have no obvious direct link with antivirulence from their characterisation in *S. cerevisiae* and other species. Therefore investigation of the virulence moderating potential of the

partial Ace2p regulon gene required deletion of each of the genes controlled by Ace2p and screening for hypervirulence compared to the wild type *C. glabrata* strain, Cg2001.

To this end, two methods of gene deletion were employed, one using a fusion PCR methodology [240] and another using a simpler one-step PCR method [241]. Deletions were created in either Cg *his3* or Cg$\Delta\Delta\Delta$ background strains by electroporation as described in section 2.3.11. Once deletions were confirmed via PCR and Southern analysis, the mutants were taken forward into phenotypic and virulence screening. Deletion mutants were created for the first time in *C. glabrata* for 10 genes including: *AMN1, ASH1, BUD9, DSE1, DSE3, ACF2, EGT2, RME1, SCW11β* and *SIC1*. The other two genes *DSE2* and *SCW11*α remain undisrupted. None of the gene deletions created in this chapter showed significant phenotypic differences from their parental strains under solid agar and growth rate screening, apart the from a mild cell separation defect displayed by both *dse1* and *egt2.*

Historically, a murine model of candidiasis employing neutropenic male CD1 mice has been used to test for *C. glabrata* virulence [7, 81]. After initial pilot studies, a modified murine model of virulence was used to screen the 10 individual Ace2p regulon deletions, with six different mutants displaying significantly increased virulence when compared to the *C. glabrata* wild type. The mutants *dse3, acf2, egt2, rme1, scw11β* and *sic1* all induced 100% mortality after 5 days compared with only 40% over 14 days for the wild type. The results indicate that the extreme hypervirulence observed in *C. glabrata ace2* mutants is indeed a multifactorial effect, with combined gene absences creating a synergistic effect on the virulence level of *C. glabrata*.

4.2 Materials and Methods

4.2.1 Construction of *ash1, bud9, dse1, dse3, egt2* and *rme1* null mutants by fusion PCR

Deletion of *C. glabrata* target genes was performed via a modified high-throughput fusion PCR gene deletion technique [240]. A deletion cassette including a NAT resistance marker was created by fusion PCR and transformed into the *C. glabrata his3* strain. Barcodes from the *S. cerevisiae* gene deletion project [242, 243] have been included for genes with *S. cerevisiae* homologues. The approach is schematically demonstrated below. Primers, which are listed in Appendix 3, are indicated with their approximate relative position to the ORF of the gene in question.

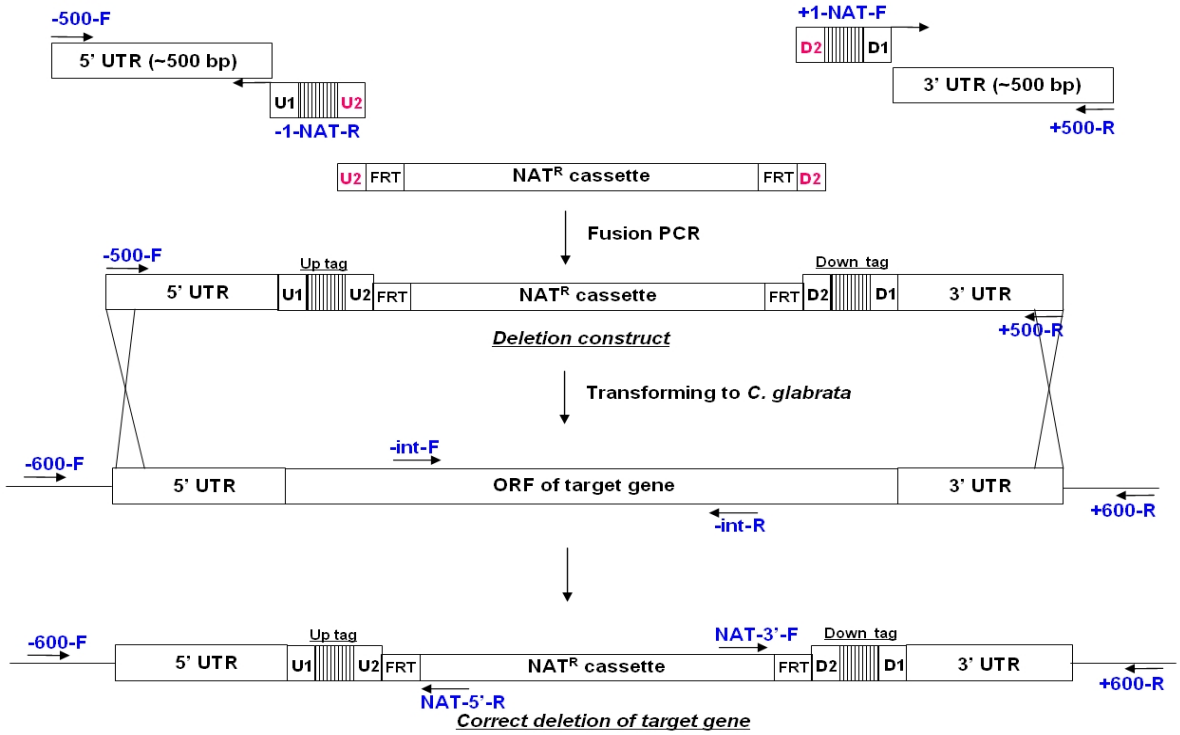


Figure 4.1 – Construction of *C. glabrata* deletion mutants by homologous recombination of a fusion PCR deletion cassette. Primers, as listed in Appendix 3, were designed to produce products containing 500 bp of homology with the 5' and 3' UTRs of the target gene and 20 bp tails of the U2 and D2 regions of the NAT^R cassette. The deletion cassette was then created by fusion PCR essentially as described by [240, 244] and transformed into the *C. glabrata his3* strain using electroporation. Flippase recognition target (FRT) sites for marker recycling and barcodes from the *S. cerevisiae* gene deletion project [242, 243] have been included for genes with *S. cerevisiae* homologues.

The deletion cassette was made through a fusion PCR process. First the 5' and 3'UTR regions of the target gene were amplified using primer pairs, -500-F and -1-NAT-R or +-NAT-F and +500-R, including an up or down tag which have been taken from the *S. cerevisiae* ORF barcoding system [243]. The 5' and 3' UTRs with homology in the U2 and D2 regions, as indicated above, are then fused with the NAT resistance cassette to create the deletion cassette [245]. The deletion cassette was transformed into *C. glabrata his3* and selected on -HIS dropout media supplemented with CloneNAT at 200 µg/mL (nourseothricin, Werner BioAgents, Germany). Colony PCR and Southern analysis were used to confirm gene deletion.

A Southern DNA probe specific to the NAT resistance cassette was constructed via PCR using the DIG PCR fluorescence labelling kit (Roche, UK) according to the manufacturer's instructions, using the primers listed in Appendix 3.

The *C. glabrata ash1* null mutant was constructed by removing 2229bps of the *C. glabrata ASH1* gene (-68 to +2161 with respect to the start codon, the stop codon is at +2136) via homologous recombination using a NAT resistance cassette as a selectable marker producing *C. glabrata* SRSG2 (*his3, ash1::*NAT_R).

The *C. glabrata bud9* null mutant was constructed by removing 1692bps of the *C. glabrata BUD9* gene (-29 to +1663 with respect to the start codon, the stop codon is at +1587) via homologous recombination using a NAT resistance cassette as a selectable marker producing *C. glabrata* SRSG3 (*his3, bud9::*NAT_R).

The *C. glabrata dse1* null mutant was constructed by removing 1747bps of the *C. glabrata DSE1* gene (-4 to +1743 with respect to the start codon, the stop codon is at +1701) via homologous recombination using a NAT resistance cassette as a selectable marker producing *C. glabrata* SRSG4 (*his3, dse1::*NAT_R).

The *C. glabrata dse3* null mutant was constructed by removing 1364bps of the *C. glabrata DSE3* gene (-44 to +1320 with respect to the start codon, the stop codon is at +1314) via homologous recombination using a NAT resistance cassette as a selectable marker producing *C. glabrata* SRSG6 (*his3, dse3::*NAT_R).

The *C. glabrata egt2* null mutant was constructed by removing 2099bps of the *C. glabrata EGT2* gene (-41 to +2058 with respect to the start codon, the stop codon is at +2028) via homologous recombination using a NAT resistance cassette as a selectable marker producing *C. glabrata* SRSG8 (*his3, egt2::*NAT_R).

The *C. glabrata rme1* null mutant was constructed by removing 1850bps of the *C. glabrata RME1* gene (-56 to +1794 with respect to the start codon, the stop codon is at +1641) via homologous recombination using a NAT resistance cassette as a selectable marker producing *C. glabrata* SRSG9 (*his3, rme1::*NAT_R).

For a list of primers used in the creation of the Ace2p regulon null mutants please see Appendix 3.

4.2.2 Construction of *amn1, acf2, scw11b* and *sic1* null mutants by Edlind method

Construction of four of the remaining partial Ace2p regulon genes was performed using a modified Edlind method [241]. Briefly, primer pairs and a one-step PCR were used to create the deletion cassette, which included 60 bps of homology ending at the start and stop codons of the target gene plus a *S. cerevisiae TRP1* deletion marker [108]. The deletion cassette was then transformed into *C. glabrata ΔΔΔ* via electroporation and selected for on -TRP dropout media. Colony PCR and Southern analysis were used to confirm gene deletion.

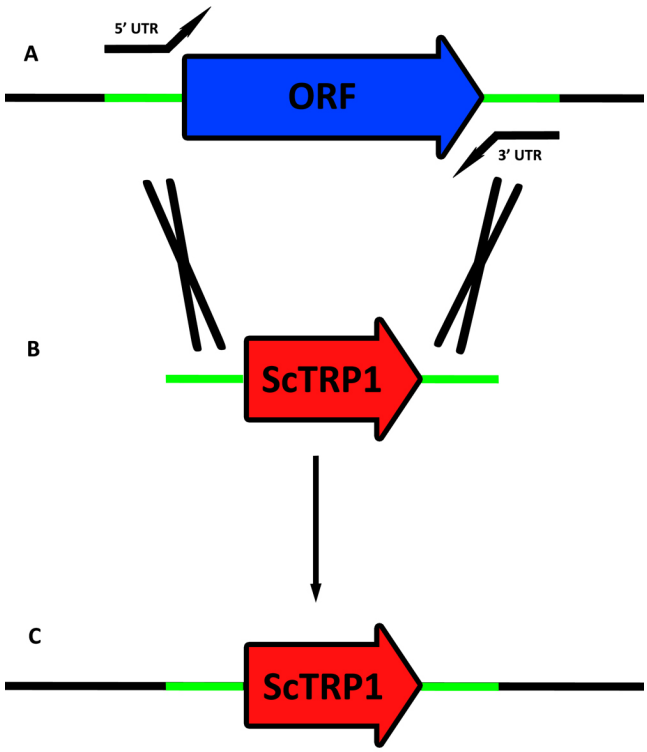


Figure 4.2 – Construction of *C. glabrata* deletion mutants by homologous recombination of a one-step Edlind method disruption cassette. A. Primers were designed with 20 bp of homology to the Sc*TRP1* marker and containing 60 bp of homology to the 5' and 3' UTRs of the target gene up to the start and stop codons. B. The disruption cassette was created via PCR to create the Sc*TRP1* marker flanked by 60 bp of homology to the 5' and 3' UTR of the target ORF. C. The disruption cassette was transformed into the *C. glabrata ΔΔΔ* strain using electroporation for disruption of the target ORF by homologous recombination.

A Southern DNA probe specific to *S. cerevisiae TRP1* was constructed via PCR using the DIG PCR fluorescence labelling kit (Roche, UK) according to the manufacturer's instructions, using the primers listed in Appendix 3.

The *C. glabrata amn1* null mutant was constructed by removing 1536bps of the *C. glabrata AMN1* gene (1 to +1536 with respect to the start codon, the stop codon is at +1533) via homologous recombination using a *S. cerevisiae TRP1* gene as a selectable marker producing *C. glabrata* SRSG1 (*his3, trp1, leu2, amn1*::*TRP1*).

The *C. glabrata acf2* null mutant was constructed by removing 2313bps of the *C. glabrata ACF2* gene (1 to +2313 with respect to the start codon, the stop codon is at +2310) via homologous

recombination using a *S. cerevisiae TRP1* gene as a selectable marker producing *C. glabrata* SRSG7 (*his3, trp1, leu2, acf2*::*TRP1*).

The *C. glabrata scw11β* null mutant was constructed by removing 1497bps of the *C. glabrata SCW11β* gene (1 to +1497 with respect to the start codon, the stop codon is at +1494) via homologous recombination using a *S. cerevisiae TRP1* gene as a selectable marker producing *C. glabrata* SRSG11 (*his3, trp1, leu2, scw11β*::*TRP1*).

The *C. glabrata sic1* null mutant was constructed by removing 849bps of the *C. glabrata SIC1* gene (1 to +849 with respect to the start codon, the stop codon is at +846) via homologous recombination using a *S. cerevisiae TRP1* gene as a selectable marker producing *C. glabrata* SRSG12 (*his3, trp1, leu2, sic1*::*TRP1*).

4.2.3 Reconstitution of *C. glabrata* gene deletions

Reconstitution of *C. glabrata* Ace2p regulon gene deletions that showed hypervirulence when compared to the parental strain was performed using the vector pBM51 [Biao Ma (personal communication)] due to the time constraints placed on this stage of the project, the reliability and availability of the pBM51 plasmid and the relative speed and ease of plasmid-based reconstitution. Briefly, primer pairs were used to create a PCR product containing only the target gene ORF from *C. glabrata* flanked by suitable digestion sites, allowing use of the pBM51 plasmid, driving the target gene expression using its *PGK1* promoter and *HIS3* 3' UTR. The poly A tails were then added to the PCR product, which was then ligated into the TA TOPO pCR2.1 vector using the TA TOPO cloning kit (Bioline, UK) as per the manufacturer's instructions and transformed into One-Shot TOP10 *E. coli* chemically competent cells (Bioline, UK) as per the manufacturer's instructions. A successfully cloned colony was confirmed via colony PCR, then grown overnight, and then the vector was extracted via a Mini-prep kit (Sigma, UK) as per the manufacturer's instructions. The target ORF was then excised from the pCR2.1 vector using unique restriction digest sites, as detailed below and described in section 2.3.5, and gel extracted using a Gel extraction kit (Sigma, UK). The ORF fragment was then ligated into pBM51 using Quick-Stick Ligase (Bioline, UK) and then transformed into *E. coli.* The vector was then extracted via Mini-prep and confirmed via PCR. The correct sequence of the target ORF and vector was confirmed via sequencing. The confirmed ORF plasmid was then transformed into the target null using electroporation and grown on selective media. The reconstituted strain was then restreaked twice from single colonies.

Reconstituted gene expression was confirmed via Northern analysis using internal probes for the target ORF, as described in section 2.3.15, comparing the null mutant with the reconstituted strain.

The *C. glabrata DSE3* reconstitution plasmid was constructed by cloning 1317 bps of the *C. glabrata DSE3* gene (1 to +1317 with respect to the start codon, the stop codon is at +1317) into pCR2.1 flanked by Sal1 and Xma1 restriction sites at the 5' and 3' ends respectively. The *DSE3* ORF was then excised from pCR2.1 via restriction digest with Sal1 and Xma1 and then ligated into pBM51 to create *C. glabrata* pSRSGR6 (*HIS3, DSE3*). pSRSGR6 was then transformed into *C. glabrata* SRSG6 to create *C. glabrata* SRSG6R (*his3, dse3*::NAT_R, pSRSGR6 (*HIS3, DSE3*)).

The *C. glabrata AFC2* reconstitution plasmid was constructed by cloning 2031 bps of the *C. glabrata ACF2* gene (1 to +2031 with respect to the start codon, the stop codon is at +2031) into pCR2.1 flanked by Sal1 and Xma1 restriction sites at the 5' and 3' ends respectively. The *ACF2* ORF was then excised from pCR2.1 via restriction digest with Sac1 and Xma1 and then ligated into pBM51 to create *C. glabrata* pSRSGR7 (*HIS3, ACF2*). pSRSGR7 was then transformed into *C. glabrata* SRSG7 to create *C. glabrata* SRSG7R (*his3, trp1, leu2, acf2*::*TRP1,* pSRSGR7 (*HIS3, ACF2*), YPCIII (*LEU2*)).

The *C. glabrata EGT2* reconstitution plasmid was constructed by cloning 1317 bps of the *C. glabrata EGT2* gene (1 to +1317 with respect to the start codon, the stop codon is at +1317) into pCR2.1 flanked by Sal1 and Xma1 restriction sites at the 5' and 3' ends respectively. The *EGT2* ORF was then excised from pCR2.1 via restriction digest with Sal1 and Xma1 and then ligated into pBM51 to create *C. glabrata* pSRSGR8 (*HIS3, EGT2*). pSRSGR8 was then transformed into *C. glabrata* SRSG8 to create *C. glabrata* SRSG8R (*his3, egt2*::NAT_R, pSRSGR8 (*HIS3, EGT2*)).

The *C. glabrata RME1* reconstitution plasmid was constructed by cloning 1644 bps of the *C. glabrata RME1* gene (1 to +1644 with respect to the start codon, the stop codon is at +1644) into pCR2.1 flanked by Sal1 and Xma1 restriction sites at the 5' and 3' ends respectively. The *RME1* ORF was then excised from pCR2.1 via restriction digest with Sal1 and Xma1 and then ligated into pBM51 to create pSRSGR9 (*HIS3, RME1*). pSRSGR9 was then transformed into *C. glabrata* SRSG9 to create *C. glabrata* SRSG9R (*his3, rme1*::NAT_R, pSRSGR9 (*HIS3, RME1*)).

The *C. glabrata SCW11β* reconstitution plasmid was constructed by cloning 1497 bps of the *C. glabrata SCW11β* gene (1 to +1497 with respect to the start codon, the stop codon is at +1497) into pCR2.1 flanked by Sal1 and Xma1 restriction sites at the 5' and 3' ends respectively. The *SCW11β* ORF was then excised from pCR2.1 via restriction digest with Sal1 and Xma1 and then ligated into pBM51 to create pSRSGR11 (*HIS3, SCW11β*). pSRSGR11 was then transformed into *C. glabrata* SRSG11 to create *C. glabrata* SRSG11R (*his3, trp1, leu2, scw11β*::*TRP1,* pSRSGR11 (*HIS3, SCW11β*), YPCIII (*LEU2*)).

The *C. glabrata SIC1* reconstitution plasmid was constructed by cloning 849 bps of the *C. glabrata SIC1* gene (1 to +849 with respect to the start codon, the stop codon is at +849) into pCR2.1 flanked by EcoR1 and Xma1 restriction sites at the 5' and 3' ends respectively. The *SIC1* ORF was then excised from pCR2.1 via restriction digest with EcoR1 and Xma1 and then ligated into pBM51 to create pSRSGR12 (*HIS3, SIC1*). pSRSGR12 was then transformed into *C. glabrata* SRSG12 to create *C. glabrata* SRSG12R (*his3, trp1, leu2, sic1*::*TRP1,* pSRSGR12 (*HIS3, SIC1*), YPCIII (*LEU2*)).

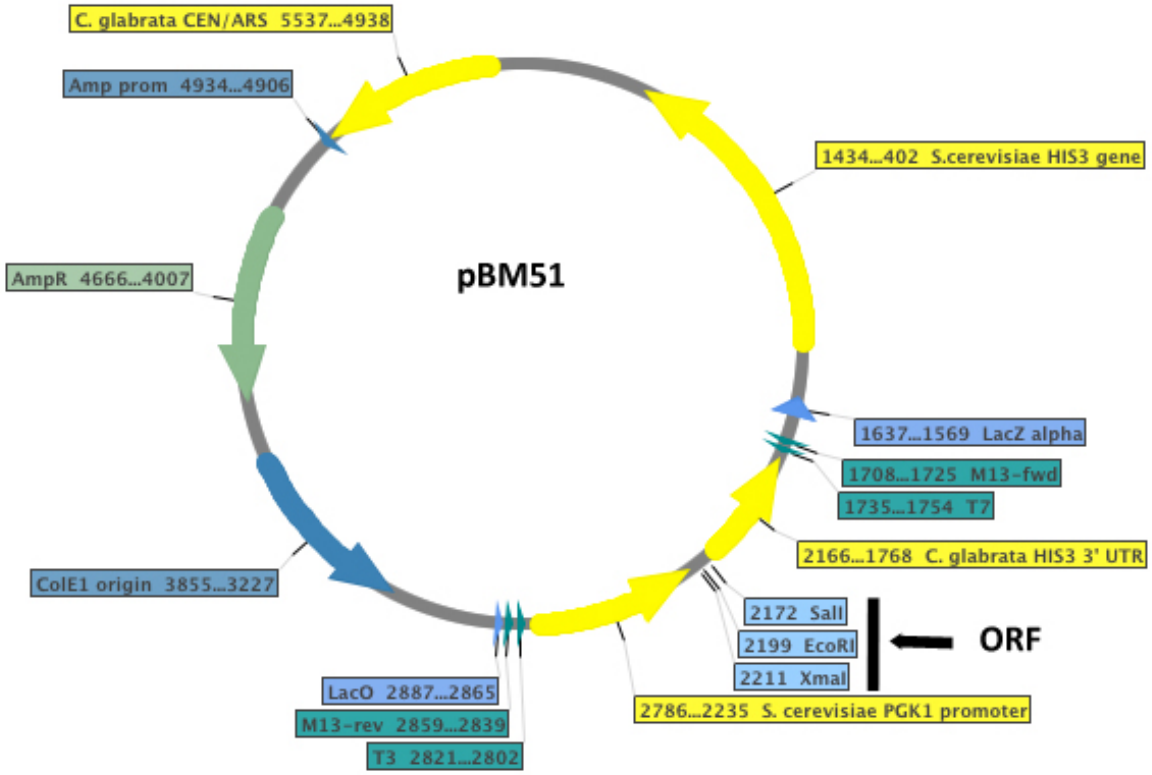


Figure 4.3 – Plasmid map of pBM51. The target ORF for reconstitution was cloned into pBM51 [Biao Ma (personal communication)] between either 2172 (Sal1) and 2211 (Xma1) or between 2199 (EcoR1) and 211 (Xma1) using the respective restriction digests.

4.2.4 Solid agar phenotypic screen

A series of phenotypic assays, described by Hampsey et al. [246] and listed in Table 4.1 below, were carried out in an attempt to characterise putative roles for these proteins.

Strains were grown overnight in 150 µL YPD in a 96-well plate at 37°C with shaking at 120 rpm. Strains were counted under a Nikon 80i eclipse microscope using a Neubauer 0.0025 mm^2 haemocytometer and diluted to approximately 1 x 10^7 cells/mL, then serially diluted to obtain 1 x 10^6, 1 x 10^5, 1 x10^4, 1 x 10^3 and 1 x 10^2 cells/mL. Strains were replicated onto the media described in the table below using a multichannel pipette that delivered 5 µL, and incubated at 37°C for three days.

Phenotype	Assay	Functional Implications
Control	YPD 37°C	-
Temperature sensitivity	YPD 4°C, Room temperature, 30°C, 42°C	General growth defect
Nutrient stress	Minimal media (YNB)	Inability to synthesise essential amino acids
pH phenotype	YPD pH7	Ability to grow at pH 7
Respiratory deficiency	3% (*v/v*) glycerol YPD	Failure to produce respiratory competent mitochondria
tBOOH (t-butylhydroperoxide)	1 mM tBOOH YPD	Oxidative stress
Ethanol sensitivity	6% (*v/v*) ethanol YPD	General protein defect
Formamide sensitivity	2% (*v/v*) formamide YPD	General protein defect
NaCl sensitivity	1.5 M NaCl YPD	Defects in osmotic stress response
Calcofluor White	10 µg/mL calcofluor white YPD	Fluorochrome with antifungal activity and high affinity for cell wall chitin. Highlights chitin biosythesis and cell wall morphogenesis mutants
SDS sensitivity	0.1% (*v/v*) SDS YPD	Defects in cell wall biogenesis
Benomyl sensitivity	0.5 µg/mL benomyl YPD	Defects in microtubule formation
Vanadate	7 mM, 2.5 mM sodium-o-vanadate YPD	Defects in protein glycosylation, secretory defects
FCS (Fetal Calf Serum)	10% (*v/v*) FCS YPD	Serum response
Caffeine sensitivity	10 mM caffeine YPD	Purine analogue affecting many cellular processes including MAPK signalling pathways
Drug sensitivity	50 µg/mL hygromycin YPD	Defects in protein glycosylation

Table 4.1 – Phenotypic conditions used to test the conditional sensitivity of the Ace2p-dependent gene nulls in a phenotypic screen [246].

4.2.5 Difference interference microscopy (DIC)

Yeast strains were grown overnight in 5 mL of YPD media at 30°C/37°C, 180 rpm. In the morning, cells were diluted to OD_{600} = 0.3 and allowed to grow at 30°C/37°C, 180 rpm for a further two to three hours, till the OD_{600} was between 0.5-1. Cells were spun down at 900 g and washed twice with PBS (137 mM NaCl, 2.7 mM KCl, 8 mM Na_2HPO_4, pH 7.3) before being re-suspended in approximately 200-500 µL of PBS. Approximately 10 µL of culture was mounted on microscope slides and visualised using a Zeiss Axiovert 200 inverted microscope with a 63x objective. The cells were photographed using a Hamamatsu ORCA-ER digital camera and images manipulated using HCImage, version 2.1.1.0, Hamamatsu Corporation, New Jersey, USA.

4.2.6 Growth rate analysis

Yeast cells were grown overnight in 5 mL of YPD media at 37°C, 180 rpm. In the morning the cells were diluted to OD_{600} = 0.1, plated out in triplicate into a 96-well plate and allowed to grow for 24 hours at 37°C in a Molecular devices Versamax Tunable Microplate reader, controlled by Softmax Pro. The OD was recorded every 3.5 minutes after having been shaken before each time point. The data was then manipulated in Excel.

4.2.7 Murine virulence studies

Virulence analysis of *C. glabrata* null mutants was carried out using a modified method as previously described by Calcagno et al. [81]. Groups of five outbred male CD1 mice were immunosuppressed via IP injection with 200 mg of cyclophosphamide per kg of body weight on day -3, day -1 and every fourth day for the duration of the study. Animals were infected with 7 x 10^7 *C. glabrata* cells in 200 µL saline via tail vein injection (IV). The mice were observed and weighed daily and sacrificed at predetermined endpoints, such as 20% weight loss.

4.2.8 Histological examination of murine samples

Small samples of murine tissue from the liver, kidney, lung and spleen were removed and fixed in 4% (*v/v*) formaldehyde solution upon death. Samples were mounted in paraffin, sectioned, and stained with haematoxylin and eosin (H & E), or Grocott's methenamine silver and light green (GMS), by C & C, London, UK.

Histological samples were observed using a Leitz Laborlux 12 light microscope and photographed using a Nikon Coolpix 990 digital camera.

4.2.9 Fungal burden

The fungal burden of the infected mice from section 4.2.8 was calculated via kidneys that were extracted from the animals at the point of sacrifice. A portion of each kidney was sectioned off, weighed, homogenised, serially diluted and plated out onto YPD in triplicate and grown overnight at

37°C. The colonies were then counted and a colony forming unit (CFU) count per gram of tissue was calculated.

4.2.10 Macrophage stimulation with yeast

Murine RAW 264.7 macrophages were seeded into 24-well plates at 2.5 x 10^5 macrophages per well and grown overnight in DMEM supplemented with 10% (*v/v*) FCS, penicillin (100 U/mL) (Invitrogen, UK), streptomycin (100 µg/mL) (Invitrogen, UK) at 37°C, 5% CO_2. Overnight cultures of yeast strains grown in the appropriate media were thoroughly washed with sterile PBS, counted and resuspended to 1.5 x 10^7 yeast/mL in DMEM media as above. Before infection, macrophages were thoroughly washed with fresh media. Yeast was then added to a yeast:macrophage ratio of 30:1 and allowed to bind and be phagocytosed for 40 minutes at 37°C, 5% CO_2. Macrophages were then washed extensively with PBS to remove unbound yeast and incubated in 0.5 mL of fresh medium for six hours at 37°C, 5% CO_2. All infections were done three times independently and triplicate wells used each time.

4.2.11 Enzyme-Linked ImmunoSorbent Assay (ELISA) cytokine analysis

RAW 264.7 TNFα and IL-6 secretion levels from the macrophage stimulation assay were measured using a Quantikine Mouse TNFα Immunoassay (R&D Systems, UK) and a Quantikine Mouse IL-6 Immunoassay (R&D Systems, UK) as per the manufacturer's instructions. The significance of the variation between the wild type and the individual null mutants was analysed using a one-way ANOVA statistical test.

4.3 Results

4.3.1 Southern blot analysis

Fusion PCR, as described in section 4.2.1, was used to construct *C. glabrata ash1, bud9, dse1, dse3, egt2* and *rme1.* PCR and Southern analysis was used to confirm correct integration at the locus (Appendix 4). Faint alternate bands were displayed for the NAT probe for *dse1* mutants 6, 7 and 8 possibly indicating multiple integration of the deletion cassette, and will therefore be excluded from further testing after the phenotypic screen as displayed in section 4.3.2 below.

The Edlind method one-step PCR, as described in section 4.2.2, was used to construct *C. glabrata amn1, acf2, scw11ϐ* and *sic1*. Between 20 and 50 colonies were screened per target gene using PCR analysis, before Southern analysis was used to confirm correct integration at the locus (Appendix 4).

4.3.2 Solid agar phenotypic screen

A selected range of phenotypic conditions as described by Hampsey et al. [246] and listed in Table 4.1 were used to test, as described in section 4.2.4, for any sensitivity of the mutants confirmed in section 4.3.1, to study gene function and to select one mutant for further *in vitro* and *in vivo* study. A parental control was used, *C. glabrata his3*, with each strain plated using a serial dilution from 1 x 10^7 to 1 x 10^4 cells. The *C. glabrata ace2* null strain was not used as a control during these experiments as it was unavailable at the time.

Normal growth rates were displayed through most of the screen with growth observed through all dilutions on all conditions apart from YPD 4°C, minimal media and 7 mM vanadate from the parental control. Slightly slower growth was noted on 2.5 mM vanadate by almost all mutants when compared with the parental strain, which could indicate a mild defect in protein glycosylation. Sensitivity to 10 mM caffeine was also shown by *Δash1 #5, Δash1 #7, Δash1 #8, Δdse1 #4* and *Δdse1 #5*, which could indicate defects various cellular processes, including Mpk1p-mediated cell wall integrity pathway [247].

The following mutants were selected for further screening: *C. glabrata ash1* #7, *bud9* #7, *dse1* #5, *dse3* #18, *egt2* #6 and *rme1* #6.

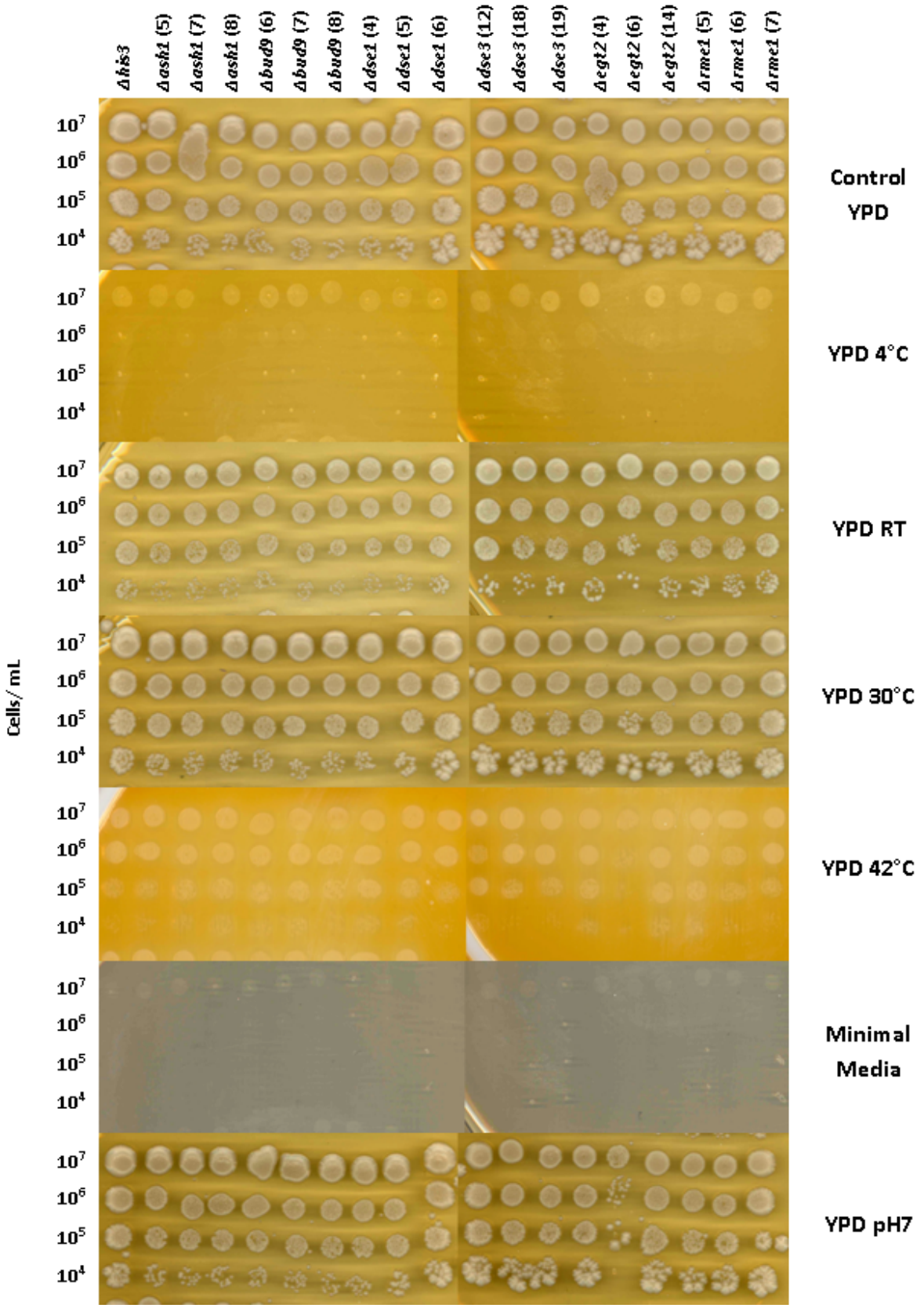


Figure 4.4 – *C. glabrata ash1, bud9, dse1, egt2* and *rme1* show no sensitivity to seven test conditions. Growth phenotypes of 18 Ace2p regulon null mutants, three nulls for each gene: *ASH1*, *BUD9*, *DSE1*, *DSE3*, *EGT2* and *RME1* and the parental strain *C. glabrata his3* (*Δhis3*). No sensitivity was shown by any of the null mutants when compared with the parental control. 5 µL of each strain was spotted in serial dilutions of 1 x 10^7, 1 x 10^6, 1 x 10^5 and 1 x 10^4 cells/ml. Strains were grown for three days on YPD at 37°C unless otherwise stated.

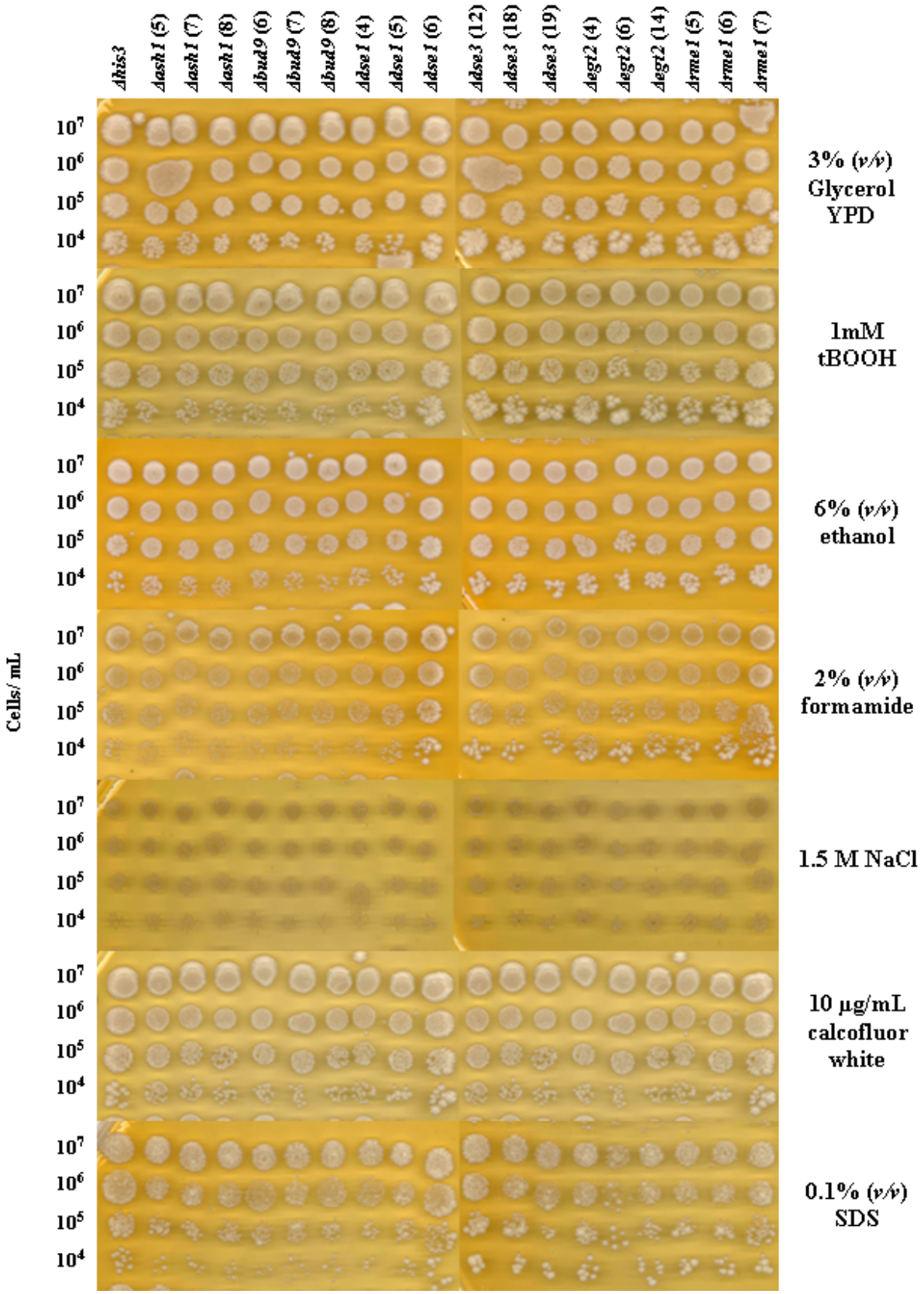


Figure 4.5 – *C. glabrata ash1, bud9, dse1, egt2* and *rme1* show no sensitivity to seven test conditions. Growth phenotypes of 18 Ace2p regulon null mutants, three nulls for each gene: *ASH1*, *BUD9*, *DSE1*, *DSE3*, *EGT2* and *RME1* and the parental strain *C. glabrata his3* (*Δhis3*). No sensitivity was shown by any of the null mutants when compared with the parental control. 5 µL of each strain was spotted in serial dilutions of 1 x 10^7, 1 x 10^6, 1 x 10^5 and 1 x 10^4 cells/ml. Strains were grown for three days on YPD at 37°C unless otherwise stated.

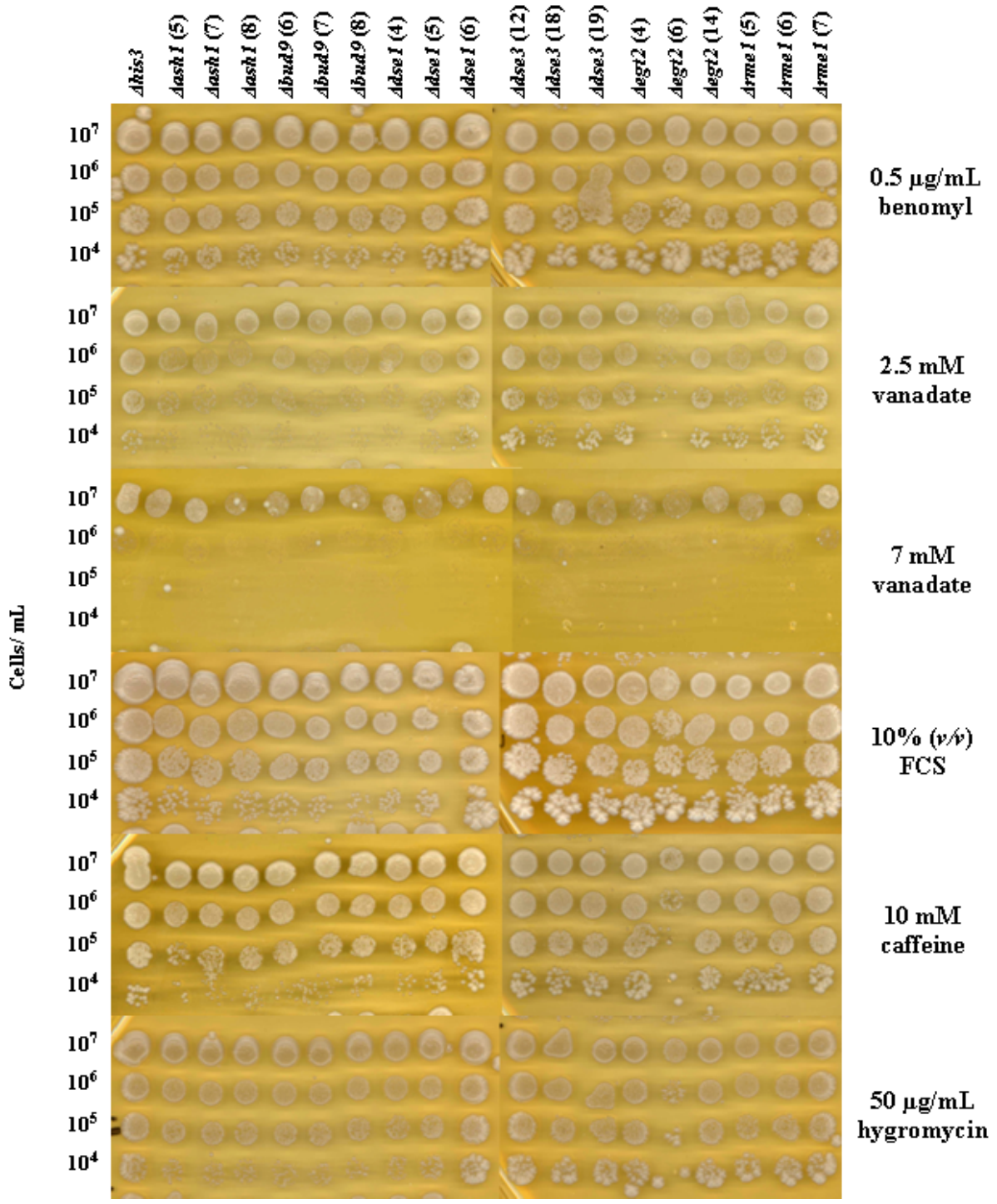


Figure 4.6 – *C. glabrata ash1, dse1, egt2* and *rme1* show mild sensitivity to vanadate and *ash1* and *dse1* show mild sensitivity to caffeine test conditions. Growth phenotypes of 18 Ace2p regulon null mutants, three nulls for each gene: *ASH1*, *BUD9*, *DSE1*, *DSE3*, *EGT2* and *RME1* and the parental strain *C. glabrata his3* (*Δhis3*). No sensitivity was shown by any of the null mutants when compared with the parental control apart from 2.5mM vanadate in which *Δash1 #5, Δash1 #7, Δash1 #8, Δdse1 #4, Δdse1 #5, Δdse1 #6, Δdse3 #18, Δdse3 #19, Δegt2 #4, Δegt2 #6, Δegt2 #14, Δrme1 #5,* and *Δrme1 #6* showed sensitivity, and 10 mM caffeine to which *Δash1 #5, Δash1 #7, Δash1 #8, Δdse1 #4* and *Δdse1 #5* showed a sensitivity. 5 µL of each strain was spotted in serial dilutions of 1 x 10^7, 1 x 10^6, 1 x 10^5 and 1 x 10^4 cells/ml. Strains were grown for three days on YPD at 37°C unless otherwise stated.

A selected range of phenotypic conditions as described by Hampsey [246] and listed in Table 4.1 were used to test, as described in section 4.2.4, for any sensitivity of the mutants confirmed in section 4.3.1, to study gene function and to select one mutant for further *in vitro* and *in vivo* study. A parental control was used, *C. glabrata ΔΔΔ*, with each strain plated using a serial dilution from 1x 10^7 to 1 x 10^4 cells. The *C. glabrata ace2* null strain was not used as a control during these experiments as it was unavailable at the time.

Normal growth rates were displayed through most of the screen with growth observed through all dilutions on all conditions apart from YPD 4°C, minimal media, 7 mM vanadate and 1 mM t-BOOH from the parental control. Sodium orthovanadate resistance has been shown to be associated with glycosylation mutants in *S. cerevisiae* due to an ability to eliminate an intracellularly formed toxic molecule [248, 249]. Mutants of *ash1, acf2* and *sic1* all showed mild sensitivity to 2.5 mM vanadate, which could indicate a small permeability change to sodium orthovanadate, which is known to inhibit phosphatase enzymes [250]. All mutants also showed mild sensitivity to 10 mM caffeine, which could indicate mild disruption of many cellular processes including Mpk1p-mediated cell wall integrity pathway [247].

The following mutants were selected for further screening: *C. glabrata amn1* #5, *acf2* #1, *scw11β* #4 and *sic1* #9.

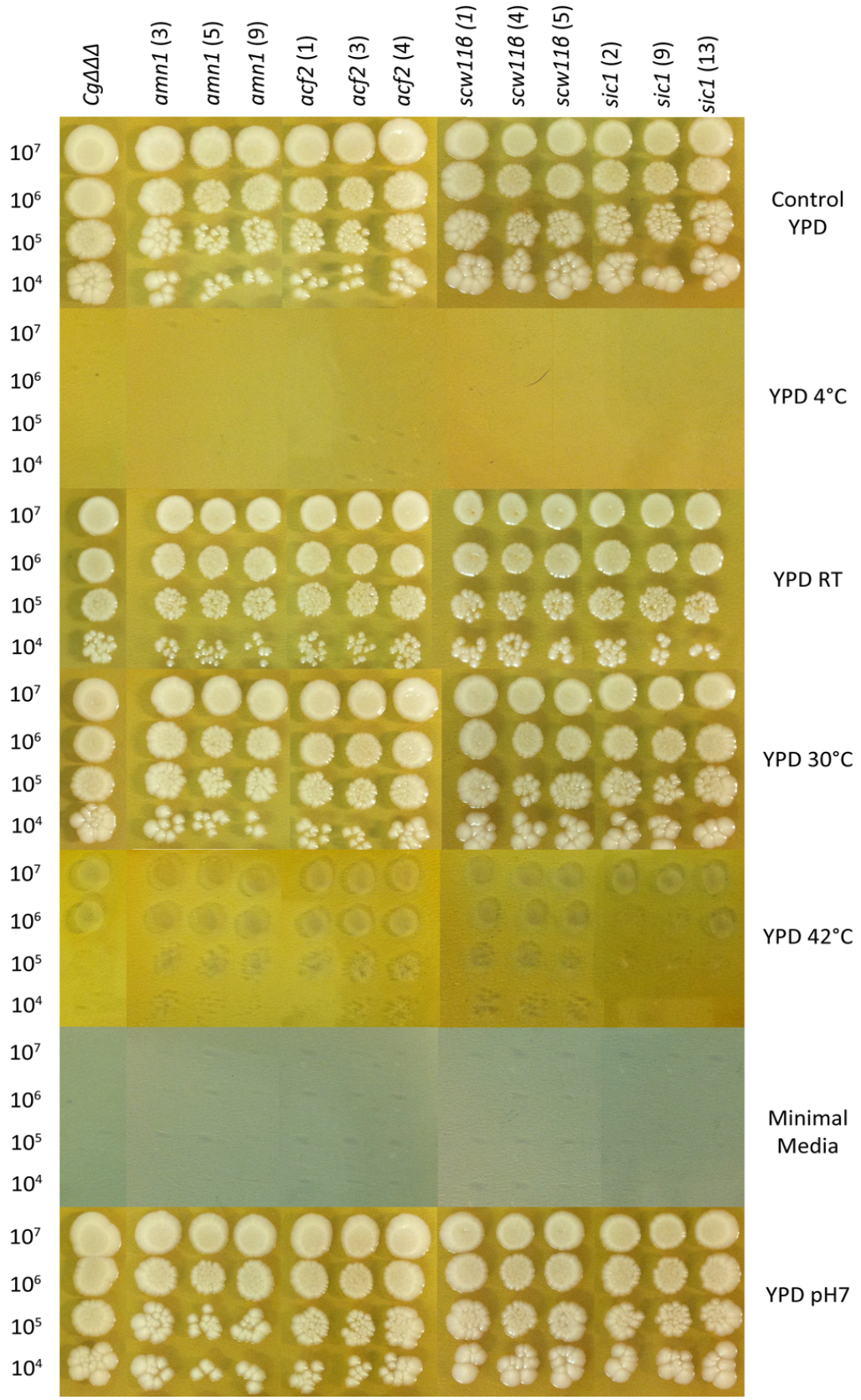


Figure 4.7 – *C. glabrata amn1, acf2, scw11β,* and *sic1* show no sensitivity to seven test conditions. Growth phenotypes of 12 Ace2p regulon null mutants, three nulls for each gene: *AMN1*, *ACF2*, *SCW11β,* and *SIC1* and the parental strain Cg*ΔΔΔ*. No sensitivity was shown by any of the null mutants when compared with the parental control. 5 µL of each strain was spotted in serial dilutions of 1 x 10^7, 1 x 10^6, 1 x 10^5 and 1 x 10^4 cells/ml. Strains were grown for three days on YPD at 37°C unless otherwise stated.

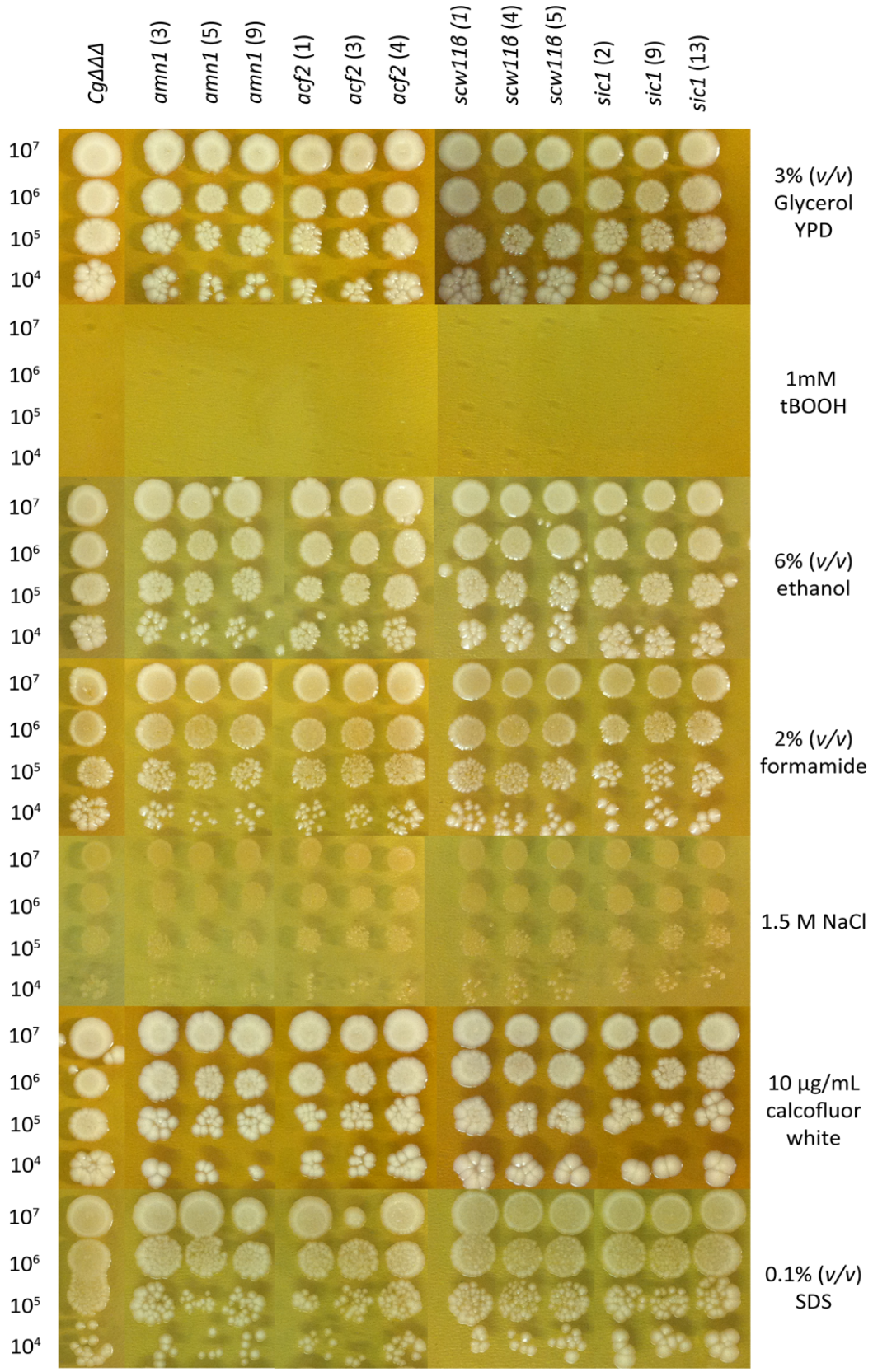


Figure 4.8 – *C. glabrata amn1, acf2, scw11β,* and *sic1* show no sensitivity to seven test conditions. Growth phenotypes of 12 Ace2p regulon null mutants, three nulls for each gene: *AMN1*, *ACF2*, *SCW11β,* and *SIC1* and the parental strain Cg*ΔΔΔ*. No sensitivity was shown by any of the null mutants when compared with the parental control. 5 µL of each strain was spotted in serial dilutions of 1 x 10^7, 1 x 10^6, 1 x 10^5 and 1 x 10^4 cells/ml. Strains were grown for three days on YPD at 37°C unless otherwise stated.

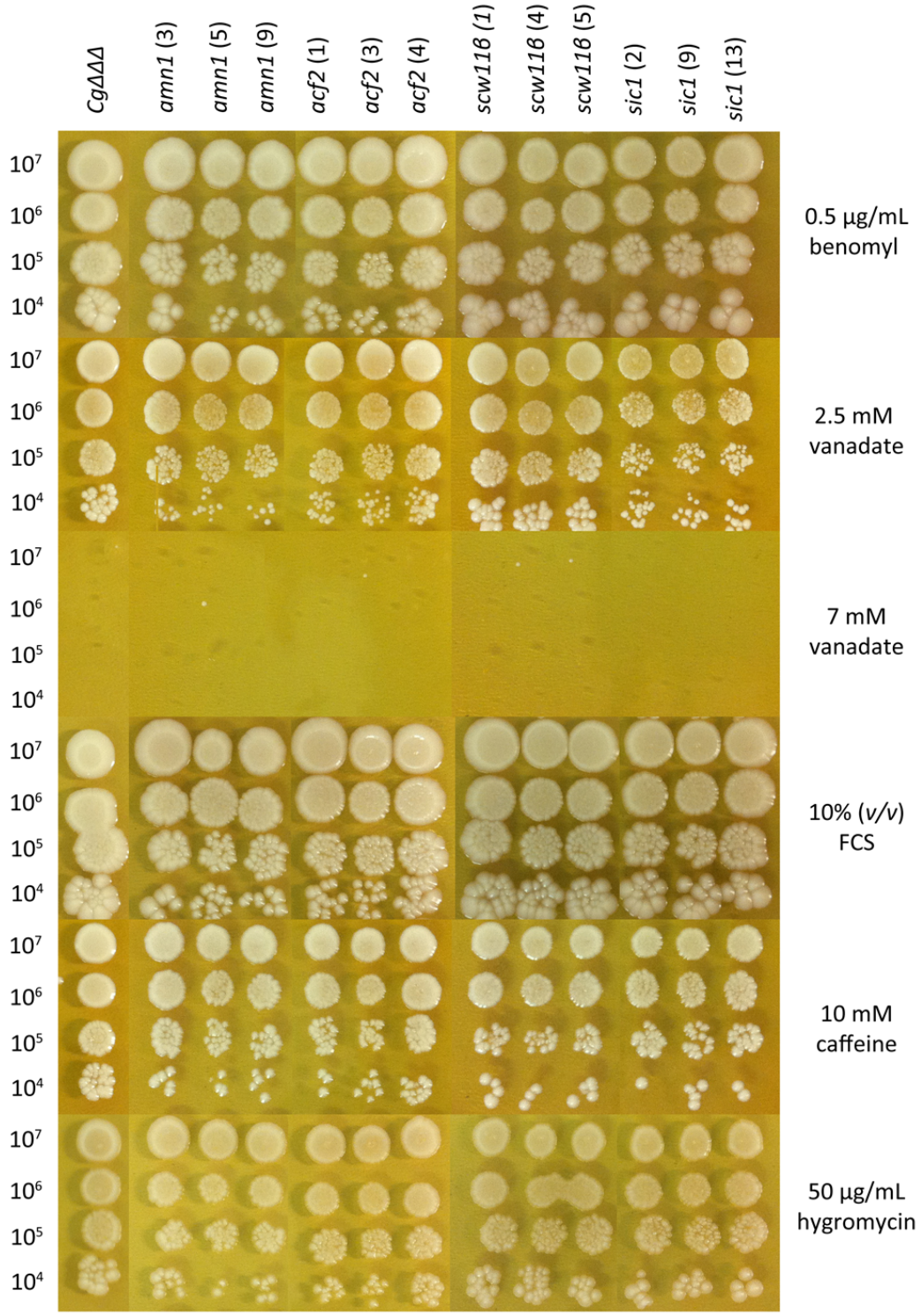


Figure 4.9 – *C. glabrata amn1, acf2* and *sic1* show mild sensitivity to vanadate and *amn1, acf2, scw11β,* and *sic1* show mild sensitivity to caffeine test conditions. Growth phenotypes of 12 Ace2p regulon null mutants, three nulls for each gene: *AMN1*, *ACF2*, *SCW11β,* and *SIC1* and the parental strain Cg*ΔΔΔ*. No sensitivity was shown by any of the null mutants when compared with the parental control apart from 2.5 mM vanadate in which all the *amn1, acf2* and *sic1* mutants showed mild sensitivity. All the mutants also showed mild sensitivity to 10 mM caffeine. 5 µL of each strain was spotted in serial dilutions of 1 x 10^7, 1 x 10^6, 1 x 10^5 and 1 x 10^4 cells/ml. Strains were grown for three days on YPD at 37°C unless otherwise stated.

4.3.3 Phenotypic microscopy

The *C. glabrata* null mutants identified in created in sections 4.2.1 and 4.2.2 were studied using DIC microscopy, as described in section 4.2.5, and shown in Figure 4.10 and Figure 4.11. A parental strain negative control and an *ace2* null HLS122 positive control (Figure 4.10 only) were included for reference. A clumpy phenotype was shown for both *dse1* and *egt2* with the remaining null mutants all showing a parental phenotype.

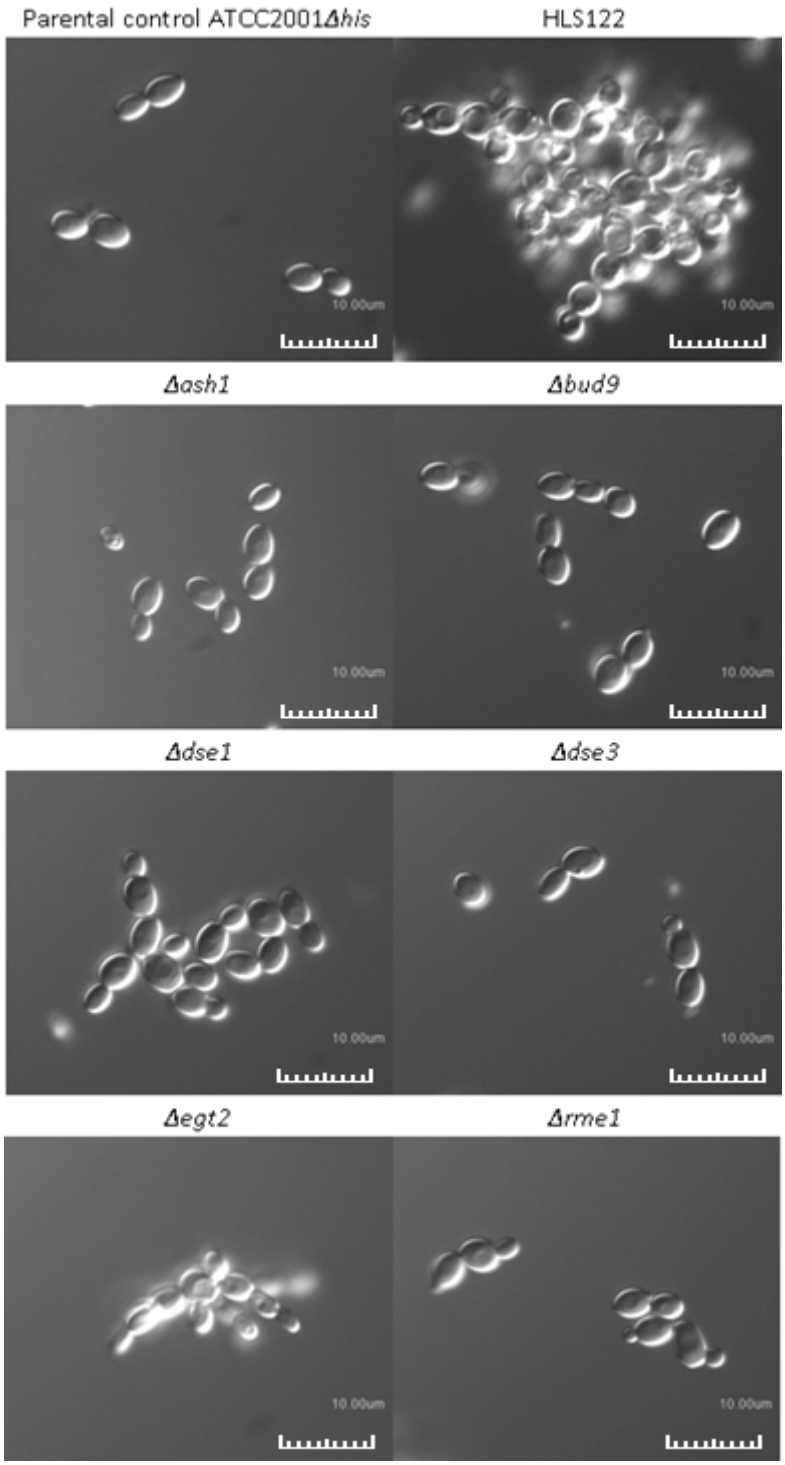


Figure 4.10 – *C. glabrata dse1* and *egt2* display a cell seperation defect similar to HLS122 (*ace2*) in liquid media. DIC microscopy of a representitive sample of each of the Ace2p regulon null mutants, their parental control and an *ace2* null, HLS122. No phenotype difference was shown between the parental control and the *ash1, bud9, dse3* and *rme1* null mutants. Both *dse1* and *egt2* null cells displayed a cell seperation defect similar, but not as pronounced, as that displayed by HLS122. This shows that both *DSE1* and *EGT2* may encode proteins that play a more significant role in cell seperation than those gene nulls that didn't display a cell separation phenotype. Yeast strains were grown overnight in YPD at 37°C, 180 rpm, diluted, and grown to OD_{600} 0.5-1, washed, mounted and visualised.

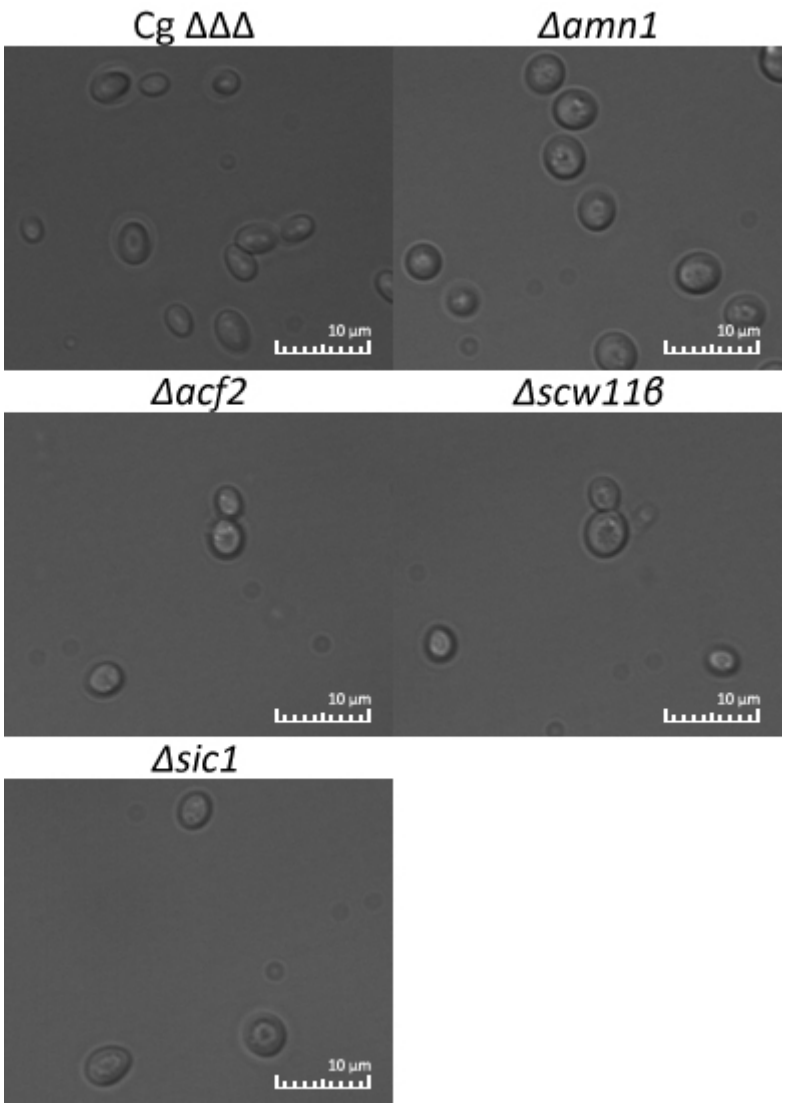


Figure 4.11 – *C. glabrata amn1, acf2, scw11β* and *sic1* show a cell separation competent phenotype similar to the parental strain Cg ΔΔΔ in liquid media. DIC microscopy of a representitive sample of each of the Ace2p regulon null mutants and their parental control Cg ΔΔΔ. No phenotypic difference was shown between the parental control and the *amn1, acf2, scw11β* and *sic1* null mutants. Yeast strains were grown overnight in YPD at 37°C, 180 rpm, diluted, and grown to OD_{600} 0.5-1, washed, mounted and visualised.

4.3.4 Growth rate analysis

Growth rate curves were created to look at the growth rates of the Ace2p regulon mutants, to determine if any of them showed any reduction in doubling time. All of the mutants showed similar characteristics to both the wild type Cg2001 and the parental strains *C. glabrata his3* and Cg *ΔΔΔ*. None of the mutant growth rates were significantly different from the wild type, therefore none of the mutants should be excluded from virulence analysis.

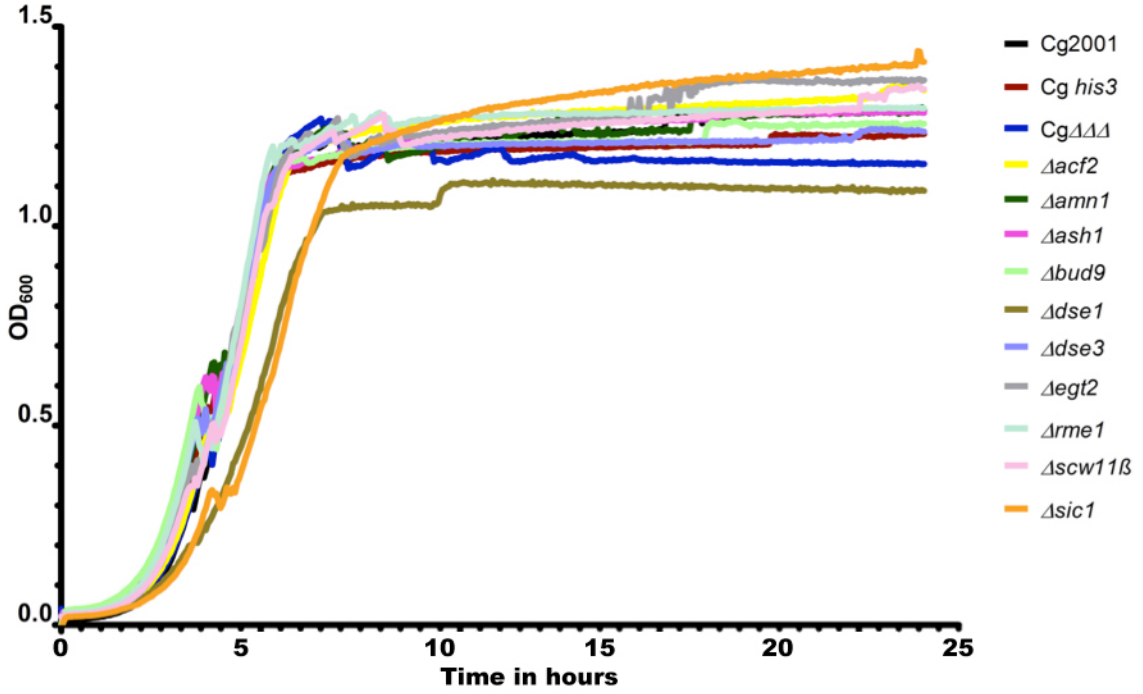


Figure 4.12 – *C. glabrata amn1, ash1, acf2, bud9, dse1, dse3, egt2, rme1, scw11ß* and *sic1* show similarity to wild type and parental growth rates. The growth rate of each of the mutants, their parental types Cg *his3* and Cg *ΔΔΔ*, as well as the *C. glabrata* wild type (Cg2001) over 24 hours. The growth rates of *amn1, ash1, acf2, bud9, dse1, dse3, egt2, rme1, scw11ß* and *sic1* showed similarity to that of their respective parental types and Cg2001.

4.3.5 Immune suppression survival pilot

An initial pilot survival analysis to test the addition of an extra immune suppression step at day -1, modifying the existing neutropenic model of disseminated candidiasis [81] to ensure neutropenia on inoculation day, resulted in 100% survival of the uninfected control group when run for the maximum experimental period of the animal license (21 days).

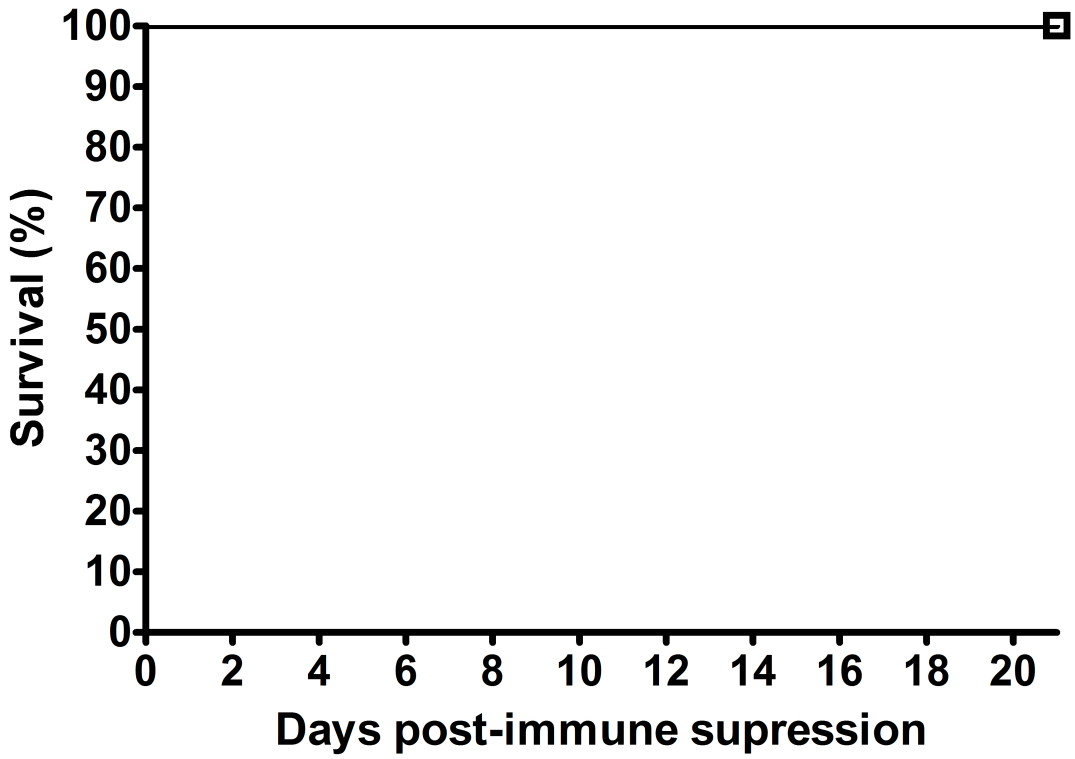


Figure 4.13 – The addition of an extra immune suppression step at day -1 does not effect uninfected control group survival. Survival of unifected mice (n = 10, open squares) subjected to the modified immune suppression regime with IP injection of 200 mg/kg cyclophosphamide at day 0, 2 and every fourth day remained at 100% through a 21 day experiment.

4.3.6 Murine virulence model of systemic candidiasis

Mutants were transformed with pBM51 and YPCIII to ensure autotrophy, and allow comparison to the *C. glabrata* wild type strain, where applicable before being tested. To assess the roles that the partial Ace2p regulon genes play in virulence a modified neutropenic murine model of systemic candidiasis was used as described in section 4.2.7. Groups of neutropenic male, CD1 mice were inoculated with 7 x 10^7 *C. glabrata amn1, ash1, bud9, dse1, dse3, dse3::DSE3, acf2, acf2::ACF2, egt2, egt2::EGT2, rme1, rme1::RME1, scw11β, scw11β::SCW11β, sic1, sic1::SIC1* and 2001 cells to assess the roles of *AMN1, ASH1, BUD9, DSE1, DSE3, ACF2, EGT2, RME1, SCW11β* and *SIC1* respectively in virulence. A comparison with *C. glabrata ace2* was not made due to time constraints and because an *ace2* deletion strain suitable for virulence analysis was not available at the time of experimentation. Each null mutant, and its reconstituted strain where applicable, are individually plotted against the *C. glabrata* wild type.

The *C. glabrata amn1* null displayed a phenotype that was indistinguishable from the wild type control resulting in 40% mortality by day five and therefore 60% survival over 14 days matching the 60% survival over 14 days for the wild type control (Figure 4.13 Log-rank (Mantel-Cox) test; p = 1)). Therefore, the host-fungal interaction is maintained in the *C. glabrata amn1* strain to wild type levels displaying a similar response in the mouse model.

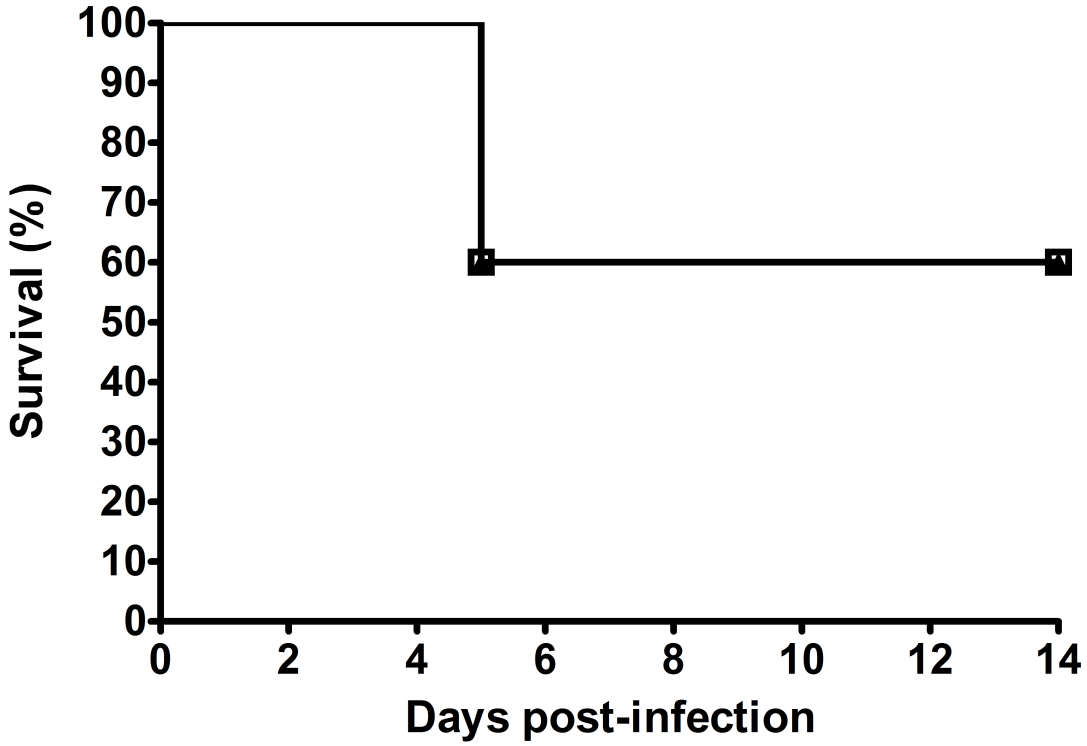


Figure 4.14 – *C. glabrata amn1* cells are not hypervirulent in a neutropenic murine model of systemic candidasis. Virulence was assayed in a modified neutropenic murine model of systemic infection [81] (n = 5 for wild type (open squares), n = 5 for null mutant (closed triangles)). Intravenous infection with the *C. glabrata amn1* null mutant at 7 x 10^7 cells/mouse resulted in a phenotype that was not significantly different when compared to the wild type strain resulting in 60% survival over 14 days.

The *C. glabrata ash1* null displayed a phenotype that resulted in increased mouse death with 80% mortality by day five and 20% survival over 14 days, but was not significantly different from the wild type control that displayed 60% survival over 14 days (Figure 4.15 Log-rank (Mantel-Cox) test; p = 0.2207)). Therefore, the host-fungal interaction is maintained in the *C. glabrata ash1* strain to wild type levels displaying a similar response in the mouse model.

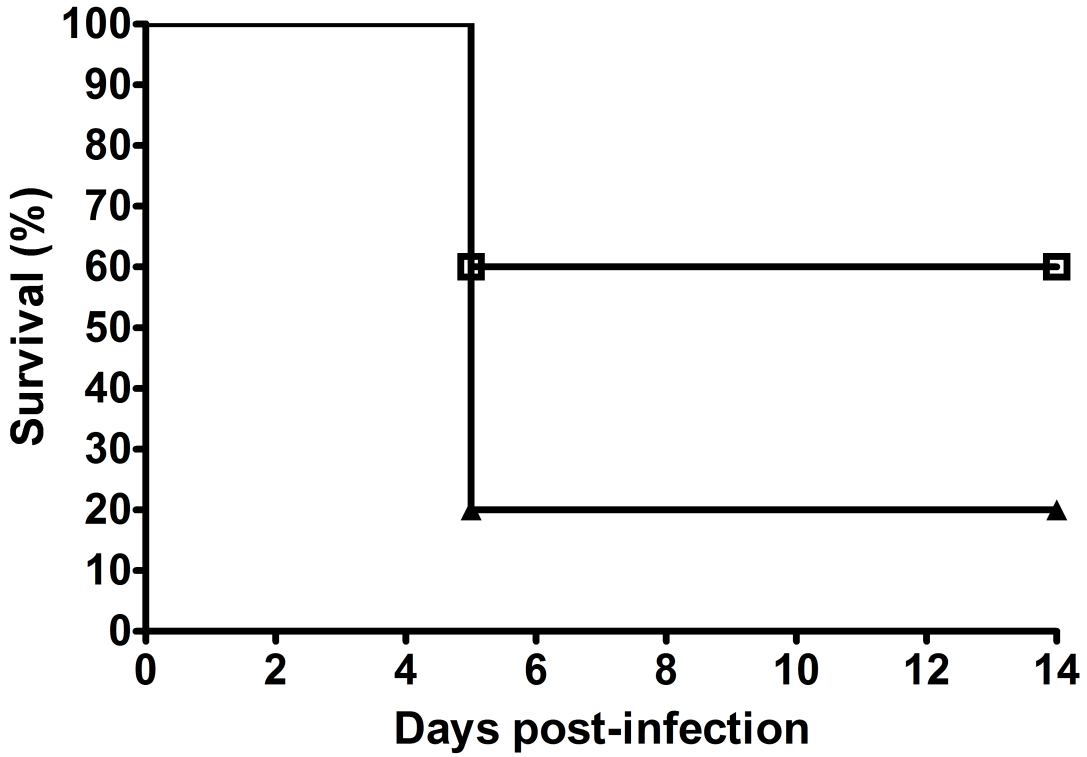


Figure 4.15 – *C. glabrata ash1* cells are not hypervirulent in a neutropenic murine model of systemic candidasis. Virulence was assayed in a modified neutropenic murine model of systemic infection [81] (n = 5 for wild type (open squares), n = 5 for null mutant (closed triangles)). Intravenous infection with the *C. glabrata ash1* null mutant at 7 x 10^7 cells/mouse resulted in a phenotype that was not significantly different when compared to the wild type strain resulting in 20% survival over 14 days.

The *C. glabrata bud9* null displayed a phenotype that resulted in increased mouse death with 80% mortality by day five and 20% survival over 14 days, but was not significantly different from the wild type control that displayed 60% survival over 14 days (Figure 4.16 Log-rank (Mantel-Cox) test; p = 0.1659)). Therefore, the host-fungal interaction is maintained in the *C. glabrata bud9* strain to wild type levels displaying a similar response in the mouse model.

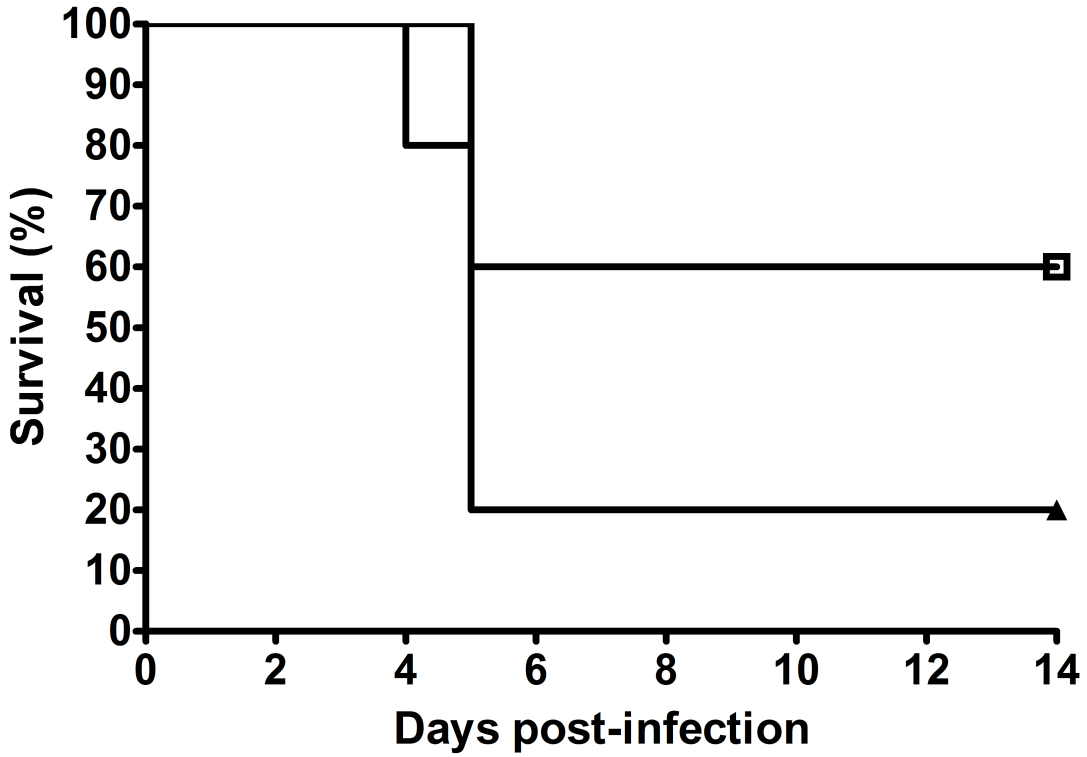


Figure 4.16 – *C. glabrata bud9* cells are not hypervirulent in a neutropenic murine model of systemic candidasis. Virulence was assayed in a modified neutropenic murine model of systemic infection [81] (n = 5 for wild type (open squares), n = 5 for null mutant (closed triangles)). Intravenous infection with the *C. glabrata bud9* null mutant at 7 x 10^7 cells/mouse resulted in a phenotype that was not significantly different when compared to the wild type strain resulting in 20% survival over 14 days.

The *C. glabrata dse1* null displayed a phenotype that was indistinguishable from the wild type control resulting in 40% mortality by day five and 60% survival over 14 days matching the 60% survival over 14 days for the wild type control (Figure 4.17 Log-rank (Mantel-Cox) test; p = 1)). Therefore, the host-fungal interaction is maintained in the *C. glabrata dse1* strain to wild type levels displaying a similar response in the mouse model.

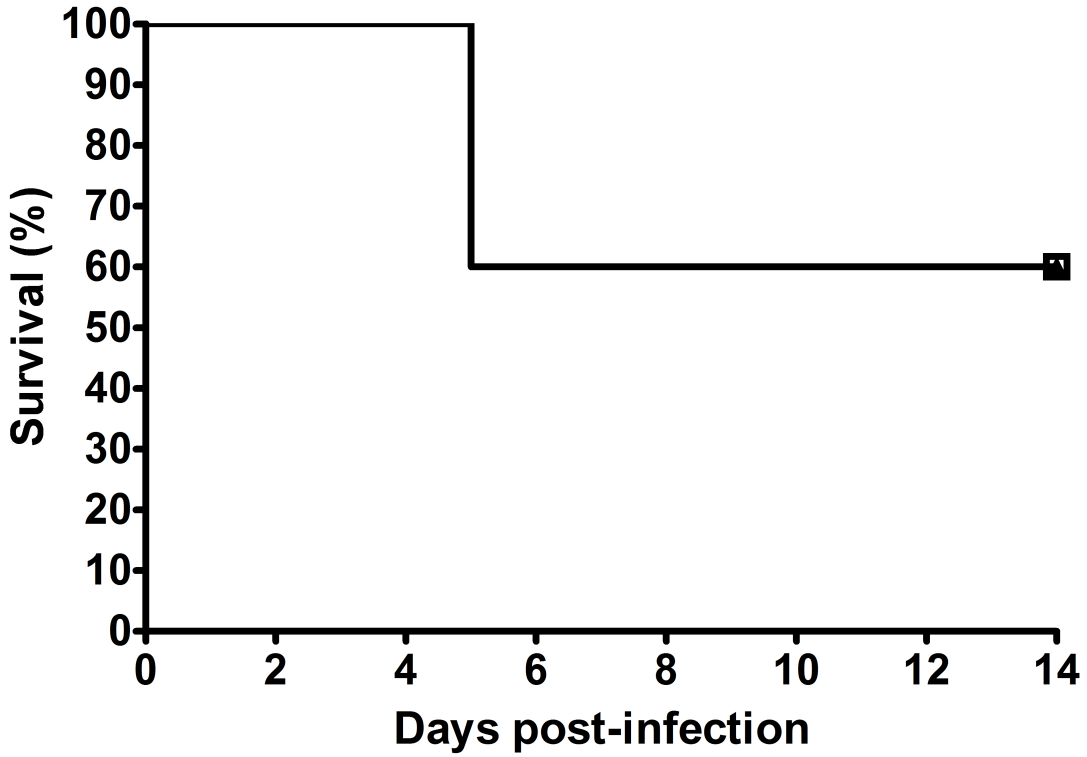


Figure 4.17 – *C. glabrata dse1* cells are not hypervirulent in a neutropenic murine model of systemic candidasis. Virulence was assayed in a modified neutropenic murine model of systemic infection [81] (n = 5 for wild type (open squares), n = 5 for null mutant (closed triangles)). Intravenous infection with the *C. glabrata dse1* null mutant at 7 x 10^7 cells/mouse resulted in a phenotype that was not significantly different when compared to the wild type strain resulting in 60% survival over 14 days.

The *C. glabrata dse3* null displayed a phenotype that was significantly different from the wild type control resulting in 40% mortality by day four and 100% mortality by day five compared with 60% survival over 14 days for the wild type control (Figure 4.18 Log-rank (Mantel-Cox) test; $p < 0.05$). The reconstituted strain returned the virulence to that displayed by the wild type. Therefore, the host-fungal interaction is altered in the *C. glabrata dse3* strain displaying a hypervirulent-like immune response in the mouse model.

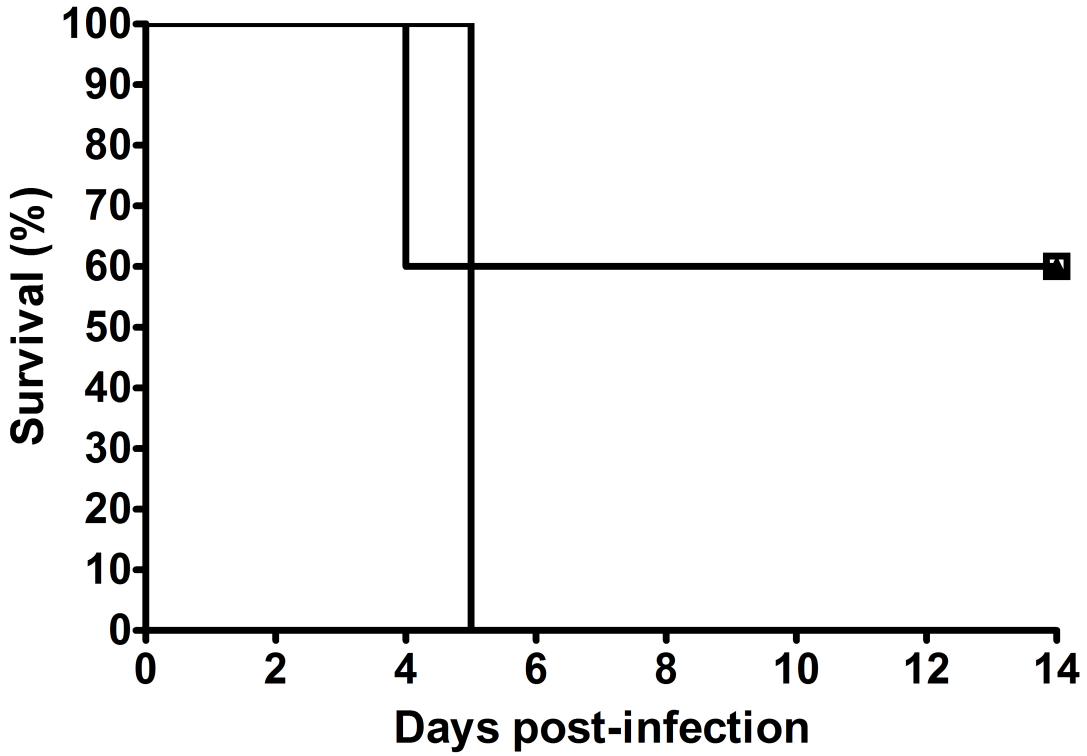


Figure 4.18 – *C. glabrata dse3* cells are hypervirulent in a neutropenic murine model of systemic candidasis. Virulence was assayed in a modified neutropenic murine model of systemic infection [81] (n = 5 for wild type (open squares), n = 5 for null mutant (no symbol), n = 5 for the reconsituted strain (closed triangles)). Intravenous infection with the *C. glabrata dse3* null mutant at 7 x 10^7 cells/mouse resulted in a hypervirulent phenotype that was significantly different when compared to the wild type strain resulting in 100% mortality after five days ($p < 0.05$, Log-rank (Mantel-Cox) analysis). Reconsitution of *DSE3* resulted in a return to wild type virulence levels.

The *C. glabrata acf2* null displayed a phenotype that was significantly different from the wild type control resulting in 100% mortality by day five compared with 60% survival over 14 days for the wild type control (Figure 4.19, Log-rank (Mantel-Cox) test; $p < 0.05$). The reconstituted strain returned the virulence to that displayed by the wild type. Therefore, the host-fungal interaction is altered in the *C. glabrata acf2* strain displaying a hypervirulent-like immune response in the mouse model.

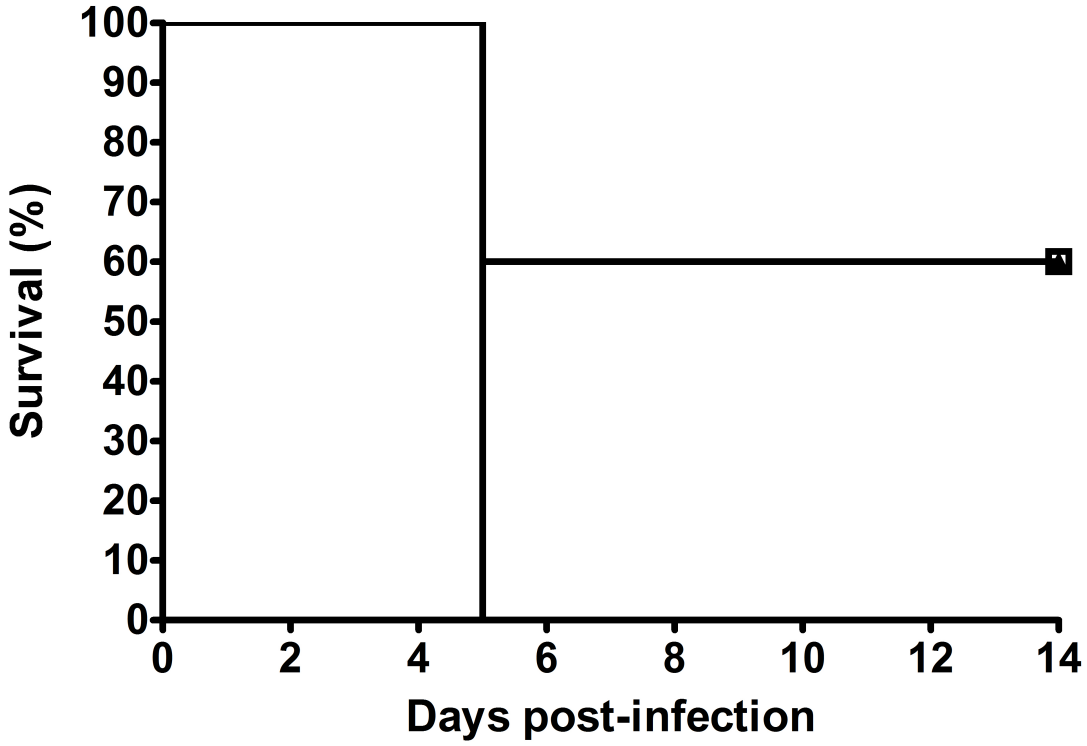


Figure 4.19 – *C. glabrata acf2* cells are hypervirulent in a neutropenic murine model of systemic candidasis. Virulence was assayed in a modified neutropenic murine model of systemic infection [81] (n = 5 for wild type (open squares), n = 5 for null mutant (no symbol), n = 5 for the reconsituted strain (closed triangles)). Intravenous infection with the *C. glabrata acf2* null mutant at 7 x 10^7 cells/mouse resulted in a hypervirulent phenotype that was significantly different when compared to the wild type strain resulting in 100% mortality after five days ($p < 0.05$, Log-rank (Mantel-Cox) analysis). Reconsitution of *ACF2* resulted in a return to wild type virulence levels.

The *C. glabrata egt2* null displayed a phenotype that was significantly different from the wild type control resulting in 100% mortality by day five compared with 60% survival over 14 days for the wild type control (Figure 4.20, Log-rank (Mantel-Cox) test; $p < 0.05$). The reconstituted strain returned the virulence to that displayed by the wild type. Therefore, the host-fungal interaction is altered in the *C. glabrata egt2* strain displaying a hypervirulent-like immune response in the mouse model.

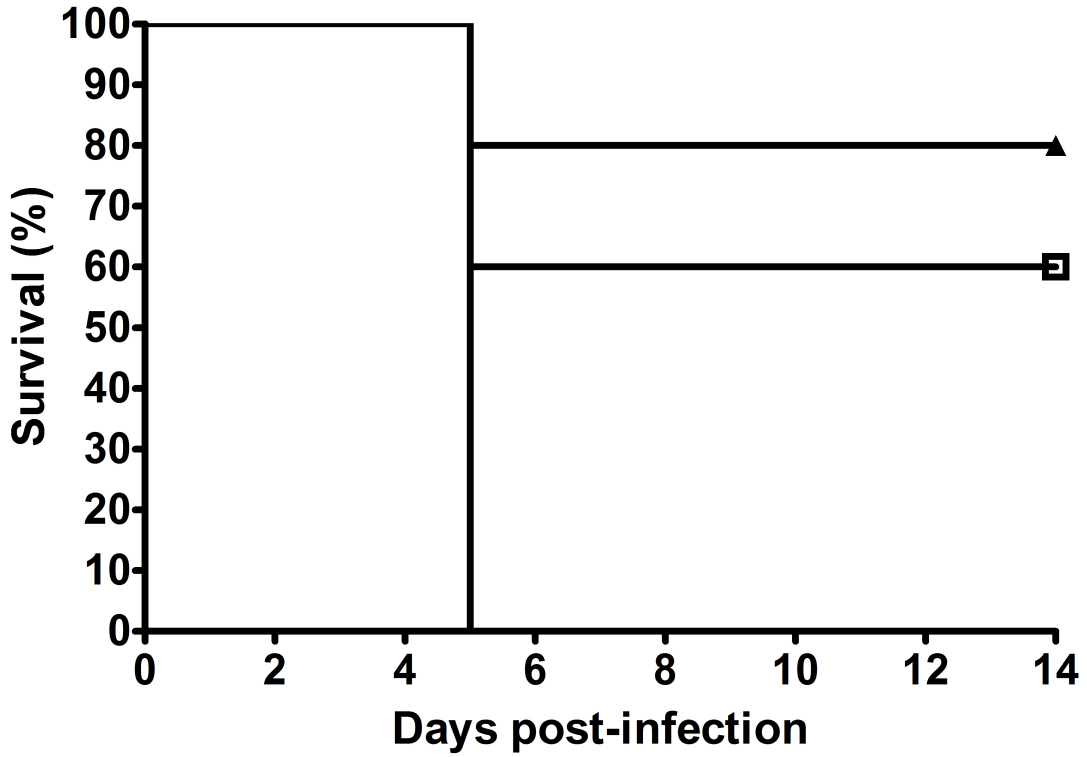


Figure 4.20 – *C. glabrata egt2* cells are hypervirulent in a neutropenic murine model of systemic candidasis. Virulence was assayed in a modified neutropenic murine model of systemic infection [81] (n = 5 for wild type (open squares), n = 5 for null mutant (no symbol), n = 5 for the reconsituted strain (closed triangles)). Intravenous infection with the *C. glabrata egt2* null mutant at 7 x 10^7 cells/mouse resulted in a hypervirulent phenotype that was significantly different when compared to the wild type strain resulting in 100% mortality after five days ($p < 0.05$, Log-rank (Mantel-Cox) analysis). Reconsitution of *EGT2* resulted in a return to wild type virulence levels.

The *C. glabrata rme1* null displayed a phenotype that was significantly different from the wild type control resulting in 100% mortality by day five compared with 60% survival over 14 days for the wild type control (Figure 4.21, Log-rank (Mantel-Cox) test; $p < 0.05$). The reconstituted strain returned the virulence to that displayed by the wild type. Therefore, the host-fungal interaction is altered in the *C. glabrata rme1* strain displaying a hypervirulent-like immune response in the mouse model.

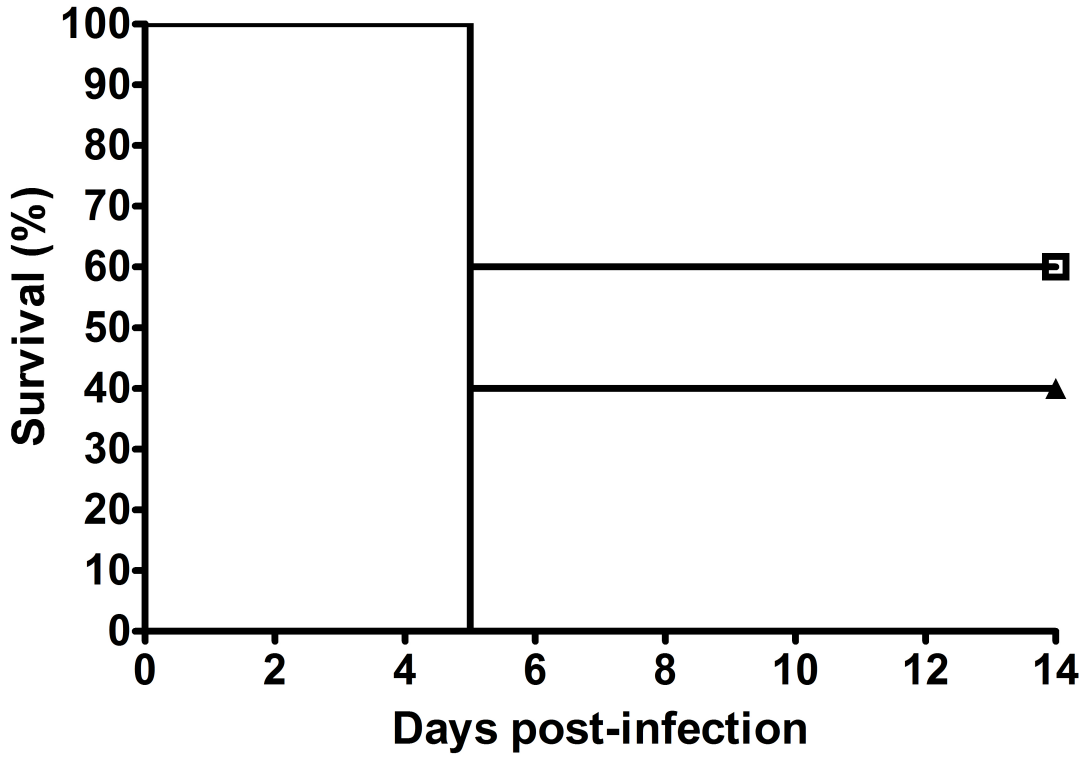


Figure 4.21 – *C. glabrata rme1* cells are hypervirulent in a neutropenic murine model of systemic candidasis. Virulence was assayed in a modified neutropenic murine model of systemic infection [81] (n = 5 for wild type (open squares), n = 5 for null mutant (no symbol), n = 5 for the reconsituted strain (closed triangles)). Intravenous infection with the *C. glabrata rme1* null mutant at 7 x 10^7 cells/mouse resulted in a hypervirulent phenotype that was significantly different when compared to the wild type strain resulting in 100% mortality after five days ($p < 0.05$, Log-rank (Mantel-Cox) analysis). Reconsitution of *RME1* resulted in a return to wild type virulence levels.

The *C. glabrata scw11β* null displayed a phenotype that was significantly different from the wild type control resulting in 60% mortality by day four and 100% mortality by day five compared with 60% survival over 14 days for the wild type control (Figure 4.22, Log-rank (Mantel-Cox) test; $p < 0.05$). The reconstituted strain returned the virulence to that displayed by the wild type. Therefore, the host-fungal interaction is altered in the *C. glabrata scw11β* strain displaying a hypervirulent-like immune response in the mouse model.

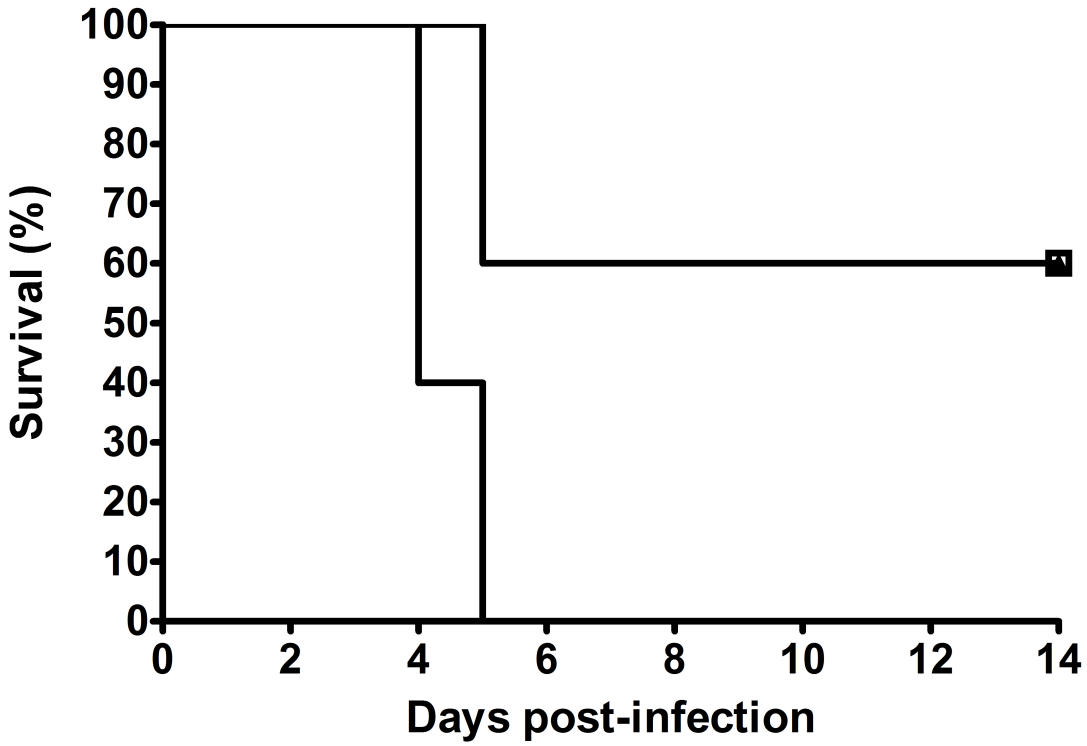


Figure 4.22 – *C. glabrata sw11β* cells are hypervirulent in a neutropenic murine model of systemic candidasis. Virulence was assayed in a modified neutropenic murine model of systemic infection [81] (n = 5 for wild type (open squares), n = 5 for null mutant (no symbol), n = 5 for the reconsituted strain (closed triangles)). Intravenous infection with the *C. glabrata scw11β* null mutant at 7 x 10^7 cells/mouse resulted in a hypervirulent phenotype that was significantly different when compared to the wild type strain resulting in 100% mortality after five days ($p < 0.05$, Log-rank (Mantel-Cox) analysis). Reconsitution of *SCW11β* resulted in a return to wild type virulence levels.

The *C. glabrata sic1* null displayed a phenotype that was significantly different from the wild type control resulting in 20% mortality by day four and 100% mortality by day five compared with 60% survival over 14 days for the wild type control (Figure 4.23, Log-rank (Mantel-Cox) test; $p < 0.05$). The reconstituted strain returned the virulence to that displayed by the wild type. Therefore, the host-fungal interaction is altered in the *C. glabrata sic1* strain displaying a hypervirulent-like immune response in the mouse model.

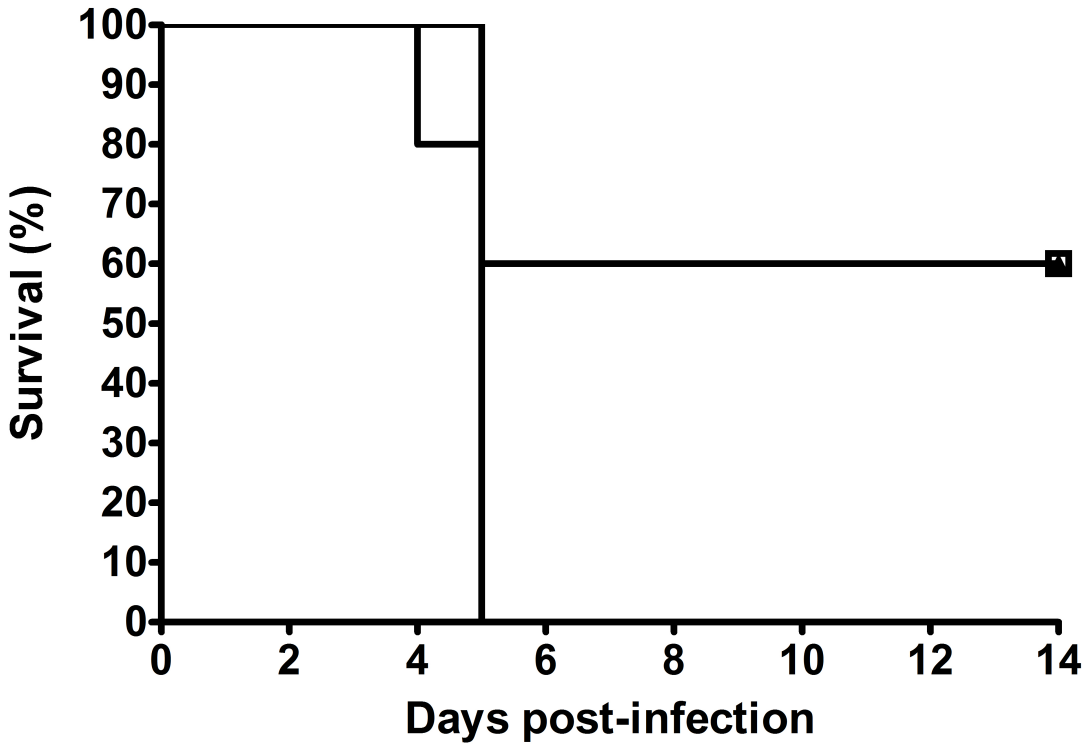


Figure 4.23 – *C. glabrata sic1* cells are hypervirulent in a neutropenic murine model of systemic candidasis. Virulence was assayed in a modified neutropenic murine model of systemic infection [81] (n = 5 for wild type (open squares), n = 5 for null mutant (no symbol), n = 5 for the reconsituted strain (closed triangles)). Intravenous infection with the *C. glabrata sic1* null mutant at 7 x 10^7 cells/mouse resulted in a hypervirulent phenotype that was significantly different when compared to the wild type strain resulting in 100% mortality after five days ($p < 0.05$, Log-rank (Mantel-Cox) analysis). Reconsitution of *SIC1* resulted in a return to wild type virulence levels.

4.3.7 Fungal burden

To estimate the fungal burden of each of the Ace2p regulon null strains, kidneys were extracted from animals at the point of sacrifice, with a portion of known weight homogenised, serially diluted and plated out onto YPD in triplicate and grown overnight. The colonies were then counted and a CFU count per gram of tissue calculated. The hypervirulent strains of *dse3*, *acf2*, *egt2*, *rme1*, *scw11ß* and *sic1* all showed significantly increased fungal burden when compared to the *C. glabrata* wild type (unpaired two tailed t-test, $p < 0.0001$). The reconstitutions of *dse3*, *acf2*, *egt2*, *rme1*, *scw11ß* and *sic1* all displayed similar fungal burden to the wild type strain.

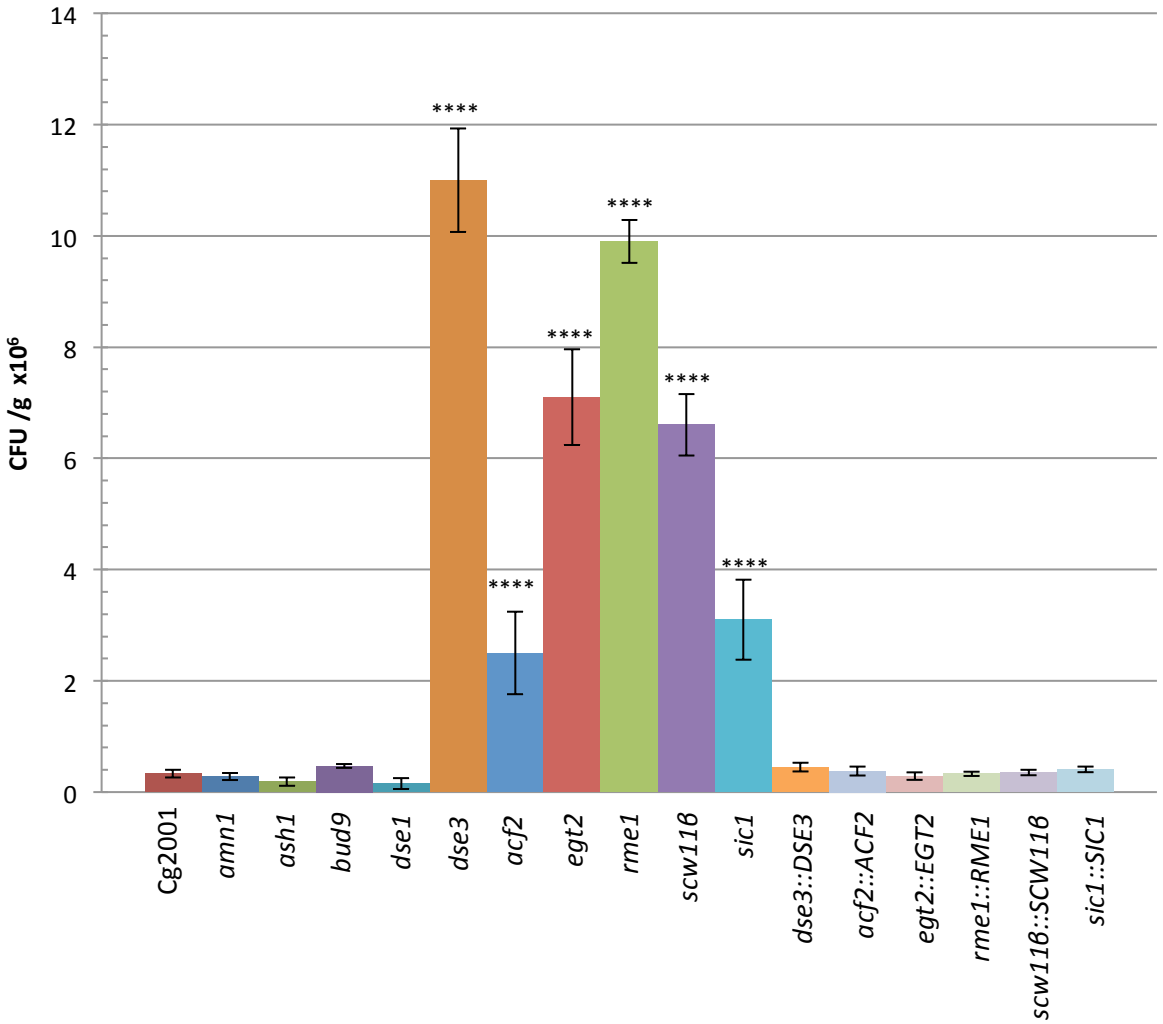


Figure 4.24 – *C. glabrata dse3, acf2, egt2, rme1, scw11ß* and *sic1* show increased fungal burden when compared with the wild type in a neutropenic murine model of candidaisis. The fungal burden as measured by kidney CFU/g from infected mice. Kidneys were extracted at the point of sacrifice, weighed, homogenised, diluted, plated out in triplicate, grown overnight at 37°C and colony forming units counted. The CFU per gram per kidney per infected animal was calculated and compared to the the wild type with *dse3*, *acf2*, *egt2*, *rme1*, *scw11ß* and *sic1* showing a significant increase in fungal burden when compared to the wild type (unpaired two tailed t-test, $p < 0.0001$). Reconstitution of *dse3*, *acf2*, *egt2*, *rme1*, *scw11ß* and *sic1* returned the fungal burden to the wild type levels.

4.3.8 Histology

Organ samples were extracted at the point of sacrifice with the tissue stained with either GMS or H & E as described in section 4.2.8. *C. glabrata* cells were observed within the parenchyma of the kidney, liver and lung, with a notable absence of more than one or two cells within the liver (Figure 4.25). The lung is observed as the primary target organ. Larger colonies for the hypervirulent strains *dse3, acf2, egt2, rme1, scw11ϐ* and *sic1* were present in the lung and kidney compared to the wild type, with *dse3::DSE3, acf2::ACF2, egt2::EGT2, rme1::RME1, scw11ϐ::SCW11ϐ* and *sic1::SIC1* reconstitutions displaying wild type levels of organ colonisation. The non-hypervirulent strains *amn1, ash1, bud9* and *dse1* also displayed wild type levels of organ colonisation. Staining by H & E displayed no signs of organ tissue inflammation for all strains and organs examined (data not shown).

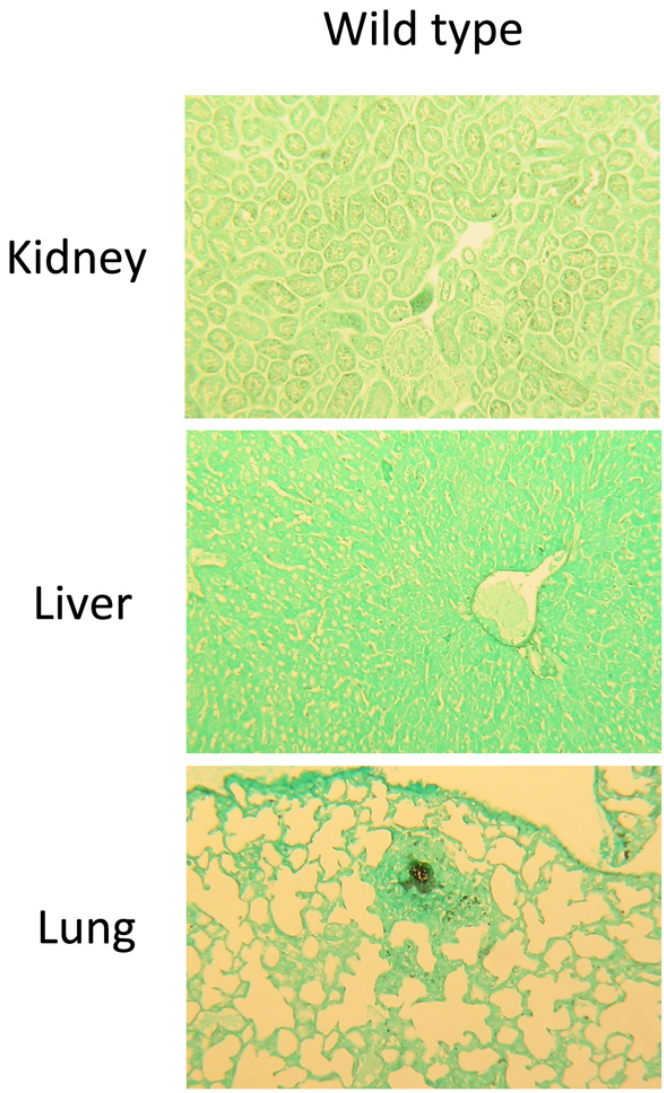


Figure 4.25a – Histological examination of tissues taken from *C. glabrata* wild type experimentally infected mice. The kidney, liver and lung from *C. glabrata* wild type infected mice were removed at sacrifice and stained using GMS. Staining revealed the lung to be the primary target organ for yeast colonisation.

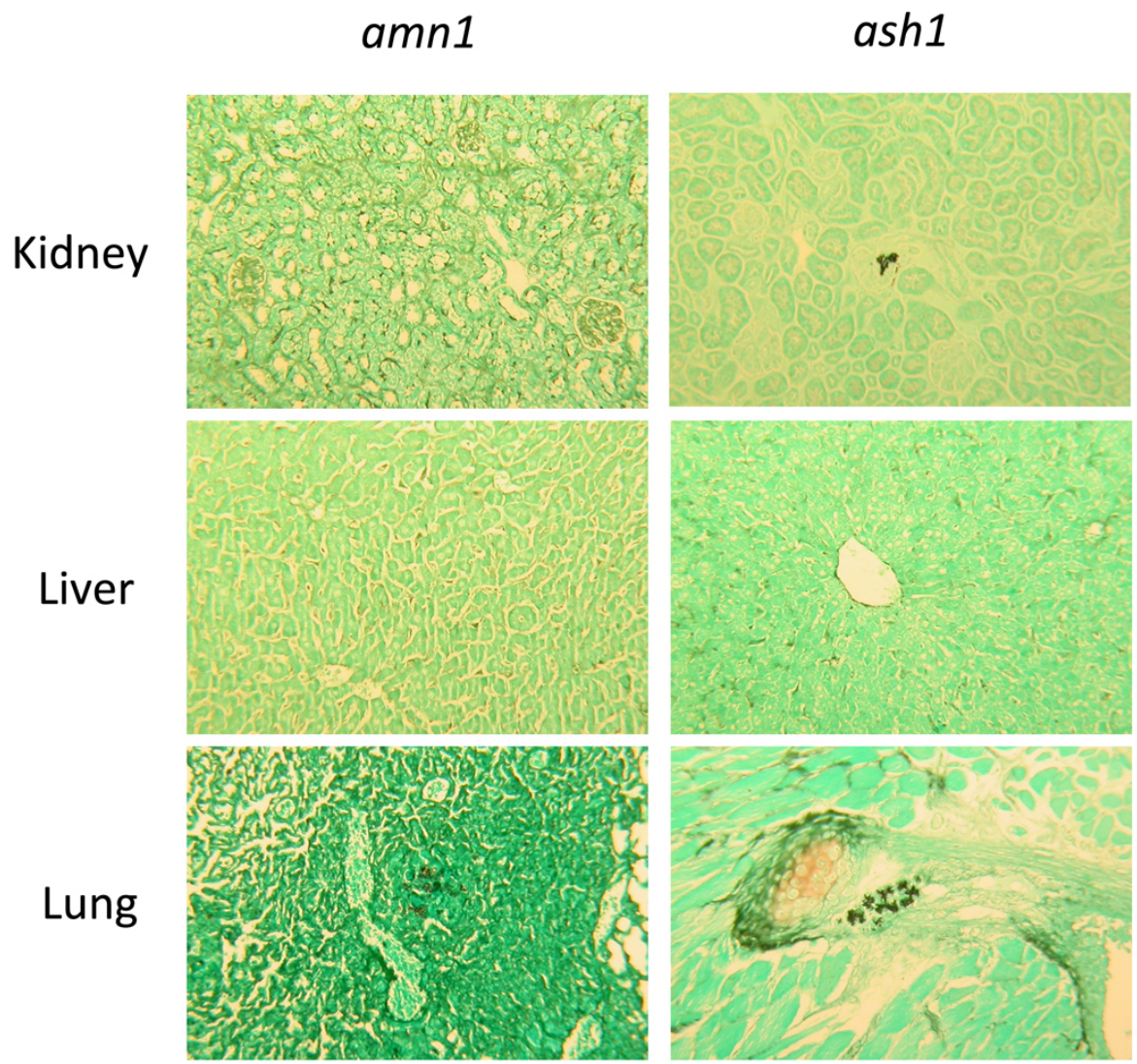


Figure 4.25b – Histological examination of tissues taken from *C. glabrata amn1* and *ash1* experimentally infected mice. The kidney, liver and lung from *C. glabrata amn1* and *ash1* infected mice were removed at sacrifice and stained using GMS. Staining revealed the lung to be the primary target organ for yeast colonisation.

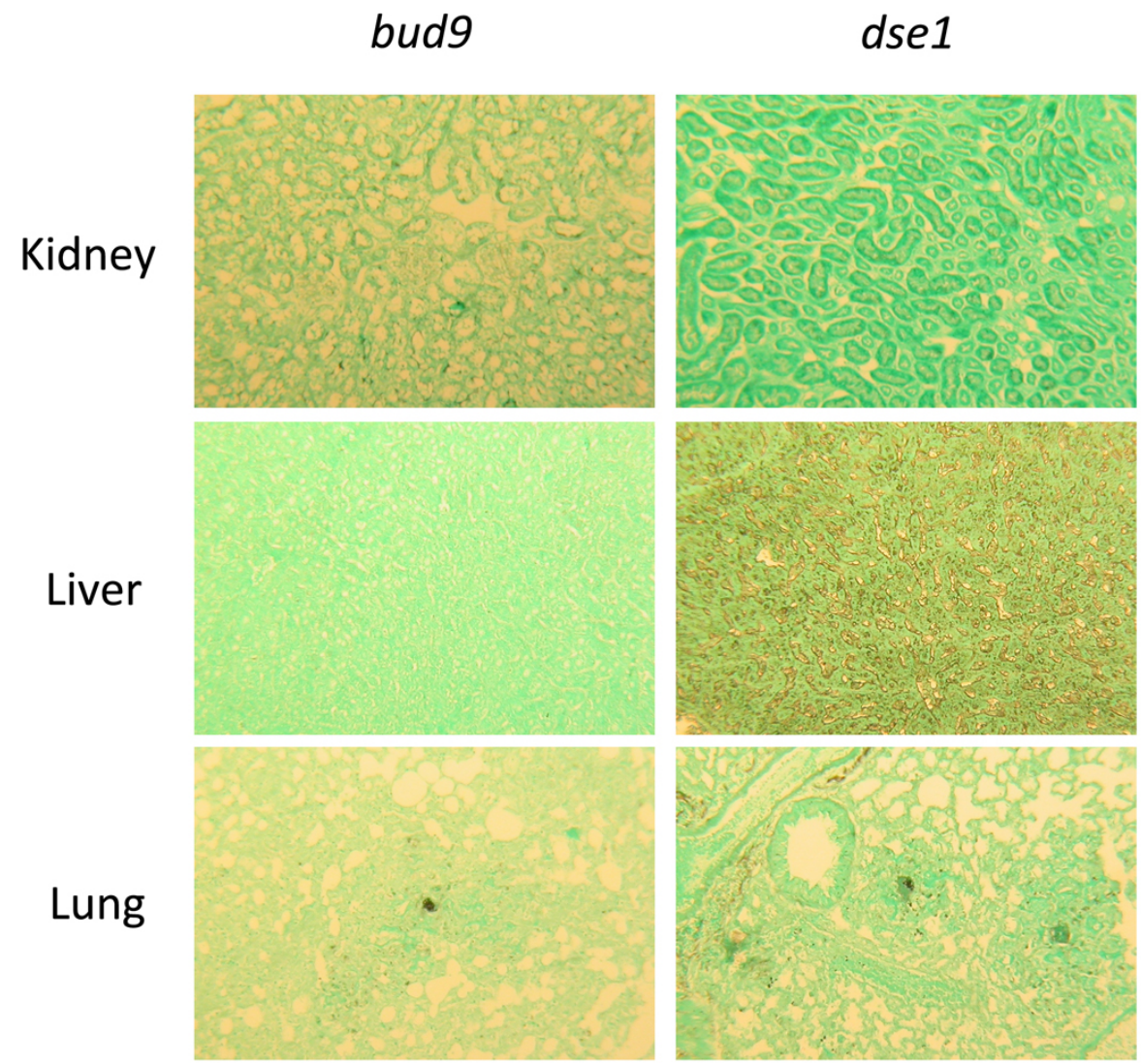


Figure 4.25c – Histological examination of tissues taken from *C. glabrata bud9* and *dse1* experimentally infected mice. The kidney, liver and lung from *C. glabrata bud9* and *dse1* infected mice were removed at sacrifice and stained using GMS. Staining revealed the lung to be the primary target organ for yeast colonisation.

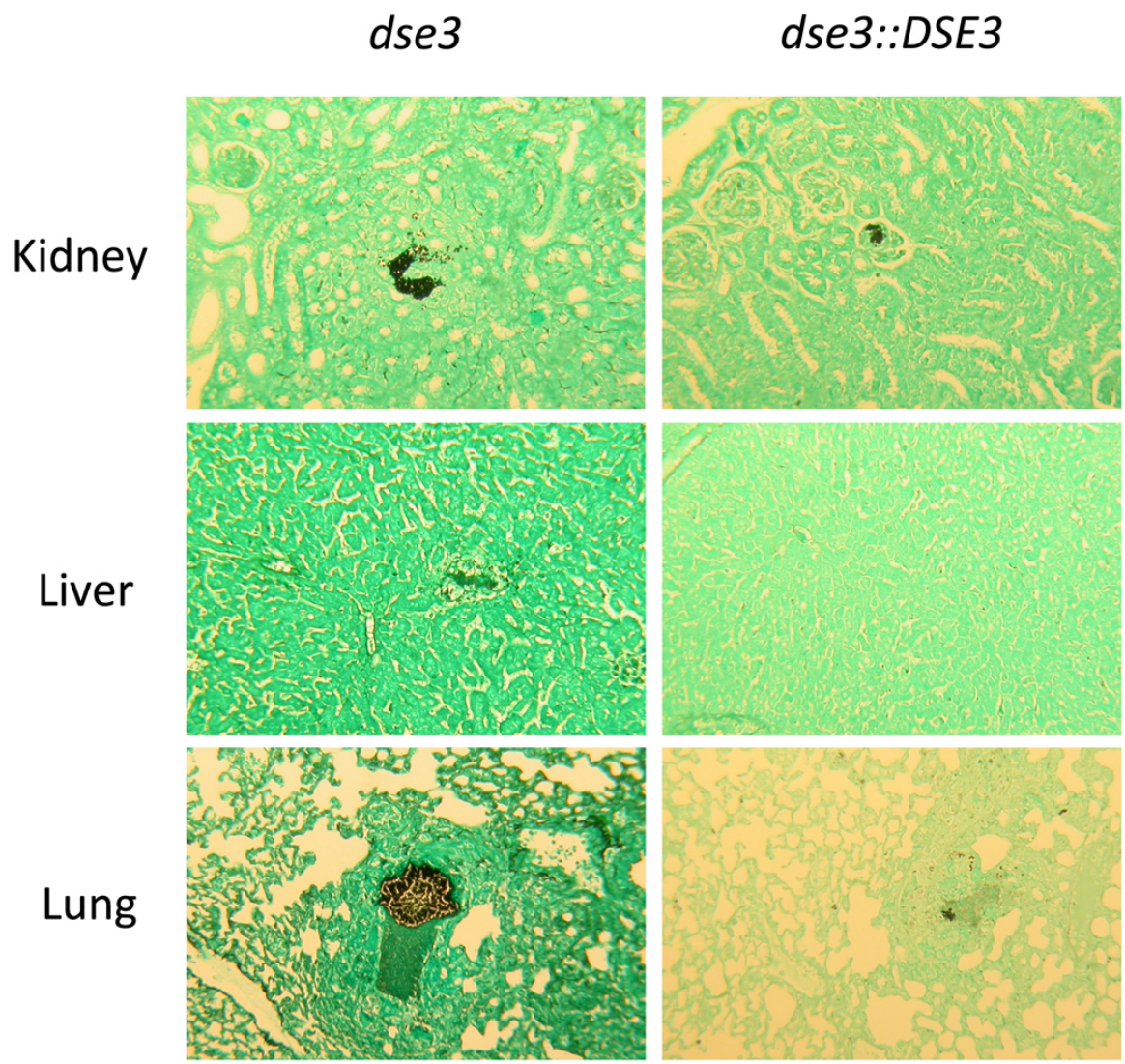


Figure 4.25d – Histological examination of tissues taken from *C. glabrata dse3* and *dse3::DSE3* experimentally infected mice. The kidney, liver and lung from *C. glabrata dse3* and *dse3::DSE3* infected mice were removed at sacrifice and stained using GMS. Staining revealed the lung to be the primary target organ for yeast colonisation. The reconstituted strain, *dse3::DSE3,* displayed similar yeast colonisation to the wild type strain.

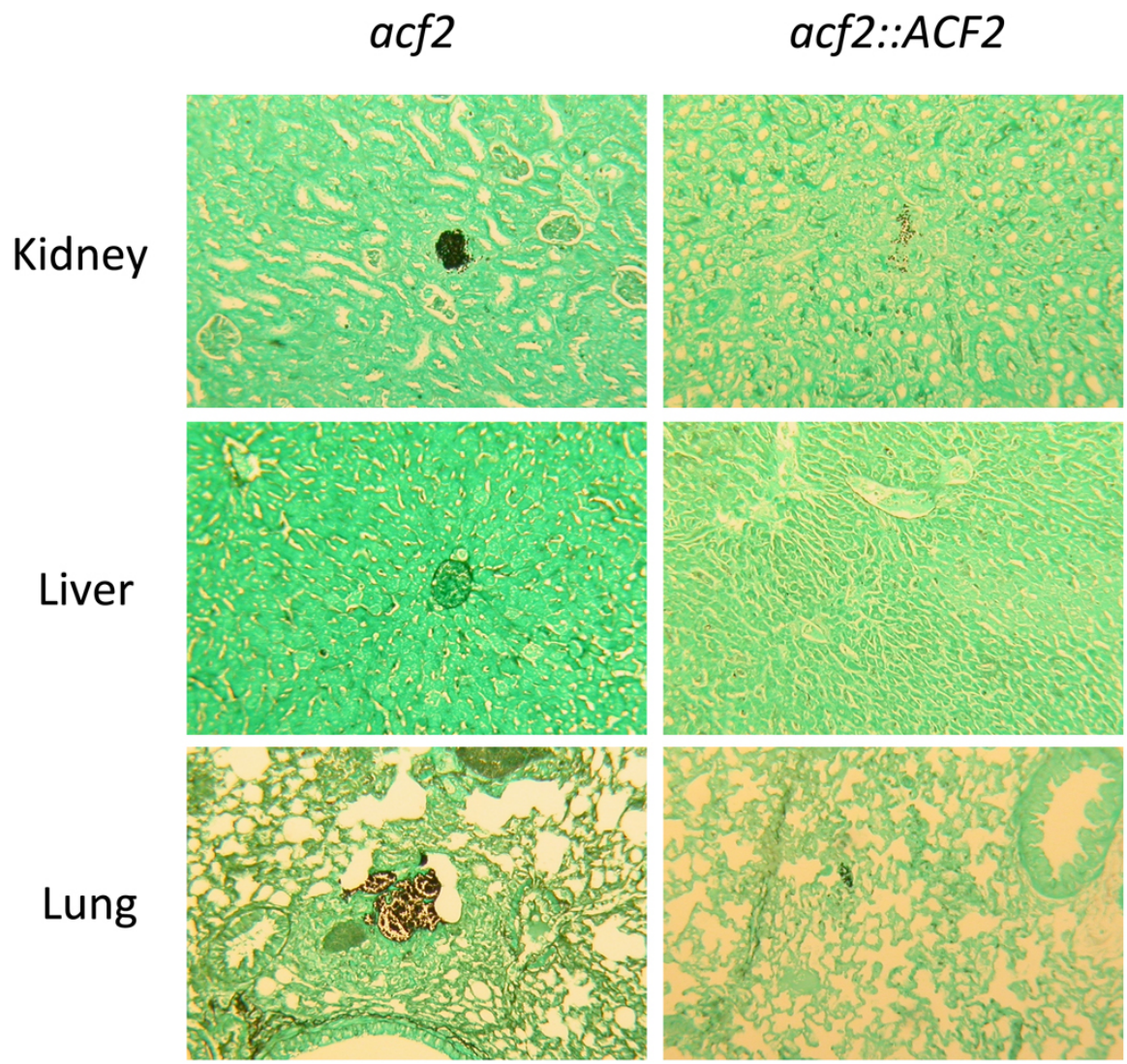


Figure 4.25e – Histological examination of tissues taken from *C. glabrata acf2* and *acf2::AFC2* experimentally infected mice. The kidney, liver and lung from *C. glabrata acf2* and *acf2::AFC2* infected mice were removed at sacrifice and stained using GMS. Staining revealed the lung to be the primary target organ for yeast colonisation. The reconstituted strain, *acf2::AFC2,* displayed similar yeast colonisation to the wild type strain.

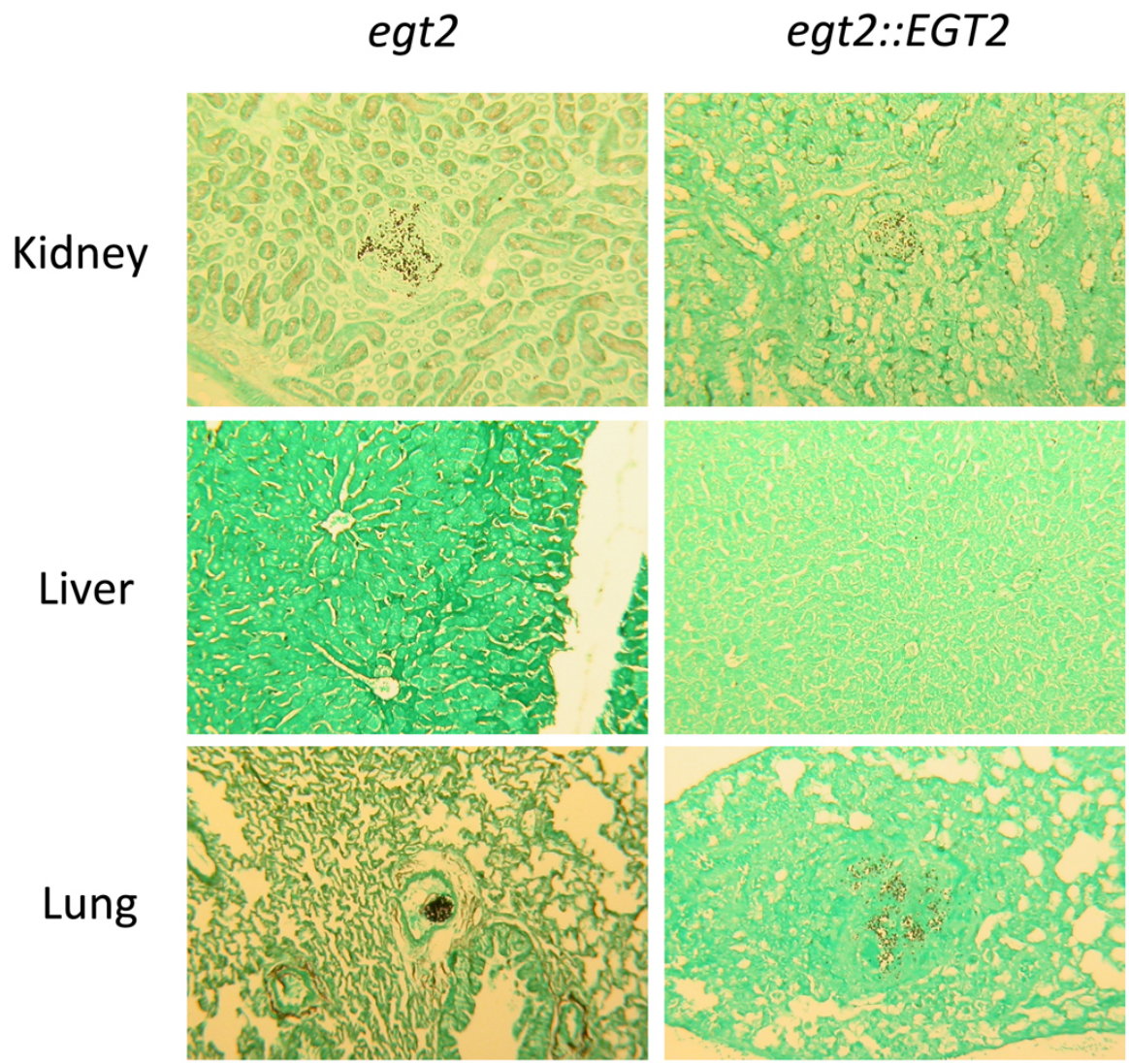


Figure 4.25e – Histological examination of tissues taken from *C. glabrata egt2* and *egt2::EGT2* experimentally infected mice. The kidney, liver and lung from *C. glabrata egt2* and *egt2::EGT2* infected mice were removed at sacrifice and stained using GMS. Staining revealed the lung to be the primary target organ for yeast colonisation. The reconstituted strain, *egt2::EGT2*, displayed similar yeast colonisation to the wild type strain.

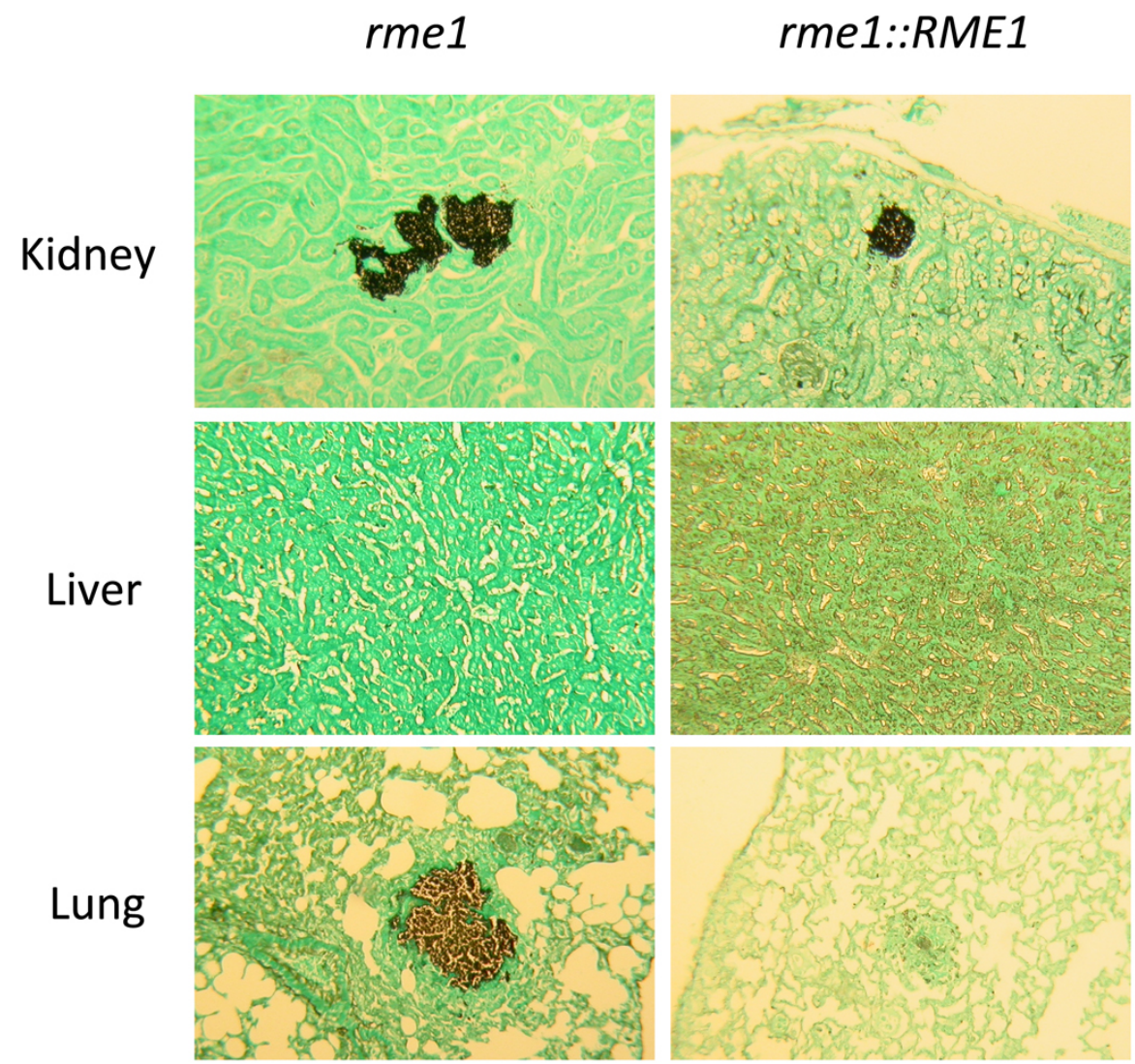


Figure 4.25f – Histological examination of tissues taken from *C. glabrata rme1* and *rme1::RME1* experimentally infected mice. The kidney, liver and lung from *C. glabrata rme1* and *rme1::RME1* infected mice were removed at sacrifice and stained using GMS. Staining revealed the lung to be the primary target organ for yeast colonisation. The reconstituted strain, *rme1::RME1,* displayed similar yeast colonisation to the wild type strain.

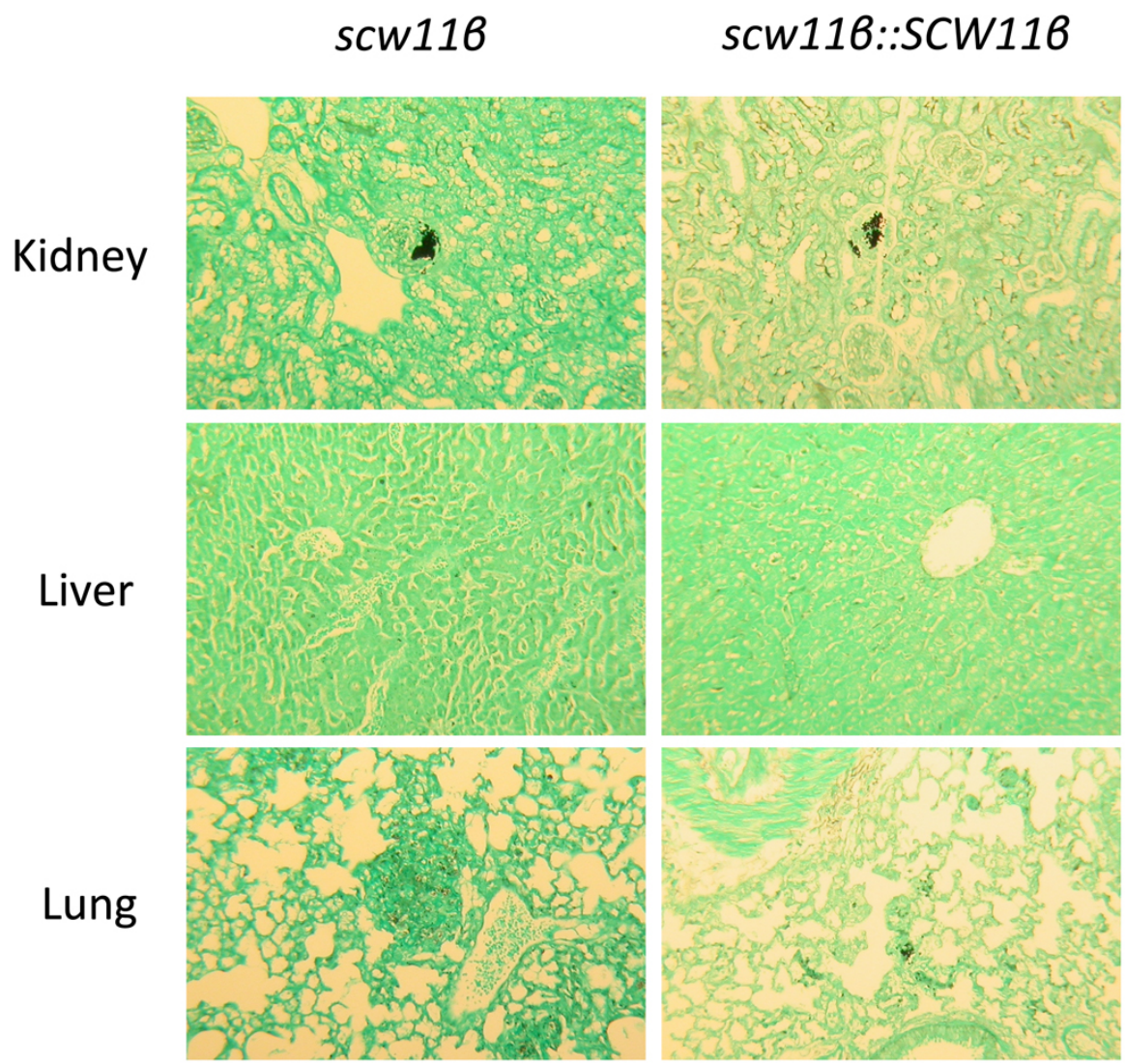


Figure 4.25g – Histological examination of tissues taken from *C. glabrata scw11β* and *scw11β::SCW11β* experimentally infected mice. The kidney, liver and lung from *C. glabrata scw11β* and *scw11β::SCW11β* infected mice were removed at sacrifice and stained using GMS. Staining revealed the lung to be the primary target organ for yeast colonisation. The reconstituted strain, *scw11β::SCW11β,* displayed similar yeast colonisation to the wild type strain.

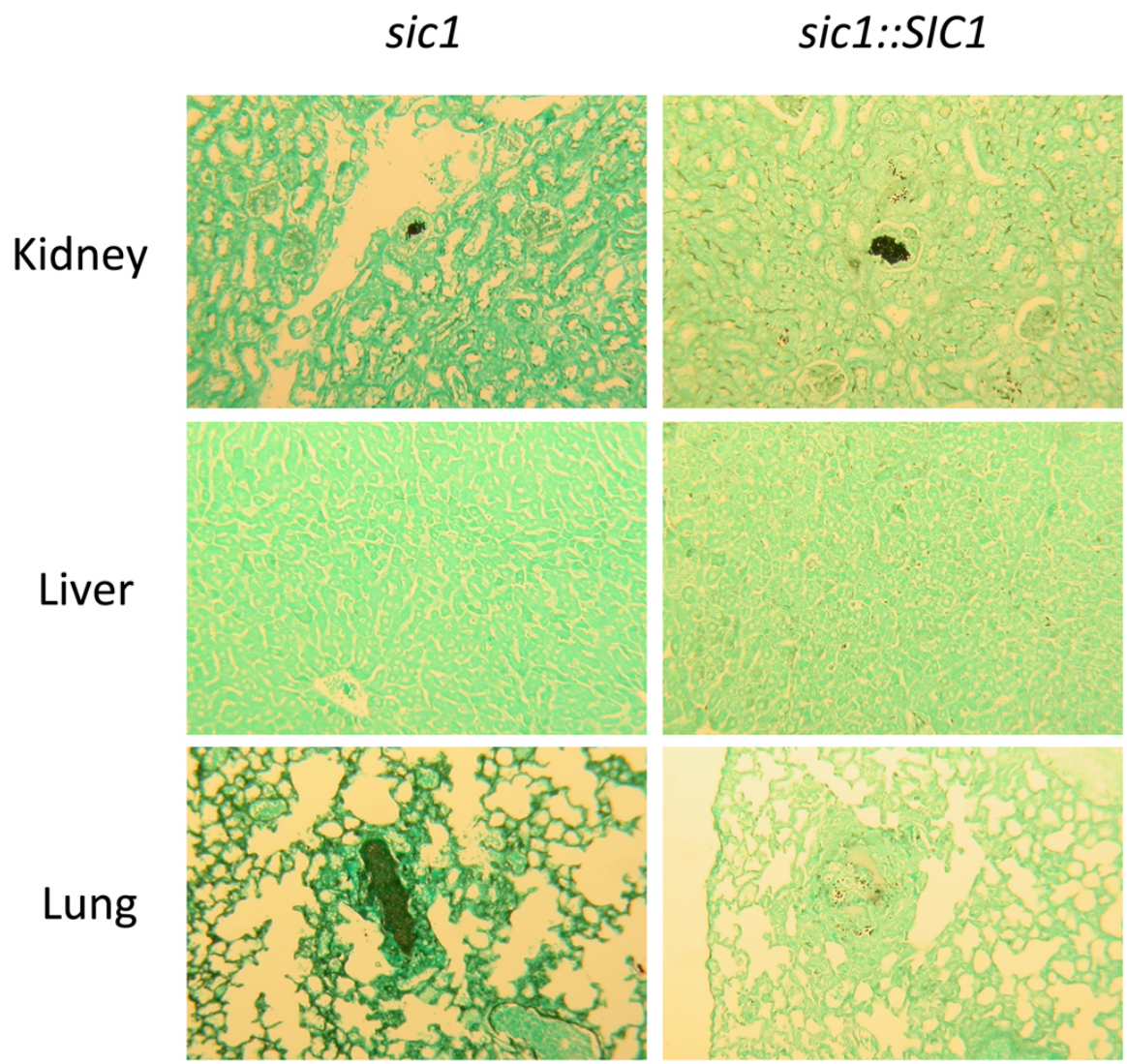


Figure 4.25h – Histological examination of tissues taken from *C. glabrata sic1* and *sic1::SIC1* experimentally infected mice. The kidney, liver and lung from *C. glabrata sic1* and *sic1::SIC1* infected mice were removed at sacrifice and stained using GMS. Staining revealed the lung to be the primary target organ for yeast colonisation. The reconstituted strain, *sic1::SIC1,* displayed similar yeast colonisation to the wild type strain.

4.3.9 Macrophage stimulation assay

To test the potential for immune over-stimulation and high levels of cytokine release, as is displayed in experiments with the *ace2* null [7], a macrophage stimulation assay was conducted. The hypervirulent nulls, *dse3*, *acf2*, *egt2*, *rme1*, *scw11β* and *sic1*, were screened for their ability to elicit TNFα and IL-6 production *in vitro* in mouse peritoneal macrophages (RAW 264.7) after a short infection as described in Section 4.2.10. The *C. glabrata sic1* null was shown to elicit a significantly different amount of TNFα and IL-6 production from the wild type using a one-way ANOVA ($p<0.005$ and $p<0.05$ respectively). The *sic1* null showed a four-fold increase in TNFα release and a 3.4-fold increase in IL-6 release compared to the wild type. Reconstitution of *SIC1* resulted in a return to wild type TNFα and IL-6 production levels.

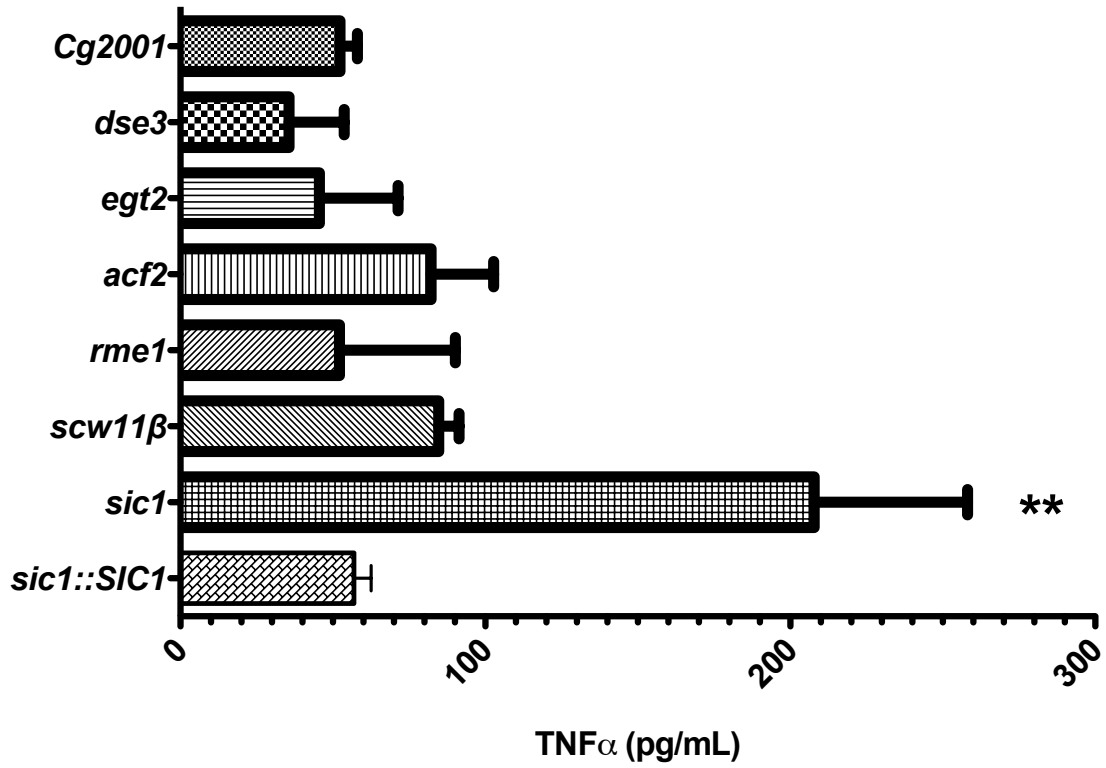


Figure 4.26 – *C. glabrata sic1* shows a significant increase in TNFα production in a macrophage stimulation assay compared to the wild type. *C. glabrata* 2001, *dse3*, *acf2*, *egt2*, *rme1*, *scw11β*, *sic1* and *sic1::SIC1* were exposed to RAW 264.7 macrophages at a ratio of 30:1 fungi:macrophage. After washing off unbound fungi, macrophages were incubated for 6 hours at 37°C, with supernatants then collected for TNFα quantification by ELISA kit (R&D Systems, UK). Results (mean with standard deviation) are pooled triplicate data from three separate experiments. *C. glabrata sic1* showed statistically significant increased levels of TNF-α elicitation compared to the wild type *C. glabrata* 2001 ($p < 0.005$, one-way ANOVA). Reconsitution of *SIC1* restored TNFα elicitation to wild type levels.

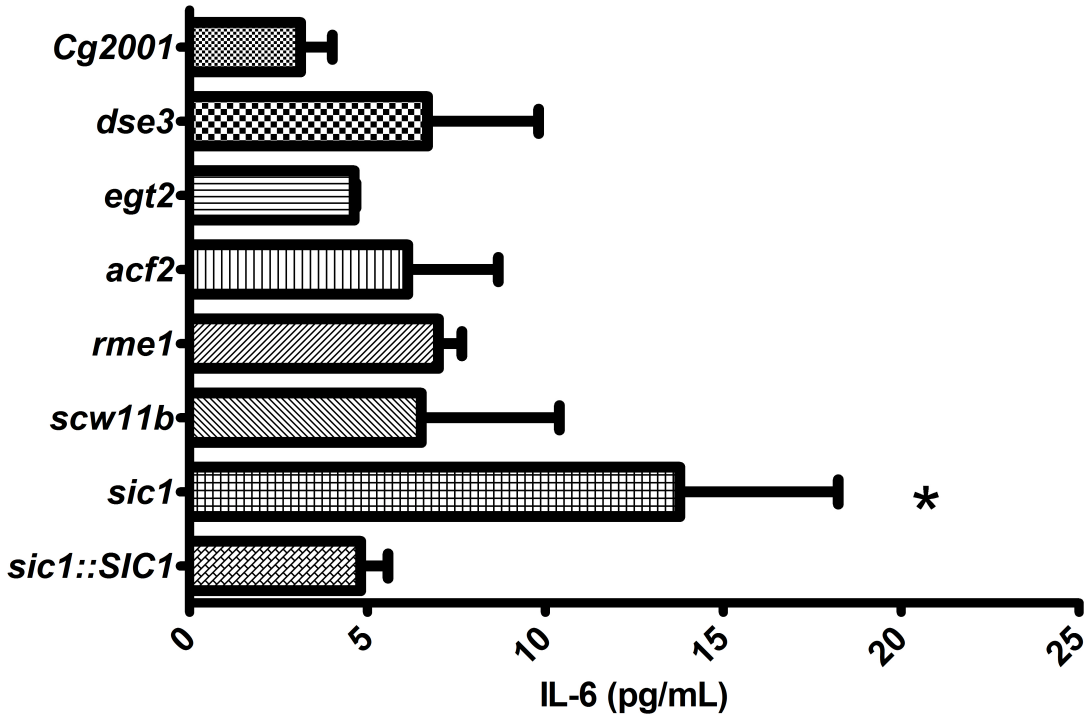


Figure 4.27 – *C. glabrata sic1* shows a significant increase in IL-6 production in a macrophage stimulation assay compared to the wild type. *C. glabrata* 2001, *dse3*, *acf2*, *egt2*, *rme1*, *scw11β*, *sic1* and *sic1::SIC1* were exposed to RAW 264.7 macrophages at a ratio of 30:1 fungi:macrophage. After washing off unbound fungi, macrophages were incubated for 6 hours at 37°C, with supernatants then collected for IL-6 quantification by ELISA kit (R&D Systems). Results (mean with standard deviation) are pooled triplicate data from three separate experiments. *C. glabrata sic1* showed statistically significant increased levels of IL-6 elicitation compared to the wild type *C. glabrata* 2001 ($p < 0.05$, one-way ANOVA). Reconsitution of *SIC1* restored IL-6 elicitation to wild type levels.

4.3.10 Reconstitution Northern Analysis

To show that reconstitution, as described in section 4.2.3, successfully resulted in the expression of the target gene within the null strains, Northern blotting, as described in section 2.3.15, was used to probe for the target gene in each null mutant and reconstituted strain. All six reconstituted strains displayed expression of the target gene and not in the null mutant as displayed in Figure 4.28.

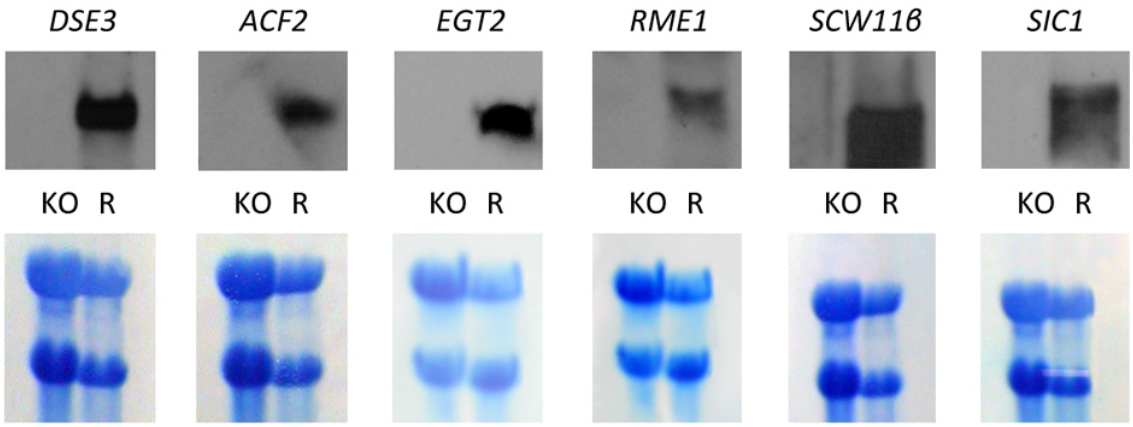


Figure 4.28 – *C. glabrata dse3::DSE3, acf2::ACF2, egt2::EGT2, rme1::RME1, scw11β::SCW11β* and *sic1::SIC1* reconstitutions display expression of the reconstituted gene. *C. glabrata dse3, dse3::DSE3, acf2, acf2::ACF2, egt2, egt2::EGT2, rme1, rme1::RME1, scw11β, scw11β::SCW11β, sic1* and *sic1::SIC1* were cultured in selective media over night, diluted down to 0.1 OD_{600} and allowed to grow for three hours. Total RNA was extracted using a Qiagen RNeasy mini kit as per the manufacturers instructions. Probes were constructed using internal primer pairs from the relevant gene as indicated above each pair of panels. Primers are listed in Appendix 3. The lower panels show methylene blue loading controls. The target gene expression is suppressed in the null strains as indicated by a lack of a band in the KO lane. All reconstituted strains display a black band in the R lane indicating expression of the reconstituted target gene.

4.4 Discussion

The results in this chapter have shown the first time that the *ACE2* virulence-moderating effect is created by multiple antivirulence genes under the transcriptional regulation of Ace2p, and that six genes, *DSE3*, *ACF2*, *EGT2*, *RME1*, *SCW11*β and *SIC1*, act as virulence-moderating genes in *C. glabrata*. Of those antivirulence genes, only the *C. glabrata sic1* null mutant shows an ability to induce inflated cytokine release in a macrophage model of immune stimulation. It has also been shown that deletion of the individual genes that form part of the Ace2p-dependent cell separation machinery, apart from *dse1* and egt2, do not create a visible cell separation defect, indicating that there is likely redundancy within the glucanases responsible for hydrolysis of the secondary septum in *C. glabrata*.

4.4.1 Deletion of the Ace2p regulon in *C. glabrata*

A reductionist approach was taken with regard the investigation of the antivirulence potential of the Ace2p regulon, by creating single gene deletions of the Ace2p-dependent genes in a suitable *C. glabrata* background strain. The first batch of six genes were created by initial attempts using the fusion PCR method for gene deletion, which created the deletion cassette using a fusion PCR cycle to join 5' and 3' UTRs of the target gene with a NAT resistance cassette. The six genes successfully disrupted were *ASH1*, *BUD9*, *DSE1*, *DSE3*, *EGT2* and *RME1*, which were confirmed by PCR and Southern analysis as shown in Appendix 4. Attempts to disrupt the remaining six Ace2p regulon genes, *AMN1*, *DSE2*, *ACF2*, *SCW11*α, *SCW11*β and *SIC1*, using the same methodology failed after many repeats. Several other deletion methodologies were then tried in an effort to disrupt the remaining six genes. Moderate success was attained using a simpler one-step PCR approach, the Edlind method, with four successful deletions confirmed by PCR and Southern analysis of the genes *AMN1*, *ACF2*, *SCW11*β and *SIC1* as shown in Appendix 4. Many attempts were made to disrupt the remaining two genes, *DSE2* and *SCW11*α, using the Edlind method and several other deletion methods, but unfortunately time ran out for their inclusion within this project.

It was assumed that deletions of both *DSE2* and *SCW11*α were possible, that the genes were not essential and that *dse2* and *scw11*α would be viable in *C. glabrata*, due to the fact that *ace2* mutants were viable and that both *DSE2* and *SCW11*α show no transcription in the absence of Ace2p as illustrated in chapter 3. It is possible, however, that the two genes are protected in some way from homologous recombination, which would prevent deletion via deletion cassette transformation, possibly due to their position within the chromosome. It is also possible that the assumption that *DSE2* and *SCW11*α are not essential could be wrong, and that they are essential for viability in *C. glabrata* and that they are expressed in low levels that are undetectable via Northern analysis in the absence of Ace2p.

4.4.2 Deletion screening

The putants for each of the 10 successfully disrupted genes were then subjected to a set of standard phenotypic tests as used within the Haynes lab, and detailed by Hampsey et al. [246], which included temperature, pH, nutrient and oxidative stress, as well as conditions to highlight cell wall and protein glycosylation deficiencies. The screen was not only designed to test for sensitivity to a series

conditions picked to show areas of possible gene function, but also to test for differences between the deletion putants, for selection of one particular mutant for each gene for virulence analysis. The phenotypic screen showed that there was no difference between the majority of the gene deletions and the parental type for all of the screen conditions, apart from a mild sensitivity of the mutants for *AMN1*, *DSE1*, *DSE3*, *ACF2*, *EGT2*, *RME1* and *SIC1* to vanadate, and a mild sensitivity of mutants for *AMN1*, *ACF2*, *SCW11β* and *SIC1* to caffeine (Figures 4.6 and 4.9). The minimal sensitivity for the majority of test conditions was expected of the partial Ace2p regulon null mutants when compared to the parental control, due to the lack of sensitivity shown by a similar screen of the *ace2* null mutant HLS122 [142]. Sensitivity to 2.5 mM vanadate could indicate a small change to the permeability of the cell to sodium orthovanadate, which is a known phosphatase inhibitor, and could indicate possible protein glycosylation and secretion defects [250]. Caffeine sensitivity is linked with defects in quite a few cellular processes, which include MAPK signalling pathways, as the caffeine molecule acts as a purine analogue once inside the cell and is currently used as phenotypic test for the evaluation of function of the Mpk1p-mediated cell wall integrity pathway [246, 247, 251].

The effects of gene deletions on cell separation were also analysed by microscopy. The results indicate that the extreme clumpy phenotype and failure of cell separation shown by *ace2* mutants in *C. glabrata* is multifactorial, and relies on the absence of expression of *CTS1* combined with the absence of other members of the cell separation machinery. Both *dse1* and *egt2* display a relatively mild cell separation defect when compared to that of *ace2* with lines of three or more joined cells consistently displayed as shown in Figure 4.10. Interestingly, the *dse1* cell separation defect displayed in the haploid *C. glabrata*, mirrors that shown in diploid *S. cerevisiae,* but not haploid *S. cerevisiae* lab strains [101]. It was suggested that Dse1p might play a role in bud site selection [163], invasive growth [166] and cross-talk between the pheromone and invasive growth pathways in *S. cerevisiae*, as well as a cell wall and filamentous growth role in *C. albicans* [169]. The current results indicate a probable role in cell separation due to the cell separation deficient phenotype and cell wall/septum hydrolysis in *C. glabrata*, and cannot confirm or deny a role in bud site selection, although a role invasive and filamentous growth within *C. glabrata* is improbable due to the lack of true hyphal formation yet to be found within the species [233]. *EGT2* encodes a GPI-anchored cell wall endoglucanase that is likely involved in cell separation in *S. cerevisiae* [127]. The cell separation defect, as shown in Figure 4.10, indicates that Egt2p also plays a role in cell separation in *C. glabrata*, and combined with the sequence homology of *EGT2* shown between the species suggests that it is a cell wall endoglucanase that plays a role in digestion of the secondary septum. One mutant from each of the gene deletions was selected to take forward through further testing

To see whether the Ace2p regulon gene deletions affected growth rates in *C. glabrata*, a 24-hour growth assay was used to plot the start and ends of the lag, exponential and stationary growth phases. Figure 4.12 shows that *C. glabrata amn1, ash1, acf2, bud9, dse1, dse3, egt2, rme1, scw11β* and *sic1* show similar growth rates to the *C. glabrata* wild type and parental strains, and therefore their growth is unaffected by the gene deletion. This means that any potential changes in virulence will not be down to a change in growth rate of the null mutants, when compared to the wild type.

By comparing the extreme cell separation deficient phenotype displayed by *C. glabrata ace2* to the individual Ace2p regulon gene deletions, it is probable that redundancy exists between the cell wall glucanases, and that the absence of *CTS1* expression, which results in a clumpy cell separation deficient phenotype [142], and therefore lack of chitin hydrolysis of the primary septum, forms a

major part of the cell separation deficiency. Considering that five genes transcriptionally regulated by Ace2p, *DSE2, ACF2, EGT2, SCW11α* and *SCW11β*, all encode cell wall associated glucanases and all show localisation to the daughter cell side of the bud neck in *S. cerevisiae*, redundancy within the genes is highly likely.

4.4.3 Virulence screening

The main focus of this study was to ascertain which genes transcriptionally regulated by Ace2p in *C. glabrata* had potential for antivirulence, in an attempt to explain the virulence-moderating effect of *ACE2.* The primary method of assaying virulence for *C. glabrata* candidiasis is the neutropenic murine model of disseminated candidiasis as defined and used in Haynes lab [7, 81]. Initial pilot studies using the *C. glabrata* wild type were performed to define a standard under the conditions to be used for the virulence analysis. It was found that a modification to the model, the addition of an extra immune suppression step at day -1 to ensure neutropenia on inoculation day, made the results more consistent and gave scope for detection of increased virulence even within small groups of animals. A test group to determine whether the addition of the extra immune suppression step caused a change in the uninfected control group's survival was run for the maximum period of the animal license (21 days), with 100% survival and no change from previously validated immune suppression regimes (Figure 4.13). It was decided that the modified neutropenic mouse model was fit for purpose, and that virulence testing of the Ace2p regulon genes was to be carried out using it.

The results show that for the first time in *C. glabrata*, six genes transcriptionally dependent on Ace2p are virulence moderating. In the modified murine model of disseminated candidiasis, *dse3*, *acf2*, *egt2*, *rme1*, *scw11β* and *sic1* all showed statistically significant hypervirulence, as tested by Log-rank (Mantel-Cox) analysis, when compared to the wild type as shown in Figures 4.18-4.23. All six deletions resulted in 100% mortality after five days compared to a 60% survival rate for the *C. glabrata* wild type, with *scw11β* and *dse3* also displaying mouse mortality on day four. Reconstitution of the hypervirulent null mutants was performed via plasmid transformation, confirmed by Northern Analysis (Figure 4.28), and assayed under the same modified model conditions to confirm the validity of the virulence phenotypes shown, with all six reconstitutions displaying a return to wild type virulence levels, statistically different from the deletion phenotypes as tested by Log-rank (Mantel-Cox) analysis, validating the hypervirulence phenotype displayed by *dse3*, *acf2*, *egt2*, *rme1*, *scw11β* and *sic1*. The other Ace2p regulon deletions *amn1*, *ash1*, *bud9* and *dse1* showed wild type levels of virulence when compared with Cg2001 (Figures 4.14-4.17), indicating that they likely play no part in the *ace2* null hypervirulent phenotype when individually disrupted.

The fungal burden created by each null strain was looked at in the kidneys of the infected mice. Fungal burden was estimated using the commonly used CFU per gram of tissue, in this case kidney, as a representative sample of colonisation. The results displayed in Figure 4.24, show that the fungal burden is increased by a factor of 10 to 100 correlating with those strains displaying hypervirulence. The strain that showed the greatest increase in virulence, *dse3*, also showed the highest fungal burden with 1.1×10^7 CFUs per gram of kidney, with *rme1*, *egt2, scw11β*, *sic1* and *acf2* decreasing in fungal burden with 9.9×10^6, 7.1×10^6, 6.6×10^6, 3.1×10^6 and 2.5×10^6 respectively. This is compared to the fungal burden of just 3.3×10^5 CFU/g shown by the *C. glabrata* wild type. This

indicates that the antivirulence displayed by the six genes of the partial Ace2p regulon in *C. glabrata* also amounts to increased survival and proliferation within the host environment and likely contributes to the increased mortality of the host.

Histological analysis of tissue from the kidney, liver and lungs of infected mice was also performed to look for yeast colonisation and proliferation within the host tissue. Given that the mice were infected with single cell solutions, *C. glabrata* displayed the ability to proliferate *in* vivo, with GMS staining (Figure 4.25) showing that the lungs were the primary target organ and that the hypervirulent *dse3*, *acf2*, *egt2*, *rme1*, *scw11β* and *sic1* strains formed larger colonies within host tissue when compared to the wild type, as was found for *C. glabrata ace2* cells by Kamran et al. [7]. The kidneys also showed an increase in yeast colonisation in the hypervirulent strains, while neither hypervirulent nor wild type strains showed much more than single yeast cells in the liver samples. The reconstituted strains displayed similar yeast colonisation and proliferation to the wild type, mirroring the return to wild type levels of virulence. No characteristic signs of inflammation were visible in H & E stained samples indicating that neither wild type *C. glabrata* nor the hypervirulent strains induce an inflammatory response from the host in the neutropenic model as was the case for *ace2* null cells [7].

The hypervirulent results show that it is possible that when the absence of each of the *DSE3, ACF2, EGT2, RME1, SCW11β* and *SIC1* genes are combined with the absence of *CTS1*, as is the case in an *ace2* mutant, the hypervirulent affect is synergistic creating the extreme hypervirulence displayed by *ace2*. To test this theory, deletions of all the seven genes, *DSE3, ACF2, EGT2, RME1, SCW11β, SIC1* and *CTS1*, need to be created within one strain, creating the equivalent of an *ace2* null with regard to the seven genes.

4.4.4 Immune activation and septic shock in Ace2p regulon hypervirulence

An immune over-stimulation effect has been reported for *ace2* and has been suggested to contribute to the hypervirulent phenotype displayed by the null strain in both CD1 and BALB/c neutropenic mouse models of candidiasis [233]. The dramatically increased cytokine release of both IL-6 and TNFα, 16- and 38-fold respectively, was suggested to contribute to the hypervirulent phenotype of *ace2*, mirroring the response involved in septic shock [233, 234]. To study the ability of the hypervirulent *dse3*, *acf2*, *egt2*, *rme1*, *scw11β* and *sic1 C. glabrata* strains to cause over-stimulation of macrophages and elicit cytokine release, a short macrophage infection assay was conducted with the resulting supernatant tested for both IL-6 and TNFα levels by ELISA. Compared to the *C. glabrata* wild type, only the *sic1* null showed the ability to significantly hyperstimulate the macrophages resulting in a 3.4-fold increase in IL-6 release ($P < 0.05$) and a four-fold increase in TNFα release ($P < 0.005$) when compared to Cg2001, with *dse3*, *acf2*, *egt2*, *rme1* and *scw11β* all exhibiting wild type levels as shown in Figures 4.25 and 4.26. Reconstitution restored *sic1* IL-6 and TNFα production to wild type levels.

Combining the *in vitro* cytokine release data with the fact that *dse3*, *acf2*, *egt2*, *rme1* and *scw11β,* took four to five days to cause mortality in the mouse model of candidiasis, it is unlikely that the hypervirulent phenotype is caused by induction of inappropriate cytokine release *in vivo* and septic shock. The same could be said for *sic1*, however its ability to induce a 3.4-fold increase in IL-6 and a

four-fold increase in TNFα production *in vitro* suggests that it contributes to the hyperstimulation displayed by the *ace2* null *in vivo* [7].

4.4.5 Potential effects of deletion of the Ace2p regulon genes

By looking at the current knowledge of the Ace2p regulon genes in *S. cerevisiae*, and the data revealed in this chapter, it is possible to hypothesise what effect some of the gene deletions will have on the *C. glabrata* cell. Amn1p is known to block G-protein signalling by binding to Tem1p and preventing the activation of the protein kinase Cdc15p, which in turn prevents activation of the protein phosphatase Cdc14p, preventing MEN activation [144]. In *S. cerevisiae*, *amn1* nulls have been shown to exhibit premature mitotic exit with inappropriate activation of MEN, and have been shown to also affect the expression of one of the other Ace2p regulon genes, *DSE3* [144, 175]. It is likely that deletion of *AMN1* in *C. glabrata* will have a similar effect, with premature MEN activation during spindle assembly or nuclear orientation checkpoints, although no obvious phenotype was displayed apart from a mild sensitivity to 10 mM caffeine, which could indicate a mild disruption of many cellular processes, including MAPK signalling pathways and the cell wall integrity pathway [246, 247, 251].

Ash1p has been shown to be a repressor of *HO* transcription and therefore controls the initiation of mating-type switching in *S. cerevisiae* [147]. Although three mating-type loci have been found within the *C. glabrata* genome and both a- and α-pheromone expressing strains exist [252], and that other parts of the mating machinery are also encoded in the genome [253], no sexual cycle has been discovered. It is therefore unknown what function Ash1p has within *C. glabrata*, although its transcriptional regulation by Ace2p and therefore its cell cycle regulated daughter cell specific expression, implies that it has a role in determining daughter cell fate. It is therefore unknown what effect its deletion could have on the *C. glabrata* cellular processes, and given that no obvious phenotype was displayed in screening apart from a mild sensitivity to 10 mM caffeine, the results from this study do not point to any function either.

Bud9p has been shown to act as a cortical landmark for bud site selection in a bipolar budding pattern [155-157]. It marks the distal pole of the cell within diploid *S. cerevisiae* cells, but is not active in haploid *S. cerevisiae*, which display axial budding rather than bipolar [155, 156]. It is unknown what role Bud9p plays in *C. glabrata*, due to its asymmetric and unipolar budding pattern [31]. However, it is possible that Bud9p marks the distal pole, from which the daughter cells tend to bud [31], acting as a cortical landmark in *C. glabrata* as Bud9p does in *S. cerevisiae*. If that is the case, deletion could cause a change in the budding pattern of the *C. glabrata bud9* null, however no such change in budding pattern was observed when compared with the parental strain as shown in Figure 4.10.

Dse1p is a gene of unknown function in both *S. cerevisiae* and *C. glabrata*. It has been suggested that Dse1p plays a role in cell wall metabolism in *S. cerevisiae*, with diploid *dse1* nulls displaying sensitivity to cell wall targeted conditions [101], and a possible role in control of cross-talk between the invasive growth and pheromone response pathway [166]; while in *C. albicans*, Dse1p has been suggested as having a role in cell wall metabolism [169]. Combined with the cell separation defect displayed in Figure 4.10, and Dse1p's bud neck localisation in *S. cerevisiae*, it is likely that Dse1p

plays a similar role in cell wall metabolism in *C. glabrata,* taking part in the degradation of the secondary septum or cell wall. Considering three out of the five Ace2p-dependent cell wall glucanases, *DSE2, ACF2,* and *SCW11β*, all failed to show a cell separation defect in their respective deletions as shown in Figures 4.10 and 4.11, it is also possible that Dse1p either plays role in regulating the action of multiple redundant glucanases, or that it plays a role in regulating the only glucanase to show a cell separation defect, Egt2p. The sensitivity to 10 mM caffeine could indicate a disruption to a range of cellular processes.

DSE3 encodes a gene of unknown function that does not share sequence homology with other characterised yeast genes, but is thought to play a role in control of daughter cell fate due its daughter cell specific expression and localisation to the bud neck [133, 143]. It is also upregulated in diploid *S. cerevisiae amn1* null cells, possibly indicating a role downstream from the MEN activation inhibitor [175]. It is unclear what role Dse3p could have within *C. glabrata*, which combined with a lack of significant display of phenotype during sensitivity screening, means that it is unknown what effect deletion of *DSE3* could have on its cellular processes. It is clear that *DSE3* has an antivirulence role, but does not elicit increased or reduced levels of cytokine release compared to the wild type; however further investigation into the function of Dse3p within *C. glabrata* is required.

DSE4 in *S. cerevisiae* is part of the glycosyl hydrolase family 81, and encodes a glucanase that localises to the daughter cell side of the bud neck [171, 176, 177]. Diploid *dse4* null cells in both *S. cerevisiae* and *C. albicans* have also been shown to display a cell separation deficient phenotype, indicating a probable role in hydrolysis of the secondary septum [130, 177]. It is therefore highly likely that the *DSE4* homologue in *C. glabrata*, *ACF2*, encodes a glucanase that plays a role in cell wall maintenance or secondary septum hydrolysis within the daughter cell. However *acf2's* lack of obvious phenotype apart from a mild sensitivity to 10 mM caffeine during testing, does not point to any clear-cut cellular role in *C. glabrata* other than as a general cell wall glucanase. However, the hypervirulence displayed by *acf2* indicates that a change has occurred to the cellular processes of the *C. glabrata* cell, perhaps in cell wall confirmation, increased glucan levels or metabolism; but its inability to elicit an increased or decreased cytokine response also indicates that if a conformational change has happened within the cell wall it has not exposed any new stimulatory antigens to the host, as would be the case in a change in β-glucan or mannan conformation [254]. It is possible that the deletion of *ACF2*, and loss of its action as a glucanase, has changed the confirmation of the cell wall to hide antigenic markers normally present on the cell surface, but not those detectable by the cytokine assays used here, increasing the difficulty of immune clearance and enhancing the survival of the yeast. It has been reported in other species that *ACE2* deletion creates a reduction in glucanase expression, and an increase in virulence, although the link between reduced glucanase expression and virulence has yet to be explained [255].

In *S. cerevisiae EGT2* encodes another cell wall glucanase, which has been shown to delay cell separation in its absence and therefore plays a role in the hydrolysis of the secondary septum and surrounding cell wall [127, 133]. A similar role in *C. glabrata* is likely due to the cell separation defect shown by *egt2* in Figure 4.10. It is interesting to note that Egt2p is the only Ace2p-dependent glucanase tested here to show a cell separation defect in its absence in *C. glabrata*, which could indicate that Egt2p is the primary glucanase involved in hydrolysis of the secondary septum during cell separation, or that it is involved in degradation of a section of the septum or surrounding cell wall that the other Ace2p-dependent glucanases do not act on. The effects of *egt2* on virulence are

similar to that of *acf2,* with no hyperstimulation of TNFα or IL-6 production, but hypervirulence is shown in the murine model. It is again, unclear what link there is between the lack of expression of a glucanase and virulence, but in the case of *egt2,* the cell separation deficient phenotype shown may play a part, perhaps causing clogging of blood vessels. That hypothesis was however, discounted for the extreme clumpy phenotype displaying *ace2,* through the use of chitinase to break up the cells prior to inoculation as discussed previously [7].

RME1 encodes a zinc finger-like protein that acts as a suppressor of meiosis, by inhibiting the expression of *IME1*, exclusively in haploid *S. cerevisiae* cells, and has been shown to promote mitosis through activation of *CLN2* expression [7, 181-185]. Disruption of *RME1* in *S. cerevisiae* has been shown to create larger than wild type cells and a reduced steady-state level of *CLN2* expression [189, 190]. It is therefore possible that deletion of *RME1* in *C. glabrata* could affect *CLN2* expression and therefore promotion of mitosis within the cell cycle, possibly causing a delay in cell cycle progression, although this was not corroborated by any obvious phenotype or growth rate under testing. The reason underlying the antivirulent potential of *RME1* is unclear. The wild type levels of TNFα and IL-6 production upon macrophage stimulation suggest that the absence of *RME1*, does not effect the cell surface receptors on the outside of the cell wall. *IME1* the target of *RME1*'s transcriptional repression has also been shown to be positively transcriptionally regulated by *RIM101* in *S. cerevisiae* [256]*. RIM101* is involved in the environmental pH response [257]*,* which has been shown to be crucial to virulence and host-environment survival. It is possible that derepression of *IME1* could infer some sort of enhanced environmental adaptation, leading to increased pathogen survival rates and hence increased virulence. Indeed, *IME1* has been linked to virulence potential through its involvement in the hyphal and pseudohyphal growth [258], neither of which were noticed in screening of the *rme1* mutant.

SCW11 encodes a cell wall associated glucanase that may have roles in cell separation and conjugation within *S. cerevisiae* [134, 193, 194]. *SCW11* deletion has been shown to cause a cell separation defect in *S. cerevisiae* [134], while it has been suggested as being essential in *C. albicans* and has been shown to be down-regulated in hyphal cells compared to yeast cells [197-200]. It is therefore likely that the two *SCW11* homologues *SCW11α* and *SCW11β* in *C. glabrata*, play a role in septum hydrolysis or cell wall metabolism, meaning that a deletion could affect septum degradation and cell separation. The results of testing of *scw11β* in Figures 4.7-4.9, however, show no obvious phenotypes apart from a mild sensitivity to caffeine, which could indicate a defect in several cellular processes and MAPK signalling pathways including the cell wall integrity pathway [246, 251]. The hypervirulent phenotype displayed by *scw11β* indicates a similar situation to *acf2*, maintaining wild type levels of immune stimulation. Again it is unknown how the absence of *SCW11β* a cell wall, septum-associated glucanase, causes increased virulence.

The final gene in the Ace2p regulon, *SIC1*, has been shown to encode a cyclin-dependent kinase inhibitor in *S. cerevisiae* that targets the Cdk1p-Clbp histone kinase complexes and prevents premature initiation of DNA replication, S-phase progression and insures genomic integrity within the cell cycle [209, 210]. It is likely that the *SIC1* homologue in *C. glabrata* performs a similar function, acting as part of a cell cycle checkpoint and controlling progression to S-phase. *SIC1* deletion might therefore cause loss of genomic stability and premature DNA replication. In *S. cerevisiae*, *sic1* nulls show partial mitotic arrest, which could be corroborated by the mild sensitivity

to 10 mM caffeine displayed in Figure 4.9, and could cause a delay in cell cycle progression, but none was presented by growth rate analysis as displayed in Figure 4.12. On the antivirulence front, it is unclear what role *SIC1* plays, although its deletion will create genome instability and possibly the ability to acquire gain of function mutations. Sic1p's inhibition target, Cdk1p, has been highlighted in maintenance of pathogenicity in the smut fungus, *Ustilago maydis* [259], however it is unknown how de-inhibition of Cdk1p-Clbp complex could aid *C. glabrata* virulence. The *sic1* null also displayed over-stimulation of TNFα and IL-6 production compared to the wild type, indicating that in the absence of *SIC1*, conformational changes in the cell wall are made. No such observations have been reported in the literature for *S. cerevisiae* or any other eukaryote, but premature DNA replication and progression to S-phase could result in any number of gene defects that could cause changes to the protein components of the cell wall.

4.4.6 Ace2p regulon hypervirulence and *ace2*

Given that the other Ace2p regulon null mutants, *amn1*, *ash1*, *bud9* and *dse1,* only showed wild type levels of virulence, it seems unlikely that they could contribute to either the hyperstimulation of cytokine response or the extreme hypervirulence shown by *ace2* [7]. Therefore the results presented in this chapter suggest that the *ace2* hypervirulent phenotype is created by a combination of antivirulence genes including *DSE3, ACF2, EGT2, RME1, SCW11ϐ* and *SIC1,* as well as the previously investigated *CTS1*, which in their individual deletions all show a hypervirulent phenotype that is significantly different from the wild type, but milder than *ace2*. The combination of their individual milder hypervirulence phenotypes could be the cause of the extreme *ace2* hypervirulence, although it is unclear how *ace2* causes such a large increase in cytokine release, given that only one of the Ace2p regulon deletions tested here elicited a four-fold increase in TNFα release and only a 3.4-fold increase in IL-6 release. Although the quantity of wild type *C. glabrata* cytokine detected between *in vivo* and *in vitro* was roughly similar [7] there is a possibility that the ratio of cytokine release between *in vivo* and *in vitro* testing as used in this study is not directly comparable, and all that can be said is that *sic1* significantly increases cytokine release *in vitro*, but the extent to what might be shown *in vivo* cannot be extrapolated. Therefore a repeat of the *sic1* cytokine release study, this time *in vivo*, is required.

It is interesting to note that all the Ace2p-dependent cell wall glucanases successfully disrupted in this study display hypervirulence in their absence, but do not elicit increased levels of cytokine release. It is, however, unclear how a cell bud neck area directed cell wall glucanase contributes to virulence in its absence.

Study of the link between cell surface carbohydrates and virulence within *C. albicans* is a well-established field with *N*- and *O*-linked mannans and other cell wall associated glycoproteins playing a role in both adherence and immune recognition (reviewed by Mora-Montes et al. [260]). With regard to the β-glucan elements of the cell wall, maintenance of cell wall integrity and glucan architecture have been shown to be crucial to virulence in *C. albicans* [261]. For the most part, the glucan components of the cell wall are hidden by an outer mannan coat that forms the first point of contact with the host environment and therefore the immune cells of the host. At certain times and within certain areas, such as budding and the bud scar, the glucan components of the cell wall within *C. albicans* are more exposed and form part of the immune recognition of the fungal cells by the

host through the β-glucan receptor dectin-1 [261, 262]. In *C. glabrata* it is likely that a similar exposure of β-glucan occurs at the point of budding, aiding immune recognition by the host and therefore clearance of the pathogen. Perhaps then, the deletion or suppression of Ace2p-dependent glucanase expression causes a change in the β-glucan component or architecture of the cell wall around the bud neck area that reduces the exposure of glucan-based antigens to the host immune system, thereby reducing immune recognition and enhancing the ability of *C. glabrata* to persist and cause disease. To see whether a change in glucan architecture is present in *C. glabrata acf2, etg2* and *scw11β*, glucan isolation and spectral analysis could be used to compare the glucan component of the cell wall of the null mutant to that of the *C. glabrata* wild type. Glucan can be isolated via acid extract as described by Müller et al. [263] and then solution-state ^{1}H NMR spectroscopy could be used to compare and contrast the structural composition of the glucans [264]. Tunnelling Electron Microscopy could also be used in a similar manner to the work performed with *C. albicans* by Netea et al. [265] to visually inspect the cell wall structure of the null mutants for comparison with the wild type, which would give an indication of any variation in thickness of the β-glucan layer or any possible conformational change of the cell wall due to the absence of glucanase activity contributed by the Ace2p-dependent glucanases. It would also be useful to perform a similar immune stimulation assay as conducted in this chapter with a macrophage strain with greater dectin-1 presentation to see whether there is a reduction in β-glucan recognition in the *C. glabrata acf2, etg2* and *scw11β* null strains compared to the wild type. Of course it may also be true that the cell wall associated glucanases within the cell wall contribute directly to the immune recognition of *C. glabrata* and therefore when absent from the cell wall cause a reduction in the immune recognition foot print of the yeast that couldn't be detected by the immune stimulation assays performed in this study that were heavily biased towards over-stimulation.

Two remaining genes, *DSE2* and *SCW11α* also encode cell wall glucanases. It would be interesting to see if they too have antivirulence potential. Unfortunately they remain uninvestigated and it is therefore necessary for further work to be done to disrupt, or silence their expression and to test their antivirulence potential and ability to elicit a macrophage hyperstimulation response to complete the partial Ace2p regulon antivirulence picture. It is clear, however, that the antivirulence effect of *ACE2* is a multifactorial affair and that its ability to cause hypervirulence in its absence may revolve around more than just the genes found to show Ace2p-depedent expression. Ace2p has been shown to affect the proteome of *C. glabrata* in many ways [231], and further investigation into the transcriptome of Ace2p in *C. glabrata* is still needed.

4.4.7 Implications of antivirulence

On the surface of it, the occurrence of antivirulence or virulence moderating genes might seem counterintuitive for a fungal pathogen like *C. glabrata*. However, for the maintenance of a gene that causes increased ability to cause disease in its absence, there must be evolutionary pressure to keep said gene. Unlike the majority of the rest of the pathogenic *Candida* species, *C. glabrata* lacks any form of true hyphal morphology and only displays pseudohyphae in nitrogen starvation conditions *in vitro* [31]. This leaves budding and efficient cell separation as the only method of colonisation, expansion and transmission between hosts available to *C. glabrata*. Therefore it has been suggested that dissemination and transmission might be a cause of evolutionary selective pressure [266], which

in this case requires maintenance of cell separation competency and therefore it is the most likely reason for the maintenance of *ACE2,* which encodes the master transcriptional regulator for the cell separation machinery [101]. It is however, harder to justify the maintenance of some of the Ace2p regulon genes, especially those that show sequence similarity and potential redundancy. For instance the cell wall glucanases *ACF2* and *SCW11ϐ* do not present a cell separation deficient phenotype when disrupted individually, which suggests that there is redundancy in the cell wall glucanases that hydrolyse the secondary septum, or that they do not play a primary role in cell separation despite being localised to the bud neck. Interestingly *EGT2* was the only cell wall glucanase tested here that showed a cell separation deficiency when disrupted, which could account for the apparent evolutionary pressure to maintain its function within the cell even though it is antivirulent. As we do not currently know the function of Dse3p within the cell, it is not possible to ascertain why it is maintained when it harbours antivirulence potential. It is, however, possible to rule out an essential role in cell separation due to the cell separation competent phenotype *dse3* null cells present. Both *RME1* and *SIC1* are involved in multiple cell cycle related processes within *C. glabrata*, therefore it is likely that maintenance of their function is critical for optimum cellular function, although they have been shown to not be essential in *C. glabrata* by their deletion.

Here we have found for the first time six more antivirulence genes in *C. glabrata* and have expanded the knowledge of the mechanisms behind the *ace2* hypervirulence effect. A possible link between the septum targeted glucanases and antivirulence has been made, but further work with these and the other antivirulence genes is required to fully understand the mechanisms behind the *ace2* antivirulence. It would be interesting to see whether other, non-Ace2p-dependent cell wall glucanases have a similar antivirulence potential. It should be noted that due to the restrictive sample sizes available within this study, negative results might not be definitive and future testing with greater samples sizes is needed to confirm the lack of hypervirulence.

The finding of six independently antivirulent genes all transcriptionally regulated by Ace2p has set out yet more targets for further investigation into this interesting and potentially significant virulence work. The mechanism of *C. glabrata* virulence *in vivo* is not yet well understood, and these studies have drawn a spotlight on previously innocuous genes, especially those showing redundancy, that might play a role *in vivo* in the potential for onset of systemic candidiasis. Transcriptome profiling of *C. glabrata in vivo* from both the wild type and *ace2* mutant is badly needed to see which genes are up and down regulated in response to the host and to pinpoint any more potential antivirulence or virulence-moderating factors changed by the deregulation of the control systems regulated by *ACE2* expression.

5 Study of the novel gene *DSE1* in yeast

5.1 Overview

During the investigation into the partial *C. glabrata* Ace2p regulon and the *ace2* hypervirulent effect, a novel gene that encoded a protein of unknown function was highlighted. The gene in question was *CAGL0K02277g*, which showed homology to the only uncharacterised *S. cerevisiae* gene to show Ace2p-dependent expression at the time, *DSE1* (*YER124C*) [101]. *DSE1* within both *S. cerevisiae* and *C. glabrata* shows no homology to other *DSE* genes such as *DSE2* and *DSE4* which encode cell wall associated glucanases as discussed in chapters 1 and 4. However, in both yeasts, *dse1* nulls display a cell separation defect and as such are thought to play a role in cell separation. Therefore an investigation into the function of this uncharacterised gene was undertaken to further our knowledge of cell separation, a crucial part of the life cycle of yeast cells and in particular *C. glabrata*, where budding marks the only dissemination and transmission mechanism available to this important fungal pathogen, as previously discussed in chapter 4.

In *S. cerevisiae*, *DSE1* has been shown to be expressed with other Ace2p-dependent genes, in the run up to cytokinesis and cell separation [101, 133]. It has also been shown to be transcriptionally repressed by the Ace2p homologue Swi5p, which has also been shown to bind to the same binding sites as Ace2p within the promoter regions of regulated genes [101, 133, 267]. Knowing that *DSE1* expression is dependent on a cell cycle regulated transcription factor it is unsurprising then that *DSE1* shows cell cycle regulated expression, which peaks in the run up to cell separation with the rest of the Ace2p-dependent genes [101, 133]. Dse1p has also been shown to localise in a similar manner to the cell separation machinery, localising to the bud neck area of the cell in *S. cerevisiae* prior to cell separation [143]. This observation indicates that Dse1p may have a role in cell separation, although precisely what role is unclear.

A reductionist approach was taken by Doolin et al. in the study of *DSE1*, among other genes, in *S. cerevisiae*, in which they showed that diploid *dse1* cells showed a cell separation defect that could not be replicated in haploid cells [101]. The diploid *dse1* cells also displayed a sensitivity to cell wall targeted test conditions including SDS, calcofluor white and caffeine, which made them speculate that Dse1p might be involved in cell wall metabolism and cell separation [101]. Data from *C. albicans* also hints at a cell wall metabolism role with a haploinsuffient *DSE1 C. albicans* strain showing increased sensitivity to calcofluor white, SDS and oxidative stress [268]. A slightly decreased chitin deposition in the cell wall was also recorded, as was an increased level of filamentous growth on both solid and liquid media and delayed adhesion contributing to reduced virulence [268]. Daher et al. also suggested that *DSE1* was an essential gene in *C. albicans* due to their failure to create a homozygous null strain [268].

Results of *DSE1* over expression also corroborate the theory of a cell wall and budding associated role, this time displaying a budding-within-birth-scar phenotype in haploid *S. cerevisiae* cells, a phenotype that has never been recorded in wild type cells, with the closest being bud sites overlapping the birth scar [163]. The birth scar is typically a highly protected area within budding yeast, defined as a zone of forbidden budding [163], which in turn hints that Dse1p may play a role

in bud site selection. Other observations from *DSE1* over expression within *S. cerevisiae* also reinforce the idea of a cell wall maintenance role, due to an observation that the cell wall integrity pathway had been activated [163].

Draper et al. suggested that Dse1p could play a role in cross-talk between the pheromone and invasive growth pathways due to its ability to bind to both a Ste4p complex and Ste11p [166]. They showed that *DSE1* over expression could induce invasive growth in *S. cerevisiae*, and that it also caused interference with the pheromone sensing pathway, conferring resistance to cell cycle arrest in G_1 in response to mating factor exposure [166]. *DSE1* deletion caused a twofold sensitivity to pheromone-induced cell cycle arrest in *S. cerevisiae*, supporting the hypothesis that Dse1p plays a role in the pheromone sensing pathway [166].

Neither *C. glabrata* nor *S. cerevisiae DSE1* show much homology with other Ace2p-dependent genes, or any other characterised genes for that matter, within *S. cerevisiae, Candida* species or other eukaryotes [170, 171]. Physical and genetic interaction data for Dse1p within *S. cerevisiae* shows 32 different possible interactions with three of them pointing to a role in bud site selection or bud formation [163-165]. Dse1p physically interacts with Boi1p, Boi2p and Zds2p, which are all thought to play a role in budding and bud site selection [163-165]. Both Boi1p and Boi2p are thought to play a role in polar growth [167]. They both localise to the bud cortex with double null mutants displaying an abnormally large, round phenotype and disruption of cell polarity maintenance [167]. Double *boi1boi2* mutants also display defective bud formation, indicating that they may play a role in more than just bud site selection [167]. Boi1p and Boi2p have been shown to interact themselves with Bem1p, a protein that helps establish the cellular polarity required for budding [165, 168], adding support to the hypothesis that *DSE1* is involved in bud site selection. Another physical interaction, this time with Ste11p, reinforces the theory that Dse1p plays a role in invasive growth and pheromone sensing, due to Ste11p's involvement in pseudohyphal growth [165, 166]. Ste11p has also been shown to play a role in virulence in *C. glabrata* and along with Ste4p has been implicated in pheromone sensing [82, 165, 166].

The data for *DSE1* suggests three potential roles within budding yeast. The first is a cell wall metabolism and cell separation role, which is supported by bud neck localisation, activation of the cell wall integrity pathway, sensitivity to cell wall targeted conditions in *dse1* nulls, a cell separation defective phenotype in certain nulls and a peak expression in the run up to cell separation. The second potential role is one of bud site selection, supported by a budding-within-birth-scar phenotype displayed with *DSE1* over expression and physical interactions with Boi1p, Boi2p and Zds2p. The third and final role is one of pheromone sensing and hyphal growth, which is supported by *DSE1* overexpression affording a resistance to pheromone induced arrest and enhanced invasive growth; *dse1* nulls showing an increased sensitivity to pheromone induced arrest; as well as Dse1p's ability to physically interact with both Ste11p and Ste4p.

None of the three roles suggested in the literature have to exist in isolation, with each one potentially overlapping the next. The true role for Dse1p in *S. cerevisiae* and *C. glabrata* is likely to be a mix of the three, although the lack of hyphal growth in *C. glabrata*, with pseudohyphal growth only visible under nitrogen starvation on solid media [31], and Ace2p-dependence mean that the cell wall metabolism and cell separation role or the bud site selection and bud formation roles are most likely in the pathogenic yeast.

Although the bulk of the work throughout this thesis has centred on *C. glabrata*, a much smaller body of work and tools exist for the pathogenic yeast when compared with its close genetic relative *S. cerevisiae*, which has been extensively studied and used as a model organism for the study of many cellular processes for decades. This means that tools for investigating the roles of unknown genes are much more developed in *S. cerevisiae* and resources such as the Yeast Knockout Library (YKO), the Yeast GFP library and genetic tools such as the Gateway cloning system (Invitrogen, UK), provide useful methods for study of the functions of Dse1p within yeast that simply aren't available in *C. glabrata* at this time. Therefore the experiments presented in this chapter will leverage the tools available for *S. cerevisiae*, combined with study in *C. glabrata* where possible, to explore possible functions for Dse1p within the two yeast species.

5.2 Materials and Methods

5.2.1 Analysis of the upstream region of *DSE1* in *S. cerevisiae* for potential Ace2p binding sites

The sequence for *S. cerevisiae DSE1* was downloaded from the *S. cerevisiae* Genome Database [170]. As described previously for *C. glabrata* genes in chapter 3, the sequence was imported into Serial Cloner, version 2.1, Serial Basics, France. The ORF was then mapped, while the intergene region upstream of *DSE1* was searched for the potential Ace2p binding site ACCAGC and its reverse complement, as defined by Dohrmann et al. [152]. Potential binding sites were then marked and the distances in base pairs to the start codon of the target gene were calculated.

5.2.2 *C. glabrata* Dse1p structural prediction

The structure of *C. glabrata* Dse1p was investigated by computational structural analysis in conjunction with Dr. Talavera (University of Manchester) [269]. Briefly, the sequence of *DSE1* from *C. glabrata* was analysed using mGenTHREADER and secondary structure recognition techniques that identified a potential structural template [270, 271]. The amino acid sequence was then aligned to the template and a model was built using Modeller [272]. The model was then checked and refined with MolProbity [273] and PROCHECK [274], as well as manual trial and error modification.

5.2.3 *C. glabrata* and *S. cerevisiae dse1* null vanadate sensitivity screen

A solid agar phenotypic screen was performed as described in sections 4.2.4 using only 0.5, 1, 2, 4, 5 and 6 mM vanadate concentrations.

5.2.4 Yeast *dse1* null polarization study

The *C. glabrata* wild type (Cg2001), *S. cerevisiae* wild type (BY4741), and the *C. glabrata* and *S. cerevisiae dse1* null cells were grown overnight in 5 mL of YPD media at 30°C, 180 rpm. Cells were spun down at 900 g and washed twice with PBS before being re-suspended in approximately 5 mL of PBS. Approximately 10 µL of culture was mounted on microscope slides and visualised using a Zeiss Axiovert 200 inverted microscope with a 63x objective. The cells were photographed using a Hamamatsu ORCA-ER digital camera. The images were manipulated and the cells measured using Image J, version 1.44p, National Institutes of Health, Maryland, USA. Briefly, the contrast was enhanced, a mask was applied and then the cells selected using the boundary select tool. Each cell was inputted into the POI manager, and measured for the smallest bounding rectangle using the measure tool. 300 cells were counted per strain, and a ratio of each individual's length to width was calculated then averaged as a measure of the strain's cell polarization.

5.2.5 Construction of Dse1p-GFP Gateway plasmid

S. cerevisiae DSE1 was cloned into pAG426GPD-ccdB [275] featuring a GFP-tag, constitutive promoter and *URA3* marker using the Gateway Cloning System (Invitrogen, UK). Briefly, the *S. cerevisiae DSE1* was cloned into a pENTRY vector using a two-step PCR method and BP clonase. The pENTRY vector containing *DSE1* was then transformed into *E. coli* TOP10 as described in section 2.3.14, and incubated at 37°C overnight on selective media. Successful transformation was confirmed using PCR as described in section 2.3.2 with the target pENTRY vector extracted from an overnight culture using a QIAprep©Spin MiniPrep kit (Qiagen Ltd, UK) as described in section 2.3.10.

The successful insert was then cloned from the pENTRY vector into the *URA3* marker GFP destination vector using LR clonase. The destination vector was then transformed into *E. coli* TOP10 as described in section 2.3.14, and incubated at 37°C overnight on selective media. Successful transformation was confirmed using PCR as described in section 2.3.2 with the target destination vector extracted from an overnight culture using a QIAprep©Spin MiniPrep kit (Qiagen Ltd, UK) as described in section 2.3.10. The successful plasmid constructs were then stored at -20°C.

5.2.6 Localisation study of *S. cerevisiae* Dse1p in known interactor nulls

To see whether Dse1p's localization was dependent on proteins shown to have physical interaction with Dse1p in *S. cerevisiae*, a plasmid containing *S. cerevisiae DSE1* tagged with GFP as constructed in section 5.2.5, was transformed into target strains from the Yeast Knockout Library YKO, selected for their physical interaction with Dse1p in *S. cerevisiae*, and the parental strain BY4741 [165, 242, 276]. A GFP-tagged Dse1p yeast strain from the commercially available Yeast-GFP library was included for comparison (Invitrogen, UK) [143]. The yeast strains were grown overnight in 5 mL of selective media at 30°C, 180 rpm. In the morning, the cells were diluted to OD_{600} = 0.3 and allowed to grow at 30°C, 180 rpm for a further two to three hours, till the OD_{600} was between 0.5-1. Cells were spun down at 900 g and washed twice with PBS before being re-suspended in approximately 200-500 µL of PBS. Approximately 10 µL of culture was mounted on microscope slides and visualised using a Zeiss Axiovert 200 inverted microscope with a 63x objective. The cells were photographed using a Hamamatsu ORCA-ER digital camera with a DA/FI/TR/Cy5-4X-A Quad-band filter set (Semrock) to observe GFP tagged proteins, while images were manipulated using HCImage, version 2.1.1.0, Hamamatsu Corporation, New Jersey, USA.

5.2.7 Growth rate analysis

Yeast cells were grown overnight in 5 mL of YPD media at 37°C, 180 rpm. In the morning the cells were diluted to OD_{600} = 0.1, plated out in triplicate into a 96-well plate and allowed to grow for 24 hours at 37°C in a Molecular devices Versamax Tunable Microplate reader, controlled by Softmax Pro. The OD was recorded every 3.5 minutes after having been shaken before each time point. The data was then manipulated in Excel.

5.3 Results

5.3.1 *DSE1* expression is Ace2p-dependent in *S. cerevisiae* and *C. glabrata*

Through Northern Analysis of a tet-regulated *C. glabrata* ACE2 strain, HLS119, *DSE1* was shown to have Ace2p-dependent expression in chapter 3 (Figure 3.1), which correlates with findings in *S. cerevisiae* [101, 133].

5.3.2 Potential Ace2p binding sites in the promoter region of both *C. glabrata* and *S. cerevisiae DSE1*

Having shown the expression of *C. glabrata DSE1* to be Ace2p-dependent in *C. glabrata* (Figure 3.1), and combined with the knowledge that *S. cerevisiae DSE1* also displays Ace2p-dependent expression [101, 133], the upstream region of *C. glabrata DSE1* was screened for potential Ace2p binding sites (ACCAGC) as defined by Dohrmann et al. [220], and presented in Figure 3.2. The same technique was then employed for *S. cerevisiae DSE1* using sequence data from the *S. cerevisiae* genome database [170]. *S. cerevisiae DSE1* shows three potential Ace2p binding sites, within its intergene region upstream of the start codon and downstream of the next closest gene ORF (*RSP5*). The site positions are mapped below in Figure 5.1 in relation to the start codon of the target gene, with all co-ordinates and sizes measured in base pairs. *C. glabrata DSE1* from Figure 3.2 is also included for reference.

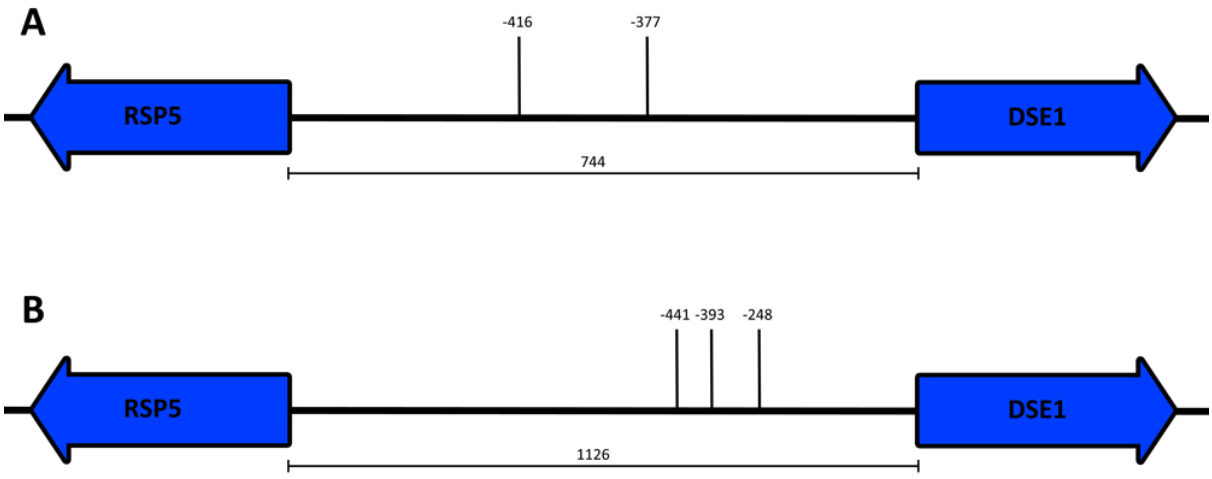


Figure 5.1 – Potential Ace2p binding sites exist in the intergene regions upstream of *DSE1*. The intergene region upstream of the *DSE1 S. cerevisiae* is displayed with potential Ace2p binding sites (ACCAGC) [220] marked for position relative to the ATG of *DSE1*. *C. glabrata DSE1* is included from Figure 3.2 for reference. All co-ordinates and measurements are in base pairs, all sequences were taken from Génolevures [171] or SGD [170]. Diagrams are not to scale. A. *C. glabrata DSE1* has two potential Ace2p binding sites between it and *RSP5*. B. *S. cerevisiae DSE1* has three potential Ace2p binding sites between it and *RSP5*.

5.3.3 *C. glabrata* Dse1p structural prediction

A structural prediction of *C. glabrata* Dse1p was created courtesy of Dr. Talavera of the University of Manchester using mGenTHREADER and secondary structure recognition techniques combined with trial and error model refinement [270, 271] as described in section 5.2.2. The resulting prediction (Figure 5.2) indicates that *C. glabrata* Dse1p has a β-propeller, which may indicate an enzymatic role.

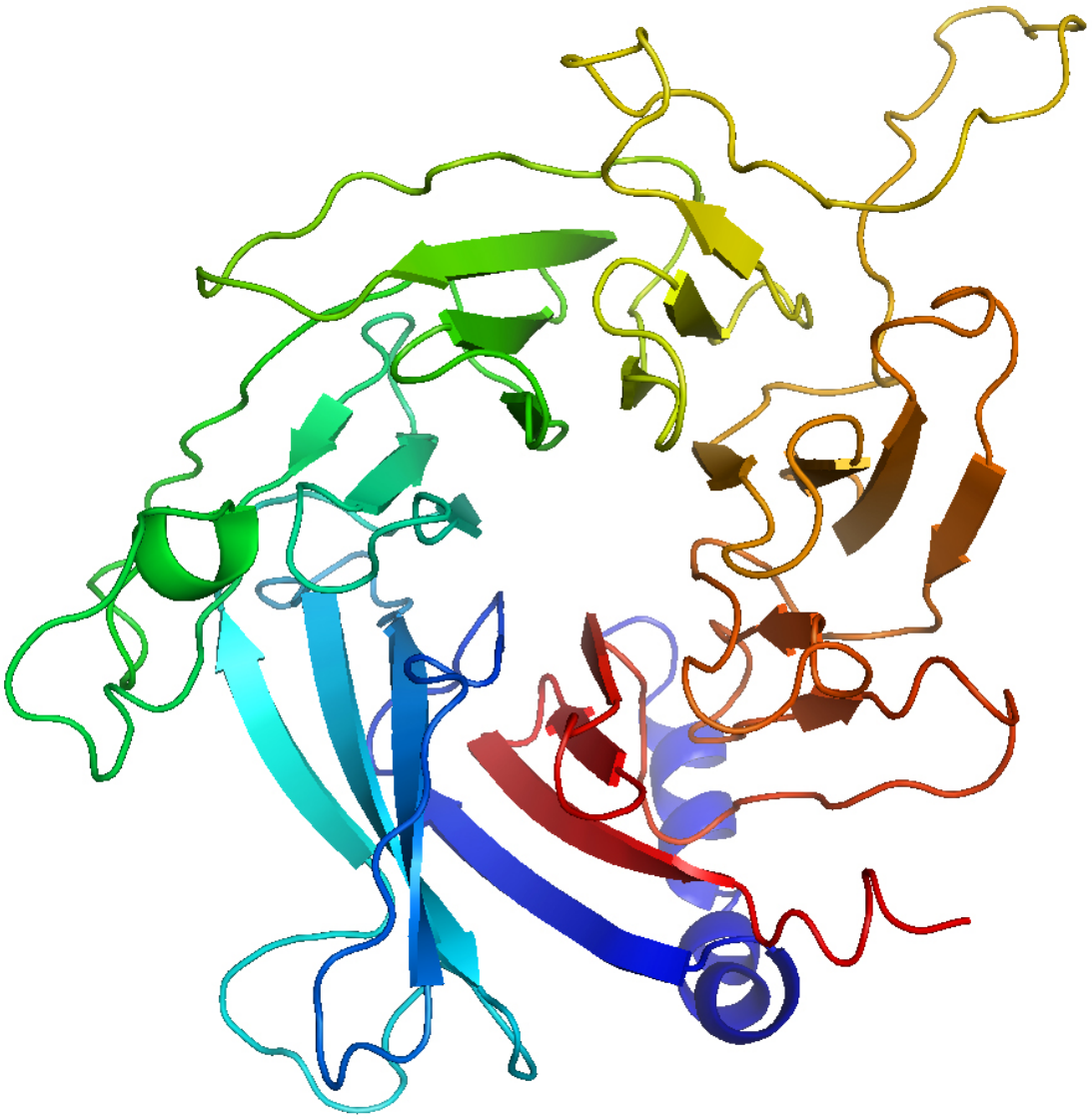


Figure 5.2 – Structural prediction of *C. glabrata* Dse1p reveals a β-propeller structure. Analysis of the predicted structure, kindly performed by Dr. Talavera, University of Manchester, of the N-terminus, minus 20bps, of *C. glabrata* Dse1p predicts a β-propeller structure. The arrows represent β-sheets and the coil an α-helix. This predicted functional structure may indicate an enzymatic function for the N-terminus of Dse1p [269].

5.3.4 C. glabrata *dse1* null phenotypic screen

A phenotypic screen was conducted in chapter 4 using a selected range of phenotypic conditions as described by Hampsey et al. [246] and listed in Table 4.1. As shown in Figures 4.4-4.6, *C. glabrata dse1* showed normal growth on all conditions except for 2.5 mM vanadate, which could indicate a mild defect in protein glycosylation, and 10 mM caffeine, which could indicate defects in various cellular processes, including MAPK signalling pathways and the Mpk1p-mediated cell wall integrity pathway [247].

5.3.5 *C. glabrata* and *S. cerevisiae* vanadate sensitivity screen

After a phenotypic screen, as shown in Figures 4.4-4.6, identified a possible sensitivity to vanadate, a screen of vanadate sensitivity using multiple concentrations of vanadate was performed on the selected candidate for *C. glabrata dse1* and the *S. cerevisiae dse1* library strain, with their respective wild types for comparison. No difference in sensitivity was observed between the *dse1* nulls and their wild type strains (Figure 5.3). *S. cerevisiae* shows increased resistance to vanadate than *C. glabrata* from 4 mM to 6 mM vanadate.

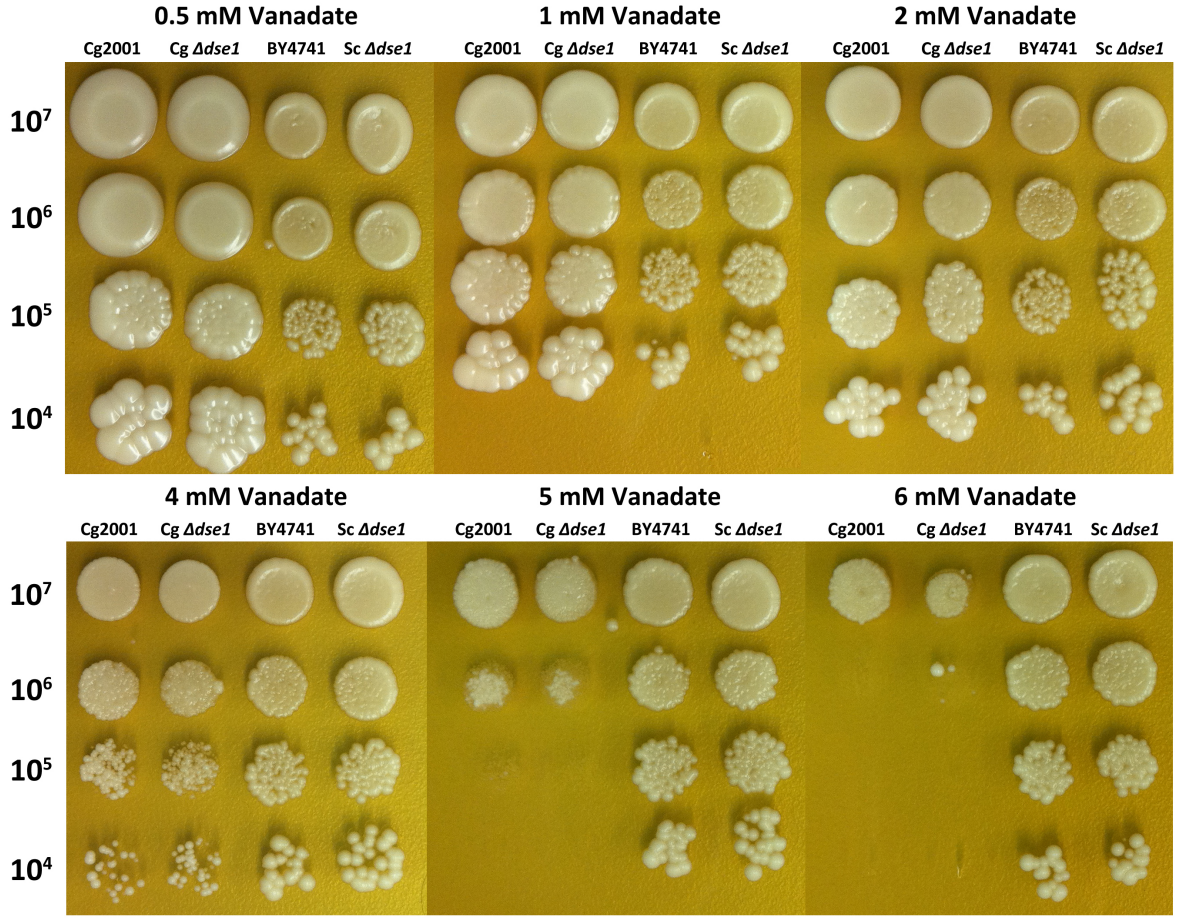


Figure 5.3 – *C. glabrata dse1* and *S. cerevisiae dse1* display no difference in vanadate sensitivity when compared to their respective wild type strains. Growth phenotypes of the wild type *C. glabrata* strain Cg2001, *C. glabrata dse1*, the *S. cerevisiae* wild type strain BY4741, and *S. cerevisiae dse1*. No sensitivity was shown by any of the null mutants when compared with the wild type control. *S. cerevisiae* shows increased vanadate resistance when compared with *C. glabrata*. 5 µL of each strain was spotted in serial dilutions of 1 x 10^7, 1 x 10^6, 1 x 10^5 and 1 x 10^4. Strains were grown for three days on YPD with the 0.5 mM, 1 mM, 2 mM, 4 mM, 5 mM or 6 mM of vanadate at 30°C.

5.3.6 Yeast *dse1* null polarization study

To ascertain whether deletion of *DSE1* causes a change in cell polarity, *C. glabrata dse1,* the *C. glabrata* wild type Cg2001, *S. cerevisiae dse1* and the S. cerevisiae wild type BY4741 were grown overnight, washed, mounted, and photographed using a microscope as described in section 5.2.4. The images were then analysed for individual cell polarity by measuring the ratio of their width and height. 300 cells were measured per strain and the results averaged. Neither *dse1* nulls from *S. cerevisiae* or *C. glabrata* show a difference in cell polarity from their respective wild types.

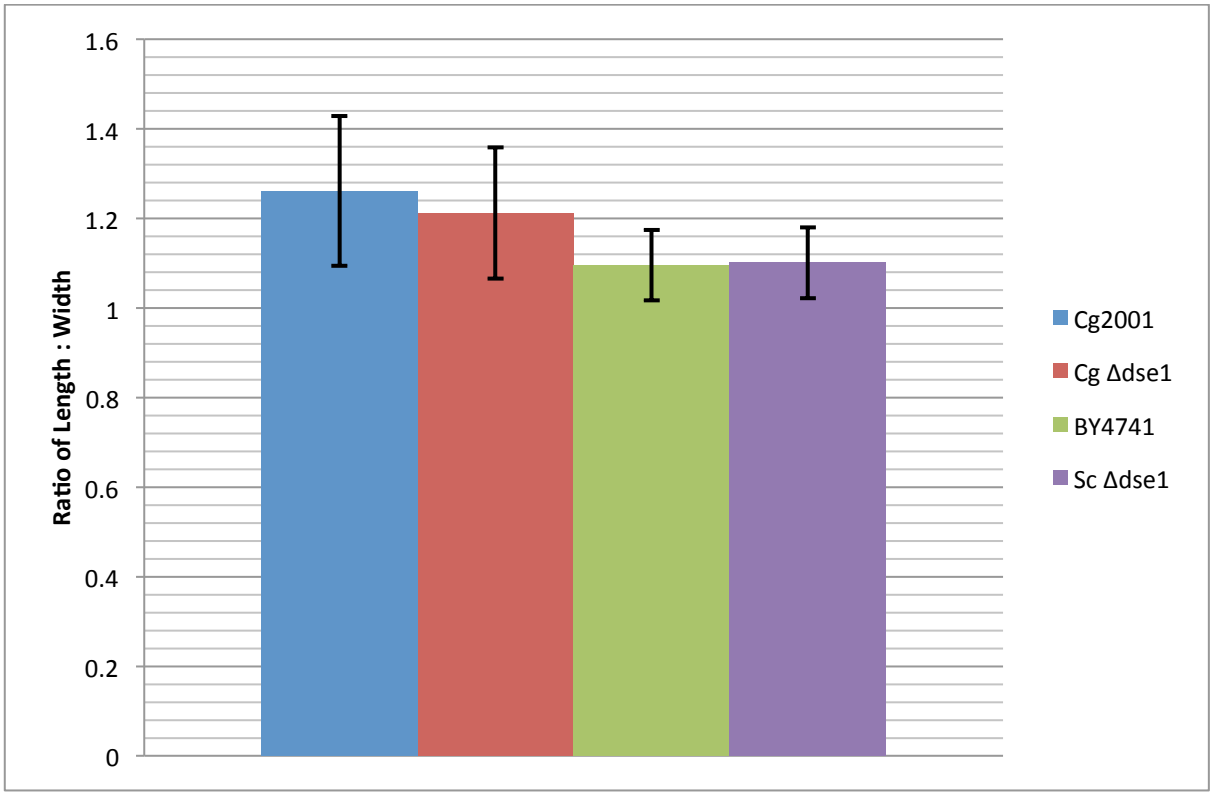


Figure 5.4 – Polarisation of *C. glabrata* and *S. cerevisiae dse1* is unchanged compared to the wild type. Chart showing cell polarisation as measured the ratio of Length:Width for a sample of *C. glabrata* wild type (Cg2001), *C. glabrata dse1* null (Cg Δdse1), *S. cerevisiae* wild type (BY4741) and *S. cerevisiae dse1* null (Sc Δdse1). No significant difference was observed between the polarity of either of the *dse1* nulls and their associated wild type strains in their respective species. Yeast strains were grown overnight in YPD at 30°C/37°C, 180 rpm, diluted, and grown to OD_{600} 0.5-1, washed, mounted and visualised. Photos were then analysed for cell polarity using Image J.

5.3.7 Localisation study of *S. cerevisiae* Dse1p in known interactor nulls

The localisation of Dse1p was visualised in known interactor nulls from the *S. cerevisiae* YKO library using a *S. cerevisiae* Dse1-GFP plasmid as constructed in section 5.2.5. The yeast strains, Dse1p-GFP library strain, BY4741 + Dse1-GFP, *boi1* + Dse1-GFP, *boi2* + Dse1-GFP, *zds2* + Dse1-GFP, *ste4* + Dse1-GFP, *ste11* + Dse1-GFP and the parental control BY4741 were studied using fluorescence microscopy as described in section 5.2.6, and shown in Figure 5.5. Dse1p shows no difference in localisation in the interactor nulls localising to the bud neck apart from *zds2,* in which it displays an altered localisation from the parental and control strains, localising to the cell wall but not the bud neck.

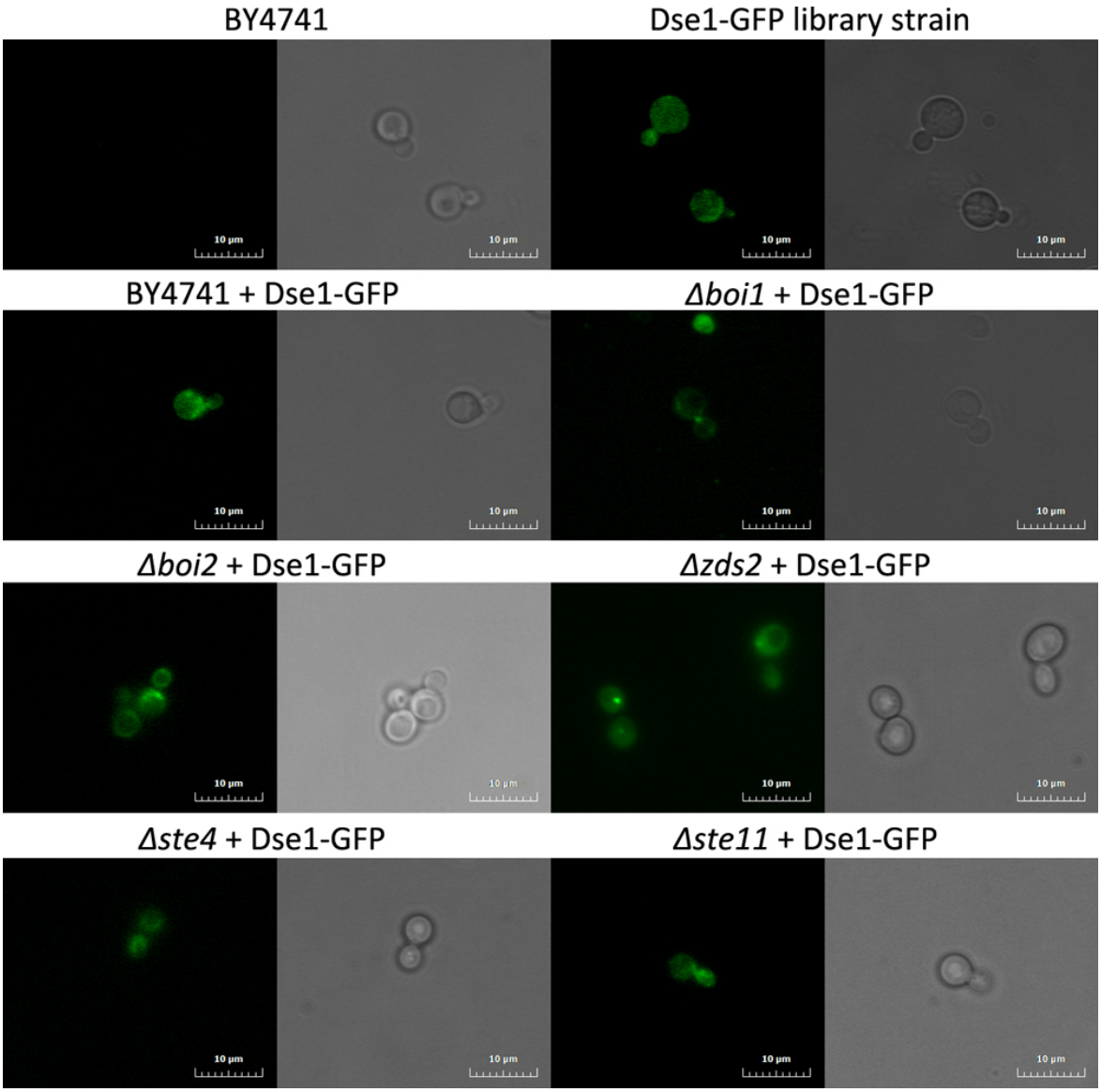


Figure 5.5 – Localisation of *S. cerevisiae* Dse1p-GFP is altered in *zds2* null mutant. Florescence microscopy of a representitive sample of the *S. cerevisiae* Dse1p-GFP library strain, as well as BY4741 and known interactors *boi1*, *boi2*, *zds2*, *ste4* and *ste11* with pSRSG-GD1 (Dse1-GFP) and their parental control BY4741. All strains show similar localisation to the Dse1-GFP library strain, with Dse1p primarily located to the bud neck area, apart from *zds2* in which Dse1p localised to the cell wall but not the bud neck. Yeast strains were grown overnight in YPD at 30°C, 180 rpm, diluted, and grown to OD_{600} 0.5-1, washed, mounted and visualised.

5.3.8 Growth rate analysis of *C. glabrata dse1*

The growth rate of the *C. glabrata dse1* null was analysed in chapter 4 as shown in Figure 4.12. The *dse1* null showed a similar growth rate compared to the *C. glabrata* wild type Cg2001 and the parental strain *C. glabrata his3*.

5.4 Discussion

The aim of the experiments in this chapter was, for the first time in *C. glabrata,* to investigate the role of the uncharacterised gene *DSE1,* both directly in *C. glabrata* and through the use of available tools within its close genetic relative, the model yeast *S. cerevisiae*.

5.4.1 Ace2p direct transcriptional regulation is likely in both *C. glabrata* and *S. cerevisiae*.

Work in *S. cerevisiae* showed that *DSE1* displays Ace2p-dependent expression, and forms part of the genes regulated by Ace2p that peak in expression during the run up to cell separation [101, 133]. To investigate whether *DSE1* also showed Ace2p-dependent expression in *C. glabrata* a study of *DSE1* expression using an *ACE2* tet-regulated strain, HLS119, was performed by Northern analysis in chapter 3. The results showed that *DSE1* displays Ace2p-dependent expression in *C. glabrata* (Figure 3.1) with transcripts for *DSE1* present when *ACE2* is expressed and absent when *ACE2* expression is inhibited. To see whether Ace2p could potentially directly regulate the expression of *DSE1* in both *C. glabrata* and *S. cerevisiae*, sequence analysis of the upstream untranslated regions of *DSE1* in both species was also performed in chapter 3. The results showed that *DSE1* in both *C. glabrata* and *S. cerevisiae* had potential Ace2p binding sites within each gene's promoter region as shown in Figure 5.1. *C. glabrata DSE1* had two potential Ace2p binding sites, one at -377 bp and one at -416 bp from the start codon, where as *S. cerevisiae DSE1* had three potential Ace2p binding sites within its promoter region at -248, -393 and -441 bp from the start codon. Combined with the known Ace2p-dependence of the gene in the two species [101, 133], the results strongly suggest that Ace2p can bind directly to the *DSE1* promoter to regulate its transcription as part of the Ace2p regulon within both species of yeast. To confirm this you could use an electrophoretic mobility shift assay to test for DNA-binding of Ace2p to the promoter sequence of *DSE1* within *C. glabrata* and *S. cerevisiae*, which coupled with the Ace2p-dependence of *DSE1* expression in both strains, would prove Ace2p's ability to directly regulate the transcription of *DSE1*.

5.4.2 β-propeller

The next stage of investigation into the role and function of *DSE1* in *C. glabrata*, was to look at the structure of the transcribed protein. To this end, structural prediction was performed in partnership with Dr. Talavera from the University of Manchester [269], which revealed that Dse1p in *C. glabrata* has a predicted β-propeller structure made of β-sheets circling a central tunnel with one α-helix coil as illustrated in Figure 5.2. The β-propeller fold takes the form of a highly symmetrical structure; normally featuring 4 to 8-fold repeats of antiparallel β-sheet motifs [277]. The antiparallel β-sheets form into 'blades', which are arranged radially around a central open tunnel, held together by the predominantly hydrophobic interactions between the sheets [277]. The circular conformation of the β-propeller structure is crucial to its function, and is held together in most cases by a β-sheet arrangement that locks the first and last blades together, described as 'molecular Velcro' [277]. Most of the known propeller proteins use the central tunnel to execute their function within the cell, co-ordinating ligand position and binding or acting as the active site in catalytic proteins [277].

β-propeller structures are predominantly found in eukaryotes, with complete genome scanning only highlighting one possible β-propeller structure within archaebacterial genomes and only four found within *E. coli* [277]. In yeast, however, 212 predicted β-propeller structures were found in *S. cerevisiae* alone, with many showing homology to Gβ proteins [277]. β-propeller structures are found in a diverse plethora of proteins ranging from G proteins carrying out signalling roles, to enzymes such as Cytochrome cd_1 and Glucose dehydrogenase [277]. β-propeller structures have also been associated with transcriptional repression, shown to exist in the β-domain of the Snn6p-Tup1p repressor complex [278]. The *TUP1* encoded protein has WD40 repeats, which form the folds of β-sheets within the β-propeller structure [278]. The WD40 repeats within the face of the radial structure form the site of interaction with DNA-binding proteins that recruit the Snn6p-Tup1p active repressor to the site of repression [278]. The Ssn6p-Tup1p complex has been shown to repress over 150 genes in *S. cerevisiae*, with homologues shown to exist in other yeast species including *Candida* species, mammals, flies and worms [278].

The discovery of a predicted β-propeller structure for *DSE1* within *C. glabrata* could indicate that Dse1p plays an enzymatic role, which could explain its Ace2p transcriptional regulation as an effector of cell separation as part of the cell separation machinery. Equally, Dse1p could play a similar role to Tup1p in transcriptional regulation, as either a repressor or activator of transcription. It is also possible that Dse1p plays a signalling role like the numerous Gβ homologues within yeast, which could support some of the suggested roles for Dse1p within *S. cerevisiae* and *C. albicans*.

5.4.3 Deletion of *DSE1* induces a cell separation defect

Having successfully disrupted *DSE1* within *C. glabrata*, the *dse1* null was subjected to a solid agar phenotypic screen in an attempt to highlight any possible roles for Dse1p within the cell in chapter 4. The screen covered conditions targeted at cell wall metabolism, glycosylation, nutrient and oxidative stress as well as temperature sensitivity. The *C. glabrata dse1* strain showed no difference in sensitivity to the majority of the conditions, only displaying a mild sensitivity to vanadate and caffeine when compared to the parental strain (Figure 4.6). Further testing of the apparent vanadate sensitivity was conducted using a greater range of concentrations. The results showed that neither the *C. glabrata dse1,* nor the *S. cerevisiae dse1* from the YKO library, display a difference in vanadate sensitivity compared to their respective wild types (Figure 5.3) indicating that the original vanadate sensitivity in Figure 4.6 might not be a real result. It's interesting to note that *S. cerevisiae* displayed considerably more resistance to the vanadate condition showing uninhibited grow on all concentrations of vanadate up to the 6 mM tested here, where as *C. glabrata* showed inhibited growth from 4 mM (Figure 5.3). Caffeine sensitivity has been linked with defects in quite a few cellular processes, which include MAPK signalling pathways, as the caffeine molecule acts as a purine analogue once inside the cell [246, 251]. Caffeine is therefore typically used in phenotypic tests to look for defects in the Mpk1p-mediated cell wall integrity pathway [247]. Therefore a mild sensitivity to caffeine could indicate that *DSE1* plays a role in the cell wall integrity pathway, either as an effector or as part of a signalling chain.

Another clue that Dse1p might be involved in cell wall maintenance, metabolism or the integrity pathway comes from the phenotype displayed by *dse1* in *C. glabrata*. Figure 4.10 showed that *dse1*

displays a cell separation deficient phenotype, forming branched chains of cells. The cell separation phenotype is not on the same scale of the clumpy phenotype displayed by *ace2 C. glabrata* cells (as shown in Figure 4.10 for comparison), but is different from the cell separation competent parental strain. This strongly indicates that Dse1p plays a role in cell separation or cell wall metabolism, which combined with the mild sensitivity to caffeine and the transcriptional regulation by Ace2p, indicates that Dse1p has a significant role in the cell separation machinery. Considering *DSE1* displays no homology to cell wall glucanases, it is likely that Dse1p does not act directly on the cell wall itself, but may form part of the initiation of the cell wall hydrolysis through recruitment, activation or repression of effectors or perhaps by forming part of a signalling chain.

It has been suggested in the literature that Dse1p could have a role in bud site selection and maintenance of cell polarity, mainly due to interaction data with Boi1p, Boi2p and Zds2p [163-165]. To test whether deletion of *DSE1* within *C. glabrata* and *S. cerevisiae* affected the maintenance of cell polarity a sample of 300 cells were photographed from each strain, which were then measured comparing the ratio of length to width as a measure of cell polarity. *C. glabrata dse1* was compared to the *C. glabrata* wild type, Cg2001, which showed no difference in polarity with a ratio of about 1.2. A comparison of *S. cerevisiae dse1* to the *S. cerevisiae* wild type BY4741 also showed no difference in polarity either, with a ratio of about 1.1. A greater range of variation was apparent for *C. glabrata* compared to *S. cerevisiae*, however ratios of polarity were within error limits across the two species showing that *C. glabrata* and *S. cerevisiae* share roughly equal polarities. These results, displayed in Figure 5.4, can discount the theory that *DSE1* deletion would affect cell polarity and suggests that if Dse1p plays a role in maintenance of polarity in *C. glabrata* and *S. cerevisiae*, it is not essential. No evidence of an abnormal budding pattern was observed for either *C. glabrata* or *S. cerevisiae dse1* during the course of this study or the images taken for Figure 5.4, again suggesting that if Dse1p plays a role in bud site selection, it is not an essential one.

Analysis of the growth rate of *C. glabrata dse1* compared to the wild type and parental strains, showed similar growth rates and curves as shown in Figure 4.12.

5.4.4 Localisation of Dse1p

To see whether the physical protein-protein interactions shown by Dse1p in *S. cerevisiae* [165] contribute to its localisation within the cell, a GFP-tagged *S. cerevisiae* Dse1p plasmid was made and used to study the localisation of Dse1p within known interactor nulls from the YKO library as described in section 5.2.6. By comparing the *S. cerevisiae* GFP library strain for *DSE1* to the YKO strains transformed with the Dse1p-GFP plasmid, it was possible to show that Dse1p localises to the bud neck, as was previously reported in the literature [143], and that the localisation of Dse1p is unchanged in the known Dse1p-interactor deletions, *boi1*, *boi2*, *ste4* and *ste11* as shown in Figure 5.5. The *S. cerevisiae zds2* null mutant showed a slightly altered Dse1p localisation, displaying localisation to the cell wall but not the bud neck. These results show that the Dse1p physical interactors Boi1p, Boi2p, Ste4p and Ste11p have no effect on the localisation of Dse1p within *S. cerevisiae*, but that Zds2p may play a role in the correct localisation of Dse1p. *ZDS2*, or Zillion Different Screens 2, has been linked with a plethora of cellular processes in *S. cerevisiae* including telomeric silencing, transcriptional silencing, mitotic exit, mRNA export, regulation of Cdc42p, calcium sensitivity, cell cycle regulation, cell wall integrity and many others, summarised by Yasutis

et al. [279]. *ZDS2* has also recently been shown to regulate the Swe1p kinase-dependent G_2/M checkpoint that is responsible for maintenance of correct polarized growth and budding, which likely acts through Cdc55p, a protein phosphatase 2A regulatory subunit [279]. This could indicate that Dse1p plays a role in the G_2/M checkpoint and that it has Zds2p-dependent localisation, possibly adding to the hypothesis of a bud site selection or polarisation role for Dse1p, or of course a role in one of the many other cellular processes Zds2p has been linked with including the cell wall integrity pathway.

5.4.5 Results and roles from the literature

The body of literature on *DSE1* from yeast and other fungi is far from comprehensive. As discussed previously, three potential roles for Dse1p have been suggested. The first is a cell wall metabolism and cell separation role, which Dse1p's Ace2p-dependence [101, 133] and bud neck localisation [143] in *S. cerevisiae*, as well as the cell separation defect and sensitivity to cell wall targeted conditions found in *S. cerevisiae dse1* nulls [101] point to. Data from a haploinsufficient *DSE1 C. albicans* strain also supports a role in cell wall metabolism [268]. In this regard the data collected in this study supports a potential role in cell wall metabolism and cell separation, with *C. glabrata dse1* nulls displaying a cell separation defect, while Dse1p localises to the cell wall and bud neck. *DSE1's* Ace2p-dependent expression within *C. glabrata* also adds to the support of a role in cell separation or associated cell wall metabolism, while its predicted β-propeller structure could also support a cell wall metabolism role. While none of the findings within this study provide any conclusive evidence for a particular role, a cell wall metabolism and cell separation role has the most support.

To investigate the potential of Dse1p to have a direct effector role in cell wall metabolism and cell separation, the next step would to be to look at the potential enzymatic qualities of Dse1p. For instance even though Dse1p shows no homology to known putative glucanases, a role in glucan degradation could still be possible and could be assayed through the use of a laminarin digestion assay [280], with laminarin a glucan substitute. Alternatively, if Dse1p does play a direct effector role in cell separation, it could be involved in chitin degradation, which could be tested using a 4-methylumbelliferyl-N-acetyl-beta-D-glucosaminide test [281] for instance.

Of course it's also possible that Dse1p plays an indirect role in cell wall metabolism, perhaps in a regulatory capacity. To test this transcriptome analysis of the *S. cerevisiae* and *C. glabrata dse1* null could be performed using RNA-seq, as described in Appendix 5, or microarray analysis which would be able to show whether any genes are up or down regulated in the *dse1* nulls and therefore show whether Dse1p has any impact either directly or indirectly over gene expression, specifically looking towards genes of the cell separation machinery.

Should a regulatory role be discovered, the next stage would be to assay for any DNA-binding potential of Dse1p. To test for DNA-binding of Dse1p, an electrophoretic mobility shift assay could be used to see whether Dse1p binds to DNA. Alternatively, a commercial transcription factor binding assay such as the DuoSet Intracellular Active Transcription Factor Assays available from R&D Systems could be used. At that point you could employ a similar DNA-foot printing assay as described in the original *S. cerevisiae* Ace2p binding site experiments by Dohrmann et al. [220], to find which sequences were protected from digestion by the binding of Dse1p to DNA. That would give you an

indication of the core of any Dse1p binding site, from which you could look to see which genes could have potential Dse1p binding sites within their promoter regions in a similar manner to that employed for Ace2p in chapter 3.

In contrast, the results displayed in the polarization study shown in Figure 5.4, indicate that a bud site selection role, which was suggested by an over-expression budding-within-birth-scar phenotype [163] and Dse1p's physical interaction with Boi1p, Boi2p and Zds2p [165], is unlikely at least in *C. glabrata* and *S. cerevisiae*, or that its role is not essential to the maintenance of cell polarity. However, a change in localisation of Dse1p within *S. cerevisiae zds2* null mutants as observed in Figure 5.5 does show that Zds2p plays some role, whether linked to bud site selection or not, in Dse1p's localisation in the cell.

To explicitly test whether Dse1p has any role in bud site selection, a look at the budding pattern of the *S. cerevisiae* and *C. glabrata dse1* nulls could be performed using cell wall staining and fluorescence microscopy in a similar manner to the study of budding within birth scar by Frydlova et al. [163], taking a sample of photos of budding cells or clumps of cell separation deficient cells and comparing the bud site selection with reference to the bud scar stained by calcofluor white and fluorescein isothiocyanate (FITC)-labelled wheat germ agglutinin (WGA-FITC).

The next stage in investigation of a cell polarity role could be to look at the localisation of known Dse1p-interactors like Boi1p, Boi2p, Zds2p, Ste4p and Ste11p within *C. glabrata* and *S. cerevisiae dse1* nulls. This would help see whether Dse1p has any effect on the localisation of known interactors and could be performed using the Gateway system as described for the creation of the Dse1p-GFP plasmid pSRSG-GD1 in section 5.2.5. If the localisation of Boi1p or Boi2p was altered in a *dse1* null for instance, it would strongly indicate that Dse1p plays at least some role in cell polarity and bud site selection. On the other hand, if Ste4p or Ste11p showed altered localisation in the *dse1* null, it would indicate that Dse1p might have a role in pseudohyphal growth.

None of the data presented within this study either supports or discourages the hypothesis of a role for Dse1p in pheromone sensing or pseudohyphal growth that was suggested by the binding of Ste11p and Ste4p as well as an over-expression invasive growth and pheromone cell cycle arrest-resistant phenotype [166], although they were not looked at specifically as neither process has been shown to be present in *C. glabrata*.

The next stage for general functional analysis of Dse1p within *S. cerevisiae* and *C. glabrata* could be performed through the construction and use of partial *DSE1* deletions in the two species. By disrupting the N- or C-terminal of *DSE1* at the locus you could assay for a change in phenotype, to see whether the function of the partial protein is preserved or whether a cell separation defect is displayed. It would also be interesting to see whether a partial *DSE1* disruption would also show caffeine sensitivity similar to the null.

A similar method could be used to study the effect of the N- and C-terminal on the correct localisation of Dse1p to the bud neck by cloning in partial fragments of the *DSE1* gene into a GFP plasmid in a similar manner to that described in section 5.2.5. Once successfully created the Dse1p fragment plasmids could then be transformed into wild type *C. glabrata* or *S. cerevisiae* for study of their localisation as performed in section 5.3.7. This would indicate which parts of Dse1p are crucial to its cellular localisation to the bud neck.

5.4.6 Summary

The results detailed in this thesis have shown for the first time that *DSE1* exhibits Ace2p-dependent expression in *C. glabrata*. It has also been shown that Ace2p binding sites exist within the *DSE1* promoter region within *C. glabrata,* strongly indicating that Ace2p exhibits direct transcriptional control over *DSE1.* Combining this data with the fact that Ace2p controls the cell separation machinery, and that Dse1p has been shown to localise to the bud neck, strongly indicates that Dse1p plays a role in cell separation either directly or through an intermediary. It is possible that Dse1p plays a role in the activation of the cell wall integrity pathway, due to sensitivity to caffeine displayed here, results shown within the literature [163], and Dse1p's apparent Zds2p-dependent bud neck localisation in *S. cerevisiae*, indicating that Dse1p may play a larger role in cell wall metabolism than just cell separation.

It has also been possible to show that cell polarity is maintained in both *C. glabrata* and *S. cerevisiae dse1* nulls, allowing us to discount a major role for Dse1p in maintenance of cell polarity despite showing Zds2p-dependent localisation in *S. cerevisiae*. No obvious bud site selection changes were observed in *dse1* nulls in either yeast species, indicating that if Dse1p has a role in bud site selection, it is not essential for the normal bud site selection displayed by the wild type strains. None of the results confirm or discount the hypothesis that Dse1p could have a role in pheromone sensing and hyphal growth, however it is unlikely to do so in *C. glabrata*, which only exhibits pseudohyphal growth *in vitro* under nitrogen starvation conditions [31]. Further work is required to confirm or discount a role in pseudohyphal growth within *C. glabrata* and to characterise the precise role Dse1p has within cell separation and cell wall metabolism.

6 Summary and Conclusions

6.1 Summary

Fungal pathogens have become an increasingly serious clinical burden, primarily due to the increased groups of patients who survive other conditions and are put 'at risk' as a result [2, 33, 34]. This at risk group involves immune suppressed patients, either because of immune deficiency diseases such as AIDS, through treatment for cancer, or those patients with transplants. Of course another increasing at risk group is the elderly, and with modern medicine, better general health and improved diet, the size of the elderly population is increasing.

Candida species have been shown to cause some 10 to 15% of all nosocomial BSIs within the United States [3], with the primary cause of candidaemia being *C. albicans* [48]. Recently, an increasing proportion of candidiasis and candidaemia infections have been caused by a relatively little known *Candida* isolate, *C. glabrata*. In contrast to *C. albicans*, *C. glabrata* lacks any true hyphal morphology, existing solely in yeast form. *C. glabrata* is also innately resistant to antifungal drugs, especially azoles, which are commonly used within the clinical setting. This has meant that positive selection of *C. glabrata* over other *Candida* and fungal species has occurred within the nosocomial setting [51], which means that an increase in resistant *Candida* species poses a serious issue for clinical treatment of *Candida* infections.

Little is known about *C. glabrata* virulence. As a close genetic relative to *S. cerevisiae* it shares many traits with the traditionally non-pathogenic commensal organism. Like other *Candida* species, *C. glabrata* is a human commensal organism also, but is categorised as an opportunistic pathogen, causing systemic disease only when a patient's immune system becomes compromised.

In 2004, Kamran et al. discovered a hypervirulence factor within *C. glabrata* [7]. What they found was an antivirulence, or virulence-moderating gene with homology to the *S. cerevisiae* cell separation transcriptional regulator *ACE2*. *C. glabrata ace2* nulls displayed an extreme hypervirulence, resulting in 100% mortality within 18-hours post infection in a neutropenic murine model of candidiasis [7]. Being a transcription factor controlling the expression of the genes of the cell separation machinery in *S. cerevisiae*, it was no surprise that *C. glabrata ace2* also displayed a clumpy, cell separation deficient phenotype. However, Kamran et al. showed, through the use of chitinase treatment, that the hypervirulence displayed by *ace2* was not due to blockade by clumps of cells but rather other factors, including the suggestion of a septic shock-like response [7].

6.1.1 The Ace2p regulon in *C. glabrata*

An investigation into the cause of the antivirulence of *ACE2* was required. To start, the genes regulated by Ace2p in *C. glabrata* had to be defined (chapter 3). Northern analysis of a tetracycline-regulated strain of *ACE2* was used to define a partial Ace2p regulon, which contained 12 genes, as well as the previously investigated *CTS1*. The 12 genes included homologues of *S. cerevisiae* genes involved in cell cycle regulation, bud site selection and cell wall associated glucanases. The genes

with expression shown to be Ace2p-dependent in *C. glabrata* include: *AMN1*, *ASH1*, *BUD9*, *DSE1*, *DSE2*, *DSE3*, *ACF2/DSE4*, *EGT2*, *RME1*, *SCW11α, SCW11β*, and *SIC1.*

To see whether the 12 genes of the Ace2p regulon were likely to be directly transcriptionally regulated by Ace2p, their promoter regions were analysed for potential Ace2p binding sites as defined by Dohrmann et al. [132]. Out of the 12 genes, 10 genes including *AMN1*, *ASH1*, *BUD9*, *DSE1*, *DSE2*, *DSE3*, *EGT2*, *SCW11α, SCW11β* and *SIC1,* have at least two potential Ace2p-binding sites within their promoter regions, indicating strongly that Ace2p exhibits direct regulation over their expression.

Once the partial Ace2p regulon was established it was possible to investigate the potential antivirulence of the individual genes of the Ace2p regulon in *C. glabrata* (chapter 4). 10 out of the 12 genes were disrupted and subjected to preliminary phenotypic testing. The deletions displayed a similar sensitivity profile to the *C. glabrata ace2* null, only showing sensitivity to vanadate and caffeine, which are linked with glycosylation and secretion defects, or cell wall integrity pathway defects respectively. Further testing showed that only *egt2* and *dse1* displayed cell separation defects in liquid media.

Virulence testing of the individual null mutants showed that six out of the 10 assayed Ace2p regulon mutants displayed significant hypervirulence in a neutropenic murine model of candidiasis when compared to the wild type control. The six mutants, *dse3*, *acf2*, *egt2*, *rme1*, *scw11β* and *sic1*, all caused 100% mortality within five days, which contrasted to the 60% survival displayed by the wild type Cg2001 over 14 days. The resulting hypervirulence was not as extreme as that displayed by the *ace2* null however, which caused 100% mortality within 18-hours post infection [7]. Given that the *ace2* hypervirulence phenotype was suggested as being caused by immune over-stimulation and septic shock, immune activation assays were performed with the hypervirulent mutants. Of the six mutants tested, only *sic1* showed significantly higher elicitation of TNFα and IL-6 production as assayed by ELISA, with a four-fold and 3.4-fold increase respectively. This indicates that *sic1* contributes, at least in part, to the immune over-stimulation induced by the *ace2* null, but the exact cause of said over-stimulation is unclear as *SIC1* plays a role in genome stability and the G_1 to S-phase progression.

Through deletion and virulence analysis it has been shown for the first time that six separate genes contribute to the antivirulence displayed by *ACE2* in *C. glabrata*, indicating that the extreme hypervirulence shown by *ace2* nulls is most likely a synergy of multiple absences of gene expression.

6.1.2 *DSE1* a novel gene likely to be involved in cell separation in *C. glabrata*

The as-yet uncharacterised gene *DSE1*, *YER124C* in *S. cerevisiae* and its homologue *CAGL0K02277g* in *C. glabrata*, was highlighted as a gene of interest in the course of investigation into the Ace2p regulon in *C. glabrata* and therefore became the subject of a study within chapter 5. *DSE1* shows Ace2p-dependent expression in both *S. cerevisiae* [101, 133] and *C. glabrata.* It is expressed in the run up to cell separation with the rest of the Ace2p-dependent cell separation machinery and has two potential Ace2p binding sites within its promoter region within *C. glabrata*. Dse1p has been

shown to localise to the bud neck, and in both *S. cerevisiae* and *C. glabrata, dse1* nulls present with a cell separation defect.

Dse1p has been suggested to play a role in three different cellular functions: cell wall metabolism and cell separation; bud site selection and maintenance of cell polarity; and pheromone sensing and hyphal growth. The data collected in this study suggests that a role in cell wall metabolism and cell separation is most likely due Zds2-dependent bud neck localisation combined with the cell separation defect and sensitivity to caffeine displayed by *C. glabrata dse1*. The predicted *C. glabrata* Dse1p structure features a β-propeller, and could indicate that Dse1p has some sort of regulatory role over the cell separation machinery, or a direct enzymatic role. More work is required to define the precise role Dse1p plays in cell separation. An assay for cell polarization showed that neither *C. glabrata* nor *S. cerevisiae dse1* cells showed any alteration in cell polarity compared to the wild type, while a change in bud site selection and budding pattern was also not observed. This puts doubt on a role for Dse1p in bud site selection and maintenance of cell polarity.

C. glabrata lacks a true hyphal morphology, and only presents pseudohyphae under nitrogen starvation conditions *in vitro* [31]. *C. glabrata* also lacks any described sexual cycle or pheromone sensing, indicating that if Dse1p plays a role in hyphal growth and pheromone sensing in *S. cerevisiae* or other yeast species, it is unlikely to do so within *C. glabrata*.

6.2 Future work

While the results presented in this thesis answer some of the questions regarding *ACE2* antivirulence, as with all research, it has raised yet more. Presented below are some experiments and lines of enquiry that could be employed to answer some of these questions and round out our knowledge of *ACE2* antivirulence within *C. glabrata* and the function of Dse1p.

Having disrupted 10 out of the 12 genes identified within the partial Ace2p regulon in *C. glabrata*, two genes *DSE2* and *SCW11*α remain undisrupted. Alternative strategies should be employed to study the effects of inhibition of their expression within *C. glabrata* with reference to any potential antivirulence. Partial disruption of the genes via traditional disruption methods like the Edlind method or Fusion PCR as described in chapter 4 could be used to inhibit the function of the two genes. Disruption of each gene's promoter region could also be used via the same methods. Alternatively the use of RNAi, which has recently been shown possible within *S. cerevisiae* and other budding yeasts [282], could be a viable method of silencing *DSE2* and *SCW11*α. The first stage would be to confirm the presence of, or restore the essential RNAi machinery, *AGO1* and *DCR1* within *C. glabrata* as has been shown possible in *S. cerevisiae* [282]. Then RNAi of *DSE2* and *SCW11*α could be performed using either *in vitro* transcription using a PCR product for the gene and a commercial kit such as the Ambion MEGAscript T7 kit (Applied Biosystems, Warrington, UK), or through the use of a custom RNAi plasmid targeted against the two genes. Once the expression of *DSE2* and *SCW11*α has been inhibited, virulence and cytokine release studies should be carried out mirroring those presented in chapter 4. This would be able to complete the picture of antivirulence of the Ace2p regulon as defined in chapter 3.

Here it has been hypothesised that the antivirulence shown by the Ace2p regulon in *C. glabrata,* as presented in chapter 4, is synergistic in its effects to create the extreme hypervirulence shown by *C. glabrata ace2* cells. To test this, multiple gene deletions of the six genes, *ACF2*, *DSE3*, *EGT2*, *SCW11*β and *SIC1* that show antivirulence could be constructed within one strain. To do this a combination of markers will be required. The Cg$\Delta\Delta\Delta$ strain affords the use of three markers, HIS, TRP and LEU, while other deletions can be created with the use of a NAT_R or GEN_R marker, and if necessary an inducible flipase marker recycling system as detailed by Reuss et al. [245]. Once a combination of the Ace2p regulon genes has been disrupted within one *C. glabrata* strain it will be possible to test for hypervirulence and see whether the combination of gene deletions enhances the hypervirulence phenotype closer to that displayed by *ace2* null mutants.

Proteomics of the *ace2* null in *C. glabrata* has shown that many more proteins are affected by the disruption of the cell separation machinery transcription factor than just those defined within the partial Ace2p regulon [231]. To fully understand the nature of the effect and highlight any other potentially up or down-regulated genes that could contribute to the hypervirulence observed in *C. glabrata ace2* nulls, transcriptomics to compare the *C. glabrata* wild type and *ace2* transcriptomes is required. Several failed attempts, as detailed in Appendix 5, were made within this study to use RNA-seq to study the *ace2* transcriptome within the host environment. However, RNA-seq or microarray analysis would help to highlight other genes for potential virulence analysis, and would aid in our understanding of the mechanisms within *C. glabrata* of not only *ace2* virulence, but also wild type virulence.

Having shown that potential Ace2p binding sites exist in genes known to display Ace2p-dependent expression, and also shown that it is possible to find and test the Ace2p-dependence of other, previously unknown Ace2p regulated genes like *BUD9* (chapter 3), analysis of other genes for the adjacent Ace2p binding site sequences would help further our understanding of the impact of *ACE2* deletion. A similar process as detailed in chapter 3 could be employed, on a gene-by-gene basis, once they have been highlighted by transcriptomics or through other means.

In vitro analysis of Ace2p binding to *C. glabrata* Ace2p-regulon genes shown to contain potential Ace2p binding sites within their promoter (chapter 3) would be able to definitively tell whether those genes are indeed directly regulated by Ace2p binding. By creating oligomers containing the promoter regions of the target genes it would be possible to assay for Ace2p binding by using an electrophoretic mobility shift assay, looking for a change in mobility of the oligomer associated with protein binding. Alternatively a transcription factor binding assay such as the DuoSet Intracellular Active Transcription Factor Assays available from R&D Systems could be used.

To look at how the deletion of *SIC1* affects the cellular process of *C. glabrata* and causes hypervirulence as shown in chapter 4, transcriptomics could be employed in a similar manner to that described for study of the *ace2* transcriptome. By identifying which genes are up and down regulated in response to *SIC1* deletion, it would hopefully be possible to look into how the deletion of a gene encoding a cyclin dependent kinase inhibitor, responsible for prevention of premature entry into S-phase and ensuring genomic integrity, results in hypervirulence within *C. glabrata*.

To see whether the *in vitro* immune over-stimulation shown by *C. glabrata sic1* cells in a macrophage infection assay mirrors what happens *in vivo,* an murine infection assay should be

carried out to collect blood to test for cytokine levels in comparison to *C. glabrata* wild type infection, as detailed previously by Kamran et al. for *ace2* cells [7]. The results will help show whether *sic1* immune over-stimulation completely explains the over-stimulation shown by *ace2* [7].

The results described in chapter 5 suggest that Dse1p may have a regulatory role within *C. glabrata*. To test this, transcriptomics could be employed as previously described for *ace2* and *sic1* cells. By comparing the transcriptome of *dse1* to that of the *C. glabrata* wild type, it would be possible to see whether any genes involved in the cell separation machinery are up or down-regulated in the absence of Dse1p and help confirm or reject the regulatory role hypothesis.

Coupled with transcriptomics to study the regulatory role of Dse1p, the DNA binding potential of Dse1p could also be looked at *in vitro.* By using a similar method as described above to study Ace2p DNA binding, an electrophoretic mobility shift assay could be used to assay for potential Dse1p binding to DNA. This would aid in the analysis of the role of Dse1p as a transcription factor, similar to other characterised β-propeller proteins within yeast.

To determine the role of the N- and C- terminals on the function of Dse1p, partial disruption of *DSE1* within *C. glabrata* could be conducted, via a disruption method as described in chapter 5 and above, and analysed for a cell separation defect and sensitivity to caffeine, as well as for a change in growth rate when compared to the wild type. This would help see which domains within Dse1p are crucial for function.

Partial disruption of Dse1p could be used to study its localisation too. By creating a partial *DSE1* fragment containing either the N- or C-terminal end of the gene from either *S. cerevisiae* or *C. glabrata* within a GFP plasmid, its localisation using fluorescence can be analysed to see which end of the protein and subsequent domains are crucial to bud neck localisation.

The results from chapter 5 also suggest that Dse1p may have a catalytic role in cell separation. To test this hypothesis, catalytic analysis of Dse1p should be carried out to test its ability to hydrolyse the components of the *C. glabrata* cell wall, namely glucan and chitin. A laminarin digest assay, for instance, could be used to test glucan hydrolysis [280], where as chitinase activity could be tested by a traditional plate assay or through the use of a rapid 4-methylumbelliferyl-N-acetyl-beta-D-glucosaminide test [281].

By following some of the lines of investigation detailed above, it would be possible to expand our knowledge of *ACE2* antivirulence and virulence of *C. glabrata* in general as well as come closer to fully characterising the still as-yet gene of unknown function *DSE1.*

6.3 Conclusions

In conclusion, we have defined the partial Ace2p regulon of genes that show Ace2p-dependent expression in *C. glabrata*, which mirrors that found in *S. cerevisiae* with the addition of two homologues of *SCW11* and the addition of *BUD9.* We have also confirmed that potential Ace2p binding sites exist within 10 out of the 12 genes of the Ace2p regulon in *C. glabrata* indicating that they are most likely directly regulated by Ace2p.

At least seven genes of the Ace2p regulon in *C. glabrata* have been shown to exhibit antivirulence, six discovered in this study plus the previously investigated *CTS1.* We can therefore conclude that the *ace2* hypervirulence displayed in *C. glabrata* [7] is multifactorial, with a combination of antivirulence genes contributing to the extreme hypervirulence displayed in a neutropenic murine model of candidiasis. We have also shown that *sic1* mutants have the ability to over-stimulate macrophages and elicit significantly increased cytokine release *in vitro*. This leads to the conclusion that the immune over-stimulation and cytokine release displayed by *ace2* cells is also multifactorial with at least *sic1* contributing to the potential septic shock response.

Due to the results presented in chapter 5, including the fact that *dse1* nulls in *C. glabrata* show a cell separation defect and sensitivity to caffeine, it is also possible to conclude that Dse1p in *C. glabrata* likely plays a role in cell separation and the cell wall, possibly in a regulatory or enzymatic role, although it may also play roles in pheromone response and hyphal growth in other yeast species.

Our understanding of the virulence mechanisms within *C. glabrata* are still in their infancy when compared to other human pathogens, despite presenting a significant and growing clinical burden (as discussed in chapter 1). The results presented in this thesis take a significant step forward in the understanding of the Ace2p regulon and *ACE2* antivirulence in *C. glabrata*, as well as virulence within *C. glabrata* as a whole. We hope that this body of work will pave the way for further research into the mechanisms and genes behind *ACE2* antivirulence and provide another step on the way to fully characterising the role and function of *DSE1.*

7 References

1. Calderone, R.A. and R.L. Cihlar, *Fungal pathogenesis: principles and clinical applications*. Mycology series 2002: Marcel Dekker.
2. Pfaller, M.A. and D.J. Diekema, *Epidemiology of invasive mycoses in North America.* Crit Rev Microbiol, 2010. **36**(1): p. 1-53.
3. Richardson, M. and C. Lass-Flörl, *Changing epidemiology of systemic fungal infections.* Clinical Microbiology and Infection, 2008. **14**: p. 5-24.
4. Auger, P., et al., *Epidemiology of tinea pedis in marathon runners: prevalence of occult athlete's foot.* Mycoses, 1993. **36**(1-2): p. 35-41.
5. Byrnes 3rd, E.J., et al., *Molecular Evidence That the Range of the Vancouver Island Outbreak of Cryptococcus gattii Infection Has Expanded into the Pacific Northwest in the United States.* Journal of Infectious Diseases, 2009. **199**(7): p. 1081-1086.
6. Rentz, A.M., M.T. Halpern, and R. Bowden, *The Impact of Candidemia on Length of Hospital Stay, Outcome, and Overall Cost of Illness.* Clinical Infectious Diseases, 1998. **27**(4): p. 781-788.
7. Kamran, M., et al., *Inactivation of transcription factor gene ACE2 in the fungal pathogen Candida glabrata results in hypervirulence.* Eukaryot. Cell, 2004. **3**: p. 546-552.
8. Rees, J.R., et al., *The Epidemiological Features of Invasive Mycotic Infections in the San Francisco Bay Area, 1992-1993: Results of Population-Based Laboratory Active Surveillance.* Clinical Infectious Diseases, 1998. **27**(5): p. 1138-1147.
9. Latge, J.-P., *Aspergillus fumigatus and Aspergillosis.* Clinical Microbiology Reviews, 1999. **12**(2): p. 310-350.
10. Pfaller, M.A. and D.J. Diekema, *Epidemiology of Invasive Candidiasis: a Persistent Public Health Problem.* Clin. Microbiol. Rev., 2007. **20**(1): p. 133-163.
11. Vazquez, J.A. and J.D. Sobel, *Candidiasis*, in *Essentials of Clinical Mycology*, C.A. Kauffman, et al., Editors. 2011, Springer New York. p. 167-206.
12. Hajjeh, R., et al., *Incidence of Bloodstream Infections Due to Candida Species and In Vitro Susceptibilities of Isolates Collected from 1998 to 2000 in a Population-Based Active Surveillance Program.* Journal of Clinical Microbiology, 2004. **42**(4): p. 1519-1527.
13. Diasio, R.B., J.E. Bennett, and C.E. Myers, *Mode of action of 5-fluorocytosine.* Biochemical Pharmacology, 1978. **27**(5): p. 703-707.
14. Ghannoum, M.A. and L.B. Rice, *Antifungal Agents: Mode of Action, Mechanisms of Resistance, and Correlation of These Mechanisms with Bacterial Resistance.* Clinical Microbiology Reviews, 1999. **12**(4): p. 501-517.
15. Mermel, L.A., et al., *Clinical Practice Guidelines for the Diagnosis and Management of Intravascular Catheter-Related Infection: 2009 Update by the Infectious Diseases Society of America.* Clinical Infectious Diseases, 2009. **49**(1): p. 1-45.
16. Cabib, E., et al., *Fungal cell wall synthesis: the construction of a biological structure.* Microbiological sciences, 1988. **5**(12): p. 370-375.
17. David W, D., *Echinocandin antifungal drugs.* The Lancet, 2003. **362**(9390): p. 1142-1151.
18. Sanglard, D., F. Ischer, and J. Bille, *Role of ATP-Binding-Cassette Transporter Genes in High-Frequency Acquisition of Resistance to Azole Antifungals in Candida glabrata.* Antimicrobial Agents and Chemotherapy, 2001. **45**(4): p. 1174-1183.
19. Henry, K., J. Nickels, and T. Edlind, *Upregulation of ERG Genes in Candida Species by Azoles and Other Sterol Biosynthesis Inhibitors.* Antimicrobial Agents and Chemotherapy, 2000. **44**(10): p. 2693-2700.
20. Perlin, D., *Resistance to echinocandin-class antifungal drugs.* Drug Resistance Updates, 2007. **10**(3): p. 121-130.

21. Narayanasamy, P., *Microbial Plant Pathogens-Detection and Disease Diagnosis:: Fungal Pathogens*2010: Springer.
22. Horsfall, J.G. and E.B. Cowling, *Plant disease: an advanced treatise*1980: Academic Press.
23. Blaustein, A.R., et al., *Interspecific Variation in Susceptibility of Frog Tadpoles to the Pathogenic Fungus Batrachochytrium dendrobatidis.* Conservation Biology, 2005. **19**(5): p. 1460-1468.
24. Rollins-Smith, L.A., et al., *Activity of antimicrobial skin peptides from ranid frogs against Batrachochytrium dendrobatidis, the chytrid fungus associated with global amphibian declines.* Developmental & Comparative Immunology, 2002. **26**(5): p. 471-479.
25. Gisder, S., et al., *A cell culture model for Nosema ceranae and Nosema apis allows new insights into the life cycle of these important honey bee-pathogenic microsporidia.* Environmental Microbiology, 2011. **13**(2): p. 404-413.
26. Higes, M., R. Martìn, and A.n. Meana, *Nosema ceranae, a new microsporidian parasite in honeybees in Europe.* Journal of Invertebrate Pathology, 2006. **92**(2): p. 93-95.
27. Calderone, R.A., *Candida and candidiasis* 2002, Washington: Amer Society for Microbiology.
28. Pfaller, M.A. and D.J. Diekema, *Rare and Emerging Opportunistic Fungal Pathogens: Concern for Resistance beyond Candida albicans and Aspergillus fumigatus.* Journal of Clinical Microbiology, 2004. **42**(10): p. 4419-4431.
29. Pfaller, M.A., et al., *In vitro susceptibilities of rare Candida bloodstream isolates to ravuconazole and three comparative antifungal agents.* Diagnostic Microbiology and Infectious Disease, 2004. **48**(2): p. 101-105.
30. Lo, H.-J., et al., *Nonfilamentous C. albicans Mutants Are Avirulent.* Cell, 1997. **90**(5): p. 939-949.
31. Csank, C. and K. Haynes, *Candida glabrata displays pseudohyphal growth.* FEMS Microbiology Letters, 2000. **189**(1): p. 115-120.
32. Richardson, M.D. and D.W. Warnock, *Fungal Infection: diagnosis and management* 3rd Edition ed2003, Oxford: Blackwell Publishing.
33. Richardson, M.D., *Changing patterns and trends in systemic fungal infections.* The Journal of antimicrobial chemotherapy, 2005. **56**: p. i5-i11.
34. Park, B.J., et al., *Epidemiology of Systemic Fungal Diseases: An Overview*, in *Essentials of Clinical Mycology*, C.A. Kauffman, et al., Editors. 2011, Springer New York. p. 27-37.
35. Sobel, J.D., et al., *Vulvovaginal candidiasis: Epidemiologic, diagnostic, and therapeutic considerations.* American Journal of Obstetrics and Gynecology, 1998. **178**(2): p. 203-211.
36. Sobel, J.D., *Pathogenesis and Treatment of Recurrent Vulvovaginal Candidiasis.* Clinical Infectious Diseases, 1992. **14**: p. S148-S153.
37. Fidel, P.L., *History and Update on Host Defense Against Vaginal Candidiasis.* American Journal of Reproductive Immunology, 2007. **57**(1): p. 2-12.
38. Kauffman, C.A., *Candiduria.* Clinical Infectious Diseases, 2005. **41**(Supplement 6): p. S371-S376.
39. Chen, S., et al., *Clinician response to Candida organisms in the urine of patients attending hospital.* European Journal of Clinical Microbiology and Infectious Diseases, 2008. **27**(3): p. 201-208.
40. Harris, A.D., et al., *Risk Factors for Nosocomial Candiduria Due to Candida glabrata and Candida albicans.* Clinical Infectious Diseases, 1999. **29**(4): p. 926-928.
41. Revankar, S., et al., *Long-term follow-up of patients with candiduria.* European Journal of Clinical Microbiology & Infectious Diseases, 2011. **30**(2): p. 137-140.
42. Worthington, H.V., et al., *Interventions for treating oral candidiasis for patients with cancer receiving treatment.* Cochrane database of systematic reviews, 2010(7).
43. Arendrup, M.C., *Epidemiology of invasive candidiasis.* Current Opinion in Critical Care, 2010.
44. Warnock, D.W., *Trends in the Epidemiology of Invasive Fungal Infections.* Nippon Ishinkin Gakkai Zasshi, 2007. **48**(1): p. 1-12.

45. Wisplinghoff, H., et al., *Nosocomial Bloodstream Infections in US Hospitals: Analysis of 24,179 Cases from a Prospective Nationwide Surveillance Study.* Clinical Infectious Diseases, 2004. **39**(3): p. 309-317.
46. Blijlevens, N.M.A., J.P. Donnelly, and B.E. De Pauw, *Impaired gut function as risk factor for invasive candidiasis in neutropenic patients.* British Journal of Haematology, 2002. **117**(2): p. 259-264.
47. Sobel, J.D., *Changing trends in the epidemiology of Candida blood stream infections: A matter for concern?* Critical Care Medicine, 2010. **38**(3).
48. Horn, D.L., et al., *Epidemiology and Outcomes of Candidemia in 2019 Patients: Data from the Prospective Antifungal Therapy Alliance Registry.* Clinical Infectious Diseases, 2009. **48**(12): p. 1695-1703.
49. Abi-Said, D., et al., *The Epidemiology of Hematogenous Candidiasis Caused by Different Candida Species.* Clinical Infectious Diseases, 1997. **24**(6): p. 1122-1128.
50. Sanglard, D. and F.C. Odds, *Resistance of Candida species to antifungal agents: molecular mechanisms and clinical consequences.* The Lancet Infectious Diseases, 2002. **2**(2): p. 73-85.
51. Pfaller, M.A., et al., *Variation in Susceptibility of Bloodstream Isolates of Candida glabrata to Fluconazole According to Patient Age and Geographic Location.* Journal of Clinical Microbiology, 2003. **41**(5): p. 2176-2179.
52. Pfaller, M.A., et al., *Variation in Candida spp. distribution and antifungal resistance rates among bloodstream infection isolates by patient age: report from the SENTRY Antimicrobial Surveillance Program (2008-2009).* Diagnostic Microbiology and Infectious Disease, 2010.
53. Pfaller, M.A., et al., *Variation in Susceptibility of Bloodstream Isolates of Candida glabrata to Fluconazole According to Patient Age and Geographic Location in the United States in 2001 to 2007.* Journal of Clinical Microbiology, 2009. **47**(10): p. 3185-3190.
54. Arendrup, M., et al., *Seminational Surveillance of Fungemia in Denmark: Notably High Rates of Fungemia and Numbers of Isolates with Reduced Azole Susceptibility.* Journal of Clinical Microbiology, 2005. **43**(9): p. 4434-4440.
55. Lin, M.Y., et al., *Prior Antimicrobial Therapy and Risk for Hospital-Acquired Candida glabrata and Candida krusei Fungemia: a Case-Case-Control Study.* Antimicrobial Agents and Chemotherapy, 2005. **49**(11): p. 4555-4560.
56. Malani, A., et al., *Candida glabrata Fungemia: Experience in a Tertiary Care Center.* Clinical Infectious Diseases, 2005. **41**(7): p. 975-981.
57. Malani, A., et al., *Is age a risk factor for Candida glabrata colonisation?* Mycoses, 2010.
58. Morrell, M., V.J. Fraser, and M.H. Kollef, *Delaying the Empiric Treatment of Candida Bloodstream Infection until Positive Blood Culture Results Are Obtained: a Potential Risk Factor for Hospital Mortality.* Antimicrobial Agents and Chemotherapy, 2005. **49**(9): p. 3640-3645.
59. Marklein, G., et al., *Matrix-Assisted Laser Desorption Ionization-Time of Flight Mass Spectrometry for Fast and Reliable Identification of Clinical Yeast Isolates.* Journal of Clinical Microbiology, 2009. **47**(9): p. 2912-2917.
60. Calderone, R.A. and W.A. Fonzi, *Virulence factors of Candida albicans.* Trends in Microbiology, 2001. **9**(7): p. 327-335.
61. Calderone, R. and P. Braun, *Adherence and receptor relationships of Candida albicans.* Microbiology and Molecular Biology Reviews, 1991. **55**(1): p. 1-20.
62. Chaffin, W., et al., *Cell Wall and Secreted Proteins of Candida albicans: Identification, Function, and Expression.* Microbiology and Molecular Biology Reviews, 1998. **62**(1): p. 130-180.
63. Hostetter, M., *Adhesins and ligands involved in the interaction of Candida spp. with epithelial and endothelial surfaces.* Clinical Microbiology Reviews, 1994. **7**(1): p. 29-42.
64. Sturtevant, J. and R. Calderone, *Candida albicans adhesins: Biochemical aspects and virulence.* Revista Iberoamericana de Micologia, 1997. **14**: p. 90-97.

65. Yue Fu, A.S.I., Donald C. Sheppard, Yee-Chun Chen, Samuel W. French, Jim E. Cutler, Scott G. Filler, John E. Edwards Jr,, *Candida albicans Als1p: an adhesin that is a downstream effector of the EFG1 filamentation pathway.* Molecular Microbiology, 2002. **44**(1): p. 61-72.
66. Fu, Y., et al., *Expression of the Candida albicans Gene ALS1 in Saccharomyces cerevisiae Induces Adherence to Endothelial and Epithelial Cells*, 1998, Am Soc Microbiol. p. 1783-1786.
67. Gaur, N. and S. Klotz, *Expression, cloning, and characterization of a Candida albicans gene, ALA1, that confers adherence properties upon Saccharomyces cerevisiae for extracellular matrix proteins.* Infection and Immunity, 1997. **65**(12): p. 5289-5294.
68. Kozel, T., et al., *Overexpression of the Candida albicans ALA1 Gene in Saccharomyces cerevisiae Results in Aggregation following Attachment of Yeast Cells to Extracellular Matrix Proteins, Adherence Properties Similar to Those of Candida albicans.* Infection and Immunity, 1999. **67**(11): p. 6040-6047.
69. Gale, C., et al., *Linkage of Adhesion, Filamentous Growth, and Virulence in Candida albicans to a Single Gene, INT1.* Science, 1998. **279**(5355): p. 1355.
70. Kozel, T., et al., *Reduced Virulence of HWP1-Deficient Mutants of Candida albicans and Their Interactions with Host Cells.* Infection and Immunity, 2000. **68**(4): p. 1997-2002.
71. Staab, J., et al., *Adhesive and Mammalian Transglutaminase Substrate Properties of Candida albicans Hwp1.* Science, 1999. **283**(5407): p. 1535.
72. Buurman, E., et al., *Molecular analysis of CaMnt1p, a mannosyl transferase important for adhesion and virulence of Candida albicans*, 1998, National Acad Sciences. p. 7670-7675.
73. Whiteway, M. and C. Bachewich, *Morphogenesis in Candida albicans.* Annual Review of Microbiology, 2007. **61**: p. 529.
74. Lo, H., et al., *Nonfilamentous C. albicans mutants are avirulent.* Cell (Cambridge), 1997. **90**(5): p. 939-949.
75. Ghannoum, M., *Potential Role of Phospholipases in Virulence and Fungal Pathogenesis.* Clinical Microbiology Reviews, 2000. **13**(1): p. 122-143.
76. Pomes, R., C. Gil, and C. Nombella, *Genetic analysis of Candida albicans morphological mutants.* Journal of general microbiology, 1985. **131**(8): p. 2107-2113.
77. Kaur, R., et al., *A yeast by any other name: Candida glabrata and its interaction with the host.* Current Opinion in Microbiology, 2005. **8**(4): p. 378-384.
78. Jones, S., G. White, and P. Hunter, *Increased phenotypic switching in strains of Candida albicans associated with invasive infections.* Journal of Clinical Microbiology, 1994. **32**(11): p. 2869-2870.
79. Brown, A.J., F.C. Odds, and N.A. Gow, *Infection-related gene expression in Candida albicans.* Curr Opin Microbiol, 2007. **10**(4): p. 307-13.
80. Kantarcioglu, A. and A. Yücel, *Phospholipase and protease activities in clinical Candida isolates with reference to the sources of strains.* Mycoses, 2002. **45**(5-6): p. 160-165.
81. Calcagno, A., et al., *Candida glabrata STE12 is required for wild-type levels of virulence and nitrogen starvation induced filamentation.* Molecular Microbiology, 2003. **50**(4): p. 1309-1318.
82. Calcagno, A.-M., et al., *Candida glabrata Ste11 is involved in adaptation to hypertonic stress, maintenance of wild-type levels of filamentation and plays a role in virulence.* Medical Mycology, 2005. **43**(4): p. 355-364.
83. Calcagno, A.-M., et al., *Candida glabrata Ste20 is involved in maintaining cell wall integrity and adaptation to hypertonic stress, and is required for wild-type levels of virulence.* Yeast, 2004. **21**(7): p. 557-568.
84. Brockert, P., et al., *Phenotypic Switching and Mating Type Switching of Candida glabrata at Sites of Colonization.* Infection and Immunity, 2003. **71**(12): p. 7109-7118.
85. Kapteyn, J., H. Van Den Ende, and F. Klis, *The contribution of cell wall proteins to the organization of the yeast cell wall.* BBA-General Subjects, 1999. **1426**(2): p. 373-383.

86. Castano, I., et al., *Telomere length control and transcriptional regulation of subtelomeric adhesins in Candida glabrata.* Molecular Microbiology, 2005. **55**(4): p. 1246-1258.
87. De Las Penas, A., et al., *Virulence-related surface glycoproteins in the yeast pathogen Candida glabrata are encoded in subtelomeric clusters and subject to RAP1-and SIR-dependent transcriptional silencing.* Genes & Development, 2003. **17**(18): p. 2245-2258.
88. Cormack, B., N. Ghori, and S. Falkow, *An Adhesin of the Yeast Pathogen Candida glabrata Mediating Adherence to Human Epithelial Cells.* Science, 1999. **285**(5427): p. 578.
89. Domergue, R., et al., *Nicotinic Acid Limitation Regulates Silencing of Candida Adhesins During UTI*, 2005, American Association for the Advancement of Science. p. 866-870.
90. Iraqui, I., et al., *The Yak1p kinase controls expression of adhesins and biofilm formation in Candida glabrata in a Sir4p-dependent pathway.* Molecular Microbiology, 2005. **55**(4): p. 1259-1271.
91. El-Azizi, M., S. Starks, and N. Khardori, *Interactions of Candida albicans with other Candida spp. and bacteria in the biofilms.* Journal of Applied Microbiology, 2004. **96**(5): p. 1067-1073.
92. Ma, B., et al., *High-Affinity Transporters for NAD+ Precursors in Candida glabrata Are Regulated by Hst1 and Induced in Response to Niacin Limitation.* Mol. Cell. Biol., 2009. **29**(15): p. 4067-4079.
93. Polakova, S., et al., *Formation of new chromosomes as a virulence mechanism in yeast Candida glabrata.* Proc Natl Acad Sci U S A, 2009.
94. Kaur, R., I. Castano, and B. Cormack, *Functional Genomic Analysis of Fluconazole Susceptibility in the Pathogenic Yeast Candida glabrata: Roles of Calcium Signaling and Mitochondria.* Antimicrobial Agents and Chemotherapy, 2004. **48**(5): p. 1600-1613.
95. Li, L., S. Redding, and A. Dongari-Bagtzoglou, *Candida glabrata, an Emerging Oral Opportunistic Pathogen.* Journal of Dental Research, 2007. **86**(3): p. 204.
96. Feng, Z., et al., *Human Beta-defensins: Differential Activity against Candidal Species and Regulation by Candida albicans*, 2005, IADR. p. 445-450.
97. Helmerhorst, E., et al., *Candida glabrata is unusual with respect to its resistance to cationic antifungal proteins.* Yeast (Chichester), 2005. **22**(9): p. 705-714.
98. Situ, H. and L. Bobek, *In Vitro Assessment of Antifungal Therapeutic Potential of Salivary Histatin-5, Two Variants of Histatin-5, and Salivary Mucin (MUC7) Domain 1.* Antimicrobial Agents and Chemotherapy, 2000. **44**(6): p. 1485-1493.
99. Tsai, H. and L. Bobek, *Studies of the mechanism of human salivary histatin-5 candidacidal activity with histatin-5 variants and azole-sensitive and-resistant Candida species.* Antimicrobial Agents and Chemotherapy, 1997. **41**(10): p. 2224-2228.
100. Schaller, M., et al., *Infection of Human Oral Epithelia with Candida Species Induces Cytokine Expression Correlated to the Degree of Virulence.* Journal of Investigative Dermatology, 2002. **118**: p. 652-657.
101. Doolin, M.-T., et al., *Overlapping and distinct roles of the duplicated yeast transcription factors Ace2p and Swi5p.* Molecular Microbiology, 2001. **40**(2): p. 422-432.
102. O'Conalláin, C., et al., *Regulated nuclear localisation of the yeast transcription factor Ace2p controls expression of chitinase (CTS1) in Saccharomyces cerevisiae.* Molecular and General Genetics MGG, 1999. **262**(2): p. 275-282.
103. Jain, C., et al., *A Pathogenesis Assay Using Saccharomyces cerevisiae and Caenorhabditis elegans Reveals Novel Roles for Yeast AP-1, Yap1, and Host Dual Oxidase BLI-3 in Fungal Pathogenesis.* Eukaryotic Cell, 2009. **8**(8): p. 1218-1227.
104. Roetzer, A., T. Gabaldón, and C. Schüller, *From Saccharomyces cerevisiae to Candida glabrata in a few easy steps: important adaptations for an opportunistic pathogen.* FEMS Microbiology Letters, 2010. **314**(1): p. 1-9.
105. Byrne, K.P. and K.H. Wolfe, *The Yeast Gene Order Browser: Combining curated homology and syntenic context reveals gene fate in polyploid species.* Genome Research, 2005. **15**(10): p. 1456-1461.

106. Marcet-Houben, M. and T. Gabaldón, *The Tree versus the Forest: The Fungal Tree of Life and the Topological Diversity within the Yeast Phylome.* PLoS ONE, 2009. **4**(2): p. e4357.
107. Roetzer, A., et al., *Candida glabrata environmental stress response involves Saccharomyces cerevisiae Msn2/4 orthologous transcription factors.* Molecular Microbiology, 2008. **69**(3): p. 603-620.
108. Kitada, K., E. Yamaguchi, and M. Arisawa, *Cloning of the Candida glabrata TRP1 and HIS3 genes, and construction of their disruptant strains by sequential integrative transformation.* Gene, 1995. **165**(2): p. 203-6.
109. Ehrlich, G.D., N.L. Hiller, and F. Hu, *What makes pathogens pathogenic.* Genome Biology, 2008. **9**(6): p. 225.
110. Dujon, B., et al., *Genome evolution in yeasts.* Nature, 2004. **430**(6995): p. 35-44.
111. Marcet-Houben, M. and T. Gabaldón, *Acquisition of prokaryotic genes by fungal genomes.* Trends in Genetics, 2010. **26**(1): p. 5-8.
112. Muñoz, P., et al., *Saccharomyces cerevisiae Fungemia: An Emerging Infectious Disease.* Clinical Infectious Diseases, 2005. **40**(11): p. 1625-1634.
113. Ferrari, S., et al., *Gain of Function Mutations in CgPDR1 of Candida glabrata Not Only Mediate Antifungal Resistance but Also Enhance Virulence.* PLoS Pathog, 2009. **5**(1): p. e1000268.
114. Alberts, B., et al., *Molecular biology of the cell*2002, New York: Garland Publishing.
115. Simon, I., et al., *Serial Regulation of Transcriptional Regulators in the Yeast Cell Cycle.* Cell, 2001. **106**(6): p. 697-708.
116. Jorgensen, P., et al., *A dynamic transcriptional network communicates growth potential to ribosome synthesis and critical cell size.* Genes & Development, 2004. **18**(20): p. 2491.
117. Fink, G., et al., *Comprehensive Identification of Cell Cycle-regulated Genes of the Yeast Saccharomyces cerevisiae by Microarray Hybridization.* Molecular Biology of the Cell, 1998. **9**(12): p. 3273-3297.
118. Breeden, L., *Periodic Transcription: A Cycle within a Cycle.* Current Biology, 2003. **13**(1): p. 31-38.
119. Koch, C. and K. Nasmyth, *Cell cycle regulated transcription in yeast.* Curr Opin Cell Biol, 1994. **6**(3): p. 451-9.
120. Althoefer, H., et al., *Mcm1 is required to coordinate G2-specific transcription in Saccharomyces cerevisiae.* Molecular and Cellular Biology, 1995. **15**(11): p. 5917-5928.
121. Kumar, R., et al., *Forkhead transcription factors, Fkh1p and Fkh2p, collaborate with Mcm1p to control transcription required for M-phase.* Current Biology, 2000. **10**(15): p. 896-906.
122. Tolliday, N., N. Bouquin, and R. Li, *Assembly and regulation of the cytokinetic apparatus in budding yeast.* Current Opinion in Microbiology, 2001. **4**(6): p. 690-695.
123. Yeong, F.M., H.H. Lim, and U. Surana, *MEN, destruction and separation: mechanistic links between mitotic exit and cytokinesis in budding yeast.* Bioessays, 2002. **24**(7): p. 659-66.
124. Walther, A. and J. Wendland, *Septation and cytokinesis in fungi.* Fungal Genetics and Biology, 2003. **40**(3): p. 187-196.
125. Yeong, F.M., *Severing all ties between mother and daughter: cell separation in budding yeast.* Molecular Microbiology, 2005. **55**(5): p. 1325-1331.
126. Klis, F.M., et al., *Dynamics of cell wall structure in Saccharomyces cerevisiae.* FEMS Microbiol. Rev, 2002. **26**(3): p. 239-256.
127. Kovacech, B., K. Nasmyth, and T. Schuster, *EGT2 gene transcription is induced predominantly by Swi5 in early G1.* Molecular and Cellular Biology, 1996. **16**(7): p. 3264.
128. Adams, D.J., *Fungal cell wall chitinases and glucanases.* Microbiology, 2004. **150**(7): p. 2029-2035.
129. Kuranda, M.J. and P.W. Robbins, *Chitinase is required for cell separation during growth of Saccharomyces cerevisiae.* Journal of Biological Chemistry, 1991. **266**(29): p. 19758-19767.

130. Baladron, V., et al., *Eng1p, an Endo-1, 3-ß-Glucanase Localized at the Daughter Side of the Septum, Is Involved in Cell Separation in Saccharomyces cerevisiae.* Eukaryotic Cell, 2002. **1**(5): p. 774-786.
131. Fujita, M., et al., *GPI7 Involved in Glycosylphosphatidylinositol Biosynthesis Is Essential for Yeast Cell Separation.* Journal of Biological Chemistry, 2004. **279**(50): p. 51869.
132. Dohrmann, P.R., et al., *Parallel pathways of gene regulation: homologous regulators SWI5 and ACE2 differentially control transcription of HO and chitinase.* Genes Dev., 1992. **6**(1): p. 93-104.
133. Colman-Lerner, A., T.E. Chin, and R. Brent, *Yeast Cbk1 and Mob2 Activate Daughter-Specific Genetic Programs to Induce Asymmetric Cell Fates.* Cell, 2001. **107**(6): p. 739-750.
134. Cappellaro, C., V. Mrsa, and W. Tanner, *New potential cell wall glucanases of Saccharomyces cerevisiae and their involvement in mating.* J. Bacteriol, 1998. **180**(19): p. 5030–5037.
135. Nelson, B., et al., *RAM: A Conserved Signaling Network That Regulates Ace2p Transcriptional Activity and Polarized Morphogenesis.* Mol. Biol. Cell, 2003. **14**(9): p. 3782-3803.
136. Kurischko, C., et al., *A role for the Saccharomyces cerevisiae regulation of Ace2 and polarized morphogenesis signaling network in cell integrity.* Genetics, 2005. **171**(2): p. 443-55.
137. Tang, Z., et al., *The kic1 kinase of schizosaccharomyces pombe is a CLK/STY orthologue that regulates cell-cell separation.* Exp Cell Res, 2003. **283**(1): p. 101-15.
138. Bogomolnaya, L.M., et al., *Hym1p affects cell cycle progression in Saccharomyces cerevisiae.* Curr Genet, 2004. **46**(4): p. 183-92.
139. Du, L.L. and P. Novick, *Pag1p, a novel protein associated with protein kinase Cbk1p, is required for cell morphogenesis and proliferation in Saccharomyces cerevisiae.* Mol Biol Cell, 2002. **13**(2): p. 503-14.
140. Kaeberlein, M., et al., *Saccharomyces cerevisiae SSD1-V confers longevity by a Sir2p-independent mechanism.* Genetics, 2004. **166**(4): p. 1661-72.
141. Weiss, E.L., et al., *The Saccharomyces cerevisiae Mob2p-Cbk1p kinase complex promotes polarized growth and acts with the mitotic exit network to facilitate daughter cell-specific localization of Ace2p transcription factor.* J Cell Biol, 2002. **158**(5): p. 885-900.
142. Findon, H.C., *Functional Analysis of C. glabrata Ace2 a Transcriptional Regulator Mediating Avirulence*, in *Microbiology* 2006, Imperial College London: London. p. 5248.
143. Huh, W.K., et al., *Global analysis of protein localization in budding yeast.* Nature, 2003. **425**(6959): p. 686-91.
144. Wang, Y., et al., *Exit from Exit: Resetting the Cell Cycle through Amn1 Inhibition of G Protein Signaling.* Cell, 2003. **112**(5): p. 697-709.
145. Ronald, J., et al., *Local Regulatory Variation in Saccharomyces cerevisiae.* PLoS Genet, 2005. **1**(2): p. e25.
146. Zheng, W., et al., *Genetic analysis of variation in transcription factor binding in yeast.* Nature, 2010. **464**(7292): p. 1187-1191.
147. Sil, A. and I. Herskowitz, *Identification of asymmetrically localized determinant, Ash1p, required for lineage-specific transcription of the yeast HO gene.* Cell, 1996. **84**(5): p. 711-22.
148. Nasmyth, K., *Molecular analysis of a cell lineage.* Nature, 1983. **302**(5910): p. 670-676.
149. Maxon, M. and I. Herskowitz, *Ash1p is a site-specific DNA-binding protein that actively represses transcription.* Proceedings of the National Academy of Sciences, 2001. **98**(4): p. 1495.
150. Chandarlapaty, S. and B. Errede, *Ash1, a Daughter Cell-Specific Protein, Is Required for Pseudohyphal Growth of Saccharomyces cerevisiae.* Mol. Cell. Biol., 1998. **18**(5): p. 2884-2891.
151. Deng, Y., R.H. Singer, and W. Gu, *Translation of ASH1 mRNA is repressed by Puf6p–Fun12p/eIF5B interaction and released by CK2 phosphorylation.* Genes & Development, 2008. **22**(8): p. 1037-1050.

152. Long, R.M., et al., *Mating Type Switching in Yeast Controlled by Asymmetric Localization of ASH1 mRNA.* Science, 1997. **277**(5324): p. 383-387.
153. Long, R.M., et al., *An Exclusively Nuclear RNA-Binding Protein Affects Asymmetric Localization of ASH1 mRNA and Ash1p in Yeast.* The Journal of Cell Biology, 2001. **153**(2): p. 307-318.
154. Long, R.M., et al., *She2p is a novel RNA-binding protein that recruits the Myo4p-She3p complex to ASH1 mRNA.* EMBO J, 2000. **19**(23): p. 6592-6601.
155. Zahner, J., H. Harkins, and J. Pringle, *Genetic analysis of the bipolar pattern of bud site selection in the yeast Saccharomyces cerevisiae.* Molecular and Cellular Biology, 1996. **16**(4): p. 1857-1870.
156. Harkins, H.A., et al., *Bud8p and Bud9p, proteins that may mark the sites for bipolar budding in yeast.* Molecular Biology of the Cell, 2001. **12**(8): p. 2497-2518.
157. Kato, Y., et al., *Cell Polarity in Saccharomyces cerevisiae Depends on Proper Localization of the Bud9 Landmark Protein by the EKC/KEOPS Complex.* Genetics, 2011.
158. Kang, P.J., et al., *Interactions among Rax1p, Rax2p, Bud8p, and Bud9p in Marking Cortical Sites for Bipolar Bud-site Selection in Yeast.* Mol. Biol. Cell, 2004. **15**(11): p. 5145-5157.
159. Schenkman, L.R., et al., *The role of cell cycle–regulated expression in the localization of spatial landmark proteins in yeast.* The Journal of Cell Biology, 2002. **156**(5): p. 829-841.
160. Kisseleva-Romanova, E., et al., *Yeast homolog of a cancer-testis antigen defines a new transcription complex.* EMBO J, 2006. **25**(15): p. 3576-3585.
161. Downey, M., et al., *A Genome-Wide Screen Identifies the Evolutionarily Conserved KEOPS Complex as a Telomere Regulator.* Cell, 2006. **124**(6): p. 1155-1168.
162. Kang, P.J., et al., *A GDP/GTP Exchange Factor Involved in Linking a Spatial Landmark to Cell Polarity.* Science, 2001. **292**(5520): p. 1376-1378.
163. Frydlova, I., et al., *Deregulation of DSE1 gene expression results in aberrant budding within the birth scar and CWI pathway activation in Saccharomyces cerevisiae.* Eukaryot Cell, 2009.
164. Drees, B.L., et al., *A protein interaction map for cell polarity development.* J. Cell Biol., 2001. **154**(3): p. 549-576.
165. Stark, C., et al., *BioGRID: a general repository for interaction datasets.* Nucleic Acids Research, 2006. **34**(suppl 1): p. D535-D539.
166. Draper, E., et al., *Dse1 may control cross talk between the pheromone and filamentation pathways in yeast.* Current Genetics, 2009.
167. Matsui, Y., et al., *Yeast src homology region 3 domain-binding proteins involved in bud formation.* J Cell Biol, 1996. **133**(4): p. 865-78.
168. Madden, K. and M. Snyder, *Cell polarity and morphogenesis in budding yeast.* Annu Rev Microbiol, 1998. **52**: p. 687-744.
169. Daher, J.Y., et al., *The Candida albicans Dse1 Protein Is Essential and Plays a Role in Cell Wall Rigidity, Biofilm Formation, and Virulence.* Interdisciplinary Perspectives on Infectious Diseases, 2011. **2011**: p. 504280.
170. SGD-project, *Saccharomyces Genome Database*, 2007, http://www.yeastgenome.org/.
171. Sherman, D.J., et al., *Genolevures: protein families and synteny among complete hemiascomycetous yeast proteomes and genomes.* Nucl. Acids Res., 2009. **37**(suppl_1): p. D550-554.
172. Kawahata, M., et al., *Yeast genes involved in response to lactic acid and acetic acid: acidic conditions caused by the organic acids in Saccharomyces cerevisiae cultures induce expression of intracellular metal metabolism genes regulated by Aft1p.* FEMS Yeast Research, 2006. **6**(6): p. 924-936.
173. Tadi, D., et al., *Selection of genes repressed by cAMP that are induced by nutritional limitation in Saccharomyces cerevisiae.* Yeast, 1999. **15**(16): p. 1733-45.

174. Sprowl, J.A., et al., *Changes in expression of cell wall turnover genes accompany inhibition of chromosome segregation by bovine protein kinase C alpha expression in Saccharomyces cerevisiae.* Cell Biology International, 2007. **31**(10): p. 1160-1172.
175. Yvert, G., et al., *Trans-acting regulatory variation in Saccharomyces cerevisiae and the role of transcription factors.* Nat Genet, 2003. **35**(1): p. 57-64.
176. Cantarel, B.L., et al., *The Carbohydrate-Active EnZymes database (CAZy): an expert resource for Glycogenomics.* Nucleic Acids Research, 2009. **37**(suppl 1): p. D233-D238.
177. Esteban, P., et al., *Characterization of the CaENG1 Gene Encoding an Endo-1,3-β-Glucanase Involved in Cell Separation in Candida albicans.* Current Microbiology, 2005. **51**(6): p. 385-392-392.
178. Encinar del Dedo, J., et al., *beta-Glucanase Eng2 Is Required for Ascus Wall Endolysis after Sporulation in the Fission Yeast Schizosaccharomyces pombe.* Eukaryotic Cell, 2009. **8**(8): p. 1278-1286.
179. McBride, H.J., Y. Yu, and D.J. Stillman, *Distinct Regions of the Swi5 and Ace2 Transcription Factors Are Required for Specific Gene Activation.* Journal of Biological Chemistry, 1999. **274**(30): p. 21029-21036.
180. Stead, D.A., et al., *Impact of the transcriptional regulator, Ace2, on the Candida glabrata secretome.* Proteomics, 2010. **10**(2): p. 212-223.
181. Covitz, P.A., I. Herskowitz, and A.P. Mitchell, *The yeast RME1 gene encodes a putative zinc finger protein that is directly repressed by a1-alpha 2.* Genes Dev., 1991. **5**(11): p. 1982-1989.
182. Mitchell, A.P. and I. Herskowitz, *Activation of meiosis and sporulation by repression of the RME1 product in yeast.* Nature, 1986. **319**(6056): p. 738-742.
183. Rine, J., G.F. Sprague, Jr., and I. Herskowitz, *rme1 Mutation of Saccharomyces cerevisiae: map position and bypass of mating type locus control of sporulation.* Mol Cell Biol, 1981. **1**(10): p. 958-60.
184. Kassir, Y. and G. Simchen, *Pathways leading to meiotic differentiation in the yeast Saccharomyces cerevisiae.* Current Genetics, 1989. **15**(3): p. 167-170.
185. Covitz, P.A. and A.P. Mitchell, *Repression by the yeast meiotic inhibitor RME1.* Genes & Development, 1993. **7**(8): p. 1598-1608.
186. Shimizu, M., et al., *Genomic footprinting of the yeast zinc finger protein Rme1p and its roles in repression of the meiotic activator IME1.* Nucleic Acids Research, 1998. **26**(10): p. 2329-2336.
187. Shimizu, M., et al., *Transcriptional repression at a distance through exclusion of activator binding in vivo.* Proceedings of the National Academy of Sciences, 1997. **94** (3): p. 790-795.
188. Li, Y., et al., *Yeast global transcriptional regulators Sin4 and Rgr1 are components of mediator complex/RNA polymerase II holoenzyme.* Proceedings of the National Academy of Sciences, 1995. **92**(24): p. 10864-10868.
189. Toone, W., et al., *Rme1, a negative regulator of meiosis, is also a positive activator of G1 cyclin gene expression.* The EMBO journal, 1995. **14**(23): p. 5824.
190. Wijnen, H. and B. Futcher, *Genetic Analysis of the Shared Role of CLN3 and BCK2 at the G1-S Transition in Saccharomyces cerevisiae.* Genetics, 1999. **153**(3): p. 1131-1143.
191. Frenz, Johnson, and Johnston, *Rme1, which controls CLN2 expression in Saccharomyces cerevisiae is a nuclear protein that is cell cycle regulated.* Molecular Genetics and Genomics, 2001. **266**(3): p. 374-384.
192. Kelly, M.T., et al., *The Candida albicans CaACE2 gene affects morphogenesis, adherence and virulence.* Molecular Microbiology, 2004. **53**(3): p. 969-983.
193. Zeitlinger, J., et al., *Program-Specific Distribution of a Transcription Factor Dependent on Partner Transcription Factor and MAPK Signaling.* Cell, 2003. **113**(3): p. 395-404.
194. Caba, E., et al., *Differentiating mechanisms of toxicity using global gene expression analysis in Saccharomyces cerevisiae.* Mutation Research/Fundamental and Molecular Mechanisms of Mutagenesis, 2005. **575**(1-2): p. 34-46.

195. Teparić, R., I. Stuparević, and V. Mrša, *Increased mortality of Saccharomyces cerevisiae cell wall protein mutants.* Microbiology, 2004. **150**(10): p. 3145-3150.
196. Stanley, D., et al., *Transcriptional changes associated with ethanol tolerance in Saccharomyces cerevisiae.* Applied Microbiology and Biotechnology, 2010. **88**(1): p. 231-239.
197. Chaffin, W.L., *Candida albicans Cell Wall Proteins.* Microbiology and Molecular Biology Reviews, 2008. **72**(3): p. 495-544.
198. Wang, A., et al., *Hyphal Chain Formation in Candida albicans: Cdc28-Hgc1 Phosphorylation of Efg1 Represses Cell Separation Genes.* Molecular and Cellular Biology, 2009. **29**(16): p. 4406-4416.
199. Mulhern, S.M., M.E. Logue, and G. Butler, *Candida albicans Transcription Factor Ace2 Regulates Metabolism and Is Required for Filamentation in Hypoxic Conditions.* Eukaryotic Cell, 2006. **5**(12): p. 2001-2013.
200. Lan, C.-Y., et al., *Regulatory networks affected by iron availability in Candida albicans.* Iron regulation in C. albicans, 2004. **53**(5): p. 1451-1469.
201. Sorgo, A.G., et al., *The effects of fluconazole on the secretome, the wall proteome and wall integrity of the clinical fungus Candida albicans.* Eukaryotic Cell, 2011: p. EC.05011-11.
202. Sorgo, A.G., et al., *Mass spectrometric analysis of the secretome of Candida albicans.* Yeast, 2010. **27**(8): p. 661-672.
203. Norice, C.T., et al., *Requirement for Candida albicans Sun41 in Biofilm Formation and Virulence.* Eukaryotic Cell, 2007. **6**(11): p. 2046-2055.
204. Toyn, J.H., et al., *The Swi5 Transcription Factor of Saccharomyces cerevisiae Has a Role in Exit From Mitosis Through Induction of the cdk-Inhibitor Sic1 in Telophase.* Genetics, 1997. **145**(1): p. 85-96.
205. Spellman, P.T., et al., *Comprehensive identification of cell cycle-regulated genes of the yeast Saccharomyces cerevisiae by microarray hybridization.* Mol Biol Cell, 1998. **9**(12): p. 3273-3297.
206. Knapp, D., et al., *The transcription factor Swi5 regulates expression of the cyclin kinase inhibitor p40SIC1.* Mol Cell Biol, 1996. **16**(10): p. 5701-5707.
207. Donovan, J.D., et al., *P40SDB25, a putative CDK inhibitor, has a role in the M/G1 transition in Saccharomyces cerevisiae.* Genes & Development, 1994. **8**(14): p. 1640-1653.
208. Nugroho, T.T. and M.D. Mendenhall, *An inhibitor of yeast cyclin-dependent protein kinase plays an important role in ensuring the genomic integrity of daughter cells.* Mol Cell Biol, 1994. **14**(5): p. 3320-3328.
209. Barberis, M., et al., *The yeast cyclin-dependent kinase inhibitor Sic1 and mammalian p27Kip1 are functional homologues with a structurally conserved inhibitory domain.* Biochem J, 2005. **387**(Pt 3): p. 639-47.
210. Schwob, E., et al., *The B-type cyclin kinase inhibitor p40SIC1 controls the G1 to S transition in S. cerevisiae.* Cell, 1994. **79**(2): p. 233-244.
211. Feldman, R., et al., *A Complex of Cdc4p, Skp1p, and Cdc53p/Cullin Catalyzes Ubiquitination of the Phosphorylated CDK Inhibitor Sic1p.* Cell, 1997. **91**: p. 221-230.
212. Nash, P., et al., *Multisite phosphorylation of a CDK inhibitor sets a threshold for the onset of DNA replication.* Nature, 2001. **414**(6863): p. 514-521.
213. Masson, A.J. and J.C. Patterson, *The structure of a β-(1→3)-D-glucan from yeast cell walls.* Biochemical Journal, 1973.
214. Kollár, R., et al., *Architecture of the yeast cell wall. Beta(1-->6)-glucan interconnects mannoprotein, beta(1-->)3-glucan, and chitin.* Journal of Biological Chemistry, 1997. **272**(28): p. 17762-17775.
215. Mazur, P., et al., *Differential expression and function of two homologous subunits of yeast 1,3-beta-D-glucan synthase.* Mol Cell Biol, 1995. **15**(10): p. 5671-5681.

216. Mio, T., et al., *Cloning of the Candida albicans homolog of Saccharomyces cerevisiae GSC1/FKS1 and its involvement in beta-1,3-glucan synthesis.* J Bacteriol, 1997. **179**(13): p. 4096-4105.
217. Kurtz, M.B. and C.M. Douglas, *Lipopeptide inhibitors of fungal glucan synthase.* Journal of medical and veterinary mycology : bi-monthly publication of the International Society for Human and Animal Mycology, 1997. **35**(2): p. 79-86.
218. Shaw, J.A., et al., *The function of chitin synthases 2 and 3 in the Saccharomyces cerevisiae cell cycle.* J Cell Biol, 1991. **114**(1): p. 111-123.
219. Munro, C.A. and N.A.R. Gow, *Chitin synthesis in human pathogenic fungi.* 2001.
220. Dohrmann, P.R., W.P. Voth, and D.J. Stillman, *Role of negative regulation in promoter specificity of the homologous transcriptional activators Ace2p and Swi5p.* Mol Cell Biol, 1996. **16**(4): p. 1746-1758.
221. Saiki, R.K., et al., *Analysis of enzymatically amplified [beta]-globin and HLA-DQ[alpha] DNA with allele-specific oligonucleotide probes.* Nature, 1986. **324**(6093): p. 163-166.
222. Liang, Q. and T. Richardson, *A simple and rapid method for screening transformant yeast colonies using PCR.* Biotechniques, 1992. **13**(5): p. 730-2, 735.
223. Sambrook, J., E.F. Fritsch, and T. Maniatis, *Molecular Cloning: A Laboratory Manual*1984, New York: Cold Spring Harbor Laboratory Press.
224. Kohrer, K. and H. Domdey, *Preparation of high molecular weight RNA.* Methods Enzymol, 1991. **194**: p. 398-405.
225. Ausubel, F.M., Brent, R., Kingston, R. E., Moore, D. D., Seidman, J. G., Smith, J. A., Struhl, K., *Current Protocols in Molecular Biology*, ed. K. Janssen1987: John Wiley and Sons.
226. Gietz, R.D. and R.A. Woods, *Transformation of yeast by lithium acetate/single-stranded carrier DNA/polyethylene glycol method*, in *Methods in Enzymology*, G. Christine and R.F. Gerald, Editors. 2002, Academic Press. p. 87-96.
227. Mandel, M. and A. Higa, *Calcium-dependent bacteriophage DNA infection.* Journal of Molecular Biology, 1970. **53**(1): p. 159-162.
228. Alwine, J.C., D.J. Kemp, and G.R. Stark, *Method for detection of specific RNAs in agarose gels by transfer to diazobenzyloxymethyl-paper and hybridization with DNA probes.* Proc Natl Acad Sci U S A, 1977. **74**(12): p. 5350-4.
229. Southern, E.M., *Detection of specific sequences among DNA fragments separated by gel electrophoresis.* Journal of Molecular Biology, 1975. **98**(3): p. 503-517.
230. Ho, H.-l., *Characterisation of the Saccharomyces cerevisiae Cell Separation Machinery: Sdm1 a Potential Nuclear Shuttler of Ace2* in *Department of Microbiology*2008, Imperial College London: London.
231. Stead, D., et al., *Proteomic changes associated with inactivation of the Candida glabrata ACE2 virulence-moderating gene.* Proteomics, 2005. **5**(7): p. 1838-1848.
232. Favorov, A.V., et al., *A Gibbs sampler for identification of symmetrically structured, spaced DNA motifs with improved estimation of the signal length.* Bioinformatics. **21**(10): p. 2240-2245.
233. Findon, H. and K. Haynes, *Chapter 7 Ace2 and fungal virulence*, in *British Mycological Society Symposia Series*, M.S. Simon V. Avery and W. Pieter Van, Editors. 2008, Academic Press. p. 97-107.
234. Netea, M.G., et al., *The Role of Toll-like Receptor (TLR) 2 and TLR4 in the Host Defense against Disseminated Candidiasis.* The journal of infectious diseases, 2002. **185**(10): p. 1483-1489.
235. Sriskandan, S. and J. Cohen, *The pathogenesis of septic shock.* Journal of Infection, 1995. **30**(3): p. 201-206.
236. Rusche, L.N., A.L. Kirchmaier, and J. Rine, *The Estabilishment, Inheritance, and Function of Silenced Chromatin in Saccharomyces cerevisiase.* Annual Review of Biochemistry, 2003. **72**(1): p. 481-516.

237. MacCallum, D.M., et al., *Different Consequences of ACE2 and SWI5 Gene Disruptions for Virulence of Pathogenic and Nonpathogenic Yeasts.* Infect. Immun., 2006. **74**(9): p. 5244-5248.
238. Braun, B.R., et al., *Identification and Characterization of TUP1-Regulated Genes in Candida albicans.* Genetics, 2000. **156**(1): p. 31-44.
239. Bates, S., et al., *Outer Chain N-Glycans Are Required for Cell Wall Integrity and Virulence of Candida albicans.* Journal of Biological Chemistry, 2006. **281**(1): p. 90-98.
240. Noble, S.M. and A.D. Johnson, *Strains and strategies for large-scale gene deletion studies of the diploid human fungal pathogen Candida albicans.* Eukaryot Cell, 2005. **4**(2): p. 298-309.
241. Edlind, T.D., et al., *Promoter-dependent disruption of genes: simple, rapid, and specific PCR-based method with application to three different yeast.* Curr Genet, 2005. **48**(2): p. 117-25.
242. Giaever, G., et al., *Functional profiling of the Saccharomyces cerevisiae genome.* Nature, 2002. **418**(6896): p. 387-91.
243. Shoemaker, D.D., et al., *Quantitative phenotypic analysis of yeast deletion mutants using a highly parallel molecular bar-coding strategy.* Nat Genet, 1996. **14**(4): p. 450-456.
244. Wach, A., *PCR-synthesis of marker cassettes with long flanking homology regions for gene disruptions in S. cerevisiae.* Yeast, 1996. **12**(3): p. 259-265.
245. Reuss, O., et al., *The SAT1 flipper, an optimized tool for gene disruption in Candida albicans.* Gene, 2004. **341**: p. 119-27.
246. Hampsey, M., *A review of phenotypes in Saccharomyces cerevisiae.* Yeast, 1997. **13**(12): p. 1099-133.
247. Kuranda, K., et al., *Investigating the caffeine effects in the yeast Saccharomyces cerevisiae brings new insights into the connection between TOR, PKC and Ras/cAMP signalling pathways.* Molecular Microbiology, 2006. **61**(5): p. 1147-1166.
248. Ballou, L., et al., *Vanadate-resistant yeast mutants are defective in protein glycosylation.* Proceedings of the National Academy of Sciences, 1991. **88**(8): p. 3209-3212.
249. Kanik-Ennulat, C., E. Montalvo, and N. Neff, *Sodium Orthovanadate-Resistant Mutants of Saccharomyces cerevisiae Show Defects in Golgi-Mediated Protein Glycosylation, Sporulation and Detergent Resistance.* Genetics, 1995. **140**(3): p. 933-943.
250. Leis, J.F. and N.O. Kaplan, *An acid phosphatase in the plasma membranes of human astrocytoma showing marked specificity toward phosphotyrosine protein.* Proceedings of the National Academy of Sciences, 1982. **79**(21): p. 6507-6511.
251. Nickas, M. and M. Yaffe, *BRO1, a novel gene that interacts with components of the Pkc1p-mitogen- activated protein kinase pathway in Saccharomyces cerevisiae.* Mol. Cell. Biol., 1996. **16**(6): p. 2585-2593.
252. Srikantha, T., S.A. Lachke, and D.R. Soll, *Three Mating Type-Like Loci in Candida glabrata.* Eukaryotic Cell, 2003. **2**(2): p. 328-340.
253. Wong, S., et al., *Evidence from comparative genomics for a complete sexual cycle in the 'asexual' pathogenic yeast Candida glabrata.* Genome Biology, 2003. **4**(2): p. R10.
254. Wheeler, R.T. and G.R. Fink, *A Drug-Sensitive Genetic Network Masks Fungi from the Immune System.* PLoS Pathog, 2006. **2**(4): p. e35.
255. Ejzykowicz, D.E., et al., *The Aspergillus fumigatus transcription factor Ace2 governs pigment production, conidiation and virulence.* Molecular Microbiology, 2009. **72**(1): p. 155-169.
256. Su, S.S.Y. and A.P. Mitchell, *Identification of Functionally Related Genes That Stimulate Early Meiotic Gene Expression in Yeast.* Genetics, 1993. **133**(1): p. 67-77.
257. Lamb, T.M. and A.P. Mitchell, *The Transcription Factor Rim101p Governs Ion Tolerance and Cell Differentiation by Direct Repression of the Regulatory Genes NRG1 and SMP1 in Saccharomyces cerevisiae.* Molecular and Cellular Biology, 2003. **23**(2): p. 677-686.
258. Strudwick, N., et al., *Ime1 and Ime2 Are Required for Pseudohyphal Growth of Saccharomyces cerevisiae on Nonfermentable Carbon Sources.* Molecular and Cellular Biology, 2010. **30**(23): p. 5514-5530.

259. Sgarlata, C. and J. Pérez-Martín, *Inhibitory phosphorylation of a mitotic cyclin-dependent kinase regulates the morphogenesis, cell size and virulence of the smut fungus Ustilago maydis.* Journal of Cell Science, 2005. **118**(16): p. 3607-3622.
260. Mora-Montes, H.c.M., et al., *Protein glycosylation in Candida.* Future Microbiology, 2009. **4**(9): p. 1167-1183.
261. Ruiz-Herrera, J., et al., *Molecular organization of the cell wall of Candida albicans and its relation to pathogenicity.* FEMS Yeast Research, 2006. **6**(1): p. 14-29.
262. Brown, G.D., et al., *Dectin-1 Mediates the Biological Effects of ß-Glucans.* Journal of Experimental Medicine, 2003. **197**(9): p. 1119-1124.
263. Müller, A., et al., *The application of various protic acids in the extraction of (1- 3)-beta-d-glucan from Saccharomyces cerevisiae.* Carbohydrate Research, 1997. **299**(3): p. 203-208.
264. Lowman, D.W. and D.L. Williams, *A Proton Nuclear Magnetic Resonance Method for the Quantitative Analysis on a Dry Weight Basis of (1-3)-beta-d-Glucans in a Complex, Solvent-Wet Matrix.* Journal of Agricultural and Food Chemistry, 2001. **49**(9): p. 4188-4191.
265. Netea, M.G., et al., *Immune sensing of Candida albicans requires cooperative recognition of mannans and glucans by lectin and Toll-like receptors.* J. Clin. Invest., 2006. **116**(6): p. 1642-1650.
266. Foreman-Wykert, A.K. and J.F. Miller, *Hypervirulence and pathogen fitness.* Trends in Microbiology, 2003. **11**(3): p. 105-108.
267. Butler, G. and D.J. Thiele, *ACE2, an activator of yeast metallothionein expression which is homologous to SWI5.* Molecular and Cellular Biology, 1991. **11**(1): p. 476-485.
268. Daher, J.Y., *Characterization of Dse1 a Candida albicans cell wall protein*, 2009, American University.
269. Talavera, D. and S. Lovell, *Candida glabrata Dse1p structural prediction*, 2009, Manchester University: Manchester.
270. Bryson, K., et al., *Protein structure prediction servers at University College London.* Nucleic Acids Research. **33**(suppl 2): p. W36-W38.
271. McGuffin, L.J. and D.T. Jones, *Improvement of the GenTHREADER method for genomic fold recognition.* Bioinformatics, 2003. **19**(7): p. 874-881.
272. Martí-Renom, M.A., et al., *Comparative Protein Structure Modelling of Genes and Genomes.* Annual Review of Biophysics and Biomolecular Structure, 2000. **29**(1): p. 291-325.
273. Davis, I.W., et al., *MolProbity: all-atom contacts and structure validation for proteins and nucleic acids.* Nucleic Acids Research, 2007. **35**(suppl 2): p. W375-W383.
274. Laskowski, R.A., et al., *PROCHECK: a program to check the stereochemical quality of protein structures.* Journal of Applied Crystallography, 1993. **26**(2): p. 283-291.
275. Alberti, S., A.D. Gitler, and S. Lindquist, *A suite of Gateway® cloning vectors for high-throughput genetic analysis in Saccharomyces cerevisiae.* Yeast, 2007. **24**(10): p. 913-919.
276. Winzeler, E., et al., *Functional characterization of the S. cerevisiae genome by gene deletion and parallel analysis.* Science, 1999. **285**(5429): p. 901.
277. Fülöp, V. and D.T. Jones, *beta Propellers: structural rigidity and functional diversity.* Current Opinion in Structural Biology, 1999. **9**(6): p. 715-721.
278. Smith, R.L. and A.D. Johnson, *Turning genes off by Ssn6-Tup1: a conserved system of transcriptional repression in eukaryotes.* Trends in Biochemical Sciences, 2000. **25**(7): p. 325-330.
279. Yasutis, K., et al., *Zds2p Regulates Swe1p-dependent Polarized Cell Growth in Saccharomyces cerevisiae via a Novel Cdc55p Interaction Domain.* Molecular Biology of the Cell, 2010. **21**(24): p. 4373-4386.
280. Klebl, F. and W. Tanner, *Molecular cloning of a cell wall exo-beta-1,3-glucanase from Saccharomyces cerevisiae.* J Bacteriol, 1989. **171**(11): p. 6259-6264.

281. O'Brien, M. and R.R. Colwell, *A rapid test for chitinase activity that uses 4-methylumbelliferyl-N-acetyl-beta-D-glucosaminide.* Appl Environ Microbiol, 1987. **53**(7): p. 1718-1720.
282. Drinnenberg, I.A., et al., *RNAi in Budding Yeast.* Science, 2009. **326**(5952): p. 544-550.
283. Jones, T., et al., *The diploid genome sequence of Candida albicans.* Proceedings of the National Academy of Sciences of the United States of America, 2004. **101**(19): p. 7329-7334.
284. Weig, M., et al., *A GAS-like gene family in the pathogenic fungus Candida glabrata.* Microbiology, 2001. **147**(Pt 8): p. 2007-19.
285. Kitada, K., E. Yamaguchi, and M. Arisawa, *Isolation of a Candida glabrata centromere and its use in construction of plasmid vectors.* Gene, 1996. **175**(1-2): p. 105-108.
286. Gietz, R.D. and S. Akio, *New yeast-Escherichia coli shuttle vectors constructed with in vitro mutagenized yeast genes lacking six-base pair restriction sites.* Gene, 1988. **74**(2): p. 527-534.
287. Hodgkin, J., *Introduction to genetics and genomics*, WormBook.
288. Nicholas, H.R. and J. Hodgkin, *The ERK MAP Kinase Cascade Mediates Tail Swelling and a Protective Response to Rectal Infection in C. elegans.* Current Biology, 2004. **14**(14): p. 1256-1261.
289. Mortazavi, A., et al., *Mapping and quantifying mammalian transcriptomes by RNA-Seq.* Nature Methods, 2008. **5**(7): p. 621-628.

Appendix 1 - Strains

A1.1 Yeast Strains

C. albicans SC5314 – Wild type [283]

C. glabrata ATC2001 (Cg2001) – Wild type (American Type Culture Collection (Rockville, MD, USA))

C. glabrata HLS119 – *Δhis3, Δtrp1, ACE2*::*tetR*::*GAL4AD*::*TRP1* [180]

C. glabrata HLS122 – *Δhis3::URA3 Δura3 Δtrp1 Δace2::HIS3 (pCgACT-14 [TRP1])* [7]

C. glabrata his3 – *Δura3*::pUC18*, Δhis3*::*URA3* [284]

C. glabrata ΔΔΔ – *Δhis3, Δtrp1, Δleu2* [285]

SRSG1 – *Δhis3, Δtrp1, Δleu2, Δamn1*::*TRP1* [This study]

SRSG1P – *Δhis3, Δtrp1, Δleu2, Δamn1*::TRP1, pBM51 (*HIS3*), YPCIII (*LEU2*) [This study]

SRSG2 – *Δhis3, Δash1*::NAT_R [This study]

SRSG2P – *Δhis3, Δash1*::NAT_R, pBM51 (*HIS3*) [This study]

SRSG3 – *Δhis3, Δbud9*::NAT_R [This study]

SRSG3P – *Δhis3, Δbud9*::NAT_R, pBM51 (*HIS3*) [This study]

SRSG4 – *Δhis3, Δdse1*::NAT_R [This study]

SRSG4P – *Δhis3, Δdse1*::NAT_R, pBM51 (*HIS3*) [This study]

SRSG6 – *Δhis3, Δdse3*::NAT_R [This study]

SRSG6P – *Δhis3, Δdse3*::NAT_R, pBM51 (*HIS3*) [This study]

SRSG6R – *Δhis3, Δdse3*::NAT_R, pSRSGR6 (*HIS3, DSE3*) [This study]

SRSG7 – *Δhis3, Δtrp1, Δleu2, Δacf2*::*TRP1* [This study]

SRSG7P – *Δhis3, Δtrp1, Δleu2, Δacf2*::*TRP1,* pBM51 (*HIS3*), YPCIII (*LEU2*) [This study]

SRSG7R – *Δhis3, Δtrp1, Δleu2, Δacf2*::*TRP1,* pSRSGR7 (*HIS3, ACF2*), YPCIII (*LEU2*) [This study]

SRSG8 – *Δhis3, Δegt2*::NAT_R [This study]

SRSG8P – *Δhis3, Δegt2*::NAT_R, pBM51 (*HIS3*) [This study]

SRSG8R – *Δhis3, Δegt2*::NAT_R, pSRSGR8 (*HIS3, EGT2*) [This study]

SRSG9 – *Δhis3, Δrme1*::NAT_R [This study]

SRSG9P – *Δhis3, Δrme1*::NAT_R, pBM51 (*HIS3*) [This study]

SRSG9R – *Δhis3, Δrme1*::NAT_R, pSRSGR9 (*HIS3, RME1*) [This study]

SRSG11 – *Δhis3, Δtrp1, Δleu2, Δscw11ϐ*::*TRP1* [This study]

SRSG11P – *Δhis3, Δtrp1, Δleu2, Δscw11ϐ*::*TRP1,* pBM51 (*HIS3*), YPCIII (*LEU2*) [This study]

SRSG11R – *his3, trp1, leu2, scw11ϐ*::*TRP1,* pSRSGR11 (*HIS3, SCW11ϐ*), YPCIII (*LEU2*) [This study]

SRSG12 – *Δhis3, Δtrp1, Δleu2, Δsic1*::*TRP1* [This study]

SRSG12P – *Δhis3, Δtrp1, Δleu2, Δsic1*::*TRP1,* pBM51 (*HIS3*), YPCIII (*LEU2*) [This study]

SRSG12R – *Δhis3, Δtrp1, Δleu2, Δsic1*::*TRP1,* pSRSGR12 (*HIS3, SIC1*), YPCIII (*LEU2*) [This study]

S. cerevisiae BY4741 – *M**A**Ta , Δhis3, Δleu2, Δmet15, Δura3* [242]

S. cerevisiae Yeast GFP-tagged DSE1 library strain – *M**A**Ta Δhis3, Δleu2, Δmet15, Δura3, HIS3, DSE1-GFP* [242]

S. cerevisiae Yeast Knockout library strains – *M**A**T*a , *Δhis3, Δleu2, Δmet15, Δura3, KanMX* [242]

S. cerevisiae YKO *dse1* – *M**A**T*a , *Δhis3, Δleu2, Δmet15, Δura3, KanMX, Δdse1* [242]

S. cerevisiae YKO *boi1* – *M**A**T*a , *Δhis3, Δleu2, Δmet15, Δura3, KanMX, Δboi1* [242]

S. cerevisiae YKO *boi2* – *M**A**T*a , *Δhis3, Δleu2, Δmet15, Δura3, KanMX, Δboi2* [242]

S. cerevisiae YKO *ste4* – *M**A**T*a , *Δhis3, Δleu2, Δmet15, Δura3, KanMX, Δste4* [242]

S. cerevisiae YKO *ste11* – *M**A**T*a , *Δhis3, Δleu2, Δmet15, Δura3, KanMX, Δste11* [242]

S. cerevisiae YKO *zds2* – *M**A**T*a , *Δhis3, Δleu2, Δmet15, Δura3, KanMX, Δzds2* [242]

SRSGB1-DGFP – *M**A**T*a , *Δhis3, Δleu2, Δmet15, Δura3, KanMX, Δboi1, pSRSG-GD1* (*DSE1-GFP*) [This study]

SRSGB2-DGFP – *M**A**T*a , *Δhis3, Δleu2, Δmet15, Δura3, KanMX, Δboi2, pSRSG-GD1* (*DSE1-GFP*) [This Study]

SRSGZ2-DGFP – *M**A**T*a , *Δhis3, Δleu2, Δmet15, Δura3, KanMX, Δzds2, pSRSG-GD1* (*DSE1-GFP*) [This study]

Appendix 2 - Plasmids

A2.1 Yeast plasmids

pBM51 – *C. glabrata* plasmid containing *HIS3, PGK* constitutive promoter and *HIS3* 3' UTR as shown in Figure 4.3 [Biao Ma (personal communication)]

YPCIII – *S. cerevisiae* episomal plasmid containing *LEU2* [286]

pAG426GPD-ccdB – Gateway GFP destination vector [275]

pSRSG-GD1 – Gateway plasmid containing GFP tagged *S. cerevisiae DSE1* [This study]

pSRSGR6 – pBM51::*CgDSE3* [This study]

pSRSGR7 – pBM51::*CgACF2* [This study]

pSRSGR8 – pBM51::*CgEGT2* [This study]

pSRSGR9 – pBM51::*CgRME1* [This study]

pSRSGR11 – pBM51::*CgSCW11ϐ* [This study]

pSRSGR12 – pBM51::*CgSIC1* [This study]

A2.2 *E. coli* plasmids

pCR2.1-TOPO – Part of the Invitrogen TOPO TA Cloning kit [Invitrogen, UK]

pSRSGE6 – pCR2.1::*CgDSE3* [This study]

pSRSGE7 – pCR2.1::*CgACF2* [This study]

pSRSGE8 – pCR2.1::*CgEGT2* [This study]

pSRSGE9 – pCR2.1::*CgRME1* [This study]

pSRSGE11 – pCR2.1::*CgSCW11ϐ* [This study]

pSRSGE12 – pCR2.1::*CgSIC1* [This study]

Appendix 3 – Primers

Name	Sequence
ASH1-600-F'	gatccaccttccacaagc
ASH1-500-F'	gcatcacggttttatatg
ASH1-1-NAT-R'	gcgtcgacctgcagcgtacggtacctattgacgcgggttccacggcgcgcctagcagcgggaaagggttcaaacgaatg
ASH1+1-NAT-F'	cgacggtgtcggtctcgtaggctaaccagagagacttaccgtcagcggccgcatccctggcataagccagtaattgg
ASH1+500-R'	aacgcaaggagtgtgtccc
ASH1+600-R'	agcgcaatccttgacttc
ASH1-Inter-F	ctgctggttcagaaagac
ASH1-Inter-R	accagaccaggatggtctcc
ASH1-DIG-INT-F	cctcaccattttagcaccag
ASH1-DIG-INT-R	agttactggagcttcatagc
ASH1-700	ggataactcagttgcgtag
ASH1+700-R'	gacgctactgatgagaaatg
BUD9-600-F'	ctatggtggtaatactgg
BUD9-500-F'	ggttttccatactgagaag
BUD9-1-NAT-R'	gcgtcgacctgcagcgtacggaataacttaggtctacgggcacggcgcgcctagcagcggcaacagcggcaataacgg
BUD9+1-NAT-F'	cgacggtgtcggtctcgtagaccgtccgattccgttaattgtcagcggccgcatccctgaagcaactcgtagttccg
BUD9+500-R'	gttcggatatgagatcttc
BUD9+600-R'	ccagaactgaatcgacctg
BUD9-Inter-F	atagagccagctcgcagccg
BUD9-Inter-R	cctgctgtctcagaatctg
BUD9-DIG-INT-F	attggatcggagcatacac
BUD9-DIG-INT-R	tctagcagttcagattcagg
DSE1-600-F'	acttgttagtctccaccgg
DSE1-500-F'	gcaatccttggtgaagagcg
DSE1-1-NAT-R'	gcgtcgacctgcagcgtacggatctagcttagtctactggcacggcgcgcctagcagcgggcatggttatgtgcgac
DSE1+1-NAT-F'	cgacggtgtcggtctcgtaggcacactgagccaactgatagtcagcggccgcatccctgctctaacaaacaatacccg
DSE1+500-R'	tagcaagcctagacggtatattgg
DSE1+600-R'	gagccttctatccacccattg
DSE1-Inter-F	acaaggaccaggacaacgtc
DSE1-Inter-R	gcgctgttgttattcccatt
DSE1-DIG-INT-F	tcaccacagcaacactgct
DSE1-DIG-INT-R	aagtacagtctgaggagac
DSE2-600-F'	cattcttctggttctggcc
DSE2-500-F'	acatctaagttgcttggg
DSE2-1-NAT-R'	gcgtcgacctgcagcgtacgatgactgggaagcgcctcaacacggcgcgcctagcagcgggaacagcagtattacac
DSE2+1-NAT-F'	cgacggtgtcggtctcgtagttgaggcgcttcccagtcatgtcagcggccgcatccctgggaatgaataggtcggaac

DSE2+500-R'	cactccaaaactcacgc
DSE2+600-R'	ggtatgttacgtagaac
DSE2-Inter-F	actttgaccaggtttgg
DSE2-Inter-R	cacatctgatggtgtcg
DSE2-DIG-INT-F	gagataggcatagagattg
DSE2-DIG-INT-R	gagatgatgataacgtaagg
DSE3-600-F'	aacacacgcatgccggtacc
DSE3-500-F'	tctgcgataggttctgtg
DSE3-1-NAT-R'	gcgtcgacctgcagcgtacggcgttacttagctgtgtgaccacggcgcgcctagcagcggagtggccgaacctctcctc
DSE3+1-NAT-F'	cgacggtgtcggtctcgtaggcctactcattaagtctcaggtcagcggccgcatccctgcaagccatgttcctccac
DSE3+500-R'	gccaatacttcttcctgc
DSE3+600-R'	cgaagtttcaattgcttcc
DSE3-Inter-F	gatgatgatgctgtgctg
DSE3-Inter-R	ctacagatccagccaatg
DSE3-DIG-INT-F	gttaccaccacatttgagtgg
DSE3-DIG-INT-R	cccgagctagcaatagag
EGT2-600-F'	gtttgaggagatacaacg
EGT2-500-F'	ctgggaagaagttatgggg
EGT2-1-NAT-R'	gcgtcgacctgcagcgtacgatcgcacatcctatcaaaggcacggcgcgcctagcagcggagtttcaaggaataggcc
EGT2+1-NAT-F'	cgacggtgtcggtctcgtagcatgactacgcattagcgcggtcagcggccgcatccctggtgtgttgtctgctttgg
EGT2+500-R'	gactggtagttaaataccg
EGT2+600-R'	gatctgctggtctcacattc
EGT2-Inter-F	tgcagtggaggttgtttc
EGT2-Inter-R	cagttcctgatgagtttg
EGT2-DIG-INT-F	gtgctcacagcttcaagatc
EGT2-DIG-INT-R	aaatggtacaacgagctc
RME1-600-F'	caatccacacagtatgatc
RME1-500-F'	ccaagggttcttcacttg
RME1-1-NAT-R'	gcgtcgacctgcagcgtacggaaagggcttcaaacttacgcacggcgcgcctagcagcggctaaagtctcctcctttc
RME1+1-NAT-F'	cgacggtgtcggtctcgtagccgggtcccaaaggtacaaagtcagcggccgcatccctgcagaaagtgggcgtgtcg
RME1+500-R'	tgaatagagtgggcaggg
RME1+600-R'	tggctacacacattgtcg
RME1-Inter-F	ttgaagcgagaactagtg
RME1-Inter-R	ataacgaggatgacgagg
RME1-DIG-INT-F	cgtctaagtgagaagcg
RME1-DIG-INT-R	tcacagctactgtagacac
SCW11a-600-F'	caatacccaatacagcatac
SCW11a-500-F'	tgttgagatgcagaaaatgc
SCW11a-1-NAT-R'	gcgtcgacctgcagcgtacggcctaaagttccctaacatgcacggcgcgcctagcagcggtgagggagtgtatctagttg
SCW11a+1-NAT-F'	cgacggtgtcggtctcgtagctctattagtcgagggtagtgtcagcggccgcatccctgctaagctacacagcaatac
SCW11a+500-R'	gttggtcttgaggctatacc

SCW11a+600-R'	cgatttctgtggatcgaac
SCW11a-Inter-F	gcggatcagttacttttacc
SCW11a-Inter-R	caaatgaggaaagcacag
SCW11a-DIG-INT-F	cacaaccattactaccacag
SCW11a-DIG-INT-R	acttgaccagaataaccagc
NAT-5'-R	catccaaagtagtagac
NAT-3'-F	atgtctatgccatgtcc
Gatway system	
pGBT9 Check For	tcatcggaagagagtagtaa
pGBT9 Check Rev	cgttttaaaacctaagagtc
pGAD424 Check For	aataccactacaatggatga
pGAD424 Check Rev	atggtgcacgatgcacagtt
Gateway ScDSE1F	acaaaaaagcaggcttcatgatgcaagataccaaatactacgaacca
Gateway ScDSE1RC	acaagaaagctgggtcctagacaacagtagtatcaatagtagatcc
ScDSE1 INT F	ctgcttattgcccatggtag
ScDSE1 INT RC	tccacatcctgcagatatgc
Edlind KO Method	
TRP Int F (n)	atgtctgttattaatttcacagg
TRP Int RC (n)	tttcttagcatttttgacga
CgAMN1+TRPF	aaactctcgctaagaatagtatttcatttaaaaaaaattggtcacaattatctataaatgtctgttattaatttcacagg
CgAMN1+TRPRC	aatgaaagggtaacggaaatgaattgaattgattttggtttttgggaattacttagcttatttcttagcatttttgacga
CgDSE2+TRPF	ttttttgacactaaacgccgacttattttattactcaaccatcaaagatttttataatgtctgttattaatttcacagg
CgDSE2+TRPRC	ctgctgttctttattattttagactttagtctaatttagaaaactgtttgaaatcatttatttcttagcatttttgacga
CgACF2+TRPF	aaagaagcacttatagctatagtacgcatcgaatccggttgatcagtttagttttctatgtctgttattaatttcacagg
CgACF2+TRPRC	ctacatattatctacttaaagaaataataaaaaaggtgggataaaatgcaagacatgtcatttcttagcatttttgacga
SCW11a+TRPF	tccaactaagatataaaacaataacaaactaatttttttaaatttttgaaacaatataatgtctgttattaatttcacagg
SCW11a+TRPRC	ggaaggctaatcacacacgataaagccttgtattgctgtgtagcttagagcttacacttatttcttagcatttttgacga
SCW11b+TRPF	atttaagacacacccatttatttcaacaattattataaagttctattaaaatataagatgtctgttattaatttcacagg
SCW11b+TRPRC	gatagttgatgaagtatccagccttcggctatcttttattgtttggatcttctaggttcatttcttagcatttttgacga
SIC1+TRPF	cgtcgaaggacaggaacaagaagttacggataaagcttacaagtgcgaaaatagataatgtctgttattaatttcacagg

SIC1+TRPRC	gaataaatgaaaatctgaaagaaaggaataaaataaatagtgaagctgttatggggactatttcttagcatttttgacga
CgAMN1 check F	ataccaaccagccgccaatc
CgAMN1 check RC	atgcaggttctacagttccc
CgDSE2 check F	gtatggcgtaagaatagg
CgDSE2 check RC	gttccgacctattcattcc
CgACF2 check F	taatgcgttcccaggatttg
CgACF2 check RC	cttagcggtaattgttgctg
CgEGT2 check F	cactgcttggtttactcttg
CgEGT2 check RC	ccaagaattcgtattcgctc
CgRME1 check F	caggcatcattagatcatgc
CgRME1 check RC	ggcatcctcagttaagtttag
CgSCW11a check F	ccaactagatacactccctc
CgSCW11a check RC	agggttatgacatatggctg
CgSCW11b check F	cccatactatcaagacc
CgSCW11b check RC	attggttggaccaaggcatg
CgSIC1 check F	gaagtctgggaaccaccaac
CgSIC1 check RC	gtgtccgaatgggaggttag
Reconsitution	
Dse3 Sal1 F	*cattggta*gtcgacatgcctagaaagtttttagg
Dse3 Xma1 RC	*ttaacatt*cccgggctaggttgcaaagtggtcac
Egt2 Sal1 F	*cgtagcca*gtcgacatgaaatttacaactacatttc
Egt2 Xma1 RC	*ttaacatt*cccgggaatcatagcaggagagcgatg
Acf2 Sal1 F	*ttaacatt*gtcgacatgtcatacaaccgccctcc
Acf2 Xma1 RC	*tactatat*cccgggtcaaatgaacgcacctgaataagc
Rme1 Sal1 F	*ttaacatt*gtcgacatgctgaggactaaagacag
Rme1 Xma1 RC	*cattggta*cccgggtcacttatttcttaccttatc
Scw11b Sal1 F	*cattggta*gtcgacatgctaccgttcatacaattac
Scw11b Xma1 RC	*ttaacatt*cccgggtcatggcaggttgtccaagatac
Sic1 EcoR1 F	*tgaacata*gaattcatgacaccttctactccgcc
Sic1 Xma1 RC	*gtaacagt*cccgggctatttcttgtctctcttaag
Reconstitution Sequencing	
Dse3 Seq 1	atgcctagaaagtttttagg
Dse3 Seq 2	taaaccgttgatcgagaagg
Dse3 Seq 3	atggctcatacacaactgcg
Acf2 Seq 1	atgtcatacaaccgccctcc
Acf2 Seq 2	taatgcgttcccaggatttg
Acf2 Seq 3	ttgcgatgttgtaaatgcag

Acf2 Seq 4	cagcaacaattaccgctaag
Acf2 Seq 5	ctatggggtatggtttctgg
Egt2 Seq 1	acaactacatttctgctcac
Egt2 Seq 2	cactgcttggtttactcttg
Egt2 Seq 3	acactaatggtacagcatcc
Egt2 Seq 4	gagcgaatacgaattcttgg
Egt2 Seq 5	gtacatccaggcaatacaac
RME1 Seq 1	atgctgaggactaaagacag
RME1 Seq 2	caggcatcattagatcatgc
RME1 Seq 3	tgatgaactgcccttaagag
RME1 Seq 4	ctaaacttaactgaggatgcc
Scw11b Seq 1	ctaactagcgatgttctcgc
Scw11b Seq 2	tcgtcatccatacagtcatc
Scw11b Seq 3	caggtgttgattccatcgac
Scw11b Seq 4	tctagaagccactaacaacc
Sic1 Seq 1	agacagagaaggcacgattc
Sic1 Seq 2	cccagtgacaaagtgatcac

Appendix 4 – Gene deletion confirmations

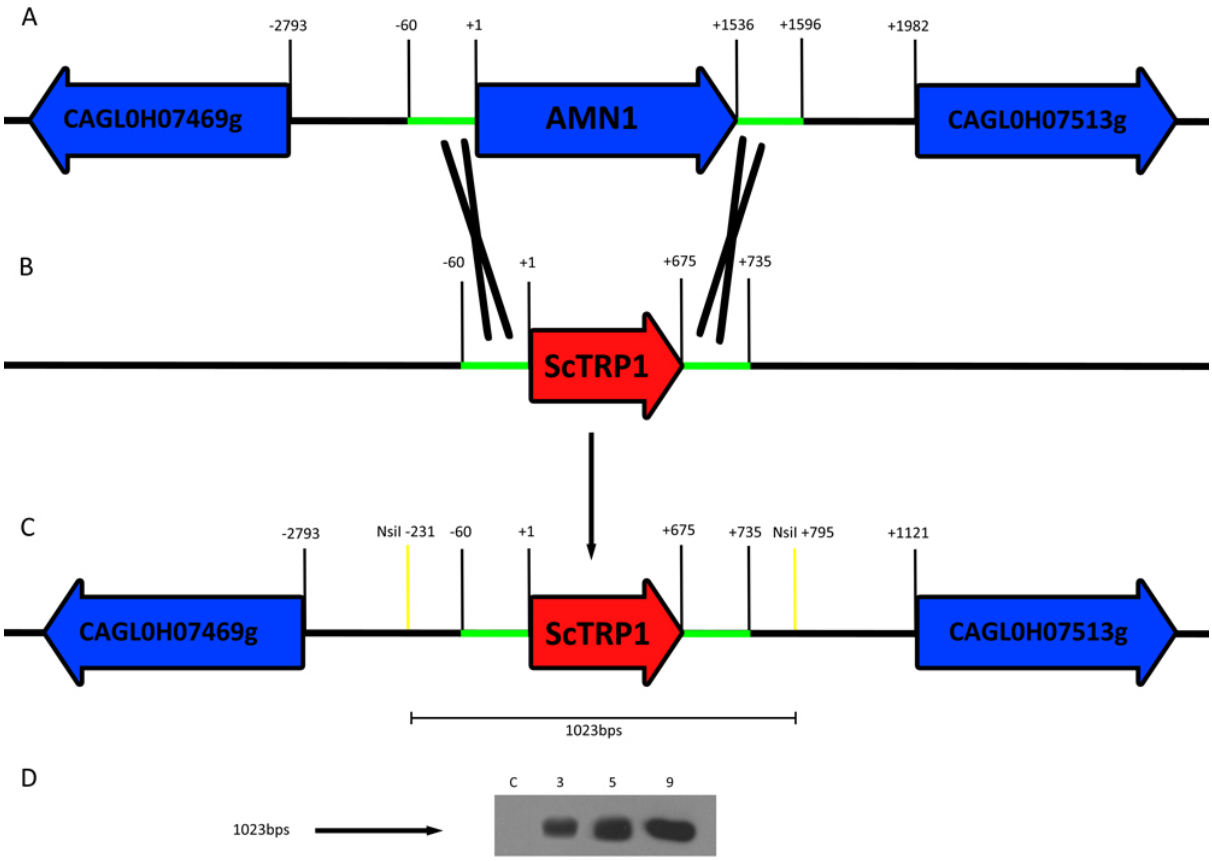


Figure S.1 – Construction and confirmation of the *C. glabrata amn1* null mutant. A null allele of *C. glabrata AMN1* was constructed as described in Chapter 4. A. The *C. glabrata AMN1* locus. Coding regions are shown in blue, ATG (+1) and stop codon (+1536) of *AMN1* are shown. The upstream and downstream genes are also shown. B. The *C. glabrata AMN1* deletion cassette. A 675 bp fragment of *S. cerevisiae TRP1* was amplified flanked by 60 bps of *AMN1* 5' and 3' as described in Chapter 4. C. Targeted integration of the *AMN1* deletion cassette at the *AMN1* locus removing 1536 bps of *AMN1* from +1 to +1536. D. Southern analysis of putative null alleles of *AMN1*. Total genomic DNA was digested with NsiI and probed with 672 bp fragment of Sc*TRP1* as described in Chapter 4. The null allele yielded a 1023 bp NSiI fragment. The presence of a band confirms that correct integration of the cassette has occurred in mutants 3, 5 and 9. The coordinates are shown relative to the start codon of *AMN1* (A) or Sc*TRP1* (B, C). The diagram is not to scale.

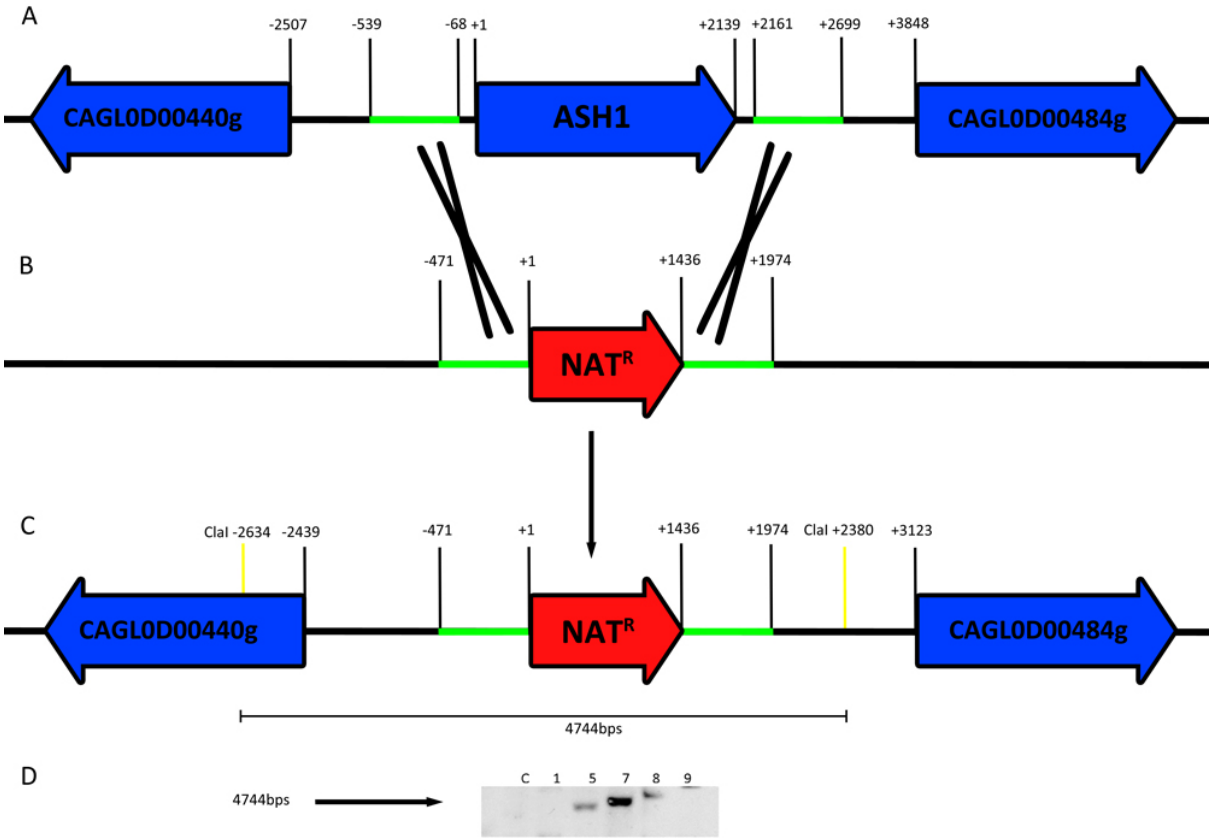


Figure S.2 – Construction and confirmation of the *C. glabrata ash1* null mutant. A null allele of *C. glabrata ASH1* was constructed as described in Chapter 4. A. The *C. glabrata ASH1* locus. Coding regions are shown in blue, ATG (+1) and stop codon (+2139) of *ASH1* are shown. The upstream and downstream genes are also shown. B. The *C. glabrata ASH1* deletion cassette. A NAT cassette was amplified flanked by 471 bps and 538 bps of *ASH1* 5' and 3' respectively as described in Chapter 4. C. Targeted integration of the *ASH1* deletion cassette at the *ASH1* locus removing 2229 bps of *ASH1* from -68 to +2161. D. Southern analysis of putative null alleles of *ASH1*. Total genomic DNA was digested with ClaI and probed with 567 bp fragment of the NAT cassette as described in Chapter 4. The null allele yielded a 4744 bp ClaI fragment. The presence of a band confirms that correct integration of the cassette has occurred in mutants 5, 7 and 8, with a slanted gel resulting in sloping bands. The coordinates are shown relative to the start codon of *ASH1* (A) or the NAT cassette (B, C). The diagram is not to scale.

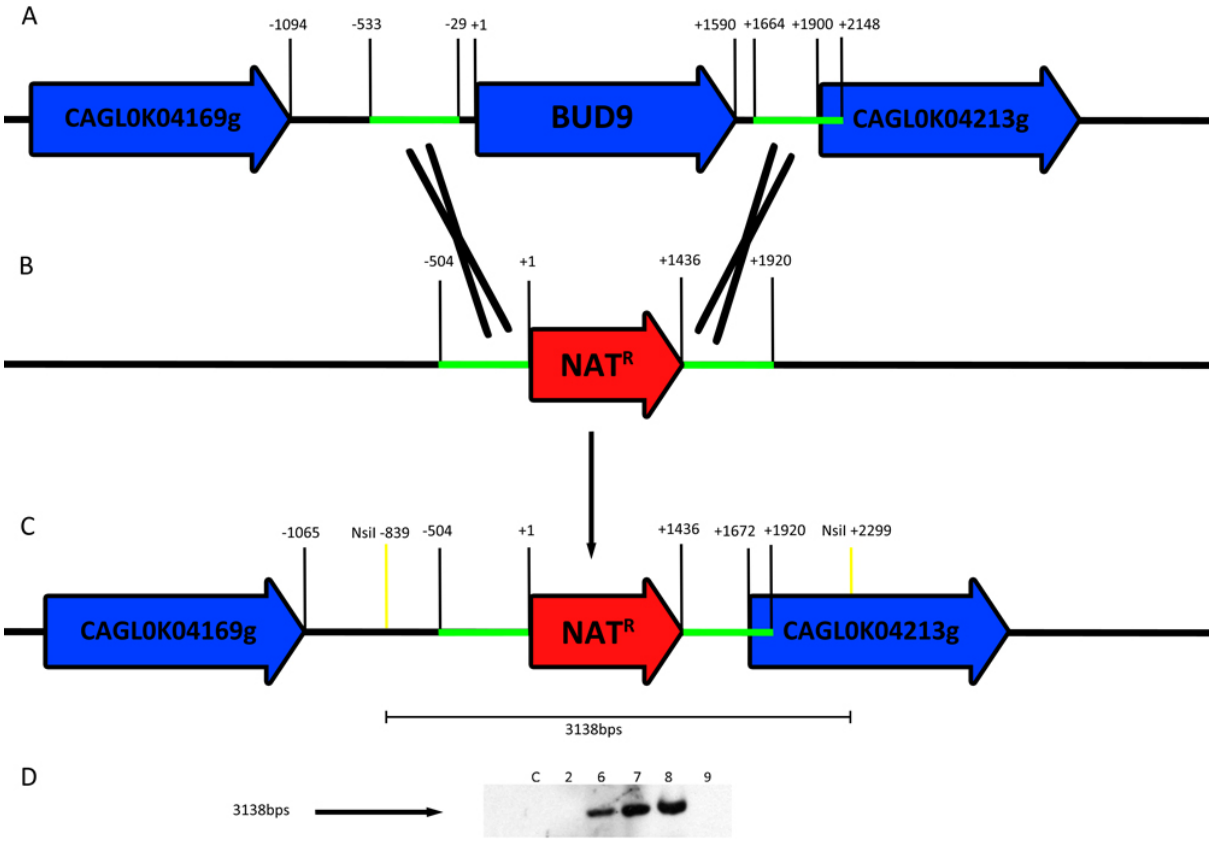


Figure S.3 – Construction and confirmation of the *C. glabrata bud9* null mutant. A null allele of *C. glabrata BUD9* was constructed as described in Chapter 4. A. The *C. glabrata BUD9* locus. Coding regions are shown in blue, ATG (+1) and stop codon (+1590) of *BUD9* are shown. The upstream and downstream genes are also shown. B. The *C. glabrata BUD9* deletion cassette. A NAT cassette was amplified flanked by 504 bps and 484 bps of *BUD9* 5' and 3' respectively as described in Chapter 4. C. Targeted integration of the *BUD9* deletion cassette at the *BUD9* locus removing 1693 bps of *BUD9* from -29 to +1664. D. Southern analysis of putative null alleles of *BUD9*. Total genomic DNA was digested with NSiI and probed with 567 bp fragment of the NAT cassette as described in Chapter 4. The null allele yielded a 3138 bp NsiI fragment. The presence of a band confirms that correct integration of the cassette has occurred in mutants 6, 7 and 8. The coordinates are shown relative to the start codon of *BUD9* (A) or the NAT cassette (B, C). The diagram is not to scale.

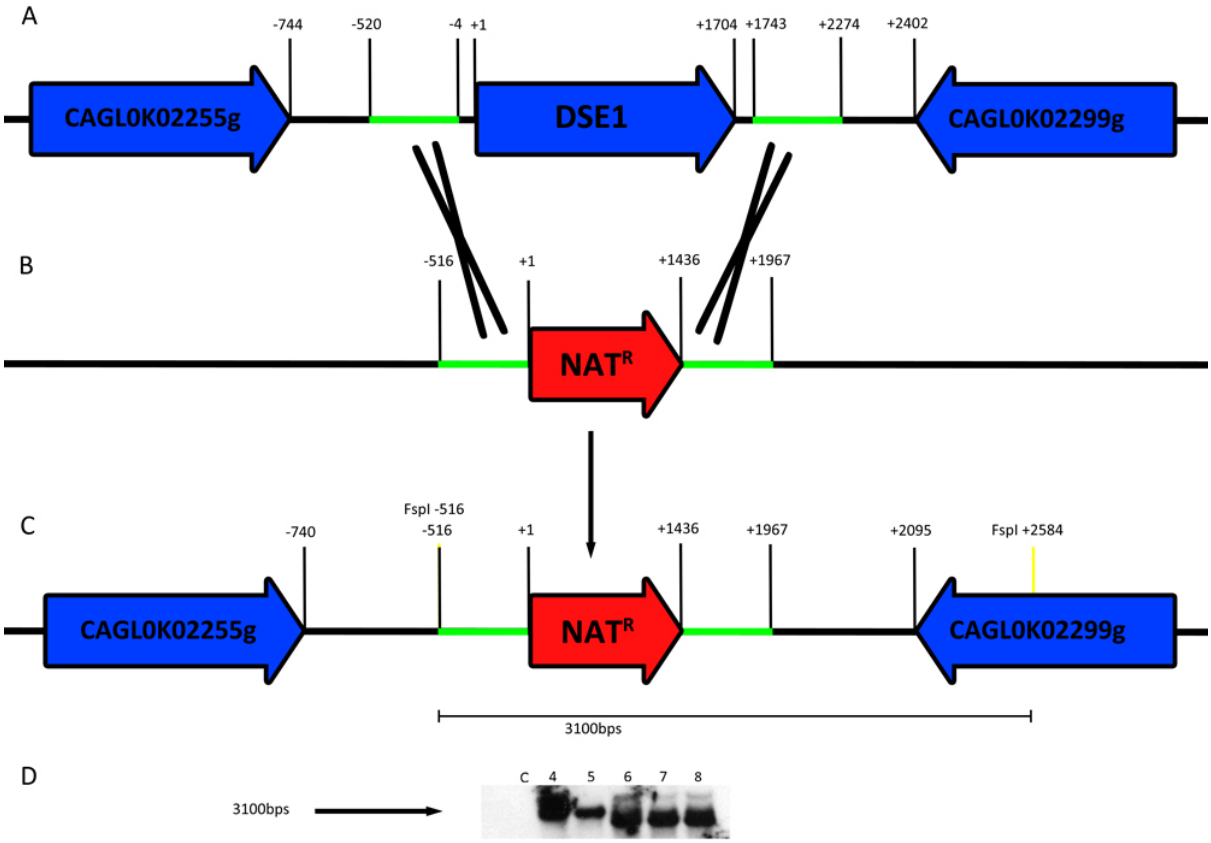


Figure S.4 – Construction and confirmation of the *C. glabrata dse1* null mutant. A null allele of *C. glabrata DSE1* was constructed as described in Chapter 4. A. The *C. glabrata DSE1* locus. Coding regions are shown in blue, ATG (+1) and stop codon (+1704) of *DSE1* are shown. The upstream and downstream genes are also shown. B. The *C. glabrata DSE1* deletion cassette. A NAT cassette was amplified flanked by 516 bps and 531 bps of *DSE1* 5' and 3' respectively as described in Chapter 4. C. Targeted integration of the *DSE1* deletion cassette at the *DSE1* locus removing 1747 bps of *DSE1* from -4 to +1743. D. Southern analysis of putative null alleles of *DSE1*. Total genomic DNA was digested with FspI and probed with 567 bp fragment of the NAT cassette as described in Chapter 4. The null allele yielded a 3100 bp FspI fragment. The presence of a band confirms that correct integration of the cassette has occurred for mutants 4, 5, 6. The coordinates are shown relative to the start codon of *DSE1* (A) or the NAT cassette (B, C). The diagram is not to scale.

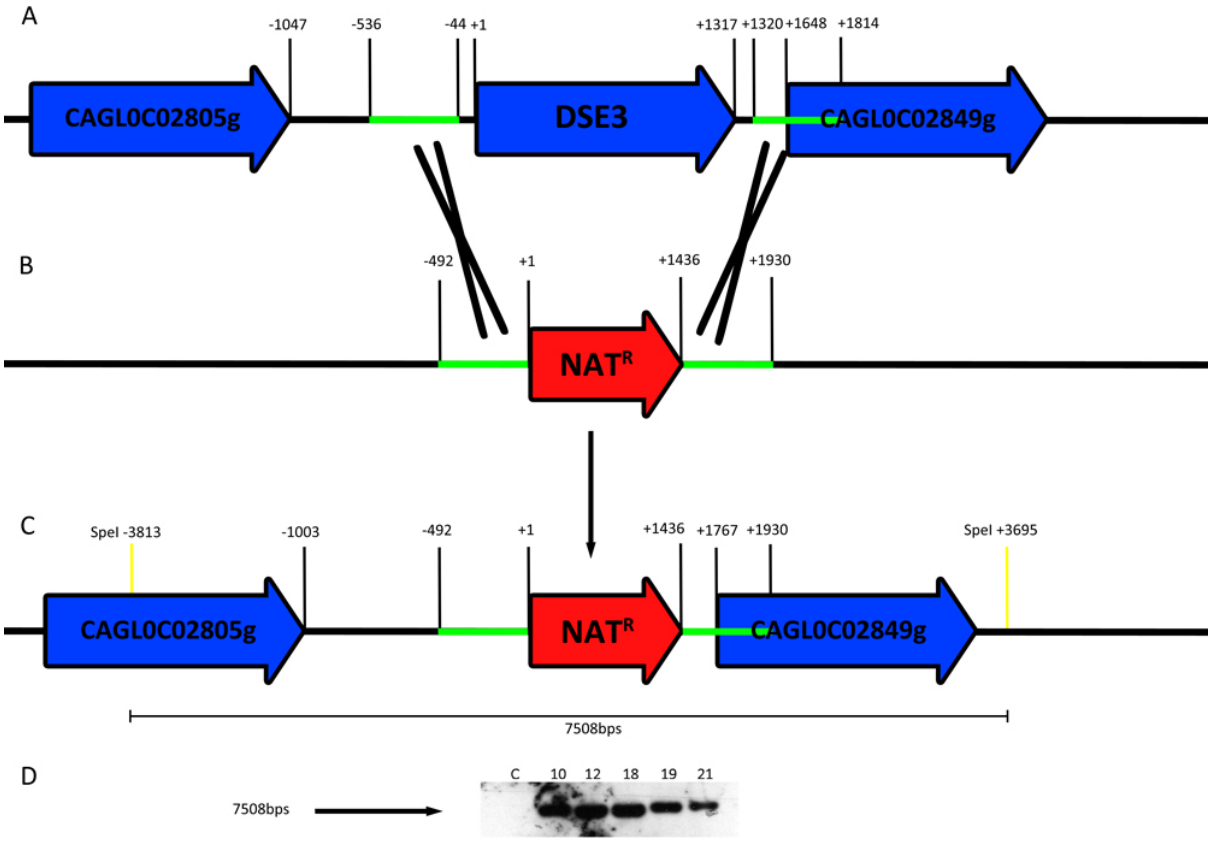


Figure S.5 – Construction and confirmation of the *C. glabrata dse3* null mutant. A null allele of *C. glabrata DSE3* was constructed as described in Chapter 4. A. The *C. glabrata DSE3* locus. Coding regions are shown in blue, ATG (+1) and stop codon (+1317) of *DSE3* are shown. The upstream and downstream genes are also shown. B. The *C. glabrata DSE3* deletion cassette. A NAT cassette was amplified flanked by 492 bps and 494 bps of *DSE3* 5' and 3' respectively as described in Chapter 4. C. Targeted integration of the *DSE3* deletion cassette at the *DSE3* locus removing 1364 bps of *DSE3* from -44 to +1320. D. Southern analysis of putative null alleles of *DSE3*. Total genomic DNA was digested with SpeI and probed with 567 bp fragment of the NAT cassette as described in Chapter 4. The null allele yielded a 7508 bp SpeI fragment. The presence of a band confirms that correct integration of the cassette has occurred for mutants 10, 12, 18, 19 and 21. The coordinates are shown relative to the start codon of *DSE3* (A) or the NAT cassette (B, C). The diagram is not to scale.

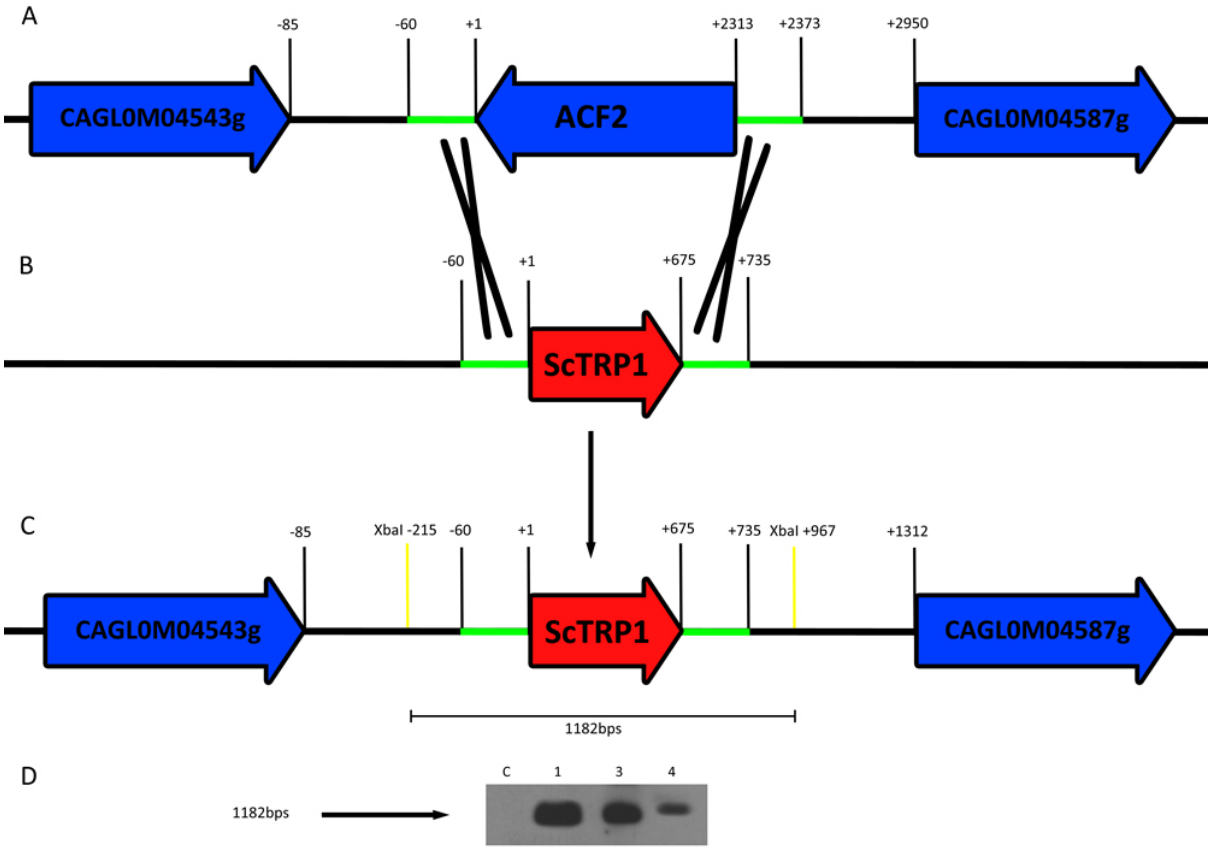


Figure S.6 – Construction and confirmation of the *C. glabrata acf2* null mutant. A null allele of *C. glabrata ACF2* was constructed as described in Chapter 4. A. The *C. glabrata ACF2* locus. Coding regions are shown in blue, ATG (+1) and stop codon (+2313) of *ACF2* are shown. The upstream and downstream genes are also shown. B. The *C. glabrata ACF2* deletion cassette. A 675 bp fragment of *S. cerevisiae TRP1* was amplified flanked by 60 bps of *ACF2* 5' and 3' as described in Chapter 4. C. Targeted integration of the *ACF2* deletion cassette at the *ACF2* locus removing 2313 bps of *ACF2* from +1 to +2313. D. Southern analysis of putative null alleles of *ACF2*. Total genomic DNA was digested with XbaI and probed with 672 bp fragment of Sc*TRP1* as described in Chapter 4. The null allele yielded a 1182 bp XbaI fragment. The presence of a band confirms that correct integration of the cassette has occurred. The coordinates are shown relative to the start codon of *ACF2* (A) or Sc*TRP1* (B, C). The diagram is not to scale.

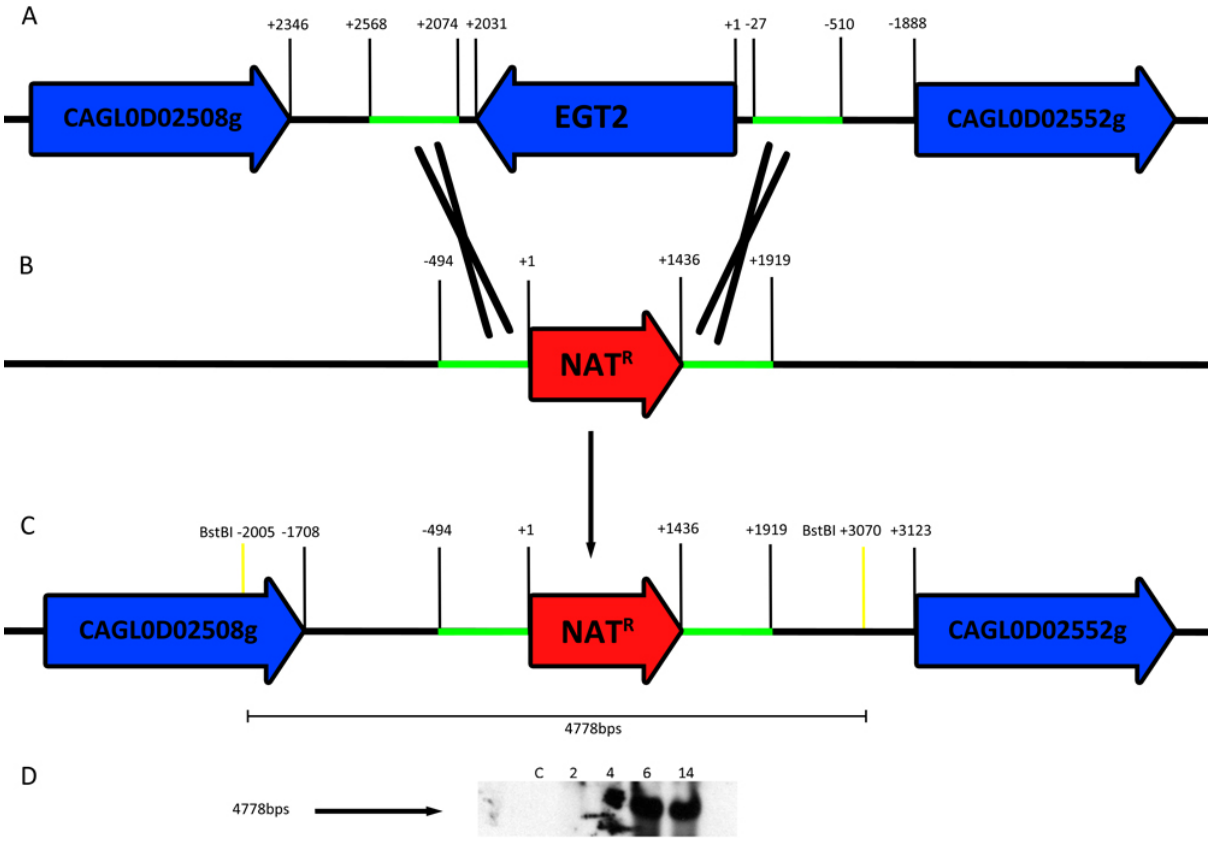


Figure S.7 – Construction and confirmation of the *C. glabrata egt2* null mutant. A null allele of *C. glabrata EGT2* was constructed as described in Chapter 4. A. The *C. glabrata EGT2* locus. Coding regions are shown in blue, ATG (+1) and stop codon (+2031) of *EGT2* are shown. The upstream and downstream genes are also shown. B. The *C. glabrata EGT2* deletion cassette. A NAT cassette was amplified flanked by 494 bps and 483 bps of *EGT2* 5' and 3' respectively as described in Chapter 4. C. Targeted integration of the *EGT2* deletion cassette at the *EGT2* locus removing 2101 bps of *EGT2* from -27 to +2031. D. Southern analysis of putative null alleles of *EGT2*. Total genomic DNA was digested with BstBI and probed with 567 bp fragment of the NAT cassette as described in Chapter 4. The null allele yielded a 4778 bp BstBI fragment. The presence of a band confirms that correct integration of the cassette has occurred for mutants 4, 6 and 14. The coordinates are shown relative to the start codon of *EGT2* (A) or the NAT cassette (B, C). The diagram is not to scale.

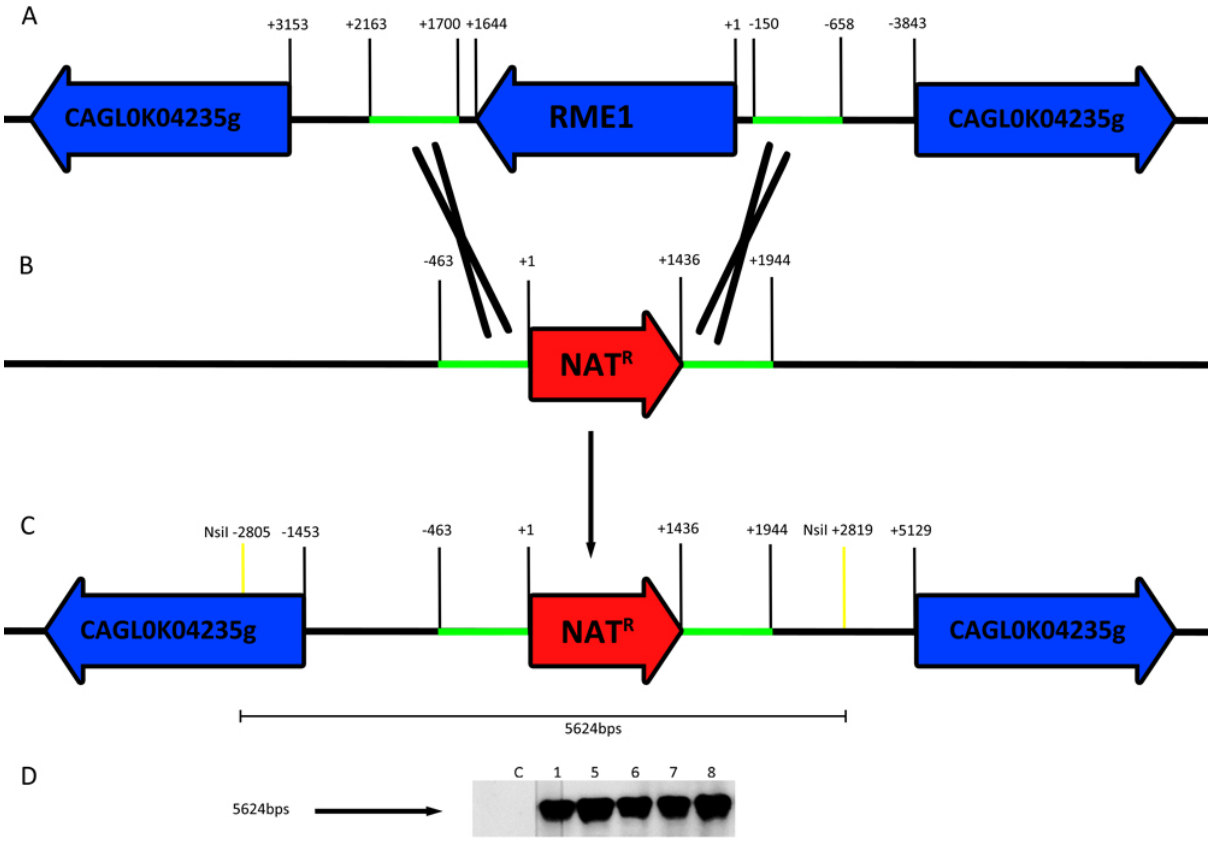


Figure S.8 – Construction and confirmation of the *C. glabrata rme1* null mutant. A null allele of *C. glabrata RME1* was constructed as described in Chapter 4. A. The *C. glabrata RME1* locus. Coding regions are shown in blue, ATG (+1) and stop codon (+1644) of *RME1* are shown. The upstream and downstream genes are also shown. B. The *C. glabrata RME1* deletion cassette. A NAT cassette was amplified flanked by 463 bps and 508 bps of *RME1* 5' and 3' respectively as described in Chapter 4. C. Targeted integration of the *RME1* deletion cassette at the *RME1* locus removing 1850 bps of *RME1* from -150 to +1700. D. Southern analysis of putative null alleles of *RME1*. Total genomic DNA was digested with NsiI and probed with 567 bp fragment of the NAT cassette as described in Chapter 4. The null allele yielded a 5624 bp NsiI fragment. The presence of a band confirms that correct integration of the cassette has occurred for mutants 1, 5, 6, 7 and 8. The coordinates are shown relative to the start codon of *RME1* (A) or the NAT cassette (B, C). The diagram is not to scale.

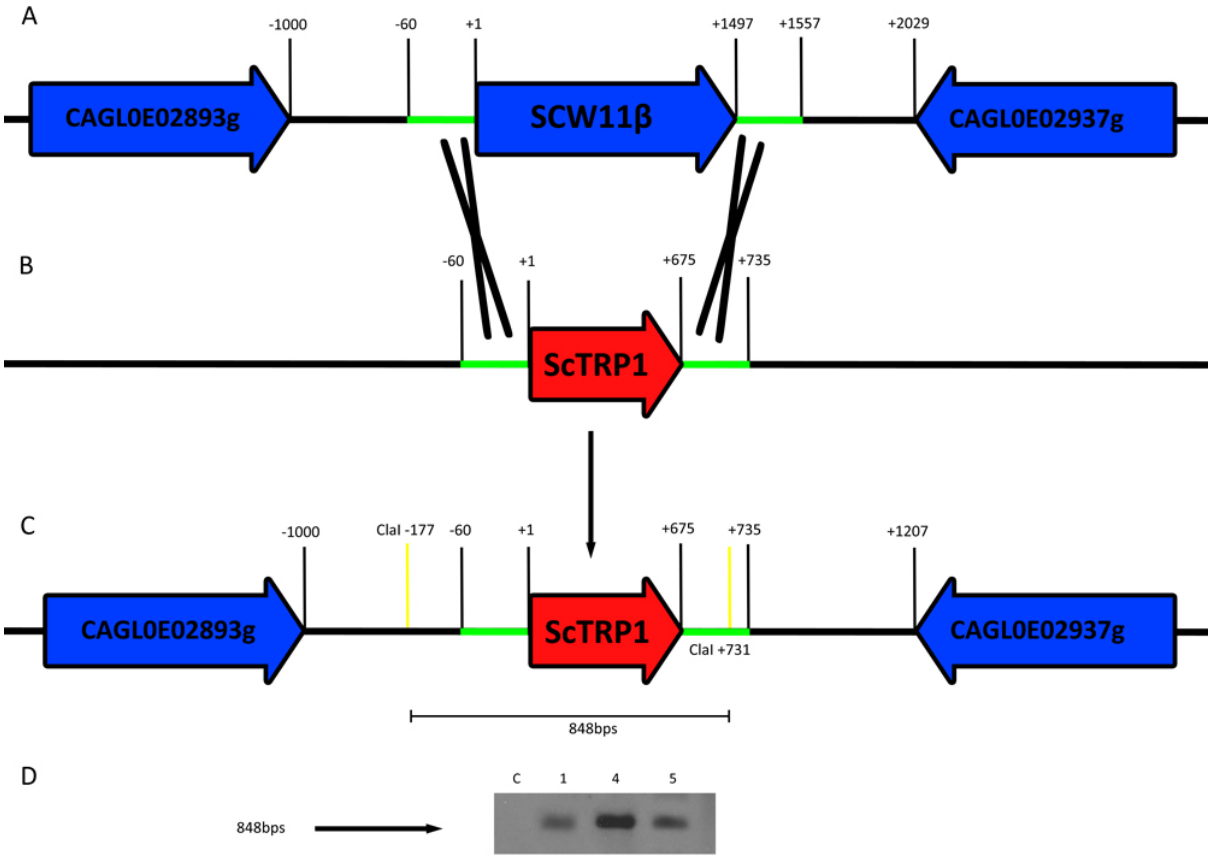


Figure S.9 – Construction and confirmation of the *C. glabrata scw11β* null mutant. A null allele of *C. glabrata SCW11β* was constructed as described in Chapter 4. A. The *C. glabrata SCW11β* locus. Coding regions are shown in blue, ATG (+1) and stop codon (+1497) of *SCW11β* are shown. The upstream and downstream genes are also shown. B. The *C. glabrata SCW11β* deletion cassette. A 675 bp fragment of *S. cerevisiae TRP1* was amplified flanked by 60 bps of *SCW11β* 5' and 3' as described in Chapter 4. C. Targeted integration of the *SCW11β* deletion cassette at the *SCW11β* locus removing 1497 bps of *SCW11β* from +1 to +1497. D. Southern analysis of putative null alleles of *SCW11β*. Total genomic DNA was digested with ClaI and probed with 672 bp fragment of Sc*TRP1* as described in Chapter 4. The null allele yielded a 848 bp ClaI fragment. The presence of a band confirms that correct integration of the cassette has occurred for mutants 1, 4 and 5. The coordinates are shown relative to the start codon of *SCW11β* (A) or Sc*TRP1* (B, C). The diagram is not to scale.

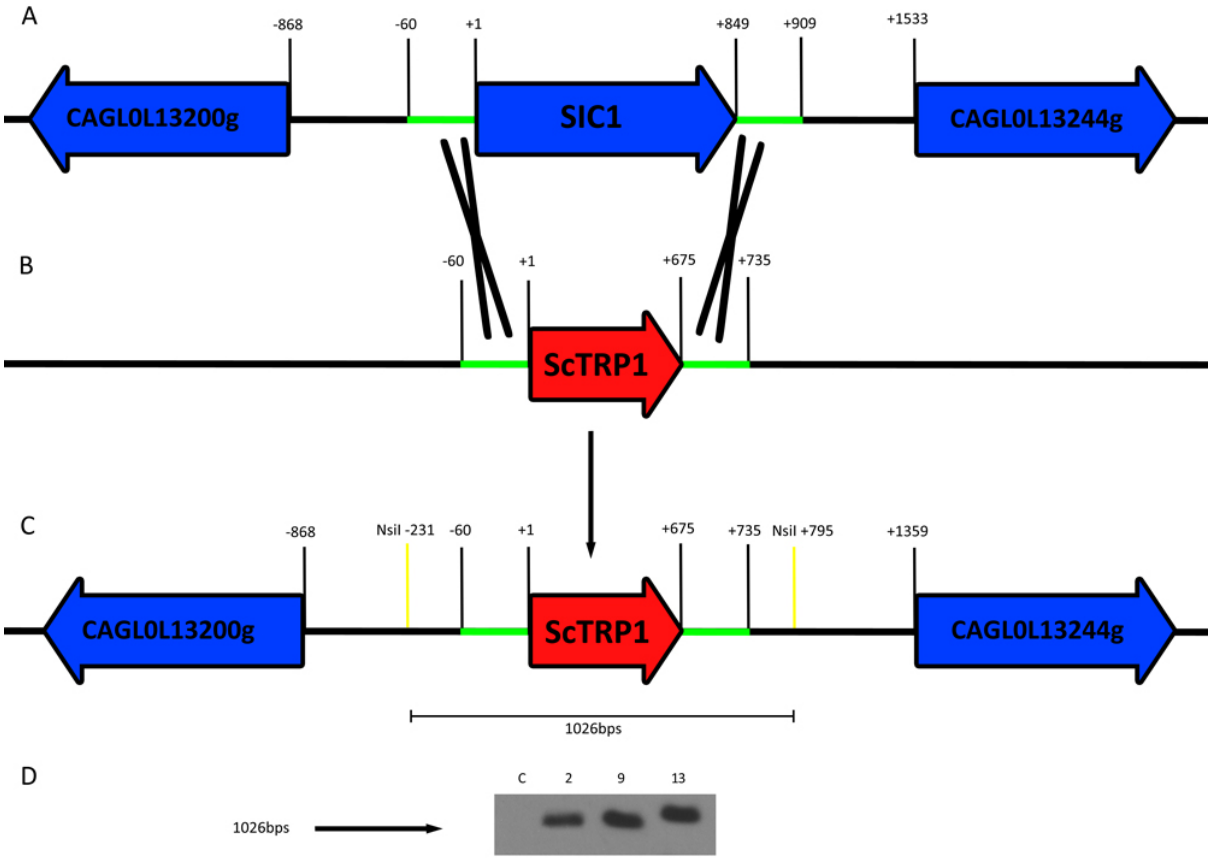


Figure S.10 – Construction and confirmation of the *C. glabrata sic1* null mutant. A null allele of *C. glabrata SIC1* was constructed as described in Chapter 4. A. The *C. glabrata Sic1* locus. Coding regions are shown in blue, ATG (+1) and stop codon (+849) of *SIC1* are shown. The upstream and downstream genes are also shown. B. The *C. glabrata SIC1* deletion cassette. A 675 bp fragment of *S. cerevisiae TRP1* was amplified flanked by 60 bps of *Sic1* 5' and 3' as described in Chapter 4. C. Targeted integration of the *Sic1* deletion cassette at the *Sic1* locus removing 849 bps of *SIC1* from +1 to +849. D. Southern analysis of putative null alleles of *SIC1*. Total genomic DNA was digested with NsiI and probed with 672 bp fragment of Sc*TRP1* as described in Chapter 4. The null allele yielded a 1062 bp NsiI fragment. The presence of a band confirms that correct integration of the cassette has occurred for mutants 2, 9 and 13. The coordinates are shown relative to the start codon of *SIC1* (A) or Sc*TRP1* (B, C). The diagram is not to scale.

Appendix 5

A5.1 *C. elegans* invertebrate model of innate immune response

Prior to vertebrate study of virulence of the Ace2p regulon it was decided that an invertebrate model of virulence would be useful in discerning which strains are likely to present with a hypervirulent phenotype without invoking ethical concerns or cost issues.

Recent work with *C. elegans* showed that it was possible to use the model nematode worm to study fungal pathogenesis, through an intermediate disease phenotype [103]. The benefit of using *C. elegans* as a model of fungal virulence is three fold; firstly, as a very well studied organism, the genome of *C. elegans* has been sequenced, annotated and a range of genetic knockouts are available [287]; secondly, an intermediate disease phenotype is possible with yeast infection giving the ability to study both hyper- and hypovirulence [103]; and finally, the maintenance of *C. elegans* cultures is cheap, they have fast generation times, do not require a licence to experiment on and there are no ethical issues about animal use to take into account. For the study of yeast pathogenesis with *S. cerevisiae* and *C. glabrata* the possible advantages to using *C. elegans* as a model of the innate immune system are clear.

An attempt was made to establish a *C. elegans* infectivity model with *C. glabrata*. It was based on the feeding model already established for *S. cerevisiae* [103], substituting *C. glabrata* for *S. cerevisiae*. Initial pilot experiments proved that just as *C. elegans* can ingest and become infected by *S. cerevisiae*, *C. elegans* could successfully ingest and become infected by *C. glabrata*. The yeast infection manifests itself as a posterior anal swelling called deformed anal region or dar. The infection is established as the yeast cells pass through the digestive tract of the nematode and adhere to the posterior anal wall, establishing an infection and causing an immune response to infection through the ERK MAP kinase pathway [288] characterised by dar. The extent of virulence is assayed by counting the number of nematodes with visible dar after a given maturation point and producing a ratio of infected to non-infected as a measure of comparative virulence.

Once the ability of *C. glabrata* to infect *C. elegans* was established, initial studies using the *C. glabrata* wild type, Cg2001, and the hypervirulent *ace2* null strain, HLS122, were performed to establish a baseline of dar for virulence analysis. Unfortunately a consistent baseline level of dar could not be established for either Cg2001 or HLS122. Many repeats and variations of food, plate media, number and age of worms, concentration of yeast, ratios of yeast to *E. coli* and also duration of experiment were tried over 18 months. It was decided that after 18 months without being able to establish a consistent baseline of wild type virulence within the *C. elegans* model it was not suitable for virulence analysis of the Ace2p regulon mutants within *C. glabrata* and therefore was abandoned in favour of direct vertebrate virulence analysis.

A brief review of the materials and methods is included below for reference.

A5.1.1 Materials and Methods

Four nematode growth medium (NGM) plates were spotted with *E. coli* OP50 and incubated overnight at 37°C. Several L4 larvae were transferred onto each plate and incubated at 20°C for four days. On day three, OP50 and yeast strains were grown overnight in 5 mL of LB or selective media at 30°C/37°C, 180 rpm.

On day four, yeast and *E. coli* were centrifuged and washed twice with sterile water. The cells were resuspended in sterile water to a concentration of 20 mg/mL for yeast and 200 mg/mL for *E. coli*. A suspension of yeast, *E. coli,* and streptomycin was made with the ratio of 3:1:4 by volume respectively for each of the target yeast strains. Triplicate plates were then made by spotting 20 µL of the suspension onto fresh NGM plates and being allowed to dry.

A *C. elegans* egg suspension was then made by washing off the worms from the four four-day *C. elegans* plates with M9 buffer (3 g KH_2PO_4, 6 g Na_2HPO_4, 5 g NaCl, 1 mL 1 M $MgSO_4$, water to 1 litre, autoclave) into a 15 mL conical tube. The eggs were collected by centrifugation at 900 g for two minutes and washed twice with M9 buffer. The pellet was then resuspended in bleach solution (0.0625 M sodium hydroxide) and mixed slowly for three minutes by inversion. The eggs were then collected via centrifugation at 2000 g for two minutes, washed twice with M9 buffer and resuspended to a concentration of 6000 eggs/mL. Approximately 30 eggs were then spotted onto the previously prepared yeast NGM plates in 50 µL of egg suspension. The plates were then incubated at 20°C for four days, observed each day.

The total number of worms were counted and compared to the number of worms showing dar on the fourth day. A triplicate plate set of *E. coli* and streptomycin only was used as a control.

A5.2 Study and comparison of the transcriptome of *Candida* species infection of murine model

Our understanding of the processes involved with *in vivo* infection of *C. glabrata* and other *Candia* species is limited. It is obvious that the study of the transcriptome of *Candida* infection is required. Study of the proteome and secretome of the hypervirulent *ace2* null in *C. glabrata* has already been completed with many proteins showing significant changes in production levels outside of the Ace2p regulon and the cell separation machinery [180, 231]. By studying and comparing the transcriptome from *C. glabrata* wild type from within the host environment and *in vitro*, the genes up and down-regulated during infection can be shown with the potential to reveal virulence factors and infection associated genes. Subsequent analysis of the transcriptome of the hypervirulent *C. glabrata ace2* from within the host will allow us to compare and contrast which genes are up and down regulated in response to the host and see which gene expression changes are different between the wild type and the hypervirulent mutant. In this way it will be possible to identify genes that contribute to the hypervirulent phenotype displayed by *ace2* null cells in *C. glabrata* [7]. Once target genes have been identified, analysis of their virulence potential can be studied in a similar manner to that employed within this study for the Ace2p regulon.

To this end a series of experiments totalling to six months work was conducted in an attempt to profile the transcriptome of both *C. glabrata* and *C. albicans* wild types from within a murine model of candidiasis, as well as the transcriptome of the *C. glabrata ace2* null, HLS122. The profiling was conducted in collaboration with the Illumina facility within the Department of Biosciences, Exeter University, Devon. It was based around the use of RNA-seq, a system of high-throughput sequencing of cDNA made from RNA samples, which promised to sequence the total RNA extracted from murine organs infected with *Candida*, and to be able to separate out the fungal transcripts from those of the host. The primary advantage of using RNA-seq over a traditional microarray was the proposed ability to handle total RNA, which would remove the requirement for extraction of the yeast infectious units prior to RNA extraction and in turn save time, give a more accurate profile of the transcriptome mid-infection and allow us to look at both the yeast and host transcriptomes simultaneously.

The experiments to compare and contrast the transcriptomes of the wild type *Candida* strains from host infections required two different host conditions, with *C. glabrata* requiring a neutropenic mouse model, and *C. albicans* requiring an immune competent model. A model of systemic candidiasis was selected, with 72 hours given for the yeast to establish a disease condition prior to harvesting. The mice were culled at 72-hours post infection, with the kidneys immediately extracted into liquid nitrogen or RNAlater (Qiagen, UK). The total RNA was then extracted, cleaned and transported to Exeter for processing on dry ice.

A similar procedure was adopted for comparison of the transcriptome of *C. glabrata ace2* infection to that of Cg2001, the *C. glabrata* wild type. *C. glabrata ace2* cells cause 100% mortality within 18-hours post infection, therefore the infection period was reduced to 15 hours to ensure RNA integrity at the point of harvesting. The mice were culled 15-hours post infection and the organs, including the lungs, harvested into RNAlater for extraction, clean-up and transport to Exeter on dry ice.

After several repeats of both infections and RNA extractions from different organs, the RNA-seq was unable to detect and discern enough *Candida* RNA from the strong mouse RNA signal after multiple runs through the Illumina G2. As running the animal experiments to generate the RNA was time consuming and not of insignificant cost, and each run of the Illumina G2 was time consuming and also carried significant cost, it was decided to abandon attempts to study the transcriptome of *Candida* species from within the host.

A brief review of the materials and methods is included below for reference.

A5.2.1 Materials and Methods

A5.2.1.1 72-hour murine infection assay for transcriptome analysis of *Candida* species

A murine infection assay using wild type *C. glabrata* (Cg2001) and *C. albicans* SC5314 was carried out using a modification of the method as previously described by Calcagno et al. [81]. Two groups of 10 outbred male CD1 mice were used, one for *C. glabrata* infection and one for *C. albicans* infection. The *C. glabrata* group of 10 mice were immunosuppressed via IP with 200 mg of cyclophosphamide per kg of body weight on day -3 and day two. Half the animals were infected with 7 x 10^7 *C. glabrata* cells in 200 µL saline via tail vein injection (IV) on day one, the other left as a control. The *C. albicans* group of 10 mice were split into two; five mice were infected with 3 x 10^4 *C. albicans* cells per gram of body weight in 200 µL saline via tail vein injection (IV) on day one, the other left as a control. The mice were observed and weighed daily and sacrificed after 72 hours post infection. The mouse kidneys were immediately extracted upon death into liquid nitrogen or RNAlater and stored at -80°C.

A5.2.1.2 15-hour murine infection assay for transcriptome analysis of *C. glabrata ace2*

A murine infection assay using wild type *C. glabrata* (Cg2001), *C. glabrata ace2* and a negative control was carried out using a modification of the method as previously described by Calcagno et al. [81]. Three groups of five outbred male CD1 mice were used, one per condition. The mice were immunosuppressed via IP with 200 mg of cyclophosphamide per kg of body weight on day -3. Two groups, Cg2001 and *ace2,* were infected with 7 x 10^7 cells in 200 µL saline via tail vein injection (IV) on day one, the third group was left as an uninfected control. The mice were observed and weighed and sacrificed after 15 hours post infection. The mouse kidneys, liver and lungs were immediately extracted upon death into RNAlater (Qiagen Ltd, UK) and stored at -80°C.

A5.2.1.3 RNA preparation for RNA-seq

Two methods for RNA extraction were used.

For liquid nitrogen flash frozen samples total kidney RNA samples were prepared via phenol (TRIzol)-chloroform extraction. All glass and ceramics were cleaned of RNAase prior to use, double autoclaved ddH_2O (daddH_2O) was used throughout, and all steps were kept on ice unless otherwise

stated. Briefly, the kidneys were ground in a frozen pestle and mortar, with regular addition of liquid nitrogen. The ground kidney was then transferred to a 50 mL tube before being homogenized for one minute in 4 mL of TRIzol Reagent (Invitrogen, UK) and incubated at room temperature for five minutes. The mixture was then shaken vigorously by hand for 15 seconds with 0.4 volumes of chloroform, before being incubated at room temperature for a further five minutes. The aqueous phase was then separated via centrifugation at 12000 g for five minutes at 4°C, and transferred to a fresh tube. The RNA was then precipitated by incubation at room temperature for 10 minutes with 0.5 mL of isopropanol per mL of solution. The RNA was then collected via centrifugation at 12000 g for five minutes at 4°C, and the supernatant removed. The RNA was then washed with 70% ethanol and allowed to air dry for 15 minutes. The RNA was then dissolved in 500 µL of daddH_2O and transferred to a fresh microfuge tube.

The RNA was then left to precipitate in one volume of LiCl buffer (4 M Lithium chloride, 20 mM Tris-Cl pH 7.5, 10 mM EDTA) for one hour at -20°C. The RNA was then collected via centrifugation at 16000 g for 30 minutes at 4°C, and washed twice with 70% ethanol before being left to air dry. The RNA was then resuspended in 50 µL of daddH_20 and cleaned using a Qiagen RNeasy Mini Kit (Qiagen Ltd, UK) as per the manufacturer's instructions, then stored at -80°C.

For kidney and lung tissue stored in RNAlater (Qiagen Ltd, UK), tissue samples were weighed and cut into 30 mg divisions, disrupted and homogenized using a rotor-stator homogenizer for 30 seconds and processed using a RNeasy Mini Kit (Qiagen Ltd, UK) as per the manufacturer's instructions.

A5.2.1.4 RNA-seq

The prepared RNA samples were sent to the Sequencing service within the Department of Biosciences at the University of Exeter, Devon, UK, for RNA-seq (Whole Transcriptome Shotgun Sequencing) [289].